Polyhedra-based analysis of computer simulated amorphous structures

D I S S E R T A T I O N

for the partial fulfillment of the requirements
for the academic degree of

Doctor rerum naturalium
(Dr. rer. nat.)

submitted to

Faculty of Mathematics and Natural Sciences
Technical University Dresden

by

Dipl.-Phys. Valentin Kokotin

born on 17 February 1983 in Noginsk

Referees: Prof. Dr. H. Eschrig
Prof. Dr. J. Rottler

Submitted on: 26.02.2010

Date of defence: 15.06.2010

ABSTRACT

Bulk metallic glasses represent a newly developed class of materials. Some metallic glasses possess combinations of very good or even excellent mechanical, chemical and/or magnetic properties uncovering a broad range of both industrial and vital applications. Besides all advantages metallic glasses have also significant drawbacks, which have to be overcome for commercial application. Apart from low critical thicknesses, brittleness and chemical inhomogeneity one important problem of metallic glasses is the lack of an appropriate theory describing their structure. Therefore, the search for new glass forming compositions as well as the improving of existing ones occurs at present by means of trial-and-error methods and a number of empirical rules.

Empirical rules for good glass-forming ability of bulk metallic glasses have been established in recent years by Inoue and Egami. Two of these rules, (i) Preference of more than 3 elements and (ii) Need of more than 12 % radii difference of base elements, seem to be closely related to topological (geometrical) criteria. From this point of view topological parameters contribute essentially to the glass-forming ability. The third rule (iii) demands a negative mixing enthalpy of base elements and refers to the chemical interaction of the atoms.

The generalized Bernal's model (hard-sphere approximation) was used for the simulation of monatomic, binary and multi-component structures. Excluding chemical interaction, this method allows the investigation of topological criteria of the glass-forming ability. Bernal's hard-sphere model was shown to be a good approximation for bulk metallic glasses and metallic liquids and yields good coincidence of experimental and theoretical results.

- The Laguerre (weighted Voronoi) tessellation technique was used as the main tool for the structural analysis. Due to very complex structures it is impossible to determine the structure of bulk metallic glasses by means of standard crystallographic methods.
- Density, radial distribution function, coordination number and Laguerre polyhedra analysis confirm amorphism of the simulated structures and are in a good agreement with available experimental results.
- The ratio of the fractions of non-crystalline to crystalline Laguerre polyhedra faces was introduced as a new parameter F_{nc}. This parameter reflects the total non-crystallinity of a structure and the amount of atomic rearrangements necessary for crystallization. Thus, the

parameter F_{nc} is related to the glass-forming ability. It depends strongly on composition and atomic size ratio and indicates a region of enhanced glass-forming ability in binary mixtures at 80 % of small atoms and atomic size ratio of 1.3. All found maxima of parameter F_{nc} for ternary mixtures have compositions and size ratios which are nearly the same as for the binary mixture with the maximum value of F_{nc}.

- A new method of multiple-compression was introduces in order to test the tendency towards densification and/or crystallization of the simulated mixtures. The results of the multiple-compression of monatomic mixtures indicate a limiting value of about 0.6464 for the density of the amorphous state. Further densification is necessarily connected to formation and growth of nano-crystalline regions.
- The results of the multiple-compression for binary mixtures shows a new maximum of the density at the size ratio of 1.3 and 30 % to 90 % of small atoms. This maximum indicates a local island of stability of the amorphous state. The maximal receivable density without crystallization in this region is enhanced compared to neighbouring regions.
- The comparison of the parameter F_{nc} and the density to the distribution of known binary bulk metallic (metal-metal) glasses clearly shows that both parameters play a significant role in the glass-forming ability.
- The polyhedra analysis shows regions with enhanced fraction of the icosahedral short-range order (polyhedron (0, 0, 12)) in the binary systems with the maximum at 80 % of small atoms and size ratio of 1.3. Comparison of the distribution of the (0, 0, 12) polyhedra to the distribution of known binary metallic (metal-metal) glasses and to the parameter F_{nc} shows that icosahedral short-range order is not related to the glass-forming ability and is a consequence of the high non-crystallinity (high values of F_{nc}) of the mixtures and non *vice versa*. Results for the ternary mixtures confirm this observation.
- A new approach for the calculation of the mixing enthalpy is proposed. The new method is based on the combination of Miedema's semi-empirical model and Laguerre tessellation technique. The new method as well as 6 other methods including the original Miedema's model were tested for more than 1400 ternary and quaternary alloys. The results show a better agreement with experimental values of the mixing enthalpy for the new model compared to all other methods. The new model takes into account the local structure at atom site and can be applied to all metallic alloys without additional extrapolations if the atomic structure of the considered alloy is known from a suitable atomistic structure model.

TABLE OF CONTENTS

CHAPTER 1
INTRODUCTION

Amorphous metallic alloys having been first reported in 1960 by Klement et al. [Kle60] represent a relatively young class of materials, which has grown from a singular observation to an expansive class of alloys with broad scientific and commercial importance. Due to exceptional physical, chemical, magnetic and/or mechanical properties (see Table 1.1) of some glasses, they have enabled applications that include low loss magnetic transformer cores, corrosion resistant coatings, pressure sensors, golf club heads, the structural hinges for digital micromirror devices etc. [Ega03, Mir06]. In addition, glassy materials have important influence on the scientific community and even daily life [Wan07a] because of constantly enhancing demand of new materials for both industrial and vital applications.

Being intensively investigated during the last 50 years metallic glasses still raise many unapprehended features. One of the most significant problems of metallic glasses is a very complicated atomic structure, which can not be investigated by means of standard crystallographic methods. When we try to find out the structure – property relationships for metallic glasses, we feel lost and have trouble knowing where to begin, because describing the atomic structure of a glass is already a major challenge [Mil08]. The name “amorphous” itself, meaning shapeless, refuses rigorous characterization and demands statistical methods.

One possible solution for describing structures of amorphous materials is Voronoi tessellation, which was firstly proposed by Finney [Fin67]. The Voronoi polyhedron describes the sort-range order around an atom. It is built around the atom and can be applied for the estimation of different topological parameters like atomic volume, local symmetry, coordination number etc. proposing a powerful way for describing the structure.

Table 1.1: The fundamental properties of the late transition metal-based bulk metallic glasses [Mil08].

Fe-based
- Soft magnetism (glass, nanocrystal)
- Hard magnetism (nanocrystal)
- High corrosion resistance
- High endurance against cycled impact deformation

Co-based
- Soft magnetism (glass, nanocrystal)
- Hard magnetism (nanocrystal)
- High corrosion resistance
- High endurance against cycled impact deformation

Ni-based
- High strength, high ductility
- High corrosion resistance
- High hydrogen permeation

Cu-based
- High strength, high ductility (glass, nanocrystal)
- High fracture toughness, high fatigue strength
- High corrosion resistance

Pd-based
- High strength
- High fatigue strength, high fracture toughness
- High corrosion resistance

Pt-based
- Very low glass transition temperature
- Very low liquidus temperature
- High glass-forming ability
- High corrosion resistance
- Good nanoimprintability

On the other hand, one of the most important characteristic values describing amorphous metallic alloys is the glass-forming ability (critical thickness or/and critical cooling rate). Heretofore there is no proper explanation, why some alloys demand on very high cooling rates and very low temperatures to persist in amorphous state and other ones can avoid crystallization by a conventional casting process at low cooling rates. At this moment the search for new compositions for bulk metallic glasses is conducted largely by an Edisonian method of trial-and-error, guided by phase diagrams and a few empirical rules [Ega03]. This is because at the moment no fundamental

theory is available for predicting the ease of glass formation. It is unlikely that this progress can be accomplished without the benefit of atomic structural models.

A general description of such materials requires the analysis of a big number of alloys and compositions. But metallic glasses are quite complex, involving both topology and chemistry (energetics), and containing commonly more than 3 (mostly 5-6) elements. This makes investigations of each individual alloy very laborious. Thus it appears virtually impossible to formulate a fundamental theory to describe the complex phenomenon for such a complex material [Ega03]. The present tendency of trying to gain knowledge on the structure and stability of amorphous materials using first-principle calculations and molecular dynamics demands at least weeks or most probably months of computational time. Therewith, the time-scale accessible by molecular dynamics and the length-scale by the first-principle calculation is too small to describe the stability of bulk glass formers.

On the other hand, the deeper look inside experimental results shows, that there is number of binary alloys with strongly enhanced glass-forming ability and critical thickness of 1 mm and more. Moreover, many multi-component good glass formers can be considered as binary alloys with minor additions of other elements [Sen03, Wan07a]. Therefore, the analysis of these binary bulk metallic glasses seems to be the simplest and the most promising way for the determination of correlations between structural properties and glass-forming ability.

According to Hermann [Her83] and Miller [Mil08] there are two different types of metallic glasses depending on type of bonding: metal-metal and metal-metalloid alloys. The structure of metal-metalloid systems cannot be understood without taking into account directed chemical bonding, and metal-metal glasses have been successfully described by Bernal's model of hard spheres, which is not so time-consuming as molecular dynamics and/or *ab initio* calculations. Bernal's model is a very simple one and can be applied for systems with additive radii only, but nevertheless, this model in implementation of the force-based algorithm of Jodrey and Tory yields very good agreement with experimental results [Mat09].

Bernal's hard sphere approximation followed by a Voronoi tessellation procedure makes it possible to investigate metal-metal amorphous structures in the

complete range of radii ratios and the whole range of concentrations and to relate their structural properties to the glass-forming ability. Molecular dynamics and first-principles calculations would take hundreds of years using actual computers for the same amount of calculations.

Besides Bernal's model and Voronoi tessellation two other method were used in this work. The first one is the Nelder-Mead simplex method, which was applied for searching of compositions with maximum packing fraction under desired conditions, since bulk metallic glasses are known to have very high density [Sen03]. The second one is the well known Miedema's semi-empirical model for calculation of the mixing enthalpy. This model developed initially for binary mixtures has got many modifications and extensions, which were compared in this work with experimental values of the mixing enthalpy of more than 1400 different alloys. A new polyhedra-based generalization of Miedema's model for multi-component systems is also suggested in this work.

1.1 History of metallic glasses

In 1960 Klement, Willens and Duwez published an article in Nature asserting that by uniform and rapid cooling from the liquid state to room temperature formation of crystalline phases was suppressed and, thus, the liquid structure of the alloy $Au_{75}Si_{25}$ was kept in the solid state, what was evidenced by the results of X-ray analysis of the samples [Kle60].

Although amorphous metallic alloys have been known before, so Buckel obtained amorphous structure in metallic Bi, Ga and $Sn_{90}Cu_{10}$ films produced by low temperature spraying (< 15 K) [Buc54]. Klement's group was the first one which produced an amorphous metal alloy by the quenching from a liquid state using the so-called splat-quenching or gun method [Duw60]. Exactly because of this, Klement's paper has been considered to be the starting point for the history of metallic glasses.

Due to the high cooling rate of ~ 10^6 K/s the atoms in the experiment of Klement did not have enough time and energy to rearrange for crystal nucleation, required for

crystallization. As a result, the liquid reaches the glass transition temperature, T_g, and solidifies as metallic glass bypassing crystallization [Tel04]. Such high cooling rates restrict the thickness of the sample to the micrometer range. A few years later Chen and Turnbull [Che69] studying ternary alloys Pd-M-Si (M = Ag, Cu, Au) found that some alloys in these systems have a critical cooling rate of about 10^2 K/s and can be obtained in the amorphous state till the thickness of 1 mm and more. These alloys can be considered as the first bulk metallic glasses (BMG). In some ternary alloys of Pd-Cu-Si and Pd-Ag-Si systems the interval of the supercooled liquid reaches 40 K, which allowed the authors to carry out the first detailed studies of crystallization in metallic glasses, as well as to prove occurrence of phase separation at temperatures higher than T_g, but below the crystallization temperature, T_x. Conducting systematic studies of Pd-TP (T = Ni, Fe, Co) and Pd-M-Si (M = Rh, Au, Ag, Cu and T) alloys in 1974, Chen received in these systems amorphous cylindrical specimens of 1-3 mm in diameter and several centimeters in length by means of casting into water [Che74]. In 1982 Lee, Kendall and Johnson produced amorphous alloy $Au_{55}Pb_{22.5}Sb_{22.5}$ in the form of balls with diameter of ~ 1.5 mm [Lee82]. This alloy was also found to show a phase separation in amorphous state. The first amorphous phase in this alloy is rich of gold, and the second one of lead. In the same year Drehman, Greer, and Turnbull received glassy spherical samples of $Pd_{40}Ni_{40}P_{20}$ up to 5 mm in diameter by a slow cooling (1.4 K/s) in vacuum. Such good results were achieved by removing the surface oxides and other inclusion through processing the alloy mixture in HCl and H_2O_2 followed by repeating the heating and cooling cycles [Dre82]. Turnbull's group obtained amorphous samples of 10 mm in diameter for this alloy with similar handling but operating in a liquid flux (boron oxide B_20_3) and not in vacuum [Kui84].

Since the 80-ies Inoue (Tohoku University's Institute for Materials Research) and Johnson (Caltech) have developed a large number of amorphous metal alloys based on La, Mg, Zr, Pd, Fe, Cu and Ti. These alloys have a wide range of the supercooled liquid state and low critical cooling rates (10^0...10^2 K/s). Such low critical cooling rates allowed to increase the quenching time up to minutes and to obtain amorphous alloys with thicknesses of more than 1 cm applying conventional casting procedure.

In 1989 Inoue, studying alloys of rare earth metals (lanthanides) with aluminum and ferrous metals, found a high glass-forming ability of La-Al-Ni system. It was also found that the alloy $La_{55}Al_{25}Ni_{20}$ has the widest interval between T_g and T_x ($\Delta T_x = T_x - T_g \approx 70$ K) known at that time. From the viewpoint of industrial applications of amorphous alloys larger values of ΔT_x make it possible to develop bulk amorphous alloys by warm consolidation of amorphous powders or ribbons [Ino89a]. Other alloys known at that time to have a wide range of ΔT_x were Pt-Ni-P (ΔT_x ~ 60 K), Pd-Ni-P (ΔT_x ~ 50 K) [Che76], and Mg-Ni-La (ΔT_x ~ 58 K) [Ino89b]. One year later Inoue discovered that alloys of La-Al-Cu system also have excellent amorphous properties. Thus the $La_{50}Al_{25}Cu_{25}$ amorphous alloy has a wide range of the supercooled state (ΔT_x ~ 59 K) and can be produced in the form of cylinders up to 0.8 mm in diameter using casting into water [Ino90a]. In 1990 Inoue, continuing investigations of amorphous alloy $La_{55}Al_{25}Ni_{20}$, produced this alloy using casting in copper molds in diameter of 3 mm [Ino90b] and two years later, replacing the 10% nickel with copper, the alloy $La_{55}Al_{25}Ni_{10}Cu_{10}$ up to 7 mm in diameter [Ino93a].

In 1991 the same group was studying the system Mg-Cu-Y. Maximum glass-forming ability was found for $Mg_{65}Cu_{25}Y_{10}$. Completely amorphous cylindrical specimens of this alloy were produced by means of casting in metal molds up to the diameter of 4 mm [Ino91]. Inoue's group developed parallel a family of Zr- based alloys: Zr-Al-Ni-Cu. These alloys have a high glass-forming ability and thermal stability. The supercooled temperature range of $Zr_{65}Al_{7.5}Ni_{10}Cu_{17.5}$ alloy is 127 K [Zha91], and the critical diameter for the alloy reaches 16 mm by the casting into water [Ino93b].

Developing of bulk metallic glasses it has been shown that these alloys may be of interest not only as a new type of material for research, but also as new materials for industrial purposes. The significance of Inoue's work was quickly recognized by Johnson, whereupon Johnson's group started searching for bulk metallic glasses in the early 90s [Loe03]. In 1993 Peker and Johnson developed 5-component alloy $Zr_{41.2}Ti_{13.8}Cu_{12.5}Ni_{10}Be_{22.5}$ [= $(Zr_3Ti)_{55}(Be_9Cu_5Ni_4)_{45}$] which is called Vitreloy 1 (Vit 1) and has a critical thickness of several centimeters [Pek93]. This work together with

Inoue's group results could be considered as the beginning of the industrial application of bulk amorphous alloys.

In 1997 Inoue's group substituted 30% nickel by copper in the alloy $Pd_{40}Ni_{40}P_{20}$ and obtained the new alloy $Pd_{40}Cu_{30}Ni_{10}P_{20}$ which has a critical cooling rate by casting in boron oxide (B_20_3) of approximately 0.1 K/s. That allows producing of $Pd_{40}Cu_{30}Ni_{10}P_{20}$ alloy in a glassy state till the thickness of more than 72 mm [Ino97a]. The family of metallic alloys Pd-Cu-Ni-P has the greatest glass-forming ability known up to now.

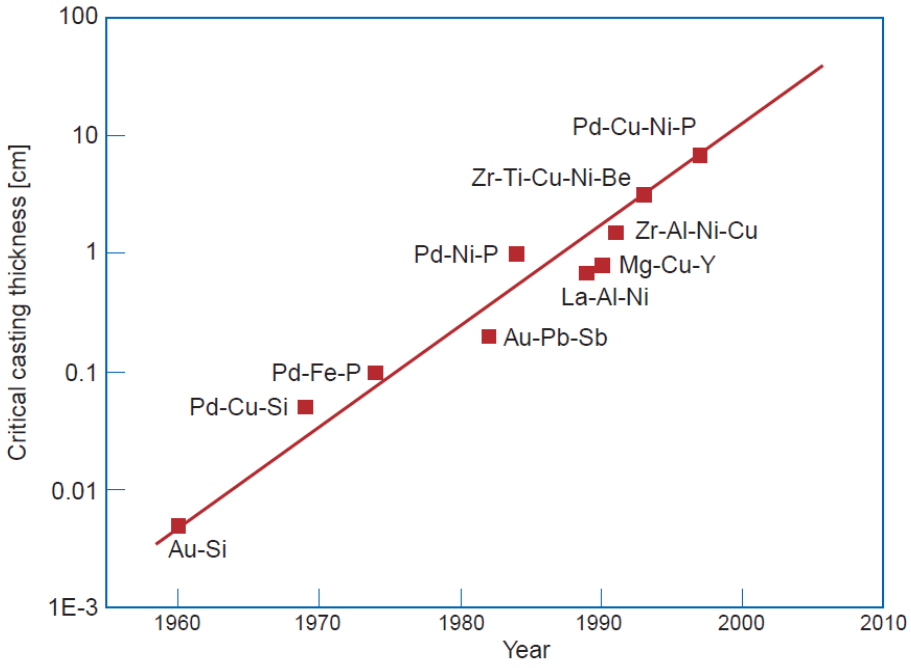

Figure 1.1: Critical casting thickness versus the year in which alloys were discovered [Tel04].

Figure 1.1 presents the critical casting thickness depending on the year the alloy was discovered. Since the discovery of the first alloy the critical thickness increased by more than 3 orders of magnitude. If the tendency will be kept, in 10-20 years new bulk metallic glasses having very high stability against crystallization, like ordinary glasses may be developed [Loe03].

1.2 Theoretical approaches and atomistic simulations for the investigation of BMGs

Atomistic simulations is a very promising and important driving force in the field of material science; many research efforts now incorporate theory and modeling to complement experimental investigations. Earliest simulations of liquids and glasses date back to the 50-ths [Ald57, Woo60]. Simulations play several key roles in research, particularly in disordered systems. They provide key tests of theory, giving unbiased insights that lead to new theoretical ideas, and connecting theory and experiment.

A major advantage of atomistic simulations is a detailed picture of processes occurring during the investigation. Simulations have been very instrumental in explaining the connection of macroscopic properties to the atomic scale structure. Simulations play also a significant role in the development and testing of theories and allow to measure properties, which are not accessible by experiments. This all allowed atomistic simulations to play a tremendous role in elucidating of what now is understood about the dynamics of glass-forming systems [Mil08].

Besides a big amount of possible applications and advantages the simulations have also their own limitations like small time- and length scales. For instance, non-empirical electronic-structure-based simulations can presently accurately handle hundreds atoms at most and are limited significantly more in size and timescales than empirical potentials. Due to the significant amounts of computations needed for calculating the energies and forces at each time step, the timescales are similarly very short.

The results of simulations depend on the interaction potentials used, and the degree to which simulations and experiments coincide is directly related to the interaction models applied to simulate the experimental system.

The use of classical potentials (hard spheres, Lennard-Jones etc.) is more common at present. More complex and more accurate potentials can correct many deficiencies of simple pair potentials. However, it is always a challenge to choose adequate models. On the one hand the empiricism required often makes the applicability

to real materials somewhat questionable, on the other hand the complex methods and potentials also demand certain assumptions and leave the question about the applicability of the model and potentials open. In addition, nominally similar potentials may produce significantly different results, with occasionally unexpected behavior that is a result of the potential and not of the real material. This sensitivity is often not considered in any detail. Even if the potentials are assumed to be acceptable for the problem, there are still important questions concerning, for example, the accuracy and reliability of the experimental results the simulations should be compared to.

BMGs consist commonly of three or more components, and developing an accurate potential for such a multicomponent system is not a trivial task. Since many qualitative questions of the glass formation are still open, it seems reasonable to use pair potentials such as hard spheres [Par05], purely repulsive soft spheres [Lai89] and the Lennard-Jones model [Bro82] for the study of general problems. Many generic properties of the glass formation have been obtained using pair potentials, and the contributions of simulations to understanding BMGs cannot be neglected. Recently, many-body potentials are being implemented to simulate more realistic systems. But it makes no difference, what potential is being used; there is always the question of how closely the results may be compared to measured properties.

Simulations are also affected by timescale limitations. Time steps in a molecular dynamics are on the order of a femto- to picoseconds. This means that to simulate a process in a time interval of about one second ~$10^{12\text{-}15}$ steps are necessary. Each step requires the calculation of interatomic interactions, what puts limit on the number of atoms (system size) that can be simulated. Due to increasing of computational power ever bigger systems and ever longer timescales are reached. At the moment simulations attained 1–10 ns and system sizes of several thousands to a few million atoms, while a decade ago simulations consisted of only 10^5 time steps and of a few thousand atoms [Sib02].

Both the timescale and time step size lead to some limitation on the simulation procedure. So, for example, on account of the short timescale the critical cooling rate of a typical simulation amounts to about 10^{12} K/s, which is much higher than experimental values used to form BMGs. Due to such high cooling rates the resulting structure and

mechanical properties might be different comparing to lower cooling rates and even simulated monatomic systems form glasses [Ben86]. This feature plays a more important role for multicomponent systems, since the local chemical equilibrium depends on the diffusion rates. Therefore, the degree of chemical ordering might be dramatically different comparing to slower cooling rates.

1.2.1 Potentials

All atomistic simulations require potentials that define the interactions between atoms in the system [Fre02]. In the Monte Carlo method the potentials are used for searching for configurations with low free energy. The interaction potentials are used to calculate the change in energy with a change in configuration.

The molecular dynamics is based on solving combined equations of motion of all atoms in the system followed by recalculation of positions, trajectories and velocities of atoms at every very small time steps (1 fs to 1 ps), what yields a full description of the time evolution of the system. The potentials are used in this method to calculate the force on an atom due to the presence of all other atoms.

Many basic questions regarding the nature of the glass transition can be adequately described by simple simulation models or interatomic potentials. These models are commonly based on pair-potentials like hard spheres, purely repulsive soft spheres and Lennard-Jones potentials. Hard spheres and Lennard-Jones potentials are mostly used to describe the amorphous state. Calculation of more specific properties requires more complicated interactions. Metallic systems can be well described by many-body interactions.

First-principles calculations may also be implemented and they are particularly useful in examining stable and metastable phases, and constructing phase diagrams. *Ab initio* methods are also being used for the parameterization of empirical potentials for molecular dynamics and other simulations.

Pair potentials: Hard spheres and Lennard-Jones

The simplest but nevertheless meaningful pair potential for describing liquids and glasses is the hard-sphere approximation. In this method the atoms are considered as hard cores – the potential energy is zero if atoms do not overlap and infinite otherwise. This model has many modifications. The general description of the hard-sphere potentials and corresponding models is presented in Section 2.1 of the present manuscript.

Another widely used model for the simulation of glass-forming systems is the Lennard-Jones potential [Sch98], which has the following form:

$$V_{\alpha\beta}(r) = 4\varepsilon_{\alpha\beta}\left[\left(\frac{\sigma_{\alpha\beta}}{r}\right)^{12} - \left(\frac{\sigma_{\alpha\beta}}{r}\right)^{6}\right], \tag{1.1}$$

where $\varepsilon_{\alpha\beta}$ and $\sigma_{\alpha\beta}$ represent the energy and length scale of the $\alpha\beta$ atomic pair, respectively.

The Lorentz–Berthelot mixing rules are usually used for the interaction of different types of atoms, for instance $\sigma_{\alpha\beta} = \frac{1}{2}(\sigma_{\alpha\alpha} + \sigma_{\beta\beta})$ and $\varepsilon_{\alpha\beta} = \sqrt{\varepsilon_{\alpha\alpha}\varepsilon_{\beta\beta}}$. This model was firstly used by Wahnström for the investigation of the dynamics and mode-coupling theory in supercooled systems [Wah91].

Many-body potentials

The use of pair potentials leads to a number of unphysical effects, for instance, regarding the elastic constants and vacancy energies. Thus, if the details of the electronic structure on the interaction between atoms become important, a many-body potential might be a solution. These potentials affect, for example, the elasticity of simulated amorphous structures.

There are a number of many-body interactions and the majority of them can be generalized in a mathematical form, which describes the energy of an atom as a function of a fictitious "electron density" from the surrounding atoms, plus a pair term. The total energy for these potentials has the following form:

$$E = \sum_i F_i(\rho_i) + \frac{1}{2}\sum_{i \neq j} \phi(r_{ij}), \tag{1.2}$$

where F_i is the embedding energy experienced by atom i due to the sum, ρ_i, of electron densities ρ_j^a from all other atoms, j. In the case of a spherically symmetric electron density, the density is written as:

$$\rho_i = \sum_{i \neq j} \rho_j^a(r_{ij}). \tag{1.3}$$

Many methods use this form of potential, for example the effective medium theory [Jac87], the Rosato–Guillope–Legrand potentials [Ros89], the Glue potentials [Erc94], the Sutton–Chen potentials [Sut90]. All this methods are generally called embedded atom models [Mil08]. Baskes [Bas92] has extended this model also to asymmetric charge densities.

1.2.2 Methods

Ab initio calculations

At present the most accurate technique for describing atomistic energies and forces is *ab initio* calculation. This method includes explicit electronic contributions to the energies. These calculations do not include empirical parameters except several approximations depending upon the method being used. Due to the accuracy first-principles methods are also the most limited ones in both time and length scales.

Ab initio calculations have found many application fields like refinement of phase diagrams by energetics of both stable and metastable phases [Zho06] (especially of ternary and multi-component alloys, due to the limited experimental data). Regarding liquids and amorphous materials such calculations have been used to study local structures and dynamics [Wan04] as well as to predict the type of atomic additions needed to suppress nucleation [Mih04]. One of the most important application fields of these calculations is the development of interatomic potentials for other simulations like molecular dynamics. Without accurate potential determination simulations can produce incorrect ground states and may totally fail. The determination of potentials using first-principles yields accurate empirical potentials and permits to avoid unphysical behavior of the simulated systems.

Constant enhancing of the computational capacity allows more and more complicated *ab initio* calculations, and even melting points can be examined [Alf05] at present.

Molecular dynamics

Molecular Dynamics simulation is a technique for computing the equilibrium and transport properties of classical many-body systems. The word "classical" means in this context that the nuclear motion of the constituent particles obeys the laws of classical Newton's mechanics. This is a very good approximation for a wide range of materials. Some of the exceptions include the translational or rotational motion of light atoms or molecules (He, H_2, D_2) or vibrational motion with frequencies higher than $\nu > k_B T / \hbar$ [Fre02]. For these systems quantum effects should be taken into account.

Real experiments and molecular dynamics have many similarities. So, the whole simulation procedure can be split into two steps similar to experimental routine: preparation of a sample followed by measurement. In the case of molecular dynamics these two steps have the following form: selection of a model system consisting of N particles and finding of an equilibrium state, and after equilibration the actual measurement can be performed. Common mistakes which can arise during the

simulation are also similar to real experiments: the sample could be prepared not correctly, the measurement might be too short to obtain satisfactory results, the system might undergo an irreversible change during the experiment, or one could also measure not what one believes [Fre02].

To receive an observable parameter value in a Molecular Dynamics simulation this parameter should be expressed as a function of the positions and momenta of the particles in the system. A definition of the temperature in a many-body system can be estimated through the energy that enters quadratically in the Hamiltonian of the system averaged over all degrees of freedom, N_f ($=3N-3$ for a system of N particles with fixed total momentum), [Fre02]. For the average kinetic energy per degree of freedom it makes:

$$\left\langle \frac{1}{2} m v_\alpha^2 \right\rangle = \frac{1}{2} k_B T \,. \tag{1.4}$$

During the simulation this equation is used as an operational definition of the temperature. From the practical point of view it is better to calculate the total kinetic energy of the system and divide this by the number of degrees of freedom. The instantaneous temperature can be expressed as:

$$T(t) = \sum_{i=1}^{N} \frac{m_i v_i^2(t)}{k_B N_f}, \tag{1.5}$$

where N_f is number of all degrees of freedom in the system and $v_i(t)$ is the instantaneous velocity of atom i. Fluctuations of the total kinetic energy cause the relative fluctuations in the temperature of about $1/\sqrt{N_f}$. For N_f on the order of 10^3, the statistical fluctuations in the temperature make about 3%. More accurate estimate of the temperature requires averaging over many fluctuations.

Molecular dynamics simulations allow a great amount of different simulations of almost all real systems under different conditions like squeezing, shearing, annealing,

rapid cooling etc. They can be also applied for the calculation of a variety of different mechanical and structural parameters like diffusion coefficients, shear viscosity, crystallization and nucleation parameters etc.

Monte Carlo simulation

The Monte Carlo approach is a statistical method lowering the energy of an initial structure under given conditions. It is clear that already for a 100 atoms system the search for a stable configuration can be very time-consuming or even impossible. It demonstrates that good numerical techniques are needed to compute positions of atoms and corresponding configurational energies. One such a technique is the Monte Carlo importance-sampling algorithm introduced in 1953 by Metropolis [Met53]. This method has found a wide range of applications in the field of the numerical simulation of dense molecular systems.

Comparing to a typical *ab initio* code the Monte Carlo programs are very short. They are only a several thousand lines long. For this reason, it is not uncommon that a simulator will write many different programs that are dedicated to a special problem or application [Fre02]. As a result, there is no a standard Monte Carlo program. However, the cores of most Monte Carlo programs are very similar.

The prime purpose of a Monte Carlo program is to compute equilibrium properties of classical many-body systems, while a random walk is constructed in such a way that the probability of visiting a particular point $r^N = (\vec{r}_1, \vec{r}_2, \ldots, \vec{r}_N)$ is proportional to the Boltzmann factor $\exp\left[-\beta U(r^N)\right]$, where $\beta = 1/k_B T$ and N is a number of particles. There are many ways to construct such a random walk. In the approach introduced by Metropolis, the following scheme is proposed [Fre02]:

1. Select a particle at random, and calculate its energy, $U_i(r^N)$;

2. Give the particle a random displacement, $\vec{r}_i' = \vec{r}_i + \vec{\Delta}$, and calculate its new energy, $U_i(r'^N)$;

3. Accept the move from r^N to r'^N with probability

$$acc = \min\left(1, \exp\left\{-\beta\left[U_i(r'^N) - U_i(r^N)\right]\right\}\right).$$

The first step of simulation in this method is the generation of points in configuration space with a relative probability proportional to the Boltzmann factor. The general approach is to prepare the system r^N that has a nonzero Boltzmann factor $\exp\left[-\beta U(r^N)\right]$. This configuration, for example, may correspond to a regular crystalline lattice with no hard-core overlaps. Next, we generate a new trial configuration r'^N with Boltzmann factor of $\exp\left[-\beta U(r'^N)\right]$ by adding a small random displacement $\vec{\Delta}$ to $\vec{r}$. The next step is to decide if the trial configuration is accepted or not. In order to make this decision, a random number from a uniform distribution in the interval [0,1] is generated. If the random number is less than *acc* the new configuration is accepted and rejected otherwise. Obviously, it is very important that the random generator does indeed generate numbers uniformly in the interval [0, 1]. Otherwise the Monte Carlo sampling will be affected [Fre02].

The resulting structure of a Monte Carlo simulation is an equilibrium configuration. Using this method and taking into account parameters of chemical elements one can simulate structures of real metallic glasses and investigate their properties.

One of the modifications of the Monte Carlo method is the Reverse Monte Carlo technique. In this method a diffraction pattern of a real alloy is taken and a structure is built in order to fit this pattern. This method is based on experimental results and has found wide application especially for BMG.

Summary

Simulations are of particular interest for BMGs in understanding factors that affect glass formation, since they can provide information of the atomic level structure allowing direct observations of the structural changes. Simulations are also very useful

for separating effects and factors that are difficult to study experimentally. For example, it has been demonstrated that the atomic size ratio has a direct effect on whether crystallization, glass formation, or phase separation will occur. For instance, Lee [Lee03] observed crystallization of $A_{50}B_{50}$ samples by the size ratios, $R(B)/R(A)$, of 0.95-1.0, while moderate size ratios of 0.60-0.95 cause glass phase formation; and with small size ratios of <0.60, the alloy phase separates into pure phases and crystallizes.

Besides the size effects there is the need to consider compositional effects of multicomponent BMGs, which give rise to phase separation and chemical ordering. Experiments have shown activation of phase separation prior to crystallization [Wan03]. Even in the absence of nucleation, phase separation has also been reported to occur in metallic glasses [Mil02].

There are still a great amount of unsolved questions concerning metallic glasses, their structure and properties; and atomistic simulations are a promising and powerful scientific equipment, which can give many answers.

1.3 Bernal´s model

When Debye and Scherrer observed the diffraction halo in liquids in 1916, it was agreed by all, that this halo demonstrates a periodicity in the liquid [Ste30]. Surely the liquid does not contain minute crystals, and if not, what causes the effects obtained and how the structure of liquids is built? Thus, the nature of this periodicity has been a long time the cause of discussion and, when in 1950s a similar diffraction halo structure was observed for rapidly cooled metallic alloys [Buc54, Duw60], this question found a second life in application to amorphous materials and become more important.

Most theories developed till 1959 frankly attempted to adapt the known structures of gaseous and crystalline matter to the intermediate state of the liquid. They were consequently physically very implausible. The same theories indeed assumed that a large part of a liquid consists of crystalline material, which is in contradiction to the fundamental property of liquids - their lack of long-range order [Ber59].

Classical works of Stewart [Ste30] and Prins [Pri36] based on X-ray and later on neutron diffraction of liquids showed liquids to possess only a short-range order, limited to the first and second coordination spheres and led Bernal to a theory he first put forward in 1937 [Ber37]. The essential feature of this theory is that it treats liquids as *homogeneous, coherent* and *essentially irregular* assemblages of molecules containing no crystalline regions or holes large enough to admit another molecule [Ber59, Ber60, Ber64, Ber67].

To confirm this idea Bernal have tried with a kind of Monte Carlo approach physical models, analogous to the formation of irregular close-packed liquids by compression from a gas. He chose a random set of points in the large cell of two- and three-dimensional lattices. If these are thought of as being rigid spheres of unit radius, the compression of such a cell is exactly equivalent to expanding a sphere surrounding each point. Starting with the nearest pair, the points were moved apart by small successive stages so that at each stage no two points are nearer than a pre-specified diameter of the spheres. Bernal has found that at a length of about 0.9 of the close-packed distance in two dimensions and 0.95 in three dimensions, no further movement is possible without introducing long-range order. It means that two-dimensional aggregates crystallize more easily than do three-dimensional aggregates and consequently the possibility of irregular co-ordinations is multiplied in three dimensions. This conclusion can be also confirmed from the great variety of polyhedra that can be escribed about the same sphere in the three-dimensional case [Ber59].

One other classical attempt to reproduce the structure of liquids was made by Bernal using balls of plasticine rolled in chalk, packed irregularly together and after that squeezed into a solid lump. Analysis of the received structure has shown 2 major features: 1 - a wide variety of polyhedra (among 65 studied polyhedra 32 different combinations of polygonal faces were found), 2 - the absolute predominance of pentagonal faces. Since the regular three-dimensional arrangements have symmetries limited to multiplicities of 2, 3, 4 and 6 (except very rare and complex structures [Fra58]) Bernal concluded that *irregular dense packing and pentagonal arrangements are necessarily connected.*

There are two basic parameters closely related to an array of spheres and accordingly to the structure of liquids and amorphous materials: (1) the packing density and (2) the radial distribution function. The packing density is the ratio of the total volume of the spheres/atoms to the total volume they occupy and the radial distribution function describes how the density varies as a function of the distance from a particular sphere.

Packing density

It is known that liquid and amorphous states commonly have densities in a certain ranges only, which is higher than that of gases and lower than of the crystalline state [Che01]. Scott [Sco60] observed that bearing-balls poured into a rigid container might form a range of random packings with different packing densities. So the same hard balls in the same container can have the densities lying between two limits of about 0.60(1) and 0.63(7). The lower limit 0.60(1) is called "loose random packing" and was observed after a slow rotation and gradual returning to the vertical position of a cylindrical container. And the upper limit 0.63(7) corresponds to the "dense random packing" and was received during gently shaking of the vessel.

In 1969 Scott [Sco69] improved the precision over previous results by an order of magnitude using up to 80 thousand steel balls and a container with irregularly spaced dimples in the walls and bottoms to ensure random packing at the boundary surfaces. The density he received for random close-packed structure was 0.6366 ± 0.0005. As a comparison to this results the ratios of solid and liquid densities of simple monatomic substance, such as the heavier rare gases, ranges between 1.14 to 1.16 (1.15(8), 1.15(2), 1.15(8) and 1.14(8) for neon, argon, krypton and xenon respectively [Sco62]), which is approximately the ratio of random to regular close packing densities 1.16(3) within experimental error.

Many attempts to define the packing density of the random close packing of hard spheres were made using different methods and yielding values from 0.610 up to 0.665 [Ber83]. Analyzing the radial distribution function of hard spheres Berryman predicted values in the range 0.64 ± 0.02, which was sufficiently well localized to distinguish this

prediction from random loose packing and ordered close packing. This value is slightly higher than that of Scott. The ratio of this density to the density of the close packed crystalline structures ($\pi/\sqrt{18} \approx 0.74048$) yields 1.15(6) which is in a pretty good agreement with the average value 1.15(4) for simple liquids.

Radial Distribution Function

The second basic parameter closely related to the structure of liquids and amorphous materials is the radial distribution function.

Using neutron diffraction Henshaw [Hen57, Hen58, Hen60] determined the radial distributions function in liquid helium, neon and argon. The relative positions of the peaks in the radial distributions for these liquids and for the random dense packing of balls are compared in Table 1.2. The radial distribution of randomly packed spheres corresponds well with that determined by x-ray and neutron diffraction for the rare-gas liquids [Sco62, Sco69].

Table 1.2: Relative position of peaks in the radial distribution of liquids (neutron diffraction data) and random dense packing of balls. The radial distances are expressed in terms of the distance to the first peak [Sco62].

	Second peak	Third peak	Fourth peak
Helium	1.8(7)	2.6(6)	3.5(8)
Neon	1.8(5)	2.7(7)	3.5(7)
Argon	1.8(1)	2.6(4)	3.4(4)
Random dense packing of balls	1.8(3)	2.6(4)	3.4(5)

Mrafko [Mra74] compared experimental and simulated radial distribution functions for $Pd_{80}Si_{20}$ amorphous alloy and found them to be identical. On the other hand, the radial distribution function of a random close-packed array of hard spheres shows a striking similarity with simple liquids, as does the difference in density between this packing and the corresponding crysta1. Therefore it is consistent to suppose liquids and amorphous alloys to have similar structures and to describe the

amorphous structure with the same model as liquids, since their structural characteristics are related more to dense liquids than crystalline solids [Fin77].

These geometrical comparisons strongly suggest that the simulated structure is essentially that of the simple liquids [Fin70a].

Summary

Random arrangements of points or particles are very useful model systems for a variety of physical and engineering problems therefore they have been studied by biologists, materials scientists, engineers, chemists, and physicists to understand the structure of living cells, liquids, granular media, glasses, and amorphous solids etc. [Tor00]. The well known Bernal's model of random close packing of hard spheres considers atoms as hard spheres and takes into account only a kind of repulsive and attractive forces, which makes this model to be the most simple but nevertheless powerful model for the structure of liquids, amorphous metals and metallic alloys. For multi-component systems, it might be called "generalized Bernal's model". The most important parameter of the model is the maximum packing fraction of about 0.636 which can be achieved with homogeneous non-crystalline arrangements of equal spheres. For multi-component mixtures of hard spheres the maximum packing fraction depends on composition and size ratio of the spheres [Her07a, Kok08].

In general the Bernal's hard sphere mixtures show the following important characteristics [Fin70b]:

- There were a large number of "collineations", or centres arranged in straight, or nearly straight, chains of up to five members.
- Arrangements of approximate fivefold symmetry occurred very frequently.
- Considering a coordination distance of up to 1.15 sphere diameters, the whole model could be broken down into only five different types of atom arrangements – or "canonical holes". Two of these (the tetrahedron and the half-octahedron) occur in regular packings; in contrast, the three other types (the lower-symmetry

trigonal prism, Archimedean antiprism and dodecadeltahedron) are absent in all regular packings.

- 73 % by number (or 48 % by volume) of these canonical holes are tetrahedral.

Though the received structures are algorithm dependent, the packing density might vary from 0.60 to 0.68 and there is no precise definition of random close packing [Tor00], the model has been the subject of extensive studies and a considerable amount of effort has gone into understanding the properties of mixtures of hard spheres [Vla03].

The model of random close packing of hard spheres seems to be of special interest as a model for amorphous materials for at least two reasons: (i) there are a series of arguments that both local and global close packing of (spherical) atoms is a characteristic feature of the structure of amorphous metallic alloys [Ega03, Mir04a, Alc08] and (ii) it is not possible to generate structure models for multi-component metallic alloys by means of *ab initio* or semi-empirical methods at the present time [Her07a].

1.4 Aim of the present work

Previous investigations have shown that metallic glasses are complex materials with non-regular structures and interesting properties. Although amorphous alloys are being intensively studied during around 50 years and many fundamental issues in metallic glasses have been explained, there are still a number of interesting scientific questions that are raised or may be studied with more care.

The fundamental reasons why liquid metallic alloys form glasses instead of crystals during solidification has been studied for a number of decades. Though, the discovery of new generations of bulk metallic glasses as well as improvement of already known ones are generally guided by rules of Inoue [Ino97, Ino00] and Egami [Ega03], which were empirically established in recent years. Two of these rules, (i) preference of more than 3 elements and (ii) need of more than 12 % radii difference of base elements, are closely related to the atomic size effect [Ino97, Ino00, Ega03, Ega84, Sen01, Mir04] and to other topological (geometrical) criteria which are considered to have fundamental

consequences for the propensity of a liquid alloy to solidify either to the crystalline state or to the glassy one. While specific proportions of radii and concentrations in binary alloys give rise to stoichiometric intermetallic crystalline compounds within the framework of the hard sphere packing model [Pas88], other radii distributions are believed to favor amorphous structures [Mir04, Mir06]. The third empirical rule demands (iii) a negative mixing enthalpy of base elements and is directly related to the chemical interaction of atoms. Though, such qualitative ideas are useful in making progress, but it would be valuable to have a deeper understanding of the size ratio effect to promote glass formation.

The atomic size ratio [Qi99, Lee03] and composition of an alloy are found to be crucial to frustrate the crystallization and, accordingly, to affect the glass-forming ability. Thus, a general investigation of topological aspects of the glass-forming ability depending on the size ratio and composition is needed. Unfortunately, there is no such investigation at the moment for the whole concentration range and sizes ratios of real metals even for binary mixtures, and only certain compositions were investigated [Lee03]. The basic reason why systematic studies are missing comes from the big amount of calculations required using even simple models. The use of molecular dynamics or *ab initio* methods makes a general investigation of topological aspects very time-consuming or even impossible at present.

On other hand, the Bernal's hard-sphere approximation is a simple model realized by relatively rapid algorithm, which allows separating out only topological aspects and investigation of geometrical contributions to short- and medium-range order, icosahedral structures and many other topological parameters in a big number of different compositions.

In addition to that, knowledge of the size ratio effect on the local ordering and phase separation behavior in the glass-forming liquid would be interesting both scientifically and for industrial applications, such as controlling of crystallization, fabrication of composites, and production of multiphase *in situ* composites by partial crystallization [Lee03].

According to aforesaid, the aim of the current contribution consists in a general investigation of the topological parameters like radial-distribution, coordination

numbers, short-range order (polyhedra analysis) etc. as well as definition and determination of non-crystallinity of the structures simulated using the Bernal's hard-sphere model. Dependences of all topological parameters on the atomic size ratio and composition will be investigated. Comparison to known good metal-metal glass-formers will be also performed in order to select parameters related to the glass-forming ability.

The first part of this work considers parameters of the monatomic hard-sphere mixtures, since these mixtures are fundamental for following investigations of binary and multi-component mixtures.

Another specific characteristic of bulk metallic glasses is the fact that the mass density is only 0.3–0.54% lower than the density of the corresponding crystallized alloy [Ino00]. This difference is significantly smaller for BMGs than for conventional glasses where it is of the order of 1–2% [Che80].

Although the relation of the packing density to the glass-forming ability makes the density to a significant factor in the glass formation, there are no complete investigations of topological parameters depending on the packing density of the mixture in the whole concentration range and "real" size ratios. The word "real" means the size ratios of real metallic systems, which is commonly in the range of 1.0 to 2.0.

The local packing fractions of separated atoms as well as the interplay of global density of a sample and the distribution of local densities in amorphous alloys also remain a topic for discussion.

Therefore, the density of the simulated structures, local packing fractions as well as influence of the density on the topological parameters will be analyzed in the present work. Thereto, a new method (multiple-compression) will be applied and compositions of multi-component mixtures having the maximum density will be found and analyzed.

Since the Bernal's model considers amorphous alloys without taking into account chemical interaction of atoms, the calculation of energetic contributions to the stability of the glassy state (glass-forming ability) becomes to a very interesting topic, especially if this investigation is based on detailed knowledge of the structure.

From this reason, the well known Miedema's semi-empirical model will be supplemented by polyhedra tessellation procedure and compared to original Miedema's model and to several known extensions of it as well.

It is obvious that the complexity of the structure of metallic glasses, especially of BMGs, cannot be understood on the basis of a sole simple principle. Nevertheless, dense packing is one of the important aspects of structure and glass-forming ability of multi-component metallic melts and will therefore be analyzed in this contribution.

CHAPTER 2
METHODS AND MODELS

This chapter summarizes the main methods used in the present work. The first Section 2.1 describes the algorithm of the hard-sphere packing which was used for the simulation of amorphous structures with predefined concentrations and radii ratios of spheres. The following Section 2.2 refers to the Voronoi tessellation technique which is also called Laguerre or weighted Voronoi technique in the general case of multi-component systems. Laguerre tessellation is the main method used in this work for the analysis of the simulated amorphous structures and some other calculations.

The high packing density of atoms in bulk metallic glasses suggests that packing densities affect the glass-forming ability. To address this idea, an algorithm was required that permits to determine atomic size distributions which give rise to particularly high packing density. The Nelder-Mead simplex method proved to be suitable for this purpose; it is described in Section 2.3.

The mixing enthalpy is one of the most important parameters in real alloys. Therefore, the Miedema's semi-empirical model for the calculation of the mixing enthalpy as well as some extrapolations and modifications of this model were investigated and compared with experimental results in Section 2.4.

2.1 Hard sphere packing algorithms

Since Bernal has published his model of liquid structures many attempts were made to prove these ideas using computing methods. As a result many different algorithms simulating liquids and amorphous materials were developed including the well known class of hard spheres packing algorithms.

The packing algorithms can be commonly divided into 2 main groups. The first one comprises the so-called sequential addition algorithms (also known as "cluster" model) and the second one is the class of collective rearrangement algorithms ("gas compression" model) [Bez02, Cla87].

2.1.1 Sequential addition algorithms

In general the main idea of the sequential addition algorithms is following. At the first step the initial configuration of spheres (a predefined arrangements of fixed spheres) is created in a container. In each following iteration step a new sphere is added to the system. This new sphere then moves in a certain direction (usually downwards simulating the effect of gravitational forces) until it is in contact with one of the already existing spheres. After that the sphere “searches” for a stable position which commonly consists of 3 contact points with other spheres. If after a certain time a stable configuration is not found the considered sphere is removed and the iteration is repeated with another new sphere. The procedure of filling continues till all spheres are packed, or till the container is filled up, and no more spheres can be placed inside the container.

Depending on the position search method such an algorithm yields different densities. So in the case of systematic choice of the lowest site the densities are around 0.606, compared with roughly 0.582 for random selection [Jod81]. These values are compatible to those for experimental loose random packings [Tor68, Got78, Jod79, Vis72]. Analyses of packings suggest that all “gravitational” packings are anisotropic. This problem can be partially solved and final structures become more homogenous if a random initial configuration is used [Jod81].

Another modification of this algorithm consists in the sequential placement of spheres around a central one or around a predefined small seed of fixed spheres. This method represents central gravitational forces. But such algorithms produce in general also inhomogeneous packings [Ada72, Ben72]. For example the density of such clusters decreases with increasing distance from the central sphere [Ben72].

The gravitational forces in sequential addition algorithms lead to an anisotropy in the direction they act since this direction plays a particular role different to that of any

other directions. In addition, the densities of such clusters are too low comparing to experimental values, if an additional densification procedure is not applied.

There are many different modifications of sequential addition algorithms, but all of them have the same problems. Boudreaux and Gregor found significant differences in the structure as a function of position and direction in their clusters; this clearly shows that this method produces packings that are not isotropic or homogeneous on any scale up to the size of the model [Bou77]. Another problem is that different sequential addition algorithms produce different structures for the same systems.

The problems of sequential addition algorithms to achieve homogeneous, dense random packing led Matheson [Mat74] to the conclusion that shaken stacks of ball-bearings are not true random packings of single spheres but are random packings composed largely of small ordered groups of spheres. It does seem clear, however, that a stepwise, non-cooperative addition of single spheres cannot simulate dense random packing.

Considering all problems of sequential addition algorithm Jodrey and Tory tried various algorithms using cooperative schemes. The one described in Ref. [Jod81] was ultimately successful.

2.1.2 Collective rearrangement algorithms

The collective rearrangement algorithms reflect a deterministic transition from a random distribution of points to a dense packing of hard spheres [Cla87] and consist in general of several steps. At the beginning a number of points are set at random within a container. After that points get radii according to the chosen size distribution and the resulting spheres are moved in order to eliminate or to reduce the overlaps. Then the spheres get new larger radii. This procedure of radii increasing and overlap reduction/elimination is repeated until any further increase in radii or any displacement of the spheres creates overlaps that cannot be eliminated.

An efficient realization of this algorithm was developed by Jodrey and Tory [Jod81]. In 1981 they proposed a new algorithm that simulates a homogeneous, dense random packing of hard spheres. The simulation embodied three fundamental ideas: 1 -

the use of periodic boundary conditions, 2 - the spreading apart of overlapping spheres via a relaxation method, 3 - the use of a form of vibration.

Applying of periodic boundary conditions indeed makes all spheres statistically equivalent and therefore eliminates wall effects. Since all spheres are statistically equivalent, anomalous effects can arise only from the interaction of a sphere with itself. But such interactions are absent in the case of sufficiently large ensembles.

The second fundamental idea is the technique of sphere moving apart along the line of centers until they are just touching. But this method generates new overlaps as old ones are eliminated. Thus, only the largest overlap of the sphere is eliminated at each step. For sufficiently dilute initial dispersions, this process converges to an overlap-free packing.

To avoid the problem with overlap elimination Jodrey and Tory used expanding and contracting of the sphere radii, that is similar to the vibrations, known to destroy unstable and metastable arrangements in experimental packings.

The algorithm of Jodrey and Tory was one of the first receiving an isotropic, homogeneous, random, overlap-free packing with a density of 0.6366. The radial distribution function showed splitting of the first peak into 2 maxima and was very similar to that obtained experimentally for liquids and amorphous materials.

The next modification of the algorithm was published four years later [Jod85]. In the new version the points become a centre of two (inner and outer) spheres. Earlier simulations, which gave lower final densities, did not have this feature. The inner diameter, d_i^{in}, reflects the true density and is set after each iteration step to the minimum center-to-center distance. The outer diameter, d_i^{out}, serves for the sphere moving procedure. The worst overlap of outer spheres is eliminated by moving both spheres by an equal distance along the line joining their centers until these centers are separated by the outer diameter. A simple two-dimensional example of 4 circles is shown in Figure 2.1. During the movement procedure new overlaps may appear and the old overlaps may change or vanish. To minimize this effect no movement takes place if the overlap to which it corresponds would be changed by the elimination of a greater overlap.

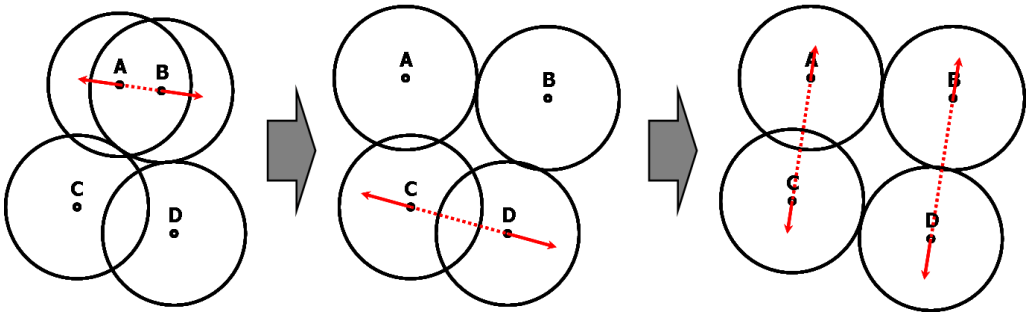

Figure 2.1: Example of the overlap elimination procedure in a four-circle system.

The outer diameter, d_i^{out}, is set initially to the value which yields a nominal density, $\eta_{nominal} = \eta(d_i^{out})$, of 1 since this value of the outer diameter must correspond to a density much greater than any attainable true value. During the algorithm the overlaps of outer spheres are eliminated and the outer diameters slowly shrink. In such a way inner and outer diameters approach each other and the eventual coincidence of true, $\eta(d_i^{in})$, and nominal, $\eta(d_i^{out})$, densities terminates the procedure.

The method appears crude in that each step removes the worst overlap without regard for the consequences. The reality is more subtle. Large shifts in positions are needed to fill big holes. The true density, $\eta(d_i^{in})$, fluctuates up and down as the inner diameter, d_i^{in}, changes. The relaxation method used here should be much more efficient than the compression of a hard-sphere gas. Overlaps are removed directly by spreading spheres apart and indirectly by shrinking the outer diameter, d_i^{out}. Although the latter process is indispensable, it has the undesirable effect of producing gaps between near neighbors. Thus, the rate of contraction is slowed as the nominal, $\eta(d_i^{out})$, and true, $\eta(d_i^{in})$, densities approach each other [Jod85].

It is clear that the end structure has only two contacting spheres and all other spheres are nearly touching. A comparison of this method with the previous one [Jod81] has shown that more spheres are very close together in the previous packing even though density was considerable less, thus it seems likely that the current packing has fewer and/or smaller holes.

This method made it possible to achieve the packing fractions between 0.642 and 0.649, which are consistent with Berryman's extrapolation from the radial distribution function for hard spheres [Ber83], though they are higher than experimental or previously simulated values.

Two years later Clark and Wiley [Cla87] presented a new algorithm for the construction of a dense random packing of a binary mixture of hard spheres. Since all previous algorithms considered packing of only equal spheres this algorithm was unique. Retaining the main ideas of Jodrey and Tory the new algorithm has also some new features.

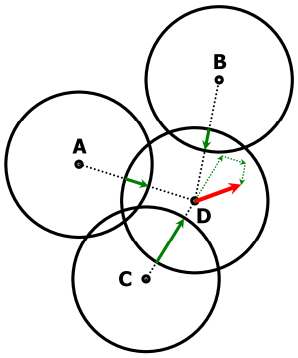

Figure 2.2: Example of the sphere moving procedure. The central sphere moves along the vector sum of the overlaps if the new maximum overlap is less than the maximum overlap among all the spheres.

The common new feature of this algorithm consisted in a new sphere movement procedure. Comparing to all previous algorithms, this one moves a sphere not along the line connecting centres of overlapping spheres, but along the vector sum of the overlaps (see Figure 2.2). In order to counteract creation or increasing of overlaps a move is accepted as long as it does not create any overlap as large as the maximum overlap among all the spheres. Thus, the maximum overlap always decreases or stays the same. If the move is not accepted, the program tries to shift this sphere in the same direction but in a shorter distance. In the case of few unsuccessful attempts the sphere will get a small random displacement. Again, the move is accepted or rejected depending on

whether the maximum overlap is less or greater than the maximum overlap among all the spheres. Each sphere in the packing is moved sequentially in this way [Cla87].

Another feature is the use of tolerance parameters, Δ_{tol1}, and, Δ_{tol2}, which define the maximum allowed overlap in the procedure of sphere increasing. Since spheres are moved proportional to the magnitude of the overlaps increasing the size of the allowed overlaps, Δ_{tol1}, speeds up the program. This feature also reduces the tendency for spheres to become locked up. The procedure of sphere moving and radii increasing is repeated until the maximum overlap does not drop below Δ_{tol1} within some specified number of steps. Then the radii are decreased slowly (each time moving the spheres to reduce overlaps) until the maximum overlap drops below some smaller tolerance, Δ_{tol2}. At this step the radii are increased and the whole procedure is repeated until the packing density approaches a constant at the end of each cycle. The following decreasing of tolerance parameters leads to further refinement of the packing.

At the steps of radii increasing all spheres also get a small random displacement without taking into account if overlaps are increasing or not. This procedure simulates a vibration and greatly improves the rate of convergence of the program.

The packing fractions Clark and Wiley obtained for simple liquids range from 0.637 to 0.645 which are in excellent agreement with the experimental results of Finney and Scott, and the computer results of Jodrey and Tory.

Bargieł and Mościński [Bar91] collected all main ideas und features of previous programs and made a new C-language program for the irregular close packing of equal hard spheres in a cubic box with periodic boundary conditions. This algorithm became the best known and useful collective rearrangement algorithm and was many times improved and generalized. The algorithm used in this work is also a modification of the force-based algorithm made by the group of Stoyan [Bez02].

At the beginning a set of points with independent centres, $\vec{r}_i$, and diameters, d_i, is randomly distributed in a container of parallelepipedal form. The distribution of diameters occurs according to an initially pre-defined size distribution. The initialization of the system is followed by the cycles of radii determination and the overlap removing procedure. Similar to the algorithm of Jodrey and Tory [Jod85] for each sphere in the

system two distinct diameters are assigned: the inner diameter $d_i^{in} = d_i d^{in}$ and the outer diameter $d_i^{out} = d_i d^{out}$. The value of the factor d^{in} is chosen so that only two spheres are in contact: $d^{in} = \min_{i,j}\left[2\left\| \vec{r}_i - \vec{r}_j \right\| /(d_i + d_j)\right]$, and there are no overlaps in the system. Thereby, the start density of the structure, $\eta(d_i^{in})$, is very small. The outer diameter factor, d^{out}, is initially calculated from the equation:

$$d^{out} = \sqrt[3]{\frac{6\eta_{nominal}}{\pi \sum_{i=1}^{N} d_i^3}}, \tag{2.1}$$

where $\eta_{nominal}$ is the nominal density, and is set initially to the value much higher than any attainable density, similar to Ref. [Jod85]. In each step the overlaps between the spheres are reduced through pushing apart overlapping spheres and using gradual shrinking of the outer diameters of the spheres by reducing of the factor d^{out}.

The outer diameter factor is reduced by the shrinking operation according to the equations

$$d^{out} = d^{out} - \left(\frac{1}{2}\right)^{\delta} d_{st}^{out} /(2\tau), \tag{2.2}$$

$$\delta = \mathrm{int}\left\{-\log_{10}\left[\frac{\pi}{6}\sum_{i=1}^{N}\left[(d_i^{out})^3 - (d_i^{in})^3\right]\right]\right\}, \tag{2.3}$$

where d_{st}^{out} is the start value of d^{out} given by Equation (2.1) and τ is the contraction rate of the outer diameter. The value of τ controls the execution time of the algorithm and has a large influence on the final packing density achieved. Increasing the value of τ increases the number of iteration steps (and obviously the execution time), but usually gives a higher packing density.

The overlap reducing leads to an increase of the factor d^{in} during the pushing, whereas shrinking reduces d^{out}. In the case of coincidence of both factors, the

simulation is stopped. Then a system of non-intersecting spheres is obtained with diameters proportional to the initial values d_i. Subsequently, the nominal density of the structure is gradually increasing by elimination of overlaps by means of the force-based algorithm at periodic boundary conditions and the increment of the radii. Cycles of overlap elimination and increase of radii are repeated till either a target density is achieved or the number of cycles reaches a preset maximum value.

This algorithm belongs to the group of force-based algorithms. It means, that the displacement of the sphere is proportional to a vector sum of "repulsion" forces, F_i, effecting the sphere i:

$$F_i = \rho \sum_{j=1}^{N} p_{ij} \frac{\vec{r}_j - \vec{r}_i}{\left\| \vec{r}_j - \vec{r}_i \right\|} \delta_{ij}, \tag{2.4}$$

where p_{ij}, is a "potential" function, ρ is a scaling factor and δ_{ij} is equal to "1" if spheres are overlapping and equal to "0" otherwise.

The choice of a suitable "potential" function is a nontrivial task but crucial to the efficiency of the algorithm. Mościński derived a new potential function, which is also suitable for systems with large differences in diameters [Bez02]. This potential ensures some positional stability of large spheres and is defined as

$$p_{ij} = d_i^{out} d_j^{out} \left(\frac{\left\| \vec{r}_j - \vec{r}_i \right\|^2}{\frac{1}{4}(d_i^{out} + d_j^{out})^2} - 1 \right), \tag{2.5}$$

In order to speed up the program the container is divided into cubic cells and the search for overlapping atoms proceeds only in the cell of the considered sphere and in the neighboring cells. Because of this feature the time used for overlap searching with respect to a given sphere is approximately constant and do not depend on number of spheres.

The algorithm used in this work for the simulation of random dense packing of spheres in three-dimensional space rests upon the force biased algorithm which has been developed and improved over the course of three decades [Jod81, Jod85, Cla87, Bez02]. It uses the Bernal's model for simple liquids and metallic glasses generalized for polydisperse hard sphere systems and simulates the structure of multi-component metallic melts.

Recent applications to crystallization phenomena in hard sphere systems [Her05, Loc06], to the problem of icosahedral local order in non-crystalline systems [Her07b], and to multi-component hard sphere systems [Her07a] have demonstrated the effective power of the algorithm.

For the present simulations the condensation process was always conducted up to the greatest possible density. This means the process was terminated when, after the completion of several cycles, no further increase in the density was observed. It is necessary to note that during a specific condensation process the number and the distribution of the (relative) size of the spheres is kept constant.

2.2 Voronoi- and Laguerre-tessellations

It is known and clear, that all properties of metallic materials depend on their internal atomic structure, so it is important to analyze their structure precisely.

A simple but very powerful way to get the complete information about the atomic structure independent if this structure is crystalline or not is the Voronoi tessellation technique [Vor08]. (A Voronoi cell is also called Dirichlet region [Dir50] and, in the case of regular atom structure, Wigner-Seitz cell [Wig33].) The main idea of this method is to form a unique polytope (Voronoi polyhedron) around each atom or point in the space so, that this polytope encloses all parts of space closer to a given atom (point) than to any other atoms (points).

Due to the simplicity and powerfulness this method has found wide fields of applications from material science (structure analysis) and biology (precise calculations of the protein volume [Goe97, Sad03]) to the modern programming (creation of the 3-dimensional (3D) objects for computer graphics [http://www.groups.csail.mit.edu])

etc. This tool is also widely and currently used to study random sphere packings, granular materials, foams, froths and glasses**.**

There are in principle two different types of algorithms for the calculation of Voronoi polyhedra: "exact" and "statistical" algorithms [Moo93]. In the fist type of algorithms the geometrical features are explicitly computed; and in the second type a number of points is set in the box and it is determined to which atom each point belongs [And88]. But the only information statistical algorithms can calculate is to approximate areas and volumes of polyhedra. In contrast to statistical methods exact algorithms yield much more information (symmetry of the first coordination sphere, coordination number, exact atomic volume etc.) and describe completely the neighborhood of the associated central atom.

If we construct planes perpendicularly bisecting vectors between a selected atom and its neighbors, and take the smallest closed polyhedron thus obtained (ensuring no planes intersect the polyhedron), we will have selected a volume in which all points within the polyhedron are closer to the central point than to any other. This polyhedron is the Voronoi polyhedron associated with the central atom.

However, as the atoms are not of the same size, bisection cannot depict the exact plane to represent the polyhedron. As a result volume and the number of faces on the polyhedron contain an error which is growing with the radii ratio increasing. The result shows over 50% differences in the number of faces and the atomic volume for the binary metallic glasses [Par07a].

Therefore, several researchers propose another method to construct polytopes in a way which takes into account the atomic size. This can be viewed as a weighted Voronoi decomposition in which the faces remain planar, but are no longer equidistant to the two atoms. The separating plane is closer to the smaller atom. Richards suggested the ratio of the distance between the atoms and the plane to equal the ratio of the atomic radii [Ric74]. This method is a kind of weighted Voronoi tessellation technique (also called Laguerre tessellation).

One of the important features is the designation of Voronoi polyhedra. Voronoi polyhedra are indexed through the number of faces with 3, 4, 5 … etc. edges. Thus for

example polyhedron with the index (0, 2, 6, 1) consists of no triangular, two tetragonal, six pentagonal and one hexagonal faces.

2.2.1 Voronoi/Laguerre tessellation algorithm

The algorithm used in this work belongs to the class of "exact" algorithms and combines both Laguerre and Voronoi techniques. The program implementing this algorithm was written by the author and can be applied to the simulated atomic structures and to the random distribution of points as well. The whole procedure can be divided into following common steps:

1. Determination of neighboring atoms;
2. Construction of planes;
3. Calculation of planes' intersection points (Triple points);
4. Removal of the triple points lying out of the target polyhedron;
5. Construction of polyhedron (triangulation);
6. Unification of close points (optional);
7. Calculation of necessary structural parameters.

All atoms are present in the algorithm by their positions $\vec{r}_i = \{x_i, y_i, z_i\}$, diameters d_i (or relative characteristic sizes) and numbers $i = 1...N$.

The first step for the two-dimensional case of binary solution is presented in the Figure 2.3. In this step the neighboring atoms, S_i ($\vec{r}_{S_i} = \{x_{S_i}, y_{S_i}, z_{S_i}\}$, d_{S_i}), to the selected sphere, O ($\vec{r}_O = \{x_O, y_O, z_O\}$, d_O), are found. The search procedure selects all atoms in the system whose centres lying closer than $R = 0.5(d_O + d_i) + kd_{\max}$ to the centre of the selected sphere, O. Where $d_{\max} = \max_{i=1...N} d_i$ corresponds the diameter of the biggest sphere in the system, d_i is diameter of the atom currently being investigated for belonging to the nearest neighbor and k is an empirical parameter. Parameter k depends on several properties of the system: atomic density, radii ratio and

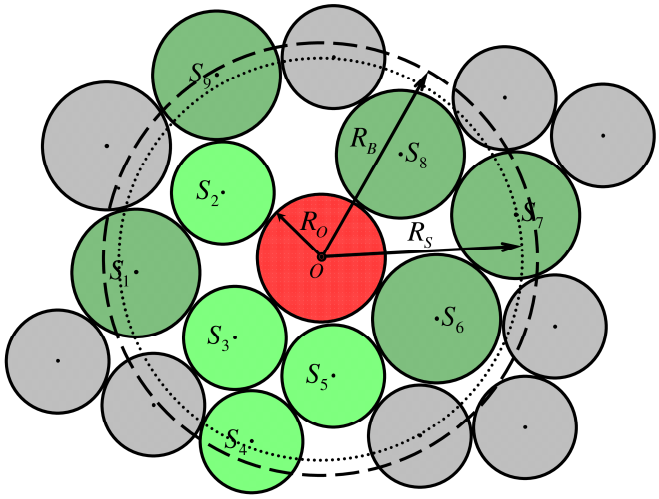

Figure 2.3: A 2-dimensional example of "searching" for neighboring atoms.

concentrations. For densities above 0.6 and radii ratios not exceeding 2.0 in the whole concentration range parameter k was found to lie between 0.60 and 0.65. Thus the *a fortiori* sufficient value of 0.7 was taken for all calculations in this work. This approach leads to the existence of an individual searching sphere for each type of atoms, as it shown in Figure 2.3 (R_S, R_B - radii of the "search" spheres for small and big atoms, respectively), and reduces the total number of neighbors found without ejection of important spheres, what significantly decreases time of the program execution. Periodic boundary conditions are applied during the searching for neighbors and the following operations.

After all neighbors were found the vectors connecting the selected sphere, O, and the surrounding spheres, S_i, are build in the following way: $\vec{n}_{S_i} = \overrightarrow{OS_i} = \{x_{S_i} - x_O, y_{S_i} - y_O, z_{S_i} - z_o\} = \{x_{n_i}, y_{n_i}, z_{n_i}\}$ (see Figure 2.4), and the contact points of spheres, $\vec{m}_i$, are set according to one of the following equations:

$$\vec{m}_i = \frac{1}{2}(\vec{r}_{S_i} + \vec{r}_O) = \{x_{m_i}, y_{m_i}, z_{m_i}\}, \tag{2.6}$$

$$\vec{m}_i = \frac{\vec{r}_{S_i} d_O + \vec{r}_O d_{S_i}}{d_i + d_{S_i}} = \{x_{m_i}, y_{m_i}, z_{m_i}\}. \tag{2.7}$$

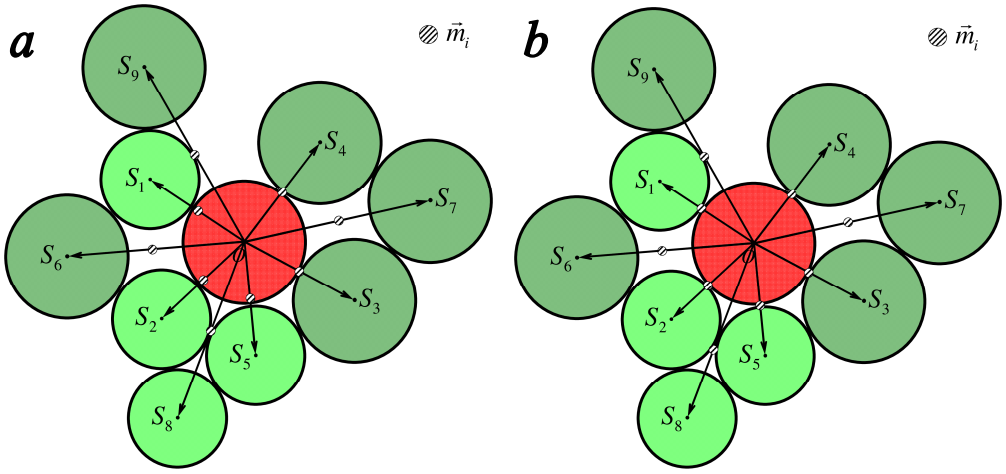

Figure 2.4: Determination of the contact points of spheres in (a) Voronoi and (b) Laguerre tessellations.

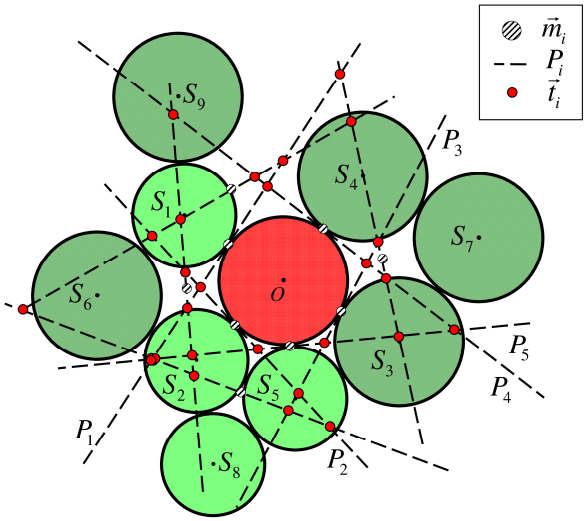

Figure 2.5: Construction of planes and planes' intersection points (triple points).

The first formula (2.6) corresponds to the case of original Voronoi tessellation, and the second one (2.7) describes the Laguerre (weighted Voronoi) tessellation technique. After the contact points determination is complete, the neighbors are sorted according to the increasing of the distance between the central atom and the corresponding contact points in order to optimize further computation time.

The next step in the algorithm is the building of the planes, P_i, (shown in Figure 2.5) passing through the contact point $\vec{m}_i$ perpendicular to the vectors $\vec{n}_{S_i}$ for all neighbors. Since $\vec{n}_{S_i}$ represent in this case normal vectors, the planes can be determined as:

$$P_i: \begin{cases} A_i x + B_i y + C_i z = D_i \\ A_i = x_{n_i}; B_i = y_{n_i}; C_i = y_{n_i} \\ D_i = A_{S_i} x_{m_i} + B_{S_i} y_{m_i} + C_{S_i} z_{m_i} \end{cases}. \tag{2.8}$$

The next step consists in the calculation of the "triple points", $\vec{t}_i = \{x_{t_i}, y_{t_i}, z_{t_i}\}$. Each triple point corresponds to the intersection point of three different planes (P_i, P_j and P_k) and can be found as a solution of the three combined equations:

$$\begin{cases} A_i x + B_i y + C_i z = D_i \\ A_j x + B_j y + C_j z = D_j \\ A_k x + B_k y + C_k z = D_k \end{cases}, \tag{2.9}$$

where $i, j, k = 1...N_S$, N_S - number of neighbors and $i \neq j, j \neq k, i \neq k$. The solution of the equations (2.9) can be found as follows:

$$\Delta = \begin{vmatrix} A_i & B_i & C_i \\ A_j & B_j & C_j \\ A_k & B_k & C_k \end{vmatrix}, \Delta_x = \begin{vmatrix} D_i & B_i & C_i \\ D_j & B_j & C_j \\ D_k & B_k & C_k \end{vmatrix}, \Delta_y = \begin{vmatrix} A_i & D_i & C_i \\ A_j & D_j & C_j \\ A_k & D_k & C_k \end{vmatrix}, \Delta_z = \begin{vmatrix} A_i & B_i & D_i \\ A_j & B_j & D_j \\ A_k & B_k & D_k \end{vmatrix}, \tag{2.10}$$

$$x_{t_i} = \frac{\Delta_x}{\Delta}, \; y_{t_i} = \frac{\Delta_y}{\Delta}, \; z_{t_i} = \frac{\Delta_z}{\Delta}$$

If the determinant of the system, Δ, is not equal to zero, the chosen three planes have one intersection point. In the other case $\Delta = 0$ some of planes are parallel and do

not have any contact points. Thus the last case is not relevant for the Voronoi/Laguerre tessellation and is not further considered.

To select all point building the polyhedron and to refuse excess points the following property of plane's equation is used. Substituting coordinates of two points lying on the same side of the plane into a plane equation one would get either positive or negative values, but in any case these values would be like-sign. In the opposite case when points lying on the different sides of the plane, these values would have opposite sings.

Applying this feature to all triple points with all planes and using as the first point the central atom O we can select all points lying outside the polyhedron according to the equation:

$$\begin{cases} A_i x_{t_i} + B_i y_{t_i} + C_i z_{t_i} > D_i \text{ - Wrong Side} \\ A_i x_{t_i} + B_i y_{t_i} + C_i z_{t_i} < D_i \text{ - Side of } O \text{ Point} \end{cases}, \; t_i \notin P_i, \qquad (2.11)$$

An example for this procedure is shown in Figure 2.6. In this case applying the only five first planes is enough to delete all unnecessary triple points and accordingly to refuse all atoms, which are not involved into the polyhedron of the atom O.

The procedure of triple points testing is implemented to each point immediately after this point is determined. This reduces significantly the total used computer time and memory, since no useless information is treated in the sequel.

Figure 2.7 presents resultant Voronoi and Laguerre polygons for the two-dimensional case. It can be seen from the comparison of Figures 2.7 (a) and 2.7 (b) that the main difference between these two methods consists in the volume of the polyhedra built. The Voronoi tessellation technique decreases the volume of big atoms and overestimates the volume of small atoms through intersecting big atoms with the planes. The areas of faces and the number of edges might be also miscalculated. The Laguerre tessellation does not have this problem and can be used for precise volume and area calculations.

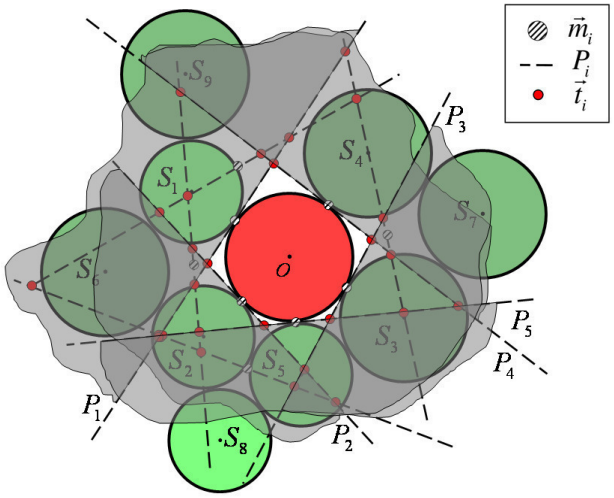

Figure 2.6: Ejection of unsuitable triple points and neighbors.

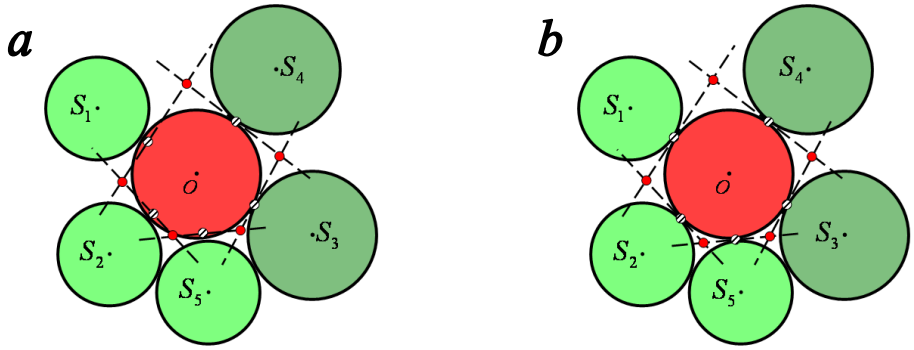

Figure 2.7: Two-dimensional examples of (a) Voronoi and (b) Laguerre polyhedra/polygons.

Triangulation technique

At this step all vertices of the polyhedron are known, but it is unclear in which order they have to be connected to each other to form the right convex polyhedron we are looking for. So for example if we connect points $\vec{t}_1$, $\vec{t}_2$, $\vec{t}_3$, $\vec{t}_4$, $\vec{t}_5$ in the Figure 2.8 (a) in a numerical sequence we will get a wrong polygon and, accordingly, the wrong polyhedron. Thus, the vertex sort procedure is applied for each face.

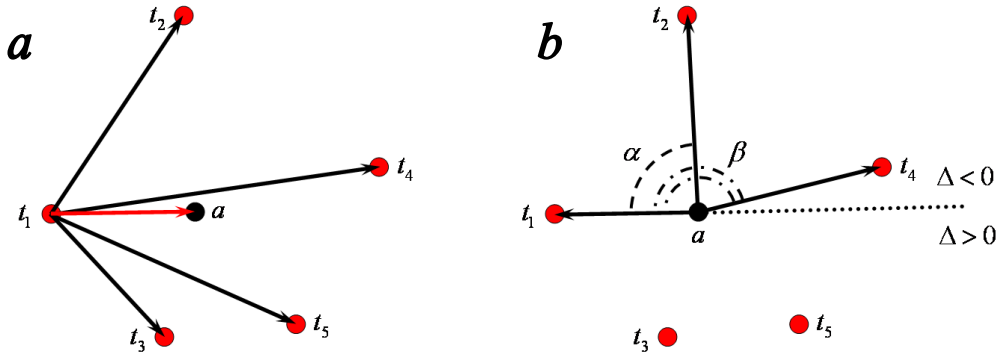

Figure 2.8: Triangulation of a polygon.

The vertex sort procedure begins with the building of the geometric center, $\vec{a}_i$, of a polygon (face of the polyhedron) according to the equation:

$$\vec{a}_i = \vec{t}_1 + \frac{1}{N_a + 1}\sum_{i=2}^{N_a}(\vec{t}_1 - \vec{t}_i), \tag{2.12}$$

where N_a is a number of vertices at the face (see Figure 2.8).

Next step is determination of the vectors $\vec{e}_i = \overrightarrow{t_i a_i}$ connecting geometric centres with triple points of the face.

Thereafter, the first point, t_1, with corresponding vector, $\vec{e}_1$, is taken and all vectors $\vec{e}_i$ building the left hand system with the first vector, $\vec{e}_1$, and plane's normal vectors are found using the equation:

$$\Delta = \begin{vmatrix} x_{e_i} & y_{e_i} & z_{e_i} \\ x_{e_j} & y_{e_j} & z_{e_j} \\ x_{n_k} & y_{n_k} & z_{n_k} \end{vmatrix} < 0, \; i \neq j, \tag{2.13}$$

where $i, j = 1...N_a$, and k is a face number. Since the face of the polyhedron is necessarily convex and the geometric center lays inside the face there is at least one point on each side of the plane going though the middle point, $\vec{a}_i$. That means that for each vector $\vec{e}_i$ there is at least one point and corresponding vector $\vec{e}_j$ building the right hand system according to the Equation (2.13). Through all the points lying on the right

side the only one having the smallest angel with the first vector is taken and gets the next number in the chain. The angel comparison occurs through the searching for the biggest cosine of the angel between vectors according to the equation:

$$\cos(\vec{e_i} \wedge \vec{e_j}) = \frac{\vec{e_i}\vec{e_j}}{\left|\vec{e_i}\right|\left|\vec{e_j}\right|} = \frac{x_{e_i}x_{e_j} + y_{e_i}y_{e_j} + z_{e_i}z_{e_j}}{\sqrt{x_{e_i}^2 + y_{e_i}^2 + z_{e_i}^2}\sqrt{x_{e_j}^2 + y_{e_j}^2 + z_{e_j}^2}}. \qquad (2.14)$$

In the case shown on the Figure 2.8 the vectors lying on the right side relative to the t_1 are t_2 and t_4, the second point t_2 has the smallest angle. Thus the second place in the sequence will be given to the point t_2 and the whole procedure is repeated with the vector $\vec{t}_2$ taken as the first one. The procedure goes on until all triple points in the face are sorted, and it is repeated for all faces of the polyhedron.

Figure 2.9 presents the resulting polygon for the two-dimensional case and a 3D polyhedron.

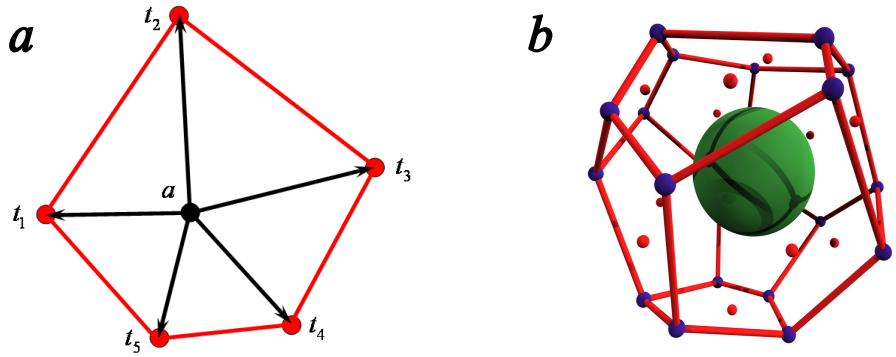

Figure 2.9: (a) Resulting polygon (face of the polyhedron) and (b) an example of a 3-dimensional polyhedron determined using the demonstrated method.

Procedure of the close vertex unification

At this step an optional operation of close triple points removing can be applied. This procedure consists in the unification of all triple points lying within the small

spherical angel with the cosine less than 0.01. This value was found to remove those faces with area less than approximately 1% of the total area of the polyhedron surfaces. In this way the degeneracy problem is minimized [She06] and the polyhedra become more physical by nature.

Figure 2.10 shows an example of a polyhedron calculated with standard technique and illustrates the effect of the close vertex unification procedure. The triple points unification moves off very small faces of the polyhedron and, accordingly, brings values of the coordination number and the form of the first coordination spheres into reasonable condition without appreciable change in relevant parameters like volume, surface area etc.

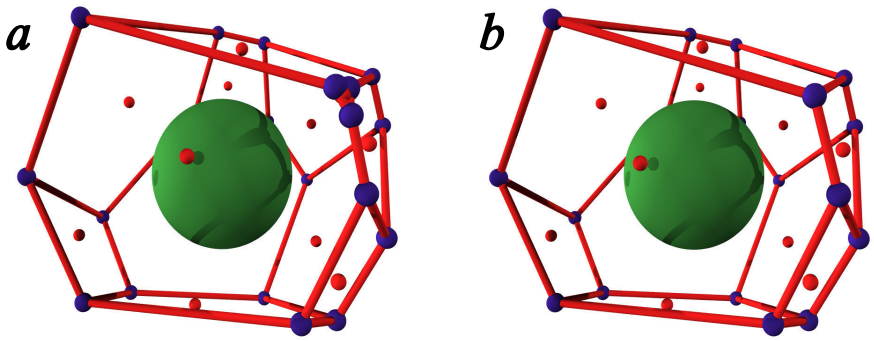

Figure 2.10: Comparison of two polyhedra calculated without (a) and with (b) applying of close vertex unification procedure.

Calculation of the area and volume of the polyhedron

After the polyhedron is built, all necessary data can be estimated. The calculation of the surface area and the volume of polyhedra is carried out according to the following equations:

$$S_{i,j} = \pm\frac{1}{2}\begin{vmatrix} x_{e_j} & y_{e_j} & z_{e_j} \\ x_{e_{j+1}} & y_{e_{j+1}} & z_{e_{j+1}} \end{vmatrix}, \qquad (2.15)$$

where $S_{i,j}$ is the area of a triangle spanned by vectors e_i and e_{i+1}. The whole area of the polyhedron can be estimated through the sum of all edges, N_e, and faces, N_s, of the polyhedron:

$$S_{Pol} = \sum_{i=1}^{N_S} \sum_{j=1}^{N_e - 1} S_{i,j} \,. \tag{2.16}$$

The volume of the pyramid built on vectors $\vec{n}_j$, e_i and e_{i+1} corresponds to the following equation:

$$V_{i,j} = \pm \frac{1}{6} \begin{vmatrix} x_{e_j} & y_{e_j} & z_{e_j} \\ x_{e_{j+1}} & y_{e_{j+1}} & z_{e_{j+1}} \\ x_{n_i} & y_{n_i} & z_{n_i} \end{vmatrix} . \tag{2.17}$$

The total volume of the polyhedron can be calculated similar to the face area as the sum of all pyramids the polyhedron is built of:

$$V_{Pol} = \sum_{i=1}^{N_S} \sum_{j=1}^{N_e - 1} V_{i,j} \,. \tag{2.18}$$

2.2.2 Comparison of Voronoi and Laguerre tessellations

As it was shown in the Figure 2.7 the Voronoi tessellation method works perfect for the monatomic systems. But in a case of the different sized atoms this algorithm causes intersections of atoms with faces of polyhedra and that leads to results that a polyhedron does not characterize the situation of the corresponding atom correctly. It is clear that these errors depend on the radii ratio, fractions of atoms and structure of the system.

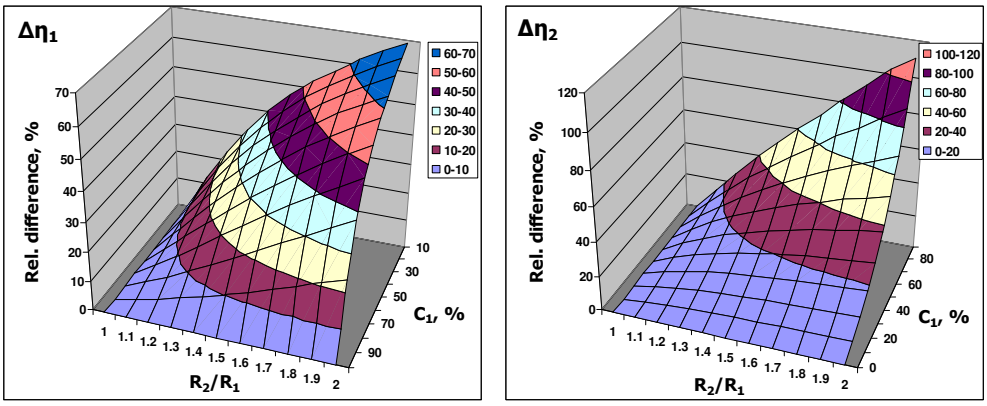

Figure 2.11: The relative difference between the partial densities calculated using Laguerre and Voronoi techniques for small, $\Delta\eta_1$, and big, $\Delta\eta_2$, spheres dependent on the radii ratio, R_2 / R_1, and concentration of small atoms, C_1.

Figure 2.11 shows the difference between the partial densities of small and big spheres calculated using Laguerre and Voronoi tessellations. As expected, the results for the monatomic systems do not depend on the chosen technique and the difference is zero. Increasing radii ratio causes significant changes of the partial densities: the difference of the partial densities of the small spheres grows up and reaches $\Delta\eta_1 = (\eta_{1,\,Laguerre} - \eta_{1,\,Voronoi}) / \eta_{1,\,Laguerre} \approx 70\%$ at the point $(R_2 / R_1, C_1)$ = (2.0, 10%). The big spheres show an opposite behavior: their polyhedra volumes become smaller causing the growth of the partial density. The difference between partial densities of Laguerre and Voronoi methods for big spheres, $\Delta\eta_2$, reaches 60% by the radii ratio of 1.5 and about 110% at the point $(R_2 / R_1, C_1)$ = (2.0, 90%), which is tremendous.

Figure 2.12 shows the relative difference between the coordination numbers estimated using Laguerre and Voronoi tessellations for small, ΔCN_1, and big, ΔCN_2, spheres. The differences of the coordination numbers do not exceed 10 % and 3 % for small and big spheres, respectively, in the shown range of concentrations and radii ratios. For the small spheres the absolute difference is negative or zero in all points, thus, the coordination number determined using Voronoi tessellation is lower than the Laguerre values. In the case of the big spheres the absolute difference becomes a more complicated form: it is negative in the area of the maximum at 40% of small atoms and

positive at the second maximum ($C_1 = 90\%$). The dividing line lays at about 70 % of small atoms (local minima between two maxima).

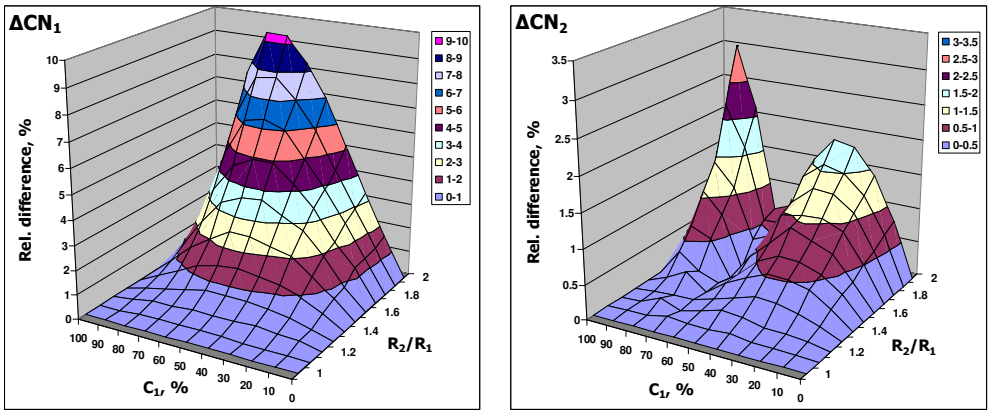

Figure 2.12: Relative differences between the total coordination numbers calculated using Voronoi and Laguerre technique for small, ΔCN_1, and big, ΔCN_2, atoms dependent on the radii ratio, R_2 / R_1, and concentration of small atoms, C_1.

As expected, the aforesaid results show considerable differences between the results obtained by Voronoi and Laguerre tessellations. The inaccuracy of the coordination number calculations limits the applicability of the Voronoi technique to maximal radii ratios of about 1.5, where the difference in coordination numbers does not exceed 2.5%. On the contrary, the local density calculations have a very strong dependence on the radii ratio and the difference makes up to 10 % when the radii ratio steps over 1.1. Thus, the Voronoi technique is suitable for the mixtures of equal spheres; in all other cases the Laguerre tessellation is preferred.

2.2.3 "Error tetrahedra"

Besides all advantages, the Laguerre tessellation is not mathematically perfect because the volume in tiny tetrahedra near each polyhedron vertex is not allocated to any atom. Such unallocated space is called error tetrahedron (or ''vertex error'' [Ger95]) and is shown as a red region in Figure 2.13.

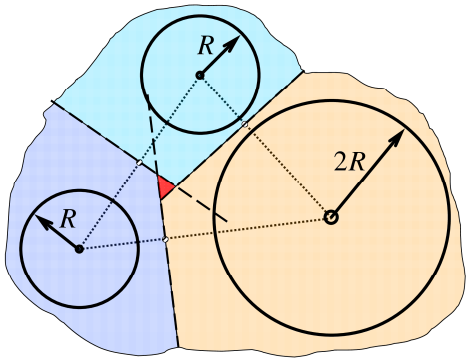

Figure 2.13: Example of the error tetrahedron (red area), which is not allocated by any atom in the case of different sized atoms.

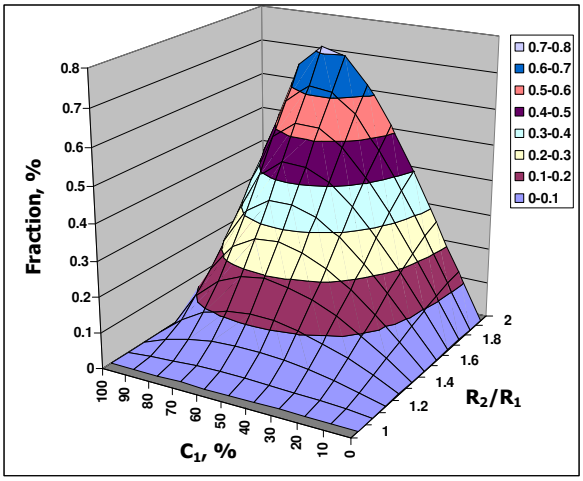

Figure 2.14: Total fraction of the "error tetrahedron" volume in the binary random dense hard-sphere mixtures depending on the radii ratio, R_2 / R_1, and concentration of small atoms, C_1.

It seams to be clear that the total volume of the error tetrahedra in the systems depends on radii ratio, composition, and structure. In the case of crystalline structure the error tetrahedron volume is absent, independent of whether the atoms have the same size or not. Density might also affect error tetrahedra. Richards and other researchers reported that the unoccupied volume lies normally below 1% [Par07a], what allows a

very precise analysis. At the moment there is no an alternative better way to study structural properties of amorphous mixtures than Laguerre tessellation.

Figure 2.14 presents the total error tetrahedron volume of dense hard-sphere binary mixtures depending on the radii ratio, R_2 / R_1, and concentration of small atoms, C_1. The fraction of unallocated volume has a monotone dependence on the radii ratio, R_2 / R_1, and, as expected, a zero value in monatomic systems ($C_1 = 0$, 100% or/and $R_2 / R_1 = 1.0$). The maximum fraction of about 0.8 % error tetrahedra is reached at the mixture ($R_2 / R_1, C_1$) = (2.0, 70%), which is close to the position of the maximal density in this system.

It should be noted that the effect of "error tetrahedra" is not a consequence of the "close vertex unification" described in Section 2.2.1. All results related to the "error tetrahedra" were calculated in this work without close vertex unification procedure.

2.3 Nelder-Mead - optimization method

It is known that amorphous materials have a high relative packing fraction. The difference in the densities between as-cast bulk amorphous glasses and the fully crystallized state is in the range of 0.30 % to 0.54% [Ino00], which is much smaller than the previously reported value range of about 2% [Che80] for ordinary (metal-metalloid) amorphous alloys with much higher critical cooling rate above 10^5 K/s. This demonstrates influence of the packing fraction on the glass-forming ability of bulk amorphous glasses and suggests that the density is an important characteristic of the amorphous state.

In the Section 2.1 it was explained how dense packings of hard spheres with fixed size distribution are simulated. But how can one find the composition of a mixture which corresponds to the maximum packing fraction in the predefined range of parameters?

Considering discrete size distributions of radii, e.g. N different species, then a specific system is characterized by the concentrations, $\{c_1, c_2, ..., c_N\}$, of the N species,

by the radii, $\{r_1, r_2, ..., r_N\}$, and by the corresponding maximum packing fraction, $\eta = \eta(x)$, which can be achieved within the non-crystalline state where (x) denotes the parameter set $\{c_1, c_2, ..., c_N, r_1, r_2, ..., r_N\}$. The problem considered here is to find parameter ranges (x) where the function η takes exceedingly high values. This problem is not trivial in the case of multicomponent systems ($N = 3,\ 4,\ 5, ...$) for at least two reasons:

(i) The number of adjustable parameters is large ($2N$) and the search for maximum values of η takes place in the $2N$-dimensional parameter space.

(ii) The calculation of one value of η for a given set of parameters takes computer time of the order of 1 to 30 min with an actual high-speed personal computer (for systems with 10.000 spheres and periodic boundary conditions).

Grid or raster methods are not suitable to solve the problem. Considering, for example, a system with 6 adjustable parameters and choosing 10 sampling points for each parameter to get a more or less good statistic, the required computing time would amount to about 200 years.

The random search method can give an impression of the character of the function η but it can not replace a systematic search. On the other hand, the simplex algorithm has been proven to work successfully and effectively in searching for extreme values of complicated functions. It is used here to determine parameter ranges where the density of systems with adjustable atomic size distribution takes local maximum values.

The Nelder-Mead method (also called “downhill simplex method”, “amoeba method” and/or “flexible polyhedron method”) is a commonly used nonlinear optimization algorithm. This method was developed by Nelder and Mead in 1965 [Nel65] and is based on an ingenious idea of Spendley [Spe62] introduced for tracking optimum operating conditions at a set of points forming a simplex in the factor-space. The main idea for the simplex evolution is to replace the worst vertex of the simplex by a better point with respect to other simplex points. This idea of Nelder and Mead is applicable for the optimization of functions of several variables.

The Nelder-Mead simplex algorithm is an enormously popular direct search method for multidimensional unconstrained minimization and has become one of the most widely used methods for nonlinear unconstrained optimization [Lag98]. Since the Nelder-Mead method does not use any derivative information of a function, this algorithm belongs to the general class of direct search methods and approximately finds an optimal value when the objective function varies smoothly.

At each step of the algorithm a nondegenerate polytope (simplex) consisting of (n + 1) vertices in the n-dimensional space adapts itself to the local landscape. It is happening through comparing function values at the vertices of the simplex followed by changing the form and direction of the simplex. Examples of simplexes include a line segment on a line, a triangle on a plane, a tetrahedron in 3-dimensional space and so forth.

This method contracts to the final minimum/maximum, it is shown to be effective and computationally compact [Nel65, Hey97] and consists in general of following steps:

1. Start simplex, S, definition:
   a) Assigning of simplex of knots, g_i $(i = 1...n+1)$,
   b) Calculation of function values at the knots, $F(g_i)$,
   c) Sorting of the knots by the function values $(F(g_i) \le F(g_{i+1})$ or $F(g_i) \ge F(g_{i+1}))$;
2. Reflection:
   a) Construction of the central point, g_M, of the n best knots,
   b) Construction of the reflection point, g_R,
   c) If $F(g_R) > F(g_1)$ then "Expansion",
   d) If $F(g_{n+1}) < F(g_R) < F(g_1)$, then "Contraction";
2. Expansion:
   a) Computation of the expanded point, g_E, in the same direction as g_R,
   b) If $F(g_E) > F(g_R)$ then $F(g_{n+1}) = (g_E)$, else $F(g_{n+1}) = (g_R)$,

c) Proceeding from the position 1.c.;

3. Contraction:
   a) Computation of the contraction point, g_C, between g_M and g_R,
   b) If $F(g_C) > F(g_{n+1})$ then $F(g_{n+1}) = (g_C)$,
   c) If $F(g_C) < F(g_{n+1})$ then "Shrinkage";
4. Shrinkage:
   a) All points are moved in the direction of the best point.

For example, a function $F(x_1, x_2, x_3, \ldots, x_n) \in P(\Re^n)$ of n independent variables should be optimized inside the permitted region $P(\Re^n)$ by means of the Nelder-Mead method. In this case $(n+1)$ points $g = \{x_1, x_2, x_3, \ldots, x_n\}$ are set in the $P(\Re^n)$ forming a simplex $S = \{g_1, g_2, g_3, \ldots, g_{n+1}\} \in P(\Re^n)$. The points g_i are named knots of a simplex. After the simplex is defined the values of the function F at the knot points of the simplex are calculated and sorted by the values of the function, so the knot with the greatest value of the function has the first number: $F(g_1) \geq F(g_2) \geq \ldots \geq F(g_{n+1})$. In case of search for a minimum of the function, the sorting would be inversed and the knot point with the lowest value would be placed at the first position: $F(g_1) \leq F(g_2) \leq \ldots \leq F(g_{n+1})$. At this step the initial simplex is constructed.

In the case of a two-dimensional parameter space the simplex represents a triangle $S = \{g_1, g_2, g_3\}$ as shown in Figure 2.15. After construction the initial simplex starts to move on a special algorithm. At the first stage the centre of gravity, g_M, of the n best knots is constructed, then the worst knot, g_{n+1}, is geometrically reflected through the centre of gravity and results in the point g_R. If the value of the function, F, at the point g_R is greater than at the best current knot, g_1, one more point, g_E, in the same direction is built. If the value of the function at g_E is better than at g_R the worst knot, g_{n+1}, will be replaced by a point g_E, thus the new simplex $S = \{g_1, g_2, g_E\}$ is formed. This procedure is called expansion. In the case $F(g_E) < F(g_R)$ the worst knot,

g_{n+1}, will be replaced by g_R. This case is called reflection. If the value of the function at the point g_R is lower than at the best unit of the simplex, g_1, the point g_I will be constructed and located on a straight line between g_{n+1} and g_R. If $F(g_I)$ is better than $F(g_{n+1})$ then the worst knot, g_{n+1}, is replaced by the point g_I. In the reverse case when $F(g_I)$ is lower than $F(g_{n+1})$, the simplex is reduced in such a way that all points of the simplex are moved in the direction of the best knot. So, in Figure 2.15, the points g_2 and g_3 are replaced by points g_2' and g_3'.

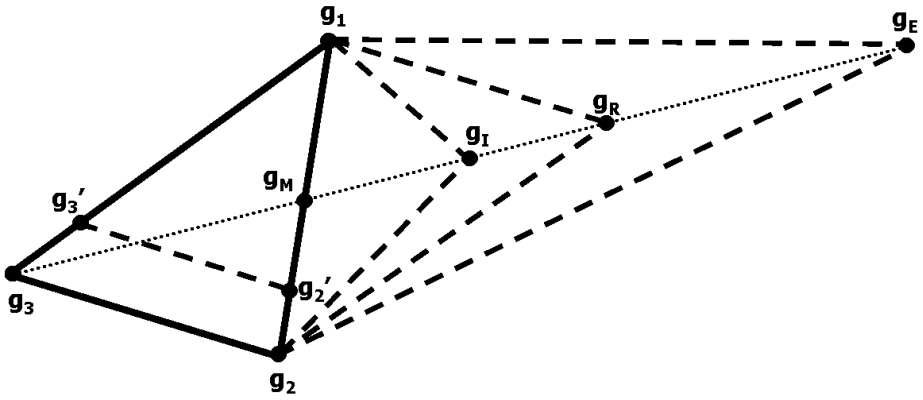

Figure 2.15: Example of the Nelder-Mead simplex algorithm of the two-dimensional case.

This method is highly opportunistic, in that the least possible information is used at each stage and no account is kept of past positions. No assumptions are made about the surface except that it is continuous and has a unique minimum in the area of the search [Nel65].

In order to restrict the tracking to the acceptability region, $P(\Re^n)$, so-called penalty-functions were applied. That means that if the simplex tries to put a new knot point in the region outside of $P(\Re^n)$ the value of the function which the knot will get for this point is worse than the worst known value in the system. So for searching of the maximum density this penalty density was taken to be zero.

More details about this algorithm and its convergence properties can be found in [Nel65, Lag98, Obe09].

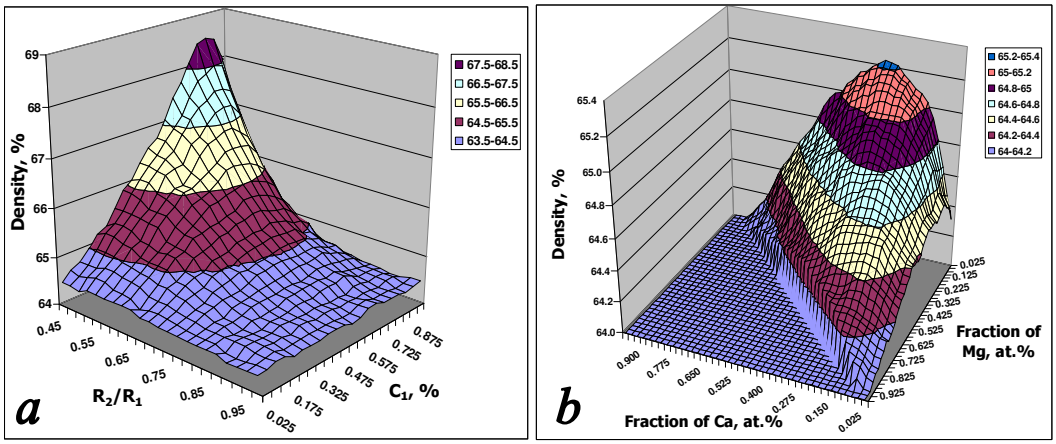

Figure 2.16: Surfaces yielded by the systematic search for the maximum density of: (a) binary system of the radii ratio range $R_2 / R_1 = 1.0 - 0.45$, depending on radii ratio, R_2 / R_1, and concentration of small atoms, C_1; (b) ternary CaMgCu system depending on atomic fractions of Ca and Mg.

For the verification of the algorithms a number of test calculations have been carried out. The size and concentration distributions of a binary system with a radii ratio range of $R_2 / R_1 = 1.0 - 0.45$ (see Figure 2.16 (a)) were optimized using the Nelder–Mead algorithm. The maximum packing fraction was obtained for $R_2 / R_1 = 0.451$ and $C_1 = 0.824$ which is in excellent agreement with the mixture $(R_2 / R_1,\ C_1) = (0.45,\ 82.5\%)$ obtained in [Her07a] for the same system by systematic screening. Another test was done referring to an experimental work on atomic packing density and its influence on the properties of Cu–Zr amorphous alloys. In Ref. [Par07b], steel balls having the size ratio of Cu and Zr atoms were mixed in the Cu concentration range from 30% to 80%. The maximum packing density was obtained for $Cu_{65}Zr_{35}$. The corresponding computer simulation using the methods described above resulted in $Cu_{66.4}Zr_{33.6}$, which is also a very good agreement with the result of the steel ball experiment [Par07b].

Another comparison of the systematic search and Nelder-Mead method was made on the ternary CaMgCu system. The search for the composition with the maximum density in this system was carried out for constant radii of elements taken from [Sen01] among two independent concentrations (C_{Ca} and C_{Mg}). The composition $Ca_{31.8}Mg_{5.6}Cu_{62.6}$ found by the Nelder-Mead method coincides very well with results of the systematic search for the same system which yields $Ca_{30}Mg_5Cu_{65}$. The resulting surface of the systematic search for CaMgCu system is shown in the Figure 2.16 (b).

2.4 Miedema's semi-empirical model

The thermodynamic properties of alloys are very important for the understanding of the relative stability of alloys and phases. There are several ways to obtain thermodynamic properties of alloys. One possibility is experimental investigation. However, it is impossible now for some alloys to perform experimental measurement due to not only technological difficulties but also expenses and time consumption. So, systematic prediction via theory is a significant and effective approach to obtain thermodynamic properties of alloys, especially for multi-component alloys.

The thermodynamic properties can be predicted from first principles calculations [Moh93, Rub95]. But there are great amounts of calculations to be performed for the prediction of the formation enthalpy of a binary alloy using the first principles, and this amount increases rapidly with increasing component number. Empirical methods cost less calculation capacity compared with the first principles, so the empirical methods are also important approaches.

2.4.1 The original model of Miedema for binary alloys

Miedema's semi-empirical model is a simple and powerful way to calculate the mixing enthalpy of alloys. This model uses only three quantities, attached to each element, that determine enthalpy changes upon alloying: molar volume,

electronegativity and the electron density at the boundary of the Wigner-Seitz cell. All parameters and constants used in the model are estimated and tabulated by Miedema and can be found elsewhere [Boe89, Bak98].

The semi-empirical model enables us to make fast predictions for values of several effects in alloys within its limitations. It is an important justification of the model that there are many examples where Miedema's approach "works". Particularly the results for systems involving at least one transition metal are satisfactory, and all known amorphous metals satisfy this condition [Bak98].

In Miedema's "semi-empirical" or "macroscopic-atom" model [Boe89] atoms are conceived as "blocks" of the element. These blocks represent Wigner-Seitz cells or, in general, they correspond to the Voronoi or Laguerre polyhedra. In this picture, when bringing dissimilar atoms into contact, energy effects occur at the interface, where the two polyhedra are in contact, and will correspondingly be proportional to the area of this interface. Thus, for dilute solution of atoms A in an excess of atoms B, this area is proportional to $V_A^{2/3}$, where V_A is the molar volume of A.

A second quantity that plays a role in the enthalpy change upon alloying is a sort of potential that is felt by the outer electrons of the atom. It resembles the electronegativity and is denoted by φ [Pau52]. The potential φ gives the energy $-e\varphi$ that is needed for bringing such an electron with negative charge e to infinity, so it has a positive sign and is expressed in Volt. This energy is proportional to $-(\varphi_A-\varphi_B)^2$, because an amount of electronic charge $\Delta Z \propto |-\varphi_A-\varphi_B|$ is transferred over this "potential" difference with a corresponding energy gain of $|\Delta Z * \Delta\varphi|$. The square $-(\varphi_A-\varphi_B)^2$ is also clear from the fact that the enthalpy effect is the same, irrespective whether $\varphi_A > \varphi_B$ or $\varphi_A < \varphi_B$. In both cases the same amount of electronic charge is transferred and the only difference is whether the electronic charge will be transferred from A to B or the inverse way. This energy contribution is called negative part of the enthalpy upon alloying $\Delta H^{inter}(\text{A in B, negative part})$, where "inter" stands for "interfacial". The actual values of the φ's, used in Miedema's model are slight

modifications of measured values, within experimental error, in order to obtain a set of parameters that adequately describe the alloying behavior.

A second term in the enthalpy is "the density at the boundary of the Wigner-Seitz cell" and is denoted by n_{ws}. This value is always positive and represents the positive term in the mixing enthalpy ΔH^{inter}(A in B, positive part). The origin of the positive term in the enthalpy lies in the fact that, when solving an A atom in a B host a discontinuity in n_{ws} is created, which is not allowed so that the discontinuity should be smoothed at the boundary by bringing electrons to higher energy levels, which explains the positive sign of this contribution. The enthalpy change is proportional to $(n_{wsA}^{1/3} - n_{wsB}^{1/3})^2$ and is, for a similar reason as outlined in the foregoing paragraph, a squared difference [Bak98].

The sum of positive and negative parts may be either positive or negative in sign, depending on the relative absolute values of both parts.

Miedema has found in a semi-empirical way the dependence between these three quantities and the chemical (interfacial) enthalpy for solving one mole of transition metal A in an excess of transition metal B

$$\Delta H^{chem}(\text{A in B}) = \frac{V_A^{2/3}}{(n_{ws}^{-1/3})_{average}} \left\{ -P(\Delta\varphi)^2 + Q(\Delta n_{ws}^{1/3})^2 + R \right\}, \qquad (2.19)$$

where P, Q and R are empirical constants for a given group of metals. P and Q are proportionality constants, and constant R is connected with the hybridization of d-type wave functions with p-type wave functions if transition metals and non-transition metals become nearest neighbors in an alloy. The term "chemical" refers to the effects due to electron transfer and smoothing of the electron density at the boundary of the Wigner-Seitz cell.

In the case of *random*, *dilute solution* of two elements having equal molar volumes (A in B with fractions c_A and c_B correspondingly) the chemical enthalpy effect upon the formation of this alloy is simply

$$\Delta H^{chem}(1 \text{ mole of A}) = c_B \Delta H^{chem}(\text{A in B}), \tag{2.20}$$

since the average contact of A atoms with B atoms is given by c_B.
Or the same per 1 mole of atoms ("A plus B"):

$$\Delta H^{chem}(1 \text{ mole of atoms}) = c_A c_B \Delta H^{chem}(\text{A in B}). \tag{2.21}$$

In the case of the different sized atoms the surface area is also different for atoms A and B. Therefore, Miedema introduces the concept of surface fraction or "surface concentration" as

$$c_A^S = \frac{c_A V_A^{2/3}}{c_A V_A^{2/3} + c_B V_B^{2/3}}, \tag{2.22}$$

$$c_A^S + c_B^S = 1. \tag{2.23}$$

And in this case one obtains

$$\Delta H^{chem}(1 \text{ mole of atoms}) = c_A c_B^S \Delta H^{chem}(\text{A in B}). \tag{2.24}$$

It is clear that in an ordered compound the surface contact between A atoms and B atoms is larger than in a completely disordered alloy. Miedema denoted the degree to which A atoms are in contact with B atoms by f_B^A. Comparison of the experimental and calculated enthalpies has shown, that f_B^A could be well described by $f_B^A = C_B^S \left[1 + \gamma (C_A^S C_B^S)^2\right]$, where $\gamma = 0$ for completely disordered alloys, $\gamma = 8$ for intermetallic compounds and $\gamma = 5$ for amorphous alloys [Wee87]. Therefore, the equation (2.24) can be generalized and rewriten in the form

$$\Delta H^{chem}(1 \text{ mole of atoms}) = c_A f_B^A \Delta H^{chem}(\text{A in B}). \tag{2.25}$$

The formation enthalpy of an alloy consists in the general case of 4 common parts depending on the type of the alloy

$$\Delta H^{form} = \Delta H^{chem} + \Delta H^{elastic} + \Delta H^{struct} + \Delta H^{topological}. \qquad (2.26)$$

The second term $\Delta H^{elastic}$ represents the so called size mismatch enthalpy. In solid solutions, where atoms of different sizes have to occupy equivalent lattice positions, an additional positive contribution to the alloying enthalpy arises due to lattice deformations necessary to accommodate atoms of different sizes. In order to estimate the mismatch enthalpy Miedema used continuum elastic theory of Eshelby and Friedel [Esh56] and received the following equation for the elastic part of the enthalpy upon alloying

$$\Delta H^{elastic}(\text{A in B}) = \frac{2K_A G_B (V_A - V_B)^2}{4G_B V_A + 3K_A V_B}, \qquad (2.27)$$

where K is the bulk modulus, G is the shear modulus and V is the molar volume. Elastic enthalpy is essential for solid solutions only, when solute atoms are randomly distributed in the lattice of the solvent. In contrast, in liquids and in solid ordered equilibrium phases this energy is almost non-existent.

The ΔH^{struct} contribution appears, according Miedema, in the solid solutions and reflects the preference for the transition metals in the 3d series to crystallize in one of the main crystallographic structures body-centered cubic (BCC), face-centered cubic (FCC) or hexagonal closely packed (HCP), depending on Z, the number of valence elections per atom. Miedema constructed, partly on the basis of band-structure calculations, partly on empirical findings the curves of Figure 2.17. This figure shows estimate values of the structural stabilities $E_\sigma(z)$ for BCC (solid line), FCC (dashed line) and HCP (dotted line) structures of metals with 3 to 10 valence electrons. It can be seen from this figure, that metals with $Z = 3,\ 4,\ 7-10$ prefer FCC or HCP structure and metals with $Z = 5,\ 6$ tend to crystallize into BCC structure.

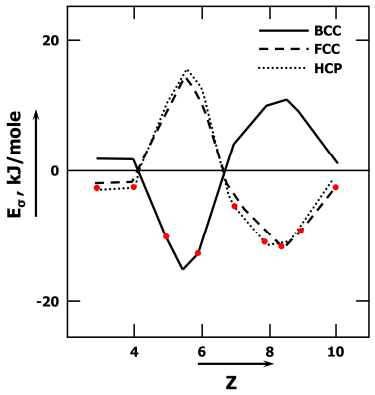

Figure 2.17: The structural stabilities $E_\sigma(z)$ of paramagnetic transition metals in the three main crystallographic structures HCP, FCC and BCC plotted versus the (average) number of valence electrons per atom [Boe89].

Since the crystal structure of a pure transition element depends on the number of valence electrons Z of the metal, the solution of one mole of A atoms in excess of B leads in fact to the transformation A to B from a structural point of view and the corresponding energy change can be written as $E_{\sigma,B} - E_{\sigma,A}$. But atoms A, which are virtually transformed into B have a different number of electrons than B itself. Therefore, the total number of electrons per atom in an alloys also differs from the value of pure B and the structural enthalpy will change by an amount $(Z_A - Z_B)\,{}^{\partial E_{\sigma,B}}\!/_{\partial Z}$. Thereby the total structural enthalpy change per mole of solvent atoms is determined by the equation:

$$\Delta H^{struct}(\text{A in B}) = (Z_A - Z_B)\frac{\partial E_{\sigma,B}}{\partial Z} + (E_{\sigma,B} - E_{\sigma,A})\,. \qquad (2.28)$$

The last term $\Delta H^{topological}$ in formula (2.26) is called topological enthalpy. For liquids the topological enthalpy, accounting for the difference between the crystalline state and the liquid state is the heat of fusion with the magnitude of about $R\bar{T}_m$, where $R = 8.31$ J/K is the gas constant and $\bar{T}_m$ is the average of the two melting temperatures.

In amorphous alloys a certain degree of relaxation towards the solid state exists, so that the enthalpy contribution will be lower. As an estimate,

$$\Delta H^{topological} = 3.5(c_A T_{m,A} + c_B T_{m,B})/1000 \text{ , kJ/mole} \tag{2.29}$$

has been proposed [Bak95].

According to this we can write the formation enthalpies of different types of alloys in the following forms

$$\begin{aligned}
&\Delta H^{form}(liquid) = \Delta H^{chem} \\
&\Delta H^{form}(solid\ \ solution) = \Delta H^{chem} + \Delta H^{elastic} + \Delta H^{struct} \\
&\Delta H^{form}(compound) = \Delta H^{chem} \\
&\Delta H^{form}(amorphous) = \Delta H^{chem} + \Delta H^{topological}
\end{aligned} \tag{2.30}$$

All previous equations can be applied for only one type of concentrated binary alloys: intermetallic compounds, and for random, dilute solutions, but not for concentrated solutions. Miedema solved this problem by just averaging according to the following equations

$$\Delta H^{chem} = c_A c_B \left[f_B^A \Delta H^{chem}(\text{A in B}) + f_A^B \Delta H^{chem}(\text{B in A}) \right] \tag{2.31}$$

$$\Delta H^{elastic} = c_A c_B \left[c_B \Delta H^{elastic}(\text{A in B}) + c_A \Delta H^{elastic}(\text{B in A}) \right] \tag{2.32}$$

$$\Delta H^{struct} = E_\sigma^{struct}(<z>) - E_\sigma^{ref}(<z>) \tag{2.33}$$

where $<z>$ is the average number of valence electrons, $E_\sigma^{struct}(<z>)$ is the value of E_σ for the most stable structure with $<z>$ electrons per atom according to the Figure 2.17, $E_\sigma^{ref}(<z>)$ is a linear extrapolation between the lattice stabilities of the two relevant metals in their equilibrium states.

2.4.2 Extensions of Miedema's model for ternary and multi-component alloys

The complexity of the determination of properties of metallic alloys rapidly increases with increasing component number. Thus, it is expensive and time consuming to measure the formation enthalpy experimentally, especially for ternary and N-component alloy systems for which $N > 3$. That is why the data for the ternary alloy systems are rather scarce, and only a few quaternary and quinary alloy systems have been measured. Therefore, there is a significant need for reliable theoretical calculations. Even though calculations are not precisely in agreement with the experimental data; researchers still accept and welcome such attempts because the theoretical calculations can give information which is helpful in the expensive and lengthy experimental measurements. That is way the extension of Miedema's model to multi-component systems is a very important task.

2.4.2.1 Miedema's approach for ternary alloys

As an approach for three- and more-component alloys Miedema suggests to neglect the interactions of third and higher order and calculate the formation enthalpy as a sum of corresponding binary alloys. Using this approach Miedema wrote the following equation for a ternary ABC alloy, which can be easily extended to the multi-component systems

$$\Delta H^{form}(ABC) = \Delta H^{form}(AB) + \Delta H^{form}(AC) + \Delta H^{form}(BC) \qquad (2.34)$$

Some researchers proposed other extensions of Miedema's semi-empirical macroscopic model to the multi-component alloys and also same modifications of it.

2.4.2.2 Method of geometrical extrapolation

The prediction of thermodynamic properties for ternary and multi-component systems using the extrapolations from binary constituent alloys is an attractive and powerful method. This method is simple and effective and requires only information that is easy to obtain. It has already been widely used in the calculation of phase diagrams and estimation of thermodynamic properties for ternary and multi-component systems in the past decades.

The results of this numerical method are closely related to the way the source binary compositions of the alloys are chosen. All geometrical methods subdivide into two groups: symmetrical and asymmetrical. Both symmetrical and asymmetrical models consider only the concentrations of elements of the N-component alloy and can be summarized as

$$\Delta H = \sum_{i=1}^{N-1} \sum_{j=i+1}^{N} W_{ij} \Delta H_{ij} \tag{2.35}$$

$$W_{ij} = \frac{x_i x_j}{y_{ij}^i y_{ij}^j} \tag{2.36}$$

where W_{ij} indicates the weight probability, y_{ij}^i corresponds to the mole fraction of the element i in the binary ij alloy, and x_i is a mole fraction of component i in a system [Cho95].

Figure 2.18 shows two kinds of symmetric and two kinds of asymmetric models as well as their corresponding selected composition points for binaries respectively. It may be seen from Figure 2.18 that, with regard to an asymmetrical model like Toop's or Hillert's, the three selected binary compositions are different in three binaries, that means, a different arrangement of three components to the three apexes of the triangle will lead to a different result for the ternary enthalpy of mixing. Evidently this kind of selection is rather arbitrary and may not work sometimes. Besides, the procedure will become very complicated as the number of components gets larger.

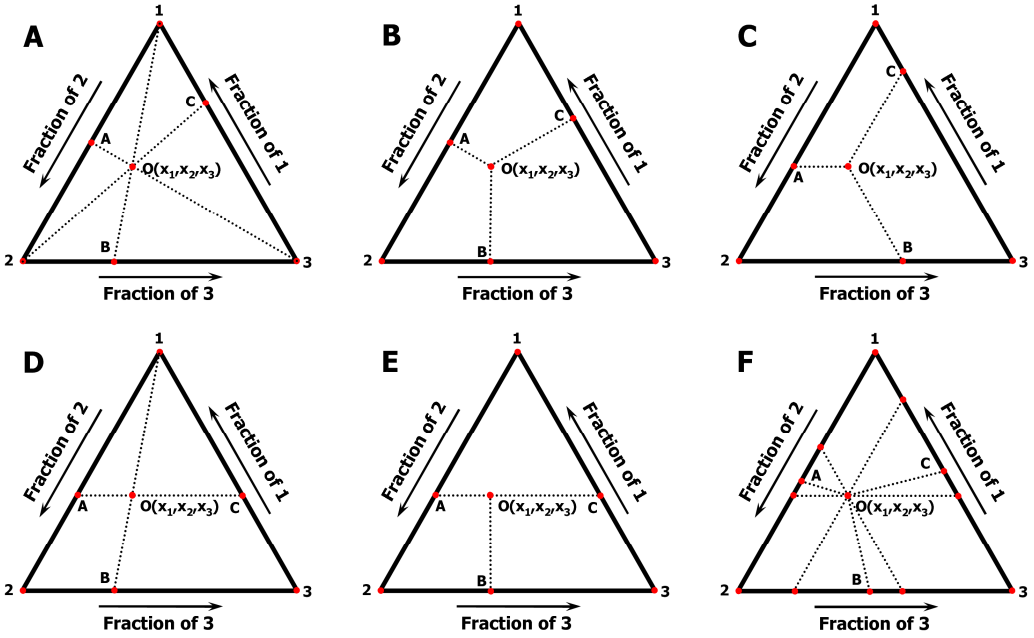

Figure 2.18: Schematic graphs of tradition geometrical models [Wan08]. Symmetrical models: (a) Kohler [Koh60], (b) Muggianu [Mug75], (c) Lück-Chou [Lüc86, Cho87]. Asymmetrical models: (d) Toop [Too65], (e) Hillert [Hil80]. Figure (f) represents the method of Chou [Cho95].

The symmetric models could avoid this problem since the selections for the three binary compositions are made in exactly the same way. However, they lead to other problems. Any reasonable model should reduce to its limiting form if the limiting conditions are met. For example, a model should turn into a binary solution mode1 if the characteristics of two components are identical, since there is a two-component alloy in this case. The symmetrical models, as it may be seen from Figure 2.18, do not have this feature and do not turn into a binary alloy, if the second component is identical to the third one.

Both symmetrical and asymmetrical models have their inherent problems and advantages. The symmetric models can not be reduced to a binary system if two components coincide. This is unacceptable at least from the theoretical point of view. For the asymmetrical models, the way of how to distribute three components into three apexes of a triangle remains undetermined. Evidence that these problems can not be

solved with symmetrical or asymmetrical models led Chou to get rid of the traditional way and to try a completely new approach to solve these problems [Cho95].

The new method developed by Chou contains a supplementary quantity λ which takes into account values of a thermodynamic parameter of binary alloys and is called "deviation sum of squares". The second new parameter in Chou's model is the "similarity coefficient" δ. Ouyang substituted the integration for summation and developed a slightly different model for the calculation of the mixing enthalpy of multi-component alloys [Oyu06a, Oyu06b]. According to Ouyang the model parameters λ and δ in their generalized forms can be written as

$$\lambda_i = \sum_{j=1}^{N-1} \sum_{k=j+1}^{N} (\Delta H_{j \text{ in } i} - \Delta H_{k \text{ in } i})^2, \; k \neq i, \; j \neq i,$$
$$\delta_{ij}^{i} = \frac{\lambda_i}{\lambda_i + \lambda_j} \tag{2.37}$$

where $\Delta H_{j \text{ in } i}$ is the dilute solution enthalpy of constituent j solved into i. According to the aforesaid arguments, the following binary composition will be selected for the calculation of the formation enthalpy of the alloy

$$y_{ij}^{i} = x_i + \delta_{ij}^{i} \sum_{k=1}^{N} x_k, \; k \neq i, \; k \neq j \tag{2.38}$$

and the whole formation enthalpy of an alloy can be written in the following form

$$\Delta H = \sum_{i=1}^{N-1} \sum_{j=i+1}^{N} \frac{x_i x_j}{y_{ij}^{i} y_{ij}^{j}} \Delta H_{ij}(y_{ij}^{i}, y_{ij}^{j}) \tag{2.39}$$

where $\Delta H_{ij}(y_{ij}^{i}, y_{ij}^{j})$ is the formation enthalpy of the constitutive binary system.

Ouyang's (Chou's) geometrical extrapolation has several advantages in comparison with symmetric and asymmetric methods. This model reduces to the simple

limiting form if one of the different limiting conditions is fulfilled. The selection of the binary compositions depends on the characteristics of all other binary systems and is not related to the succession of elements, what allows to exclude any arbitrariness in selecting models and arranging the three components to apexes of composition triangle.

2.4.2.3 Method of sequential addition

Another possibility to calculate the formation enthalpy of a multi-component alloy is a so-called "sequential addition" or in the case of a ternary alloys a "two-step calculation" method [Wan07b]. In this method the whole procedure for a N-component alloys is split into $N-1$ steps. The first step is alloying of two elements A and B according to the alloy composition, and the second step is the introducing of the third metal C into the received mixture of the first two metals. After that the procedure is repeated for the fourth element of the alloy and so on for all metals in the system. The formation enthalpy of an alloy can be calculated in this case as

$$\Delta H_{ABCD...} = \Delta H_{AB} + \Delta H_{C(AB)} + \Delta H_{D(ABC)} + ... \tag{2.40}$$

where $\Delta H_{C(AB)}$ and $\Delta H_{D(ABC)}$ are the formation enthalpies of quasi-binary solutions "C in AB" and "D in ABC" respectively. The three main parameters of Miedema's model for AB quasi-elements can be defined for ABC etc. as weighted average values from the constituent elements [Wan07b]

$$\begin{aligned} x_{AB} &= x_A + x_B \\ V_{AB} &= (x_A V_A + x_B V_B)/x_{AB} \\ \varphi_{AB} &= (x_A \varphi_A + x_B \varphi_B)/x_{AB} \\ n_{wsAB} &= (x_A n_{wsA} + x_B n_{wsB})/x_{AB} \end{aligned} \tag{2.41}$$

This procedure reduces the calculation of a N-component alloy to $N-1$ calculations of binary and quasi-binary alloys using Equation (2.31).

It is clear that alloys ABC, BCA, CBA etc. are the same in nature; therefore the results for an ABC alloy should not depend on the sequence of elements in it. But the use of Equations (2.40) and (2.41) obviously leaves traces on the results. To avoid this problem Wang proposed to compute the formation enthalpies of all possible combination followed by their averaging. Thus, for example the total formation enthalpy of the ternary alloy ABC can be written in the following form

$$\Delta H_{ABC} = \frac{1}{3}\left[\left(\Delta H_{AB} + \Delta H_{C(AB)}\right) + \left(\Delta H_{AC} + \Delta H_{B(AC)}\right) + \left(\Delta H_{BC} + \Delta H_{A(BC)}\right)\right] \qquad (2.42)$$

where ΔH_{ij} are formation enthalpies calculated using Equations (2.30) and (2.31) of the original Miedema's model.

2.4.2.4 L.C. Zhang's pseudo-ternary solution method of multi-component alloys

L.C. Zhang presented and approved successfully another method for the calculation of the formation enthalpy of multi-component alloys [Zha07a]. He suggested to divide the elements an alloy consists of into 3 groups by their chemical affinity and after that to calculate the formation enthalpy of the alloy using the Miedema's formula (2.34) for ternary alloys. According to L.C. Zhang the (Ti, Zr, Nb)–(Cu, Ni)–Al alloys, for example, can be considered as a pseudo-ternary alloy system, where (Ti, Zr, Nb) are regarded as the first group A, (Cu, Ni) as the second one B and Al as the third one C. The corresponding parameters V, φ, n_{ws} of each pseudo-component (i.e. A, B and C) can be calculated using the weighted average principle similar to Equation (2.41) of Wang's model.

The pseudo-ternary solution does make more physical sense compared to Wang's method, since elements having similar parameter values in Miedema's model also have similar behavior. But this method is sensitive to the rules how the elements are classified and thus it can not be fully automatized. The results depend on the way

the elements are grouped, but this dependence is not so drastic, as it is in the case of the symmetrical geometrical models.

2.4.3 Parameter S(c)

Since the early 1980s, Kleppa *et al.* investigated the standard enthalpies of formation of more than 270 binary intermetallic compounds of early transition metals with late transition and noble metals using different experimental techniques [Gou01]. Comparing the experimental data obtained by Kleppa *et al.* with the calculated values from Miedema's theory, over 90% of the calculated values are more negative than the experimental ones [Zha02a]. R.F. Zhang explains such a behavior with the atomic size difference and its influence on the contact interface and the bonding energy, which is believed to play an important role in affecting the precision of the calculation, but has not been considered in Miedema's original theory [Zha07b]. The contact between the two dissimilar Wigner-Seitz cells could not be matched ideally, especially for binary systems with a large atomic size difference. In other words, the shapes of the two contacting unit cells would be deformed, because the contact interfaces would always differ from the surface area of the solute atom. Therefore, the effect of changing contact interface area should be taken into account in calculating the formation enthalpy. Meanwhile, the atomic size difference would frequently lower the package density of the crystalline lattice and thus increase the binding energy between the two dissimilar atoms, because the electron cloud would become further away from the nuclei. In order to take these effects into account R.F. Zhang proposed to add a pre-factor $S(c)$ into Equation (2.19), which is defined by

$$S(c) = 1 - S_V(c) = 1 - \frac{c_B^S \left| V_A^{2/3} - V_B^{2/3} \right|}{c_A^S V_A^{2/3} + c_B^S V_B^{2/3}} \tag{2.43}$$

where $S_V(c)$ is called as an influential factor and c represents the alloy composition [Zha02a, Che05, Zha05, Zha07b]. Under such definition, the pre-factor $S(c)$ is unity, if

the two constituent metals have the same atomic sizes, and goes to zero with increasing radii difference.

According to the definition, the chemical part of the formation enthalpy when metal A is solved in metal B is expressed by the following formula

$$\Delta H^{chem}(\text{A in B}) = S(c)\frac{V_A^{2/3}}{(n_{ws}^{-1/3})_{average}}\left\{-P(\Delta\varphi)^2 + Q(\Delta n_{ws}^{1/3})^2 + R\right\} \tag{2.44}$$

Continuing and reviewing this work Wang introduced another form of the pre-factor $S(c)$, which is thought to be as correct as the asymmetry of the R.F. Zhang's variant of the pre-factor. It is written as

$$S(c) = 1 - C_W \frac{c_A c_B |V_A - V_B|}{c_A^2 V_A + c_B^2 V_B} \tag{2.45}$$

where C_W is an empirical parameter that describes the effect of the atomic size difference in a semi-quantitative manner and is taken to be 0.5 and 2.0 for liquid alloys and compounds, respectively [Wan07b].

2.4.4 Simplification of Bangwei Zhang

B. Zhang proposed to simplify the original Miedema's model by the replacement of the surface concentrations c_A^S, c_B^S and the contact parameters f_A^B, f_B^A by the atomic concentrations of the corresponding elements c_A and c_B, respectively [Zha02b]. Thus the formulae (2.24) and (2.31) change their form to the following equations

$$\Delta H^{chem}(\text{1 mole of atoms}) = c_A c_B \Delta H^{chem}(\text{A in B}) \tag{2.46}$$

$$\Delta H^{chem} = c_A c_B \left[c_B \Delta H^{chem}(\text{A in B}) + c_A \Delta H^{chem}(\text{B in A}) \right] \tag{2.47}$$

This simplification reduces the total number of calculations and can be applied for simple estimates.

2.4.5 A new and improved extension of Miedema's model

All mentioned models try to predict thermodynamic properties of ternary alloys from the properties of the related binary systems. It is assumed that the properties of the corresponding binaries are not modified by the addition of a third element. As a result the actual structure of the ternary alloy including existing fluctuations as well as the important many-particle interactions are not taken into account. Thus, the drawbacks of these approximations and the uncertainty of the results grow with the increasing number of elements the alloy consists of. To avoid these problems a completely new approach is proposed here which combines the fundamentals of Miedema's model and the detailed structure of multi-component alloys.

The Miedema's model is based on the examination of atoms as Wigner-Seitz cells, and the chemical part of the formation enthalpy is calculated considering the boundaries of these cells by means of Equation (2.19) for dilute solutions. All following formulae for the chemical enthalpy (2.20)-(2.25) and (2.31) as well as all extensions of the model for ternary and multi-component alloys (2.34)-(2.42) and the additional $S(c)$ parameter (2.43)-(2.45) try to accommodate the basic Equation (2.19) to different kinds of structures and properties of alloy. One can avoid the disadvantages of these approaches only by the incorporation of the very local atomic structure. Thus, a combination of the Voronoi/Laguerre tessellation technique and the basics of Miedema's model is proposed as a simple and powerful way to calculate the chemical part of the formation enthalpy. On the basis of this idea a completely new model has been suggested in the present work.

The Equation (2.19) represents the chemical part of the formation enthalpy of an atom A completely surrounded by B atoms. Since this part is proportional to the contact area of atom A, the mixing enthalpy corresponding to atom B_i contacting atom A can be expressed as

$$\Delta H^{chem}(\text{A to B}_i) = \frac{1}{2}\frac{S_{A-B_i}}{S_A}\Delta H^{chem}(\text{A in B}) \qquad (2.48)$$

where S_A is the total surface area of the atom A, S_{A-B_i} corresponds to the contact area of the atom A with the B_i atom and $\Delta H^{chem}(\text{A in B}_i)$ is a chemical part of the formation enthalpy calculated using the equation (2.19). The pre-factor 0.5 is needed due to the fact that every contact face and energy effects belongs to two atoms. The information about contact areas as well as about the type of neighboring atoms can be simply obtained from the Laguerre tessellation algorithm.

The whole procedure of the formation enthalpy calculation for amorphous alloys or liquids has the following sequence:

1. Structure simulation of multi-component alloys using the hard spheres packing algorithm;
2. Analysis of the received structure by means of Laguerre tessellation;
3. Calculation of the mixing enthalpy of each atom in the system and averaging of enthalpies yields the total mixing enthalpy of the alloy.

The first and the second step are described in Sections 2.1 and 2.2; the third one is accomplished using following equations:

$$\Delta H^{chem}(\text{of A atom}) = \sum_i \Delta H^{chem}(\text{A in B}_i) \qquad (2.49)$$

$$\Delta H^{chem}(\text{1 mole of atoms}) = \frac{1}{N}\sum_{j=1}^{N}\sum_i \Delta H^{chem}(\text{A}_j \text{ in B}_i) \qquad (2.50)$$

where N is the number of atoms in the system. Equation (2.49) represents the total contribution of one atom A to the mixing enthalpy of the alloy; and Equation (2.50) calculates the average value of all atoms in the system and gives the total mixing enthalpy of the alloy per mole of atoms.

This method does not need any additional calculations if the structure of the alloy is known. It also takes into account local structure fluctuations and does not have any restrictions on the component number, which makes this method applicable to any type of alloys. The only limitations arise due to the structure simulation algorithm.

The procedure of the enthalpy calculation was realized as one computer program combining three algorithms (hard sphere packing, Laguerre tessellation and Miedema's model) and takes about 2 to 5 minutes on the standard personal computer for an alloy consisting of 5000 atoms. The input file contains the alloy composition and all additional parameters necessary for calculation of the formations enthalpy depending on the type of the alloy. All data which are of interest for bulk metallic glasses are summarized in an additional data-base file. The program includes of 4 additional algorithms: Ouyang's geometrical extrapolation, method of sequential addition according to Wang, pseudo-ternary solution method of L.C. Zhang and the simplified method of B. Zhang. Additional parameters of Wang and R.F. Zhang are also included into the program for corresponding methods.

CHAPTER 3
SIMPLE LIQUIDS AND AMORPHOUS ELEMENTS

In this chapter results of simple (monatomic) packings of hard spheres will be discussed. Structure simulations were performed using the force-based algorithm of Jodrey and Tory. In order to get a good convergence of results and assimilate simulations to experimental investigations a number of identical independent mixtures of 5000 equal hard spheres (corresponds to lamps of about 5 nm of a real amorphous structure) were simulated. It was found that the simulation of 20 statistically independent mixtures gives good statistic and a low error of final results. Thus, the total number of analyzed spheres amounts to 100000 (~ 13-15 nm real samples). After simulation each system was analyzed by means of Laguerre tessellation, radial distribution function etc. All results were averaged over all statistically identical mixtures.

The results are also compared to the simulated samples of smaller sizes consisting of 50 and 500 atoms, in order to test the system with respect to size effects.

3.1 Density

The density distributions of 20 samples each consisting of 5000 atoms and the local density distribution of all 100k spheres are presented in the Figures 3.1 (a) and (b), respectively. The total density varies in a small range from 0.6417 to 0.6433, the average density was found to be 0.6425 ± 0.0003, which is in a good agreement with experimental results of Berryman [Ber83] and Clarke [Cla87], but is slightly higher than Scott's 0.636(6) [Sco69]. The density distribution of all spheres has a broad maximum

in a range of the density from 0.53 to 0.73 which can be very well described by a Gauss distribution function.

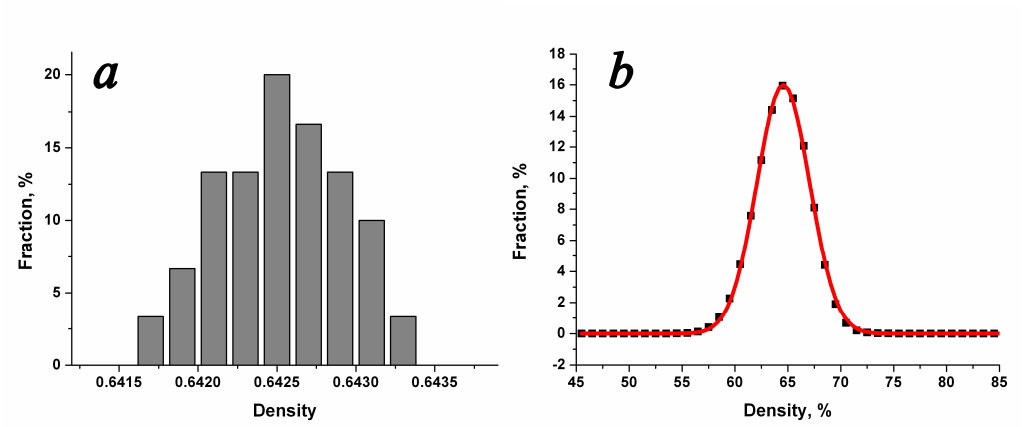

Figure 3.1: (a) Density distribution of 20 simulated mixtures, and (b) distribution of the local density of all 100000 simulated spheres.

As a measure of the goodness of the fitting can be used the so-called coefficient of determination, R^2. The R^2 is a statistical measure of how well the fitting curve approximates the real data points. Adjusted R^2 ($adj.R^2$) is a modification of R^2 that adjusts for the number of explanatory terms in a model. Unlike R^2, the $adj.R^2$ increases only if the new term improves the model more than would be expected by chance. The $adj.R^2$ is always less than or equal to R^2. The values of the $adj.R^2$ vary from 0 to 1. An $adj.R^2$ of 1.0 indicates that the regression curve perfectly fits the data.

The $adj.R^2$ of the Gauss fitting amounts in this case to 0.99927, and the average density calculated from the fitting is 0.6457 ± 0.0002. The latter value of the density is a little bit higher than the former one due to the different type of estimation and numerical errors.

These distributions clearly show that the samples are inhomogeneous on the atomic scale and the local packing density varies in the broad range from 55 % to 75 %. Increasing the observation window reduces the inhomogeneity, and at linear dimensions of about 15 sphere radii the systems become statistically homogeneous.

3.2 Radial distribution function

The radial distribution function (RDF) was also averaged over 20 mixtures. The result is shown in the Figure 3.2. In the range up to 10 radii the radial distribution function has 6 maxima their positions and theoretical descriptions are listed in the Table 3.1. Planar configurations in the Table 3.1 can be considered as sectional views of the corresponding 3D atomic arrangements. While SC, BBC and FCC columns shows possible 3D atomic arrangements on the example of simple, body-centered and face-centered cubic structures, respectively.

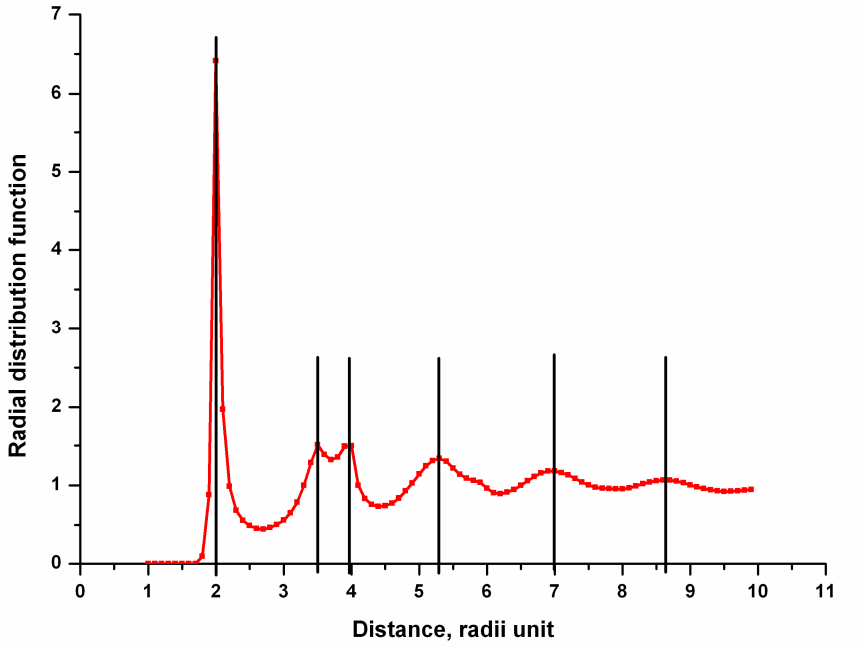

Figure 3.2: Average radial distribution function of 20 samples.

The first peak of the radial distribution fuction corresponds to the direct contacting spheres; the second one is split into two maxima. This splitting is characteristic for amorphous atomic packings [Fin77] and is observed experimentally in all metallic glasses, but not in liquids [Lee03]. The second maxima confirms configurations of spheres similar to the relative arrangement between (0 0 0) and (1 1 1) atoms in a simple cubic structure (or (0 0 0) and (.5 .5 1) in the case of FCC lattice). The

third maximum is presented in all shown crystalline structures and corresponds to thee direct touching spheres. Peaks 4, 5 and 6 have much more diffuse form and indicate more complicated structures comparing to the first 3 peaks.

Table 3.1: Positions of RDF maxima from Figure 3.2 and their descriptions.

Peak	Position	Theoretical descriptions				
		Distance	Planar configurations	SC	BCC	FCC
1	2.00	$2R = 2.00$	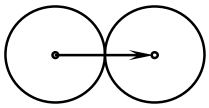	{0 0 1}	{.5 .5 .5}	{0 .5 .5}
2	3.50	$2\sqrt{3}R \approx 3.46$	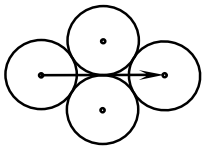	{1 1 1}	-	{.5 .5 1}
3	3.97	$4R = 4.00$	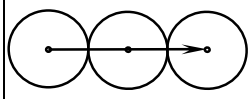	{0 0 2}	{111}	{0 1 1}
4	5.28	$2\sqrt{7}R \approx 5.29$	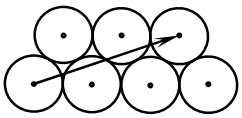	-	-	{.5 1 1.5}
5	6.99	$4\sqrt{3}R \approx 6.93$	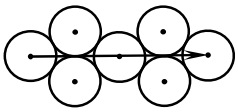	{2 2 2}	{0 0 3} {1 2 2}	{1 1 2}
6	8.64	$2\sqrt{19}R \approx 8.72$	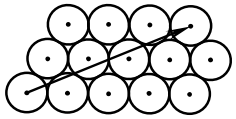	{1 3 3}	{1 2 3}	-

After the distance of about $8R$ (R - radius of atoms) the distribution became nearly random indicating homogeneity of the samples. The form of radial distribution function demonstrates the presence of short- and medium-range order limited to first 4-5 coordination spheres without any evidence of long-range order and translation symmetry. Thus, structures like these packings of hard spheres fulfill Bernal's necessary conditions for amorphous materials: homogeneity, coherence and irregularity. Though the second peak is split, the radial distribution function is very similar to those of simple liquids [Hen60, Sco62].

3.3 Coordination numbers

There are a number of methods for the determination of the coordination number, which lead to different but comparable values. The method providing the lowest values considers only "kissing" atoms as neighbors and is commonly used for crystalline structures. In the case of disordered structures this method yields underestimated values and cannot be applied.

The second well known method is integration of the radial distribution function in the [0, R_{min}] range, where R_{min} position of the first minimum. Due to the simplicity this method is commonly applied for the estimation of the coordination number from diffraction patterns and/or other experimental results. This method, however, has a number of disadvantages. The resulting value strongly depends on the quality of the initial experimental results and the selection of the first minimum position. In addition, this method yields only an average value over the sampling points. Except for a small number of binary alloys, this method does not produce information about the partial correlations of certain atomic species.

The method used in this work determines the coordination number of an atom as the number of faces of the corresponding polyhedron. This determination excludes inaccuracies arising in the first two methods and can be easily applied for disordered structures and crystalline materials as well. According to the determination, the coordination number in this case is the number of real geometrical neighbors calculated for all atoms separately and averaged over the whole sample. The values calculated using this method are commonly about 1.0 higher than the values of the second method.

The coordination number distribution of a monodisperse system and the corresponding Gauss fitting are shown in a Figure 3.3. The fitting yields 0.9996 for the $adj.R^2$ and the average coordination number of 14.039 ± 0.007, which is in a good agreement with [Ber64]. The distribution ranges between 10 and 19 neighbors of an atom and shows strong fluctuation of the coordination number and, accordingly, of local structure while the average coordination number has small deviation and confirms homogeneity of the samples on the $15R$ scale, where R is radius of atoms.

Results of Bezrukov for similar monatomic mixtures calculated using the method of "kissing" spheres with 1% tolerance show, that the coordination numbers are in the range 1 to 10 and the average value of the coordination number is about 6.05 [Bez02].

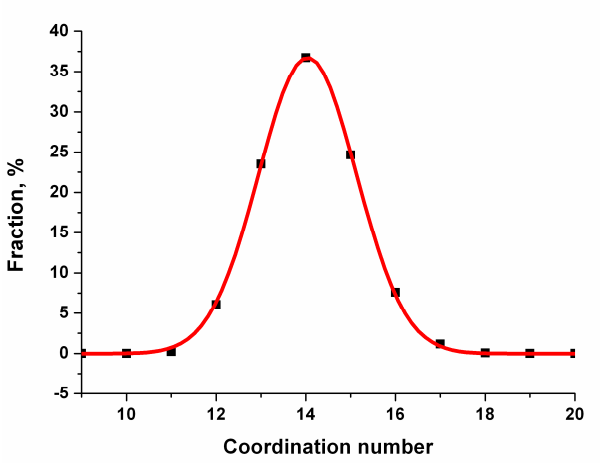

Figure 3.3: Coordination number distribution of 100000 simulated spheres and corresponding Gauss fitting curve.

Similarity of the distribution range sizes reflects the similarity of simulated structures. But the different average values are connected to the different behavior of these two types of coordination number determination. So, the values of the "kissing" atoms method have a decreasing tendency with increasing disorder in the systems, while the method of geometrical neighbors yields higher values with increasing disorder in the system. Though, both of these methods have similar values in the case of crystalline arrangements.

3.4 Polyhedra analysis

A polyhedron obtained by Voronoi of Laguerre tessellation can be characterized by a sequence of numbers $(n_3, n_4, ...)$. n_k is the number of faces with k edges.

Structure model can be characterized by the statistics of $(n_3, n_4, ...)$ polyhedra of the corresponding Voronoi or Laguerre mosaic.

There are two different kinds of polyhedra fraction determination. The first one calculates the fraction as the whole number of atoms involved into similar polyhedra [Lek07]. The second one describes the distribution of polyhedra in terms of the fraction of atoms, which a placed in the middle of the polyhedron [Fin70a, Mat09]. It is clear, that the first method yields larger values as the second one.

The corresponding comparative ratio between these two methods can be estimated as a number of atoms, which are involved into a corresponding polyhedron (13 for icosahedral short-range order) taking into account the probability that two similar polyhedra are somehow connected. Two polyhedra can be connected by a common vertex, a common edge, or a common face. For example, the value of $(2*13-5)/2=10.5$ seems to be a good approximation for randomly distributed 2-4 % of (0, 0, 12) polyhedra, since in this case (0, 0, 12) polyhedra contact statistically one similar polyhedron by a common face, and the contact area consist of 5 atoms. The total number of atoms involved into (0, 0, 12) polyhedra ranges in this case between about 20 and 45 %.

In these work the terms of middle atoms is used for description of the polyhedra fractions.

The polyhedra analysis of all simulated structures has shown that monatomic mixtures consist of about 1060 different polyhedra types and only 29 of them have concentrations of more than 1 percent. These polyhedra and their percentages are listed in the Table 3.2. A small amount of atoms (~0.18 %) was found to possess a crystalline BCC short-range order. These BCC polyhedra are randomly distributed in the samples and do not show any evidence of long-range order or crystallization. From the statistical point of view, real amorphous alloys contain atoms with crystalline short-range order. But separated non-interacting crystalline polyhedra do not cause crystallization and the whole alloy is still random, coherent and isotrop.

All other polyhedra do not show any evidence of local crystal-like order.

Total percentage of the major polyhedra in the Table 3.2 amounts to 64.46 %. This means, that approximately one third of the sample volume is occupied by about

1000 different types of minor polyhedra. The average local density yielded by the major polyhedra amounts to 0.6493, which is slightly higher than the density of the whole system but very close to it.

Table 3.2: 29 Major polyhedra with corresponding frequency in percent.

Type of polyhedron	Av. local density	Percentage, %
(0, 3, 6, 4)	0.6583	6.27
(0, 2, 8, 4)	0.6463	5.89
(0, 3, 6, 5)	0.6487	5.74
(0, 4, 4, 6)	0.6483	4.5
(0, 1, 10, 2)	0.662	3.94
(0, 3, 6, 6)	0.6352	3.03
(1, 3, 4, 5, 1)	0.6486	2.76
(0, 2, 8, 3)	0.6613	2.19
(0, 4, 4, 7)	0.6395	2.16
(0, 2, 8, 5)	0.6295	2.14
(1, 1, 8, 3, 1)	0.6499	1.87
(0, 2, 8, 2)	0.6729	1.84
(1, 3, 5, 4, 2)	0.6349	1.72
(1, 2, 6, 3, 1)	0.6609	1.66
(0, 1, 10, 3)	0.6415	1.64
(0, 0, 12)	0.6873	1.63
(1, 2, 6, 4, 1)	0.6491	1.48
(1, 0, 9, 3)	0.6712	1.43
(1, 2, 6, 5, 1)	0.6353	1.27
(1, 3, 5, 3, 2)	0.6445	1.22
(1, 2, 7, 3, 2)	0.6349	1.2
(0, 4, 4, 5)	0.655	1.18
(0, 4, 5, 4, 1)	0.6368	1.13
(1, 4, 3, 5, 2)	0.6387	1.12
(1, 3, 4, 6, 1)	0.6371	1.12
(1, 2, 7, 2, 2)	0.6489	1.11
(0, 4, 5, 5, 1)	0.6267	1.11
(0, 3, 7, 4, 1)	0.6225	1.07
(1, 2, 5, 5)	0.6617	1.04

Average densities of polyhedra from the Table 3.2 are presented in the diagram below (Figure 3.4). The densest polyhedron is a dodecahedron (0, 0, 12), which corresponds to the icosahedral short-range order. Considering the assumption that the high density and a good glass-forming ability are necessarily connected, the

dodecahedron as well as two other densest polyhedra in this system (1, 0, 9, 3) and (0, 2, 8, 2) should be liable for the glass-forming ability. But the total amount of these three polyhedra (~5%) indicates their small contribution to the total density of the system.

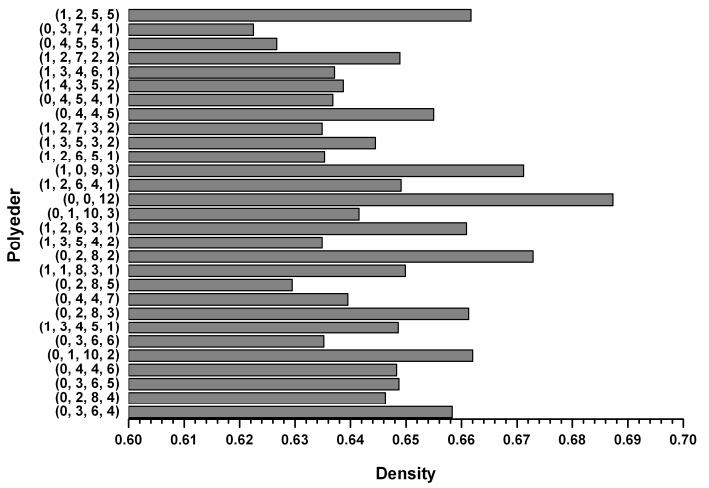

Figure 3.4: Average densities of 29 major polyhedra.

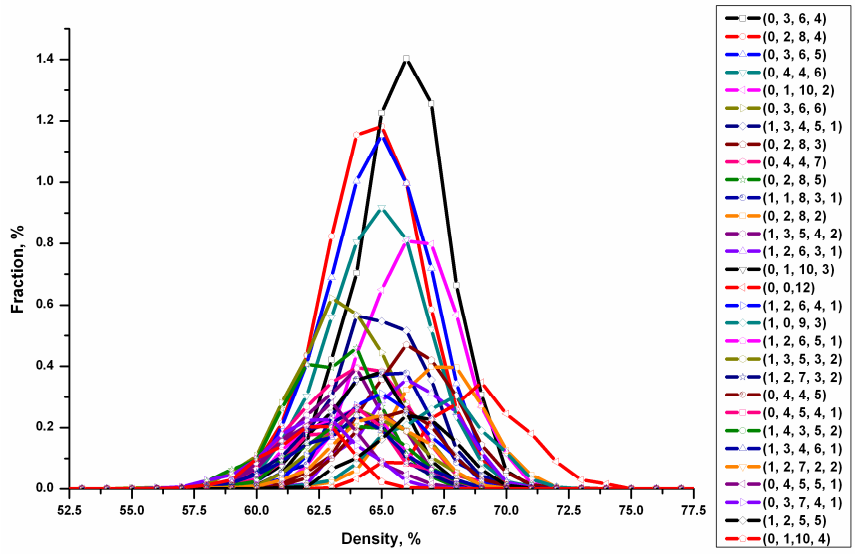

Figure 3.5: Density distribution of the 29 major polyhedra.

Another interesting parameter of the polyhedra is their density distribution, which is shown in the Figure 3.5. The density distributions of almost all polyhedra have

similar ranges from about 0.58-0.59 to 0.70-0.72 except polyhedra with low concentrations and the dodecahedron. The distribution of the last one has nonzero values between 0.63 and 0.75, which goes up to the values higher than the density of crystal structures like FCC and HCP. This feature of icosahedral short-range order can hypothetically allow a considerable increase of the density of an amorphous alloy. But there are also limiting conditions like incompatibility of icosahedra with translation symmetry, which does not allow to fill the whole structure with only dodecahedrons, and other polyhedra are necessary.

3.5 Non-crystalline to crystalline faces ratio

A Laguerre polyhedron characterizes not only the local density but also the geometry of the cluster formed by the central sphere and its nearest neighbors. Moreover, each face is common to two adjacent clusters and describes how these clusters are interconnected. The number, n_e, of vertices of a face connecting two neighboring mosaic cells is used as an approximate measure for the type of the local symmetry axis which is perpendicular to the considered face. If the number of vertices, n_e, is 3, 4 or 6, then the local symmetry axis is approximately compatible with local translational order [Sch67]. If $n_e = 5,\ 7,\ 8\ldots$, then the local symmetry is incompatible with local translational order and, consequently, favors non-crystalline (liquid, amorphous, glassy) structures. The statistics of the number of vertices of the mosaic cell faces is discussed in this work in terms of the parameter

$$F_{nc} = \sum_{e\neq 3,4,6} n_e \Big/ \sum_{e=3,4,6} n_e , \qquad (3.1)$$

where the summation is taken over all cells of the considered model. The parameter F_{nc} characterizes the affinity of a system to stabilize non-crystalline states and can also be considered as a quantitative measure for geometric frustration [Nel89]. Strictly speaking, the incompatibility of $n_e = 5,\ 7,\ 8\ldots$, with translational (crystalline) order

applies to the symmetry of the elementary cell of a crystal, and it may happen that the Laguerre polyhedron of a single atom inside an elementary cell has faces with five edges. This means that the above condition – higher values of F_{nc} mean higher affinity to stabilizing non-crystalline states – applies in the sense of spatial statistics.

The value of the parameter F_{nc} of simulated monatomic systems amounts to 0.9403. The percentages of polygons depending on the edge number are listed in the Table 3.3. Nonagons and decagons, as well as polygons with more edges occur very seldom. In fact no dodecagons (12 edges) and only one hendecagon (11 edges) were found among all 100000 investigated spheres.

Table 3.3: Percentage of faces depending on number of edges.

Number of face edges	Percentage, %
3	4.4909
4	17.9889
5	42.1751
6	29.0594
7	5.4733
8	0.7323
9	0.0734
10	0.0063

The absolute predominance is shown by the pentagon. According to its concentration of about 42 % and to the average coordination number of about 14 this polygon is statistically present at least by 5 faces at each polyhedron. Such a concentration superiority is in a good agreement with previous results of Bernal [Ber64]. The second largest concentration of about 30 % belongs to hexagons, what is also clear, since hexagonal orientation is familiar to FCC and HCP structures and leads to the highest possible density of $\pi/\sqrt{18} \approx 0.74048$ in a monatomic system. Thus, hexagons are necessarily connected to the high density, as well as pentagons (icosahedral short-range order).

3.6 Compression tests

Each simulation of an amorphous structure approaches the density of the system to some value, which is limited by the algorithm and lies between 0.62 and 0.66 according to different papers [Ber83]. But it is clear that structure as well as properties is connected to the density.

We can, probably, never reach the "real" maximal value of the density in random, homogeneous and coherent systems without crystallization, since there is no legible boundary between the amorphous and the crystalline states and it is not clear what structural changes should we define as the beginning of crystallization, and when amorphous state turns into crystalline or partial crystalline. In addition, amorphous materials might also contain crystalline polyhedra, what also complicates the determination of the limiting density.

One of the possibilities to approach the maximum density of the monatomic systems is a multiple compression, which was applied in order to investigate the behavior of monatomic systems depending on compression cycle number. In this algorithm a sphere packing received after the Jodrey and Tory compression procedure is used as start configuration for a new similar compression cycle. Each compression cycle begins with reducing of the radii, what causes a relaxation of the structure and makes the following compression possible. The whole procedure is repeated until the prescribed number of cycles is done. One can assume this algorithm as a step by step compression of a system followed by structure analysis after each step. One of the limiting values, which should be taken into account, is the increasing of the crystallinity caused by high density.

This section presents results of the multiple compression test implemented for 3 different sizes of a system: 50, 500 and 5000 atoms. The number of compression cycles was limited to 20 for most of the simulations, since further compression results in a high quantity (> 1%) of atoms with crystalline polyhedra (commonly FCC). For each set of parameters 10 identical simulations (called samples) were made in order to get a satisfactory statistic.

3.6.1 Density

Figure 3.6 (a) presents behavior of the density of 10 samples (5000 atoms each) up to 50 compression cycles. The black thick curve corresponds to the average value of the density of all 10 samples. Whereas at the first cycles of the algorithm the densities of all samples do not differ by more than 0.001, at higher step numbers the difference increases up to values of 0.006. This behavior shows a strong variety of the final results determined presumably on small differences of the start configurations.

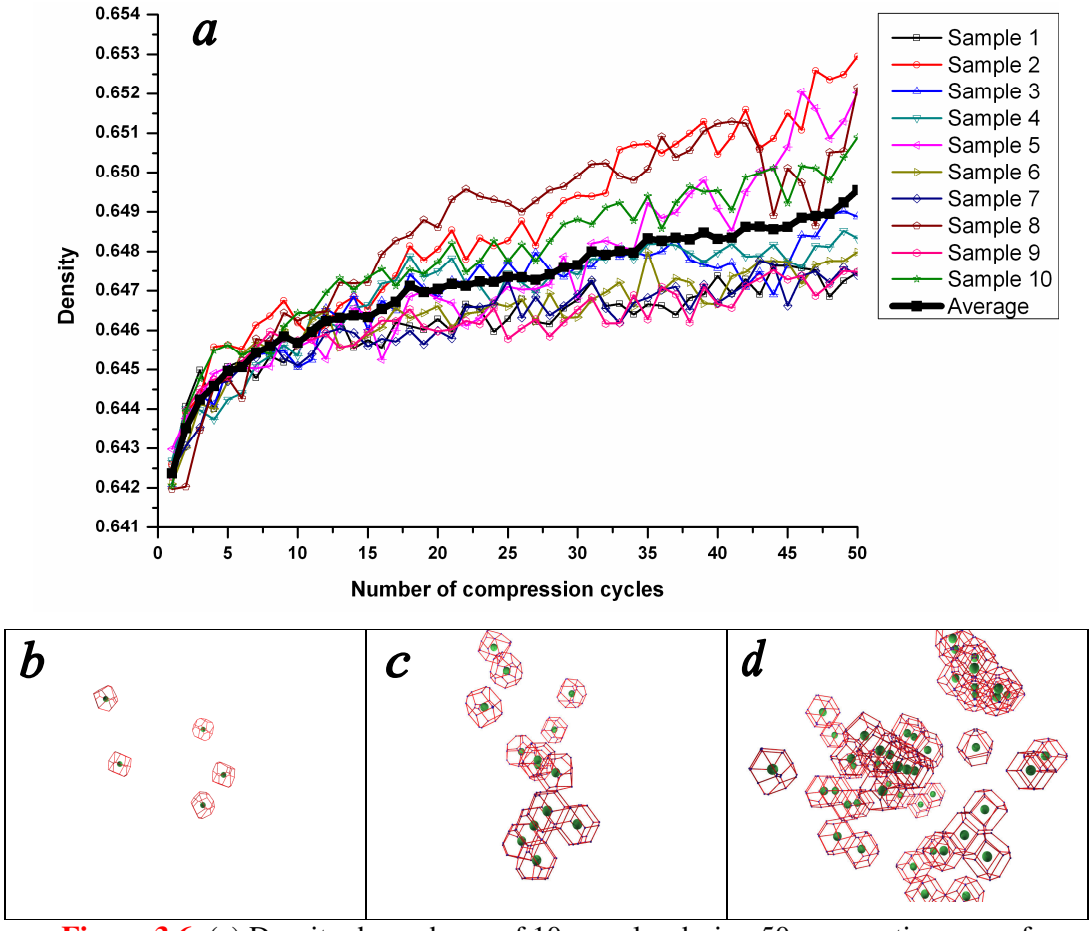

Figure 3.6: (a) Density dependence of 10 samples during 50 consecutive runs of compression algorithm and (b-d) crystalline polyhedra (BCC and FCC cells) found after 15, 25 and 50 compression cycles.

After about 20 compression cycles, when the average density crosses the value of 0.647, the total amount of crystalline polyhedra (FCC and BCC) exceeds 1%. This scope was chosen as empirical limit of the amorphous state in monatomic systems, since larger amounts of crystalline areas can be determinated by experimental methods like X-Ray diffraction (XRD) etc. Therewith, systems with small amounts of crystalline polyhedra exhibit instability of such polyhedra and fluctuations of their concentrations in the range between 0.2 to 0.4%. After the value of about 1% (depending on the sample) is reached, these polyhedra become more stable and indicate normal crystal growth.

Figures 3.6 (b-d) present crystalline polyhedra or, what is the same, single crystalline cells (BCC and FCC) after 15, 25 and 50 compression cycles. Up to about 20 compression cycles only separated crystalline cells can be found (Figures 3.6 (b)). Further compression changes this behavior, and after about 25 compression cycles crystalline cells start to interact and to build nano-crystalline regions.

In the range between 20 to 50 compression cycles the average density of 5000 atoms systems shows a linear dependence on the compression cycle number. That is directly connected to the grow of existing nano-crystalline regions and to the appearance of new ones.

From these reasons, the compression cycle number was limited to 20 as an appropriate approximation for the limiting value of the amorphous state.

Another interesting aspect of this algorithm is the dependence on the sample size. Figure 3.7 represents the density dependence for 3 kinds of mixtures (50, 500 and 5000 atoms) up to 20 compression cycles.

Spheres of the samples in Figure 3.7(a) become jammed after 3 compression cycles at most, and the structure as well as the density and other parameters does not change during next cycles. The density varies for these samples between 0.6277 and 0.6405 and the concentration of atoms having BCC-like first coordination sphere amounts to about 0.6 %.

Samples consisting of 500 atoms (Figure 3.7(b)) give much more interesting results. The behavior of most of the samples is the same as for the samples with 5000

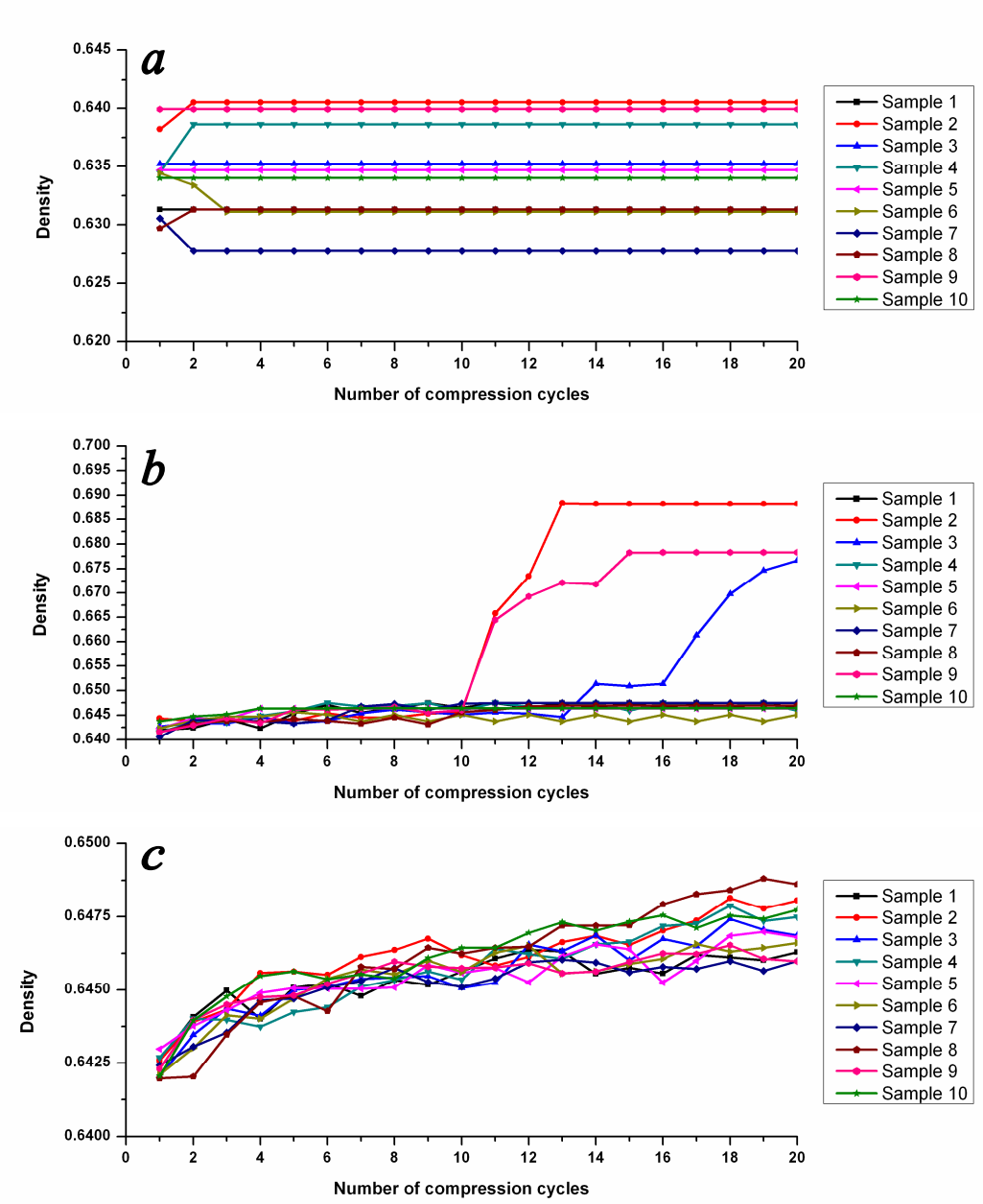

Figure 3.7: Density dependence of 10 monatomic mixtures during 20 consecutive runs of compression algorithm for different sample sizes: (a) 50 (b) 500 and (c) 5000 atoms.

spheres in Figure 3.7(c). Curves 2, 3 and 9 differ from the average value and approach the densities of 0.6882, 0.6766 and 0.6783, respectively, which is close to the density of the BCC structure $\sqrt{3}\pi/8 \approx 0.68017$. The violent kind of density change reflects the

behavior of real system. For example, when in an undercooled liquids a crystallization center appears, the whole system immediately crystallizes.

During the searching for optimal parameters for the algorithm of Jodrey and Tory some systems of 500 atoms showed almost perfect FCC structure after about 15 compression cycles (data not shown). During the compression, these system get firstly a distorted BCC structure and only after that they get densities approaching the well known limiting value of $\pi/\sqrt{18} \approx 0.74048$ for FCC and HCP lattices. The BCC to FCC transition occurs commonly within only one compression cycle and has an explosion-like behavior.

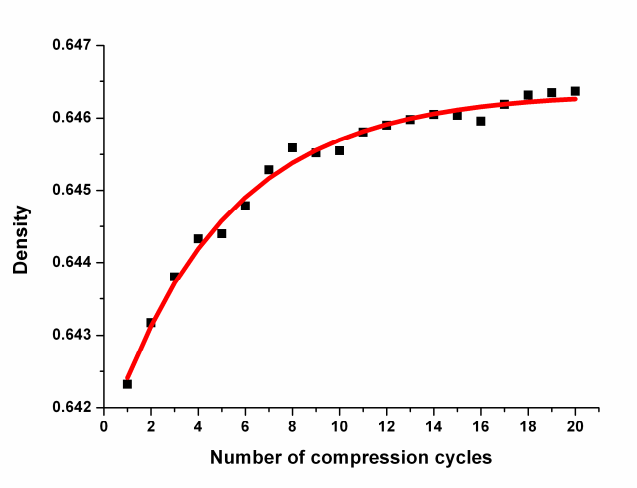

Figure 3.8: Exponential fitting of the average density.

The behavior of the average density among first 20 compression cycles of 5000 mixtures can be well described by the exponential curve $y = y_0 + a\exp(bx)$, see Figure 3.8. Parameter y_0 corresponds to the maximum or minimum attainable value of y, a represents the quasi-velocity and direction (depends on the sing of b) of the function change and b is a scale factor which is related to the internal parameters of the packing algorithm. Since packings parameters stay the same, the only quantity the parameter b depends on in this work is the number of different sphere types.

The fitting function for the results in Figure 3.8 was found to have following form with $adj.R^2$ of 0.98906: $y = 0.64635 - 0.00481\exp(-0.20076x)$. Value 0.64635 accords to the maximum attainable density in this mono system without crystallization which is in a good agreement with previous results of Berryman [Ber83] and observation, that after the density of about 0.647 is reached a sufficient amount of crystalline polyhedra are present in the structure.

3.6.2 Radial distribution function

The average radial distribution functions of the samples after up to 50 compression cycles are shown in the Figure 3.9. With increasing samples density (compression) the form of the radial distribution function undergoes changes. The maxima become sharper and some new peaks appear. After 30 compression cycles a new peak can be seen at about 2.88. This maximum corresponds to the {001} positions of the FCC lattice with the distance $2\sqrt{2}R \approx 2.8284R$ ($R = 1.0$ - radius of atoms) and reflects a certain degree of crystallization in the system. Sharpening of peaks {.5 .5 1} at 3.50, {0 1 1} at 4.0 and {0 1 1.5} at ~5.28 points to the growing of FCC crystals up to about 6 atoms in diameter. Another new peak is situated at ~4.56 and corresponds to {0 .5 1.5}.

According to Figure 3.9 the size of FCC regions can be estimated as $4R$ after 10 and 20 compression cycles, which corresponds to separate single FCC cells/polyhedra. After 30, 40 compression cycles a new peak at ~4.56 appears and all other peaks with distances below 4.56 become sharper, thus the size of FCC regions reaches $5R$, which corresponds to crystallites of about 2 cells in size. Further compression up to 50 cycles causes the appearance of a new peak at about 7.21 reflecting agglomeration of FCC cells into regions of about $8R$ in size (approximately 5 cells).

This confirms the observation that after about 20 compression cycles the system earns a significant degree of crystallinity, and in the following the increasing of the density occurs due to the growth of the crystalline areas. This confirms the choice of 20 compression cycles to be reasonable for the investigation of amorphous structures.

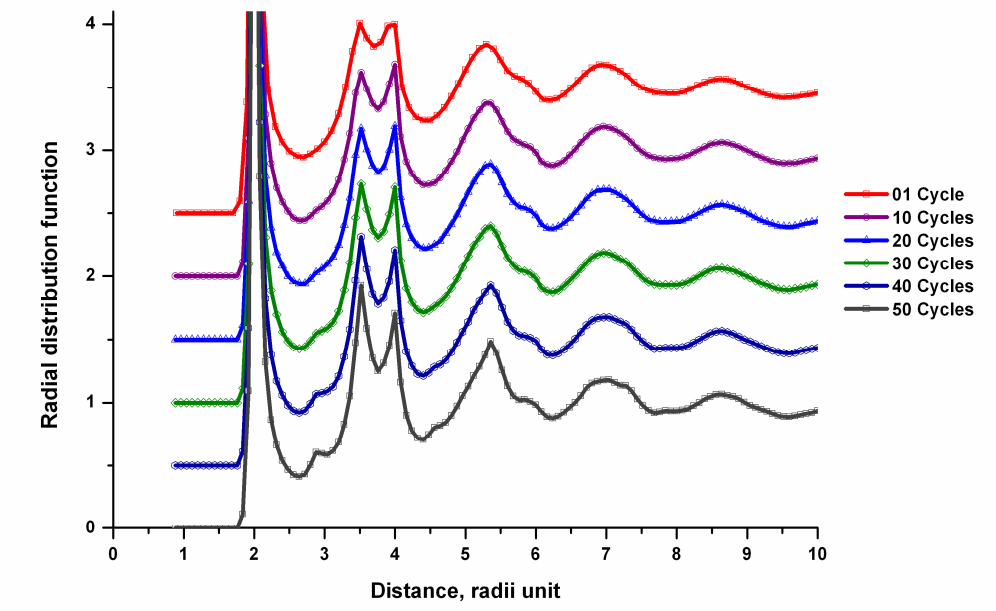

Figure 3.9: Radial distribution functions depending on the number of the compression cycles (shifted by the amount of 0.5 each).

Another interesting feature of the radial distribution function is the fact, that the ratio of the altitudes of the second (~3.50) and third (~4.00) peaks shows a density dependence. While after the first compression cycle the third peak is higher than the second one, after 30 compression cycles and at the densities of about 0.6476 both peaks have approximately the same altitude. Further densification up to 50 compression cycles makes the second peak more prevailing.

3.6.3 Coordination numbers

Average coordination numbers of the systems consisting of 50, 500 and 5000 spheres depending on the number of compression cycles are shown on Figure 3.10(a). The behavior of the coordination number for 50 atoms systems supports the assumption that structure jamming occurs at a constant coordination number of 14.18 after the third compression cycle. Strong fluctuations of the coordination number and low final values (approaching value of 14, which is typical for BCC structure) point to a high propensity towards crystallization of the 500 atoms systems and insufficient statistic. The average

coordination number of the 5000 atoms structures has a smoother curve and tends to a medium final value.

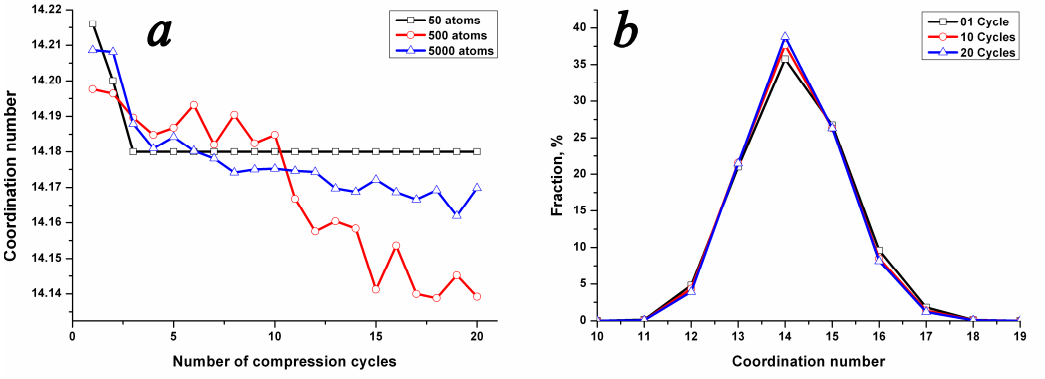

Figure 3.1.10: (a) Coordination number for 3 kinds of systems and (b) coordination number distribution of the "5000 atoms" systems for different number of compression cycles.

The coordination number distribution Figure 10 (b) shows minor changes during the compression. The limits of the distribution do not change and remains between 11 and 18 atoms. The probability of an atom to have 14 neighbors grows from 35 to about 39 percent during 20 compression cycles. Configurations of 13 nearest atoms have almost the same frequency and the percentage of all other structures decreases with the number of cycles. This shows that all atoms independent of the actual coordination number tend to have 14 closest neighbors.

3.6.4 Polyhedra analysis

Polyhedra distribution analysis of the 5000 atom systems after 20 compression cycles has yielded 900 different types of polyhedra. 23 of them have percentages of more than 1 % and can be assumed as major configurations listed in the Table 3.4. The total fraction of the major polyhedra amounts to ~63.53 does not change essentially during compression, but the individual concentrations undergo changes. Figure 3.11

shows fractions of 29 major polyhedra found after the first cycle depending on the compression cycle number.

Table 3.4: 23 Major polyhedra with corresponding percentages (> 1%) of the 5000 atoms samples after 20 compression cycles.

Type of polyhedron	Av. local density	Percentage, %
(0, 4, 4, 6)	0.6568	7.7
(0, 3, 6, 4)	0.6629	7.64
(0, 3, 6, 5)	0.6537	7.35
(0, 2, 8, 4)	0.6492	5.91
(0, 1, 10, 2)	0.664	3.5
(0, 3, 6, 6)	0.6389	3.48
(0, 4, 4, 7)	0.6477	3.38
(1, 3, 4, 5, 1)	0.6514	2.81
(0, 2, 8, 3)	0.6644	2.29
(0, 2, 8, 5)	0.6285	1.98
(1, 3, 5, 4, 2)	0.6388	1.9
(0, 4, 4, 5)	0.6632	1.66
(0, 2, 8, 2)	0.6751	1.47
(1, 4, 3, 5, 2)	0.6427	1.46
(0, 1, 10, 3)	0.6412	1.38
(1, 1, 8, 3, 1)	0.6511	1.33
(1, 3, 5, 3, 2)	0.6487	1.32
(1, 2, 6, 4, 1)	0.6506	1.27
(1, 2, 6, 3, 1)	0.6647	1.26
(1, 3, 4, 6, 1)	0.6414	1.23
(0, 0, 12)	0.6891	1.13
(1, 2, 7, 2, 2)	0.6518	1.06
(1, 2, 6, 5, 1)	0.637	1.02

After 20 compression cycles the polyhedra (0, 3, 6, 4), (0, 2, 8, 4), (0, 3, 6, 5) and (0, 4, 4, 6) still occupy the first 4 places, but their sequence has changed. The percentage of (0, 4, 4, 6) rapidly increases from 4.5 to 7.7% during compression and this polyhedron becomes the most widely distributed one. The second biggest change was observed for the concentration of (0, 3, 6, 4), which is increasing from 6.27 up to 7.64%. All other percentages do not change much and stay at roughly the same level. Figure 3.11 confirms this observation and shows a strong difference of about 2 percent between the first 4 and all other major polyhedra.

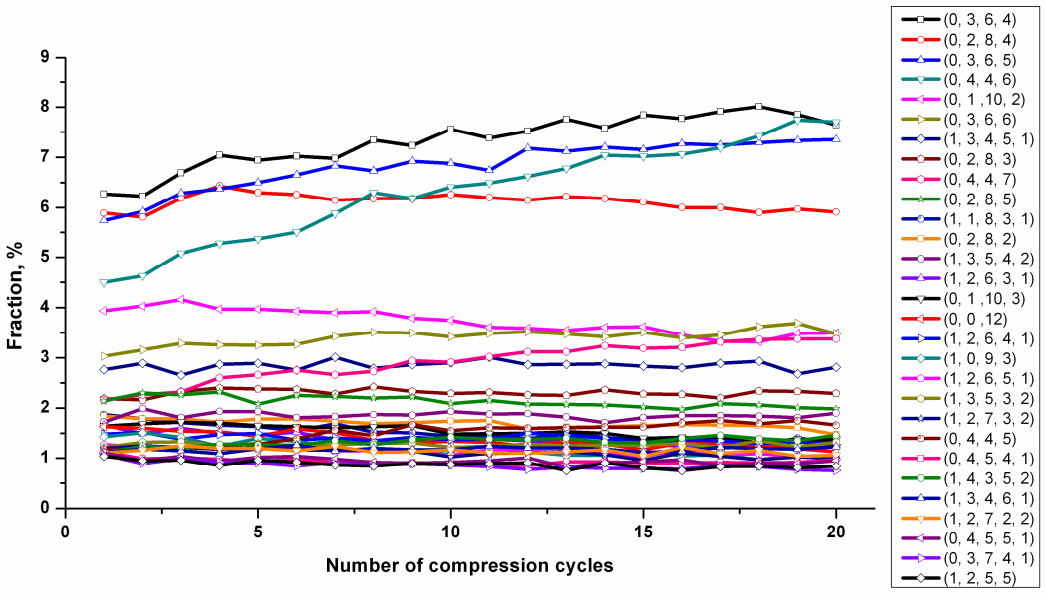

Figure 3.11: Fraction of 29 major polyhedra depending on the step number.

The average density of polyhedra undergoes only minor changes of less than 1 % and the densest polyhedron is always the dodecahedron (0, 0, 12). That kind of behavior indicates stability and completeness as well as small relaxation of individual polyhedra and the whole structure of simulated monatomic samples.

In comparison to the average density of polyhedra the density distribution has a stronger dependence on the number of the compression cycles. Figure 3.12 presents density distributions of 4 major polyhedra and the dodecahedron. The density distributions of (0, 3, 6, 4), (0, 3, 6, 5) and (0, 4, 4, 6) have a similar behavior during compression: the right side of the distribution is shifted to greater densities and the maximum becomes bigger, especially for the polyhedron (0, 4, 4, 6). The density distribution of the (0, 2, 8, 4) as of (0, 0, 12) hardly change. In the latter case the summit of the maxima becomes broader and lower representing a wide region of stability of the icosahedral short-range order and configurational indeterminateness of this polyhedron in monatomic systems. It is directly related to the fact, that the radii ratios of 1.099 (small atom is inside) is needed to get a stable icosahedron.

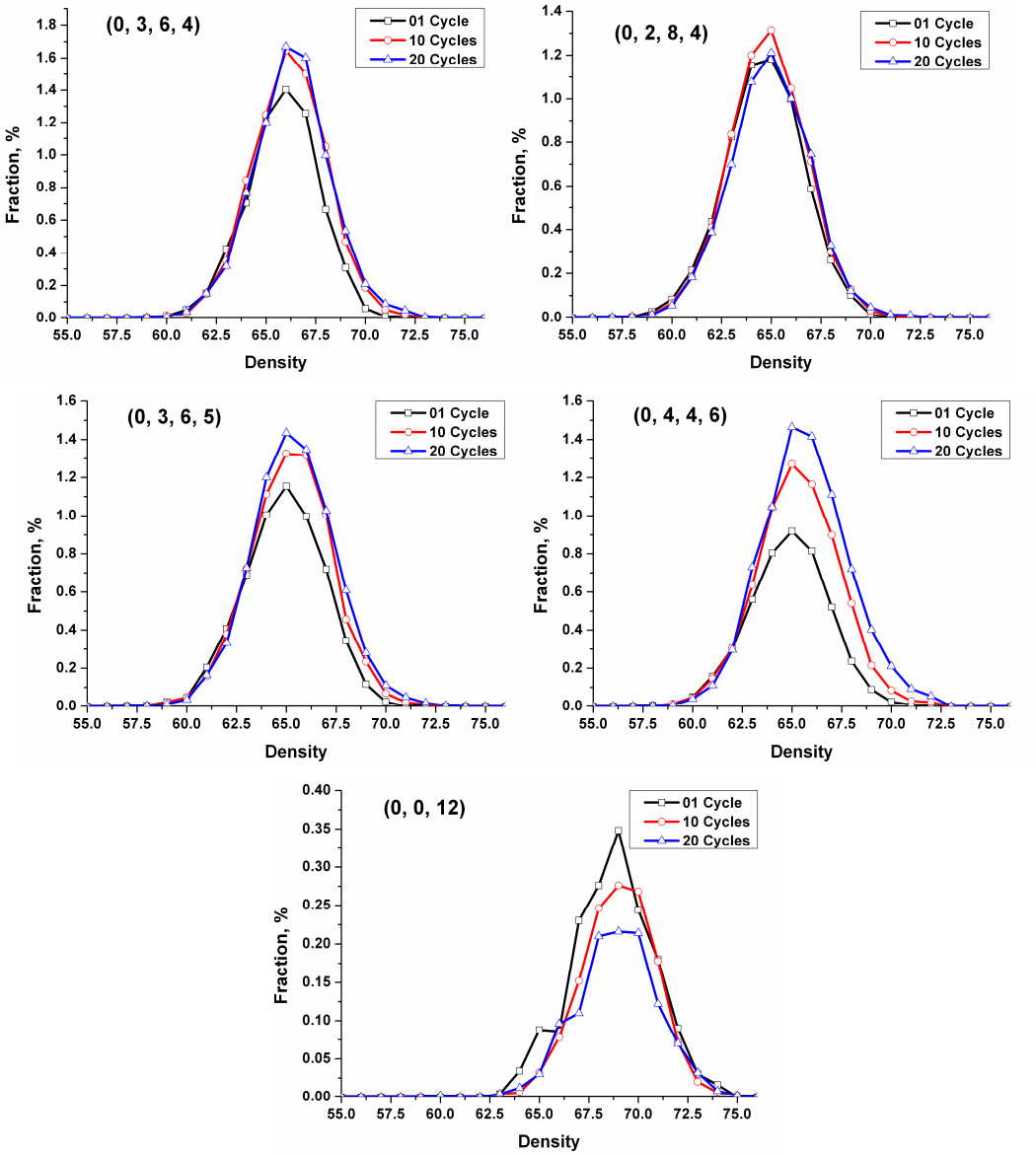

Figure 3.12: Density distribution of 5 major polyhedra depending on the compression cycle number.

3.6.5 Non-crystalline to crystalline faces ratio

Parameter F_{nc} shows a strong dependence on the compression cycle number, see Figure 3.13(a). It decreases from about 0.96 to 0.86 during 20 compression cycles, what indicates the instability of the amorphous state in monatomic structures. Such a

behavior coincides with experimental results. For instance, pure nickel requests cooling rates of ~10^{10} [Lu02] and is very unstable in the amorphous form. Therefore, pure elements/monatomic systems are unstable in the amorphous state and have a very strong tendency towards crystallization.

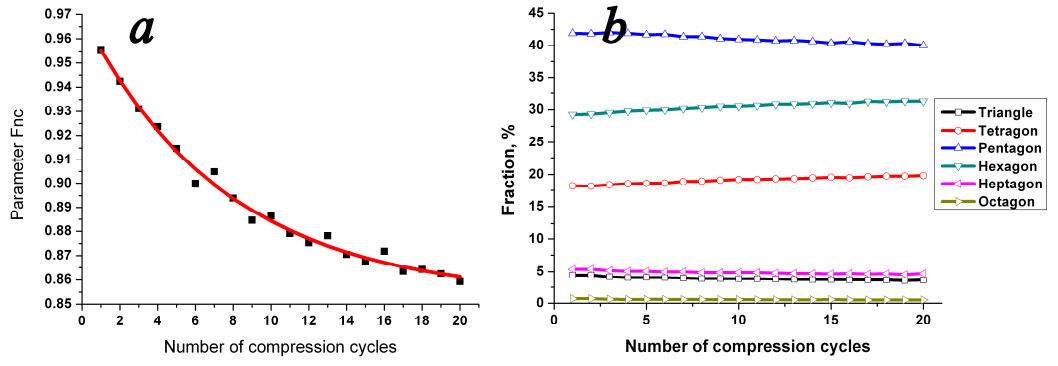

Figure 3.13: Dependence of (a) parameter F_{nc} and corresponding exponential fitting, (b) percentages of different polygons on the number of compression cycles.

The data points in Figure 3.13(a) can be very well fitted by the same exponential function as used in Section 3.6.1: $F_{nc} = 0.85267 + 0.11698 \exp(-0.13071x)$. The $adj.R^2$ is 0.98951 and indicates the validity of the chosen function. The approaching value of about 0.85 corresponds to the minimal values of the parameter F_{nc} without crystallization of the structure. This results coincide with the observation that the systems of 500 atoms have a downward winding of the parameter F_{nc} (data not shown) after the value of about 0.848 is crossed downwards.

After 20 compression cycles the parameter F_{nc} has a linear descending dependence reflecting crystallization of the sample.

The fractions of the individual polygons do not undergo noticeable changes during the first 20 compression cycles. Quantities of triangles and heptagons (7 edges) have similar values of about 4-5 % and similar slightly decreasing curves. The amount of pentagons also diminishes from 42 to 40 %. The percentages of tetragons and

hexagons have an opposite behavior and increase by about 2 %. The quantity of octagons stays at the same level of ~ 0.6%.

CHAPTER 4
BINARY AMORPHOUS MATERIALS

This chapter summarizes results for binary mixtures of hard spheres simulated using the force-based algorithm of Jodrey and Tory. A good convergence of results was received through the averaging of 20 identical mixtures consisting of 5000 spheres each. Thus, the total number of spheres in a system amounts to 100000; it accords to a particle of about 15 nm in a real structure. The periodic boundary conditions were applied.

Depending on the size all spheres have an index 1 or 2: 1 marks small spheres and 2 – big ones. The mixture composition is commonly presented by the fraction of small spheres in the range $C_1 = 0...100\%$, and the radii ratio was limited to $R_2 / R_1 = 1.0...2.0$, since almost all real alloys have their radii ratios in this region.

Each simulated structure was analyzed by means of Laguerre tessellation, RDF etc. and all results were averaged over 20 identical mixtures.

Results for mixtures with $C_1 = 0,\ 100\%$ and/or $R_2 / R_1 = 1.0$ are taken from the previous chapter for monatomic mixtures.

4.1 Density

Figure 4.1 presents the density, η, of the binary mixtures depending on the radii ratio, R_2 / R_1, and the concentration of small atoms, C_1. As it can be seen, the density has only one extreme value and shows monotone dependence on the radii ratio. The position of the maximum density drifts from 50 to 80% of small atoms with the radii ratio increasing from 1.1 to 2.0; and the maximum value of the density reaches ~0.675 in the latter case. That is in a very good agreement with results of Clark and Wiley [Cla87]. They found the maximum value of about 0.68 for the system with radii ratio of

2.0 and 80 % of small atoms. Their results also indicate the shifting of the maximum to larger concentration of small atoms.

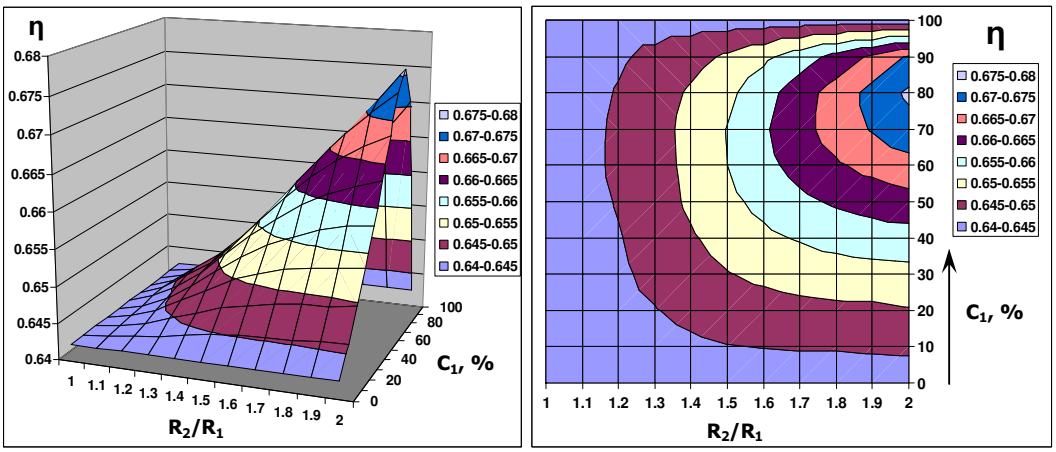

Figure 4.1: Density, η, of binary hard-sphere mixtures depending on radii ratio, R_2 / R_1, and concentration of small atoms, C_1.

The limiting value of the density in the binary system of hard spheres corresponds to the radii ratio approaching infinity. The resulting structure looks like a dense packing of the big spheres in which all holes are filled up with the small spheres having the same dense packing. If the packing density of the big and, accordingly, small spheres is η, the total density of the structure can be estimated as $\eta_{Total} = \eta + \eta(1-\eta)$. In the case of FCC and HCP structures ($\eta = \pi / \sqrt{18}$) the limiting density value amounts to ~0.93265 and is the densest possible structure. For the densest possible amorphous structure of a binary systems the density amounts to $\eta_{Total} \approx 0.875$. However such structures are unachievable in real alloys.

Park has found a maximum density of Cu-Zr systems for $Cu_{65}Zr_{35}$ composition [Par07]. He also found, that this composition possess minimal plastic strain, maximal values of Young's modulus and yield strength as well as maximal crystallization temperature of amorphous ingots. On other hand high density reduces diffusion and increases viscosity, what in its turn reduces nucleation and crystal grow favoring amorphization.

Aforesaid emphasizes the role of the density in the glass-forming ability.

According to extrapolation from the Figure 4.1 the mixture conforming to the maximum density of CuZr system ($R_2 / R_1 = 1.25$ [Par07]) is situated by $C_1 = 65\%$. That is in a very good agreement with Park's results.

Figure 4.2 shows the values of the partial local packing fractions for small, η_1, and big, η_2, spheres depending on radii ratio and concentration of small atoms. The partial local packing density is defined by the sphere volume divided by the volume of the corresponding Laguerre cell. The local packing fractions are determined as the ratio between volume of polyhedron and volume of the corresponding atom inside the polyhedron. The behavior of local densities is monotonous for both types of spheres. The big spheres being surrounded by the small ones become appreciable denser with increasing radii ratio and fraction of small spheres. Their density are about 79 % at the point (R_2 / R_1, C_1) = (2.0, 90%). On the other hand the small spheres do not get enough neighbors and their first coordination spheres gradually lose "kissing" spheres. Therefore, the density decreases to about 45 % when the system approaches the point (R_2 / R_1, C_1) = (2.0, 10%).

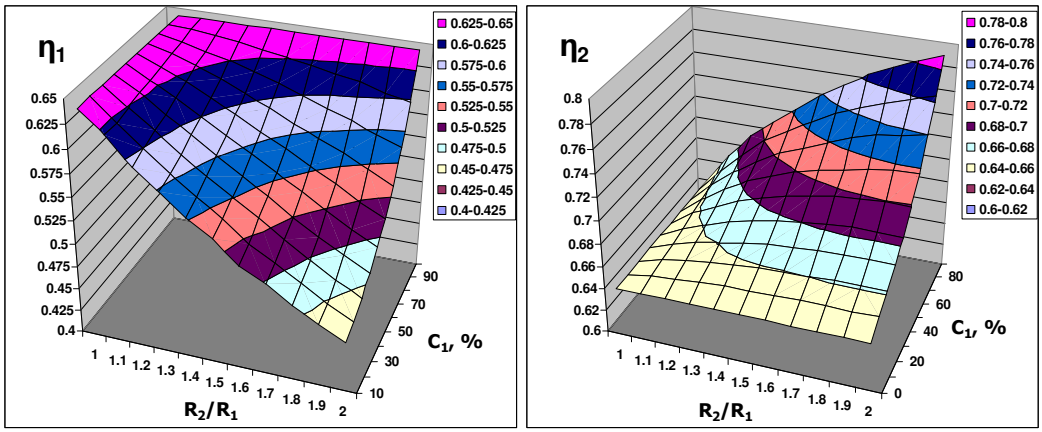

Figure 4.2: Partial local packing fractions of small, η_1, and big, η_2, spheres vs. radii ratio, R_2 / R_1, and concentration of small atoms, C_1.

4.2 Radial distribution function

The radial distribution functions of the mixtures with radii ratio of $R_2 / R_1 = 1.5$ are shown in Figure 4.3 depending on the concentration of small atoms, C_1. The RDF's of all other simulated binary systems can be found in the Appendix A4.1.

Increasing fraction of small atoms, C_1, leads to the structural changes. The amount of contacting similar atoms changes proportional to the concentration of atoms. Therefore, with the increasing of the small atoms concentration, the peaks corresponding to the contacts of small-to-small spheres (2.0, 3.5 and 4.0) are growing up and the big-to-big peaks (3.0, 5.2 and 6.0) are vanishing. The big-to-small and small-to-big peaks (2.5, 4.8) have maximum intensity by 50 % of small atoms.

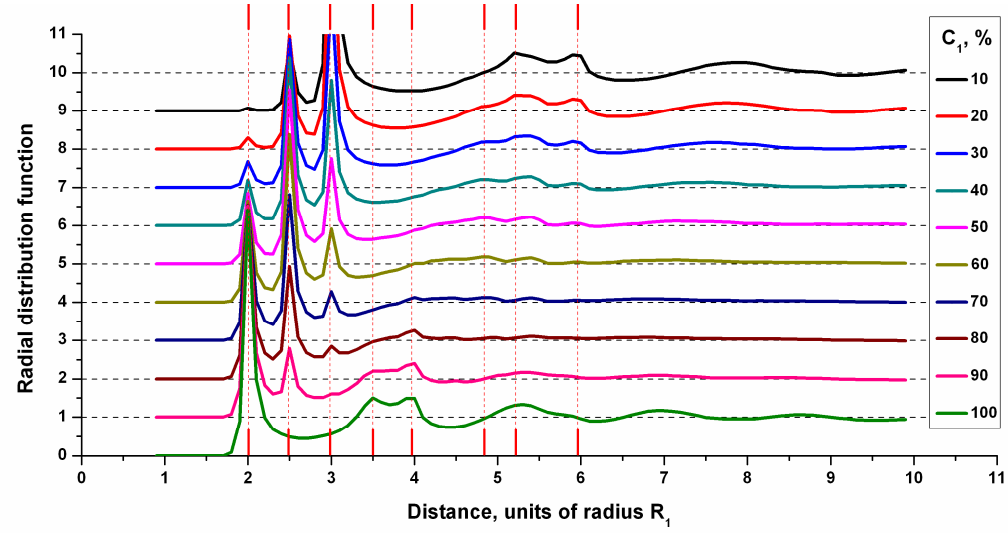

Figure 4.3: Radial distribution functions of the system with radii ratio, R_2 / R_1, of 1.5 depending on the concentration of small atoms, C_1.

All radial distribution functions show a gradual dependence on the concentration of small atoms, C_1, and radii ratio, R_2 / R_1, and indicate no abrupt structure changes (see also Appendix A4.1). The medium-range order has the interesting feature that at medium concentrations of small atoms (especially by 70 and 80%) the radial

distribution functions points to the minimum of the medium-range order. This is reflected by the property that the radial distribution becomes constant at a distance of about 4.5 for the composition mentioned while for all other compositions peaks appear at higher distances. Other binary systems as well as monatomic mixtures possess an appreciable degree of medium-range order, what is indicated by the presence of significant diffuse peaks of the radial distribution functions.

As it can be seen from the figures in Appendix A4.1, this effect appears by the radii ratios of 1.3 and becomes more obvious with increasing radii ratio.

Other radial distribution functions of binary systems presented in the Appendix A4.1 have a similar behavior.

4.3 Coordination numbers

Total coordination numbers for small, CN_1, and big, CN_2, spheres of binary mixtures of hard spheres depending on radii ratio, R_2 / R_1, and concentration of small atoms, C_1, are shown in Figure 4.4. Other coordination numbers are situated in the Appendix A4.2.

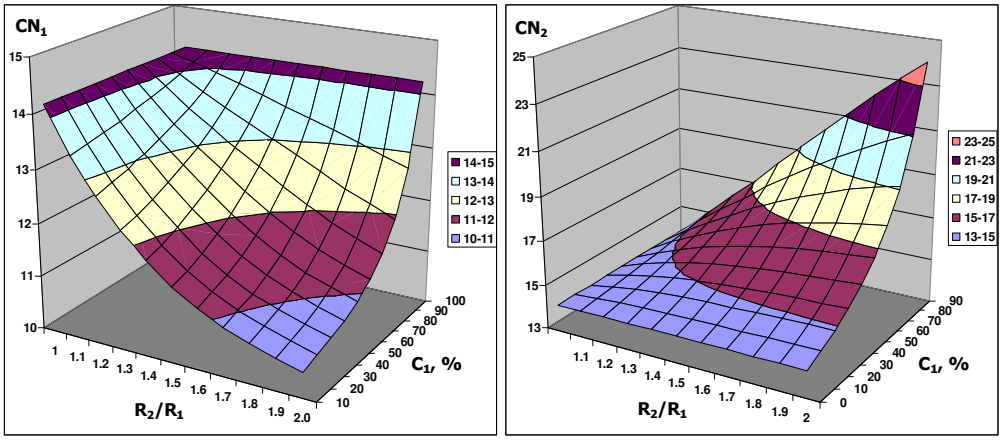

Figure 4.4: Total coordination numbers of small, CN_1, and big, CN_2, spheres of binary hard spheres mixtures depending on radii ratio, R_2 / R_1, and concentration of small atoms, C_1.

Coordination numbers have a strong faired concentration and radii ratio dependence without any leaps. The coordination number of small spheres, CN_1, decreases from 14.21 (monatomic mixtures) to about 10.47 ($R_2/R_1 = 2.0$ and $C_1 = 10\%$) with increasing radii ratio and reduction of small atoms fraction. The coordination number of big spheres, CN_2, also has monotone but increasing behavior; it grows from 14.21 (monatomic system) to about 23.99 ($R_2/R_1 = 2.0$, $C_1 = 10\%$) with increasing radii ratio and percentage of small atoms.

Partial coordination numbers ($CN_{1-1}, CN_{1-2}, CN_{2-1}$ and CN_{2-2}) also depend strongly on the composition and do not show any extrema (see also Appendix A4.2).

4.4 Polyhedra analysis

The common polyhedra analysis of all simulated mixtures has shown the presence of about 1400 up to 2000 and more (depending on composition) different polyhedron types. 41 polyhedra were found to have a percentage of more than 1% at least at one point of the raster $C_1 = 0...100\%$ and $R_2/R_1 = 1.0...2.0$ with the steps 10% and 0.1, respectively. These polyhedra are grouped according to the topological affinity and listed in Table 4.1.

The amount of all polyhedra typical for crystalline structures has a maximum value of 0.18 % in the monatomic parts of raster ($R_2/R_1 = 1.0$ and/or $C_1 = 0,\ 100\%$) and decreases with increasing polydispersity. The percentage of crystalline polyhedra amounts to about 0 to 0.12 % at $R_2/R_1 = 2.0$ depending on the concentration of small atoms, C_1.

Table 4.1 shows that the major polyhedra can be divided into 12 common groups according to the topological affinity. The two most frequent major polyhedra groups are (0, 2, 8, x) and (0, 3, 6, x); their percentages are presented in Figure 4.5 depending on radii ratio and concentration of small atoms. These three distributions decrease with increasing polydispersity in the system. The (0, 3, 6, x) group has a monotone

Table 4.1: Major polyhedra of binary hard sphere mixtures with fractions of more than 1% at least at one point of the raster. New polyhedra (in comparison to monatomic system) marked by red color.

Polyhedron	CN	Polyhedron	CN	Polyhedron	CN	Polyhedron	CN
(0, 1, 10, x)		**(0, 3, 6, x)**		**(0, 4, 5, x, 1)**		**(1, 3, 4, x, 1)**	
(0, 1, 10, 2)	13	(0, 3, 6, 3)	12	(0, 4, 5, 4, 1)	14	(1, 3, 4, 4, 1)	13
(0, 1, 10, 3)	14	(0, 3, 6, 4)	13	(0, 4, 5, 5, 1)	15	(1, 3, 4, 5, 1)	14
(0, 1, 10, 4)	15	(0, 3, 6, 5)	14			(1, 3, 4, 6, 1)	15
(0, 1, 10, 5)	16	(0, 3, 6, 6)	15	**(1, 2, 5, x)**			
		(0, 3, 6, 7)	16	(1, 2, 5, 4)	12	**(1, 3, 5, x, 2)**	
(0, 2, 8, x)				(1, 2, 5, 5)	13	(1, 3, 5, 2, 2)	13
(0, 2, 8, 1)	11	**(0, 3, 7, x, 1)**				(1, 3, 5, 3, 2)	14
(0, 2, 8, 2)	12	(0, 3, 7, 4, 1)	15	**(1, 2, 6, x, 1)**		(1, 3, 5, 4, 2)	15
(0, 2, 8, 3)	13	(0, 3, 7, 5, 1)	16	(1, 2, 6, 2, 1)	12		
(0, 2, 8, 4)	14			(1, 2, 6, 3, 1)	13	**(x, x, x, x)**	
(0, 2, 8, 5)	15	**(0, 4, 4, x)**		(1, 2, 6, 4, 1)	14	(0, 0, 12)	12
(0, 2, 8, 6)	16	(0, 4, 4, 4)	12	(1, 2, 6, 5, 1)	15	(1, 4, 3, 5, 2)	15
		(0, 4, 4, 5)	13			(1, 0, 9, 3)	13
		(0, 4, 4, 6)	14	**(1, 2, 7, x, 2)**		(1, 1, 8, 3, 1)	14
		(0, 4, 4, 7)	15	(1, 2, 7, 2, 2)	14		
				(1, 2, 7, 3, 2)	15		

distribution without any extrema in contrast to the (0, 2, 8, x) group which has a broad maximum with a fraction of about 15 % in the range $R_2 / R_1 = 1.1...1.3$ and $C_1 = 20...80\%$.

The most famous and mysterious structural element of amorphous materials is the (0, 0, 12) polyhedron. Bernal called it “clue to the whole geometry of irregular or liquid structures” [Ber64]. There are many discussions in the literature, if amorphous state is connected to this polyhedron or not [Mat09, Lek07].

It is historically established that Polyhedron (0, 0, 12) is sometimes called icosahedron, but it is delusion. In fact, the name of this polyhedron is dodecahedron (pentagon dodecahedron), since it consists of 12 pentagons. Dodecahedron is a reciprocal figure for icosahedron and it corresponds to the icosahedral short-range order.

Fraction of dodecahedra shows a strong dependence on polydispersity. The distribution has a strong maximum with a top at (R_2 / R_1, C_1) = (1.3, 80%), and the

whole preferred region for the building of (0, 0, 12) spreads between radii ratios, R_2 / R_1, of about 1.1 to 1.6 and 50 to 90% of small atoms, C_1, (pigment indigo area).

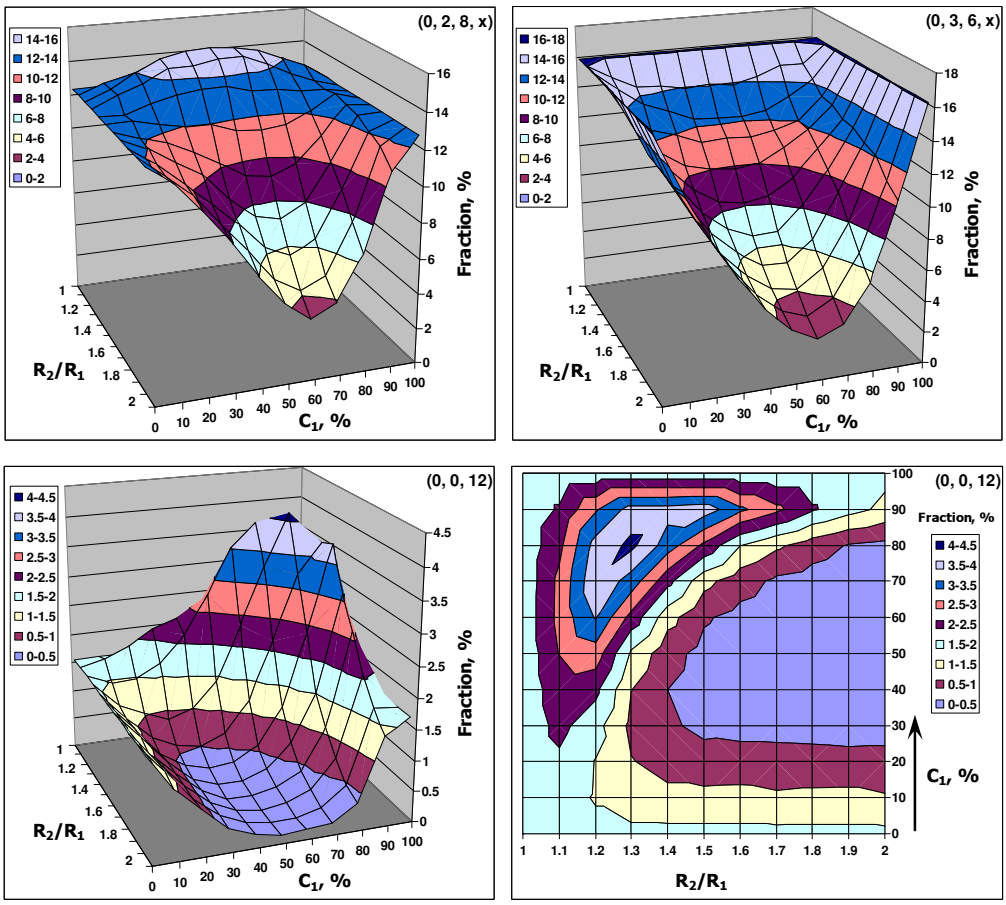

Figure 4.5: Fractions of the 2 most frequent major polyhedra groups (0, 2, 8, x), (0, 3, 6, x) and dodecahedron (0, 0, 12) vs. radii ratio, R_2 / R_1, and concentration of small atoms, C_1.

The maximum fraction of about 4.1% means that at this point up to about 50 % of atoms are involved into icosahedral short-range order.

By medium concentrations of small atoms when the radii ratio exceeds 1.5 (blue-violet area) fraction of dodecahedra becomes almost negligible.

The percentages of other major polyhedra groups are presented in the Appendix A4.3.

4.5 Non-crystalline to crystalline faces ratio

The dependence of the non-crystalline to crystalline polyhedra faces ratio, F_{nc}, on radii ratio, R_2 / R_1, and concentration of small atoms, C_1, is presented in Figure 4.6. Parameter F_{nc} shows a great variety. The maximum value of about 1.09 appears at the mixture (R_2 / R_1, C_1) = (1.3, 80%). After the radii ratio exceeds about 1.5, F_{nc} rapidly decreases.

The distributions of separated polygons are presented in Appendix A4.4. Pentagons have the absolute numerical superiority (⅓ to ½ of the total amount) and contribute essentially to the F_{nc} parameter. An interesting feature is that the amount of pentagons and hexagons decreases during the polydispersity increases, while all other polygons occur more frequently. The total fraction of nonagons, decagons and other high polygonal figures does not exceed the value of 0.15 % for all shown concentration and radii ratio ranges.

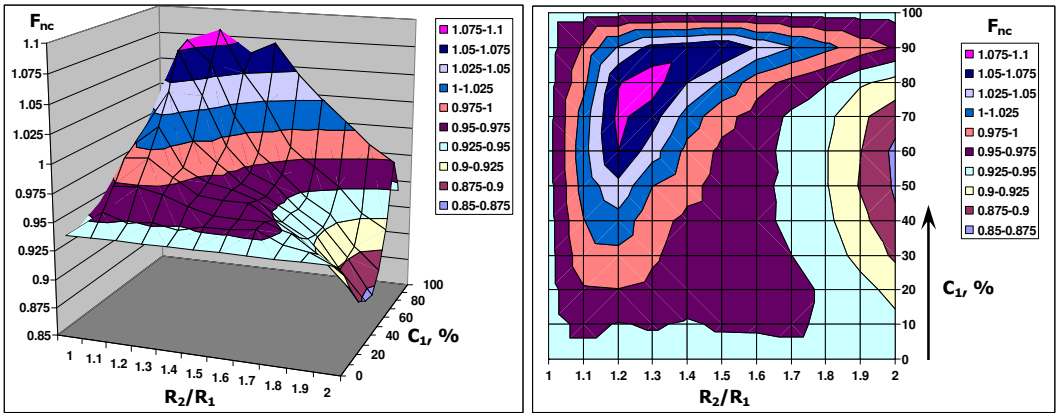

Figure 4.6: F_{nc} vs. concentration of small atoms, C_1, and radii ratio, R_2 / R_1, in binary systems.

4.6 Partial correlations

Figure 4.7 shows density–density correlation functions at selected positions on the trajectories $R_2 / R_1 = 1.3$ and $C_1 = 80\%$, labeled as T_1 and T_2, respectively.

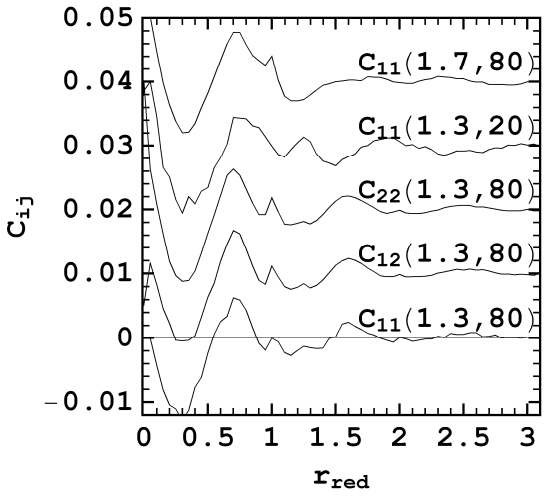

Figure 4.7: Partial density-density correlation functions, $C_{ij}(r_{red})$, for parameter values on three different positions of trajectories T_1 and T_2; $r_{red} = r - (R_i + R_j)$. The $C_{ij}(r_{red})$ curves are shifted on the ordinate by $\langle \rho \rangle^2$ plus a multiple of 0.01.

The three partial correlation functions of the system with the maximum value of F_{nc} show the same behavior. The comparison of C_{11} (small-to-small) of the two systems (R_2 / R_1, C_1) = (1.3, 80%) and (1.3, 20%) shows differences in the subpeak at $r_{red} = 1$ which changes from a peak to a shoulder of the main peak situated at $r_{red} = 0.7$ when the fraction of small spheres is reduced by the factor of 4. Simultaneously, the peak at $r_{red} = 1.3$ increases considerably due to the enhanced number of big spheres ($R_2 / R_1 = 1.3$). There are also remarkable differences at $r_{red} > 1.5$. However, the changes of the correlation functions along trajectory T_1 are monotonous. The same is true for the changes of the correlation function along T_2 illustrated by C_{11} of the two systems

(R_2/R_1, C_1) = (1.3, 80%) and (1.7, 80%) in Figure 4.7. It should be noted that the present results are valid for non-crystalline systems with high packing fractions. Different effects can be observed at lower packing fractions. For example, recent studies of binary mixtures of colloidal hard spheres showed dramatic changes of density fluctuations [Eck02] and a marked change of the dominant wavelength in the pair-correlation function [Bau07].

4.7 Compression tests

This part discusses results of the multiple compression tests of the binary hard spheres mixtures in the whole range of concentrations, C_1, and radii ratios, R_2/R_1, limited to 2.0. In order to get an acceptable statistics for each point of the (R_2/R_1, C_1) raster 10 samples with identical parameters were simulated and compressed. The final results were averaged over these 10 samples. Behavior of the samples during densification was found to be very similar to monatomic liquids. Thus, in compliance with the Section 3.6 number of compression cycles was limited to 20, preventing crystallization of the samples.

4.7.1 Density

Behavior of the density for each point on the raster $R_2/R_1 = (1.0,\ 1.1,\ \ldots\ 2.0)$ and $C_1 = (0,\ 10,\ \ldots 100\%)$ was investigated in a similar way as in Section 3.6. Fitting by the exponential function $y = y_0 + a\exp(bx)$ yields in this case $adj.\,R^2$ in the range from 0.95 to 0.99 with an average value of 0.98 without any evidences of the dependence on radii ratio, R_2/R_1, or fraction of small spheres, C_1. Thus, the chosen fitting function is a good approximation for the behavior of the density in a binary system undergoing step-by-step compression.

The constant b amounts to -0.249, this value is slightly lower than for the monatomic system. The dependence of the parameters $y_0(\eta)$ and $a(\eta)$ on the radii

ratio, R_2/R_1, and concentration of small atoms, C_1, is shown in Figure 4.8. The maximum attainable density without crystallization, $y_0(\eta)$, is not monotonous and shows a broad maximum at the radii ratio of 1.3 and the concentration of small atoms in the range 30 to 90 %. This behavior differs from the density shown in the Figure 4.1. The compression quasi-velocity, $a(\eta)$, is negative in the whole range of concentrations and radii ratios and is related to the value of the density.

According to aforesaid about influence of the density on the glass-forming ability the region of the "new" maximum of the density at $R_2/R_1 = 1.3$ should allocate good binary glass formers. As it will be shown later, there are a big number of real binary metallic (metal-metal) glasses situated on this maximum and having the critical thickness of 1mm and more.

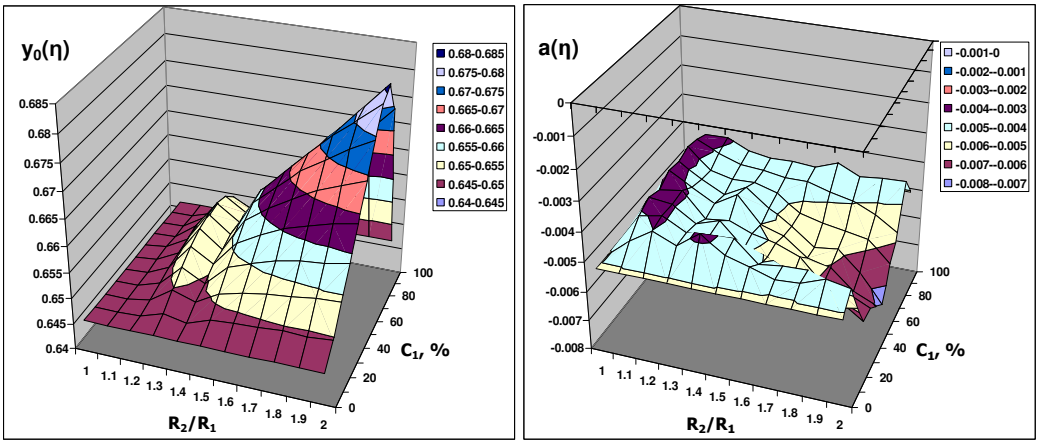

Figure 4.8: Maximal attainable density, $y_0(\eta)$, and quasi-velocity, $a(\eta)$, of the exponential fitting $y = y_0 + a\exp(bx)$ of the density, η, change upon multiple compression depending on coordination of small, C_1, atoms and radii ratio, R_2/R_1.

4.7.2 Coordination numbers

During the multiple-compression tests the coordination numbers, CN, undergo minor changes. Figure 4.9 shows differences in the coordination numbers between the

first and the last (20th) compression cycles for small, $CN_1^{1st} - CN_1^{20th}$, and big, $CN_2^{1st} - CN_2^{20th}$, spheres. Due to high degree of fluctuations and low differences they were averaged over concentrations, C_1, Figure 4.9 (a) and radii ratios, R_2 / R_1, Figure 4.9 (b). Monotone behavior of coordination numbers allows such averaging.

Both coordination numbers do not differ in more than about 0.12. Since the difference $CN_1^{1st} - CN_1^{20th}$ (blue lines) is positive, the coordination number of small atoms, CN_1, decreases in the whole range of concentrations and radii ratios. The maximum difference of coordination numbers for small spheres $CN_1^{1st} - CN_1^{20th}$ is located at the point (R_2 / R_1, C_1) = (~1.8, ~50%), since blue curves have maxima at these values.

The difference $CN_2^{1st} - CN_2^{20th}$ (red lines) of the coordination numbers of big spheres does not show any extreme values. Up to the radii ratio of 1.5 and 50 % of small atoms the difference $CN_2^{1st} - CN_2^{20th}$ is positive and represents the decreasing of the coordination number for big spheres during compression. This tendency changes to the opposite when the radii ratio, R_2 / R_1, of 1.5 is overstepped or concentration of small atoms, C_1, is higher than 50 %. In this case average coordination number of big spheres decreases during compression.

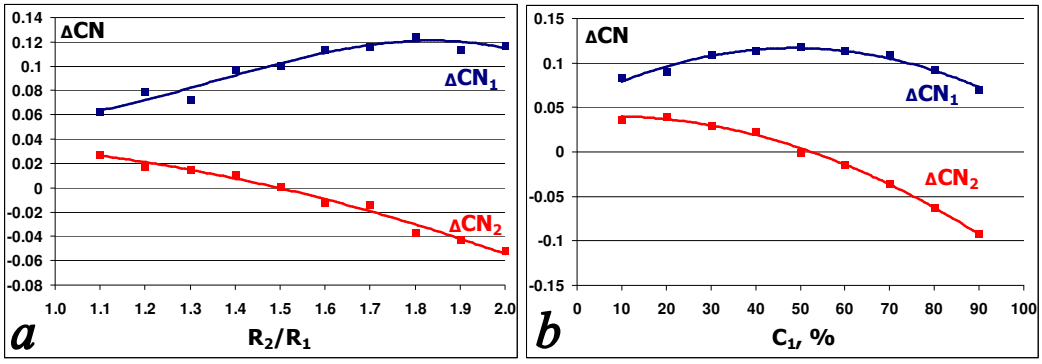

Figure 4.9: Differences of coordination number between 1st and 20th steps of compression for small, $\Delta CN_1 = CN_1^{1st} - CN_1^{20th}$, and big, $\Delta CN_2 = CN_2^{1st} - CN_2^{20th}$, spheres averaged over concentrations (a) and radii ratios (b).

4.7.3 Non-crystalline to crystalline faces ratio

The behavior of the parameter F_{nc} for each point on the raster $R_2 / R_1 = (1.0,\ 1.1,\ \ldots\ 2.0)$ and $C_1 = (0,\ 10,\ \ldots 100\%)$ was investigated in the same way as in Section 3.6. Parameters y_0 and a of the exponential fitting $y = y_0 + a\exp(bx)$ of the non-crystalline to crystalline faces ratio, F_{nc}, upon multiple-compression depending on coordination of small atoms, C_1, and radii ratio, R_2 / R_1, are shown in Figure 4.10. The average $adj.R^2$ amounts to 0.8312 and also does not show evidence of the dependence neither on radii ratio nor on concentration.

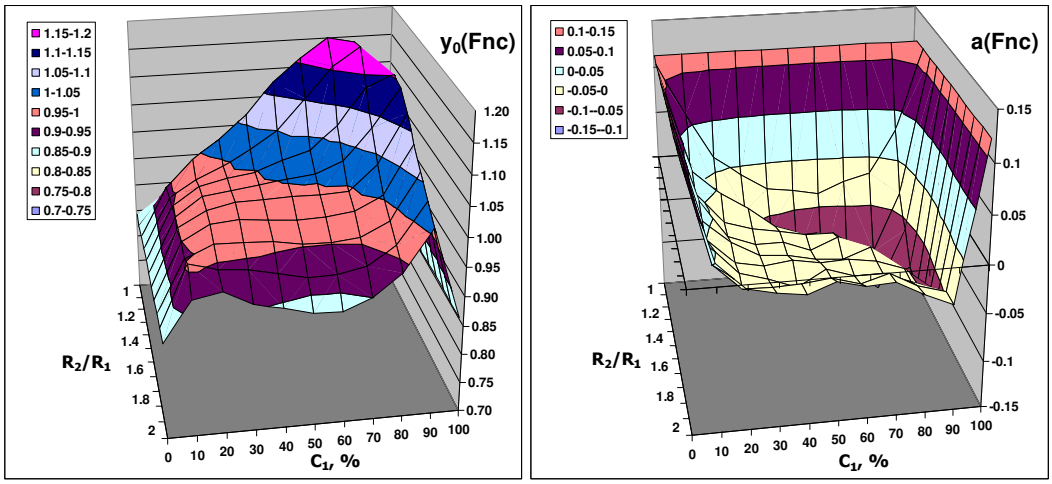

Figure 4.10: Parameters $y_0(F_{nc})$ and $a(F_{nc})$ of the exponential fitting $y = y_0 + a\exp(bx)$ for non-crystalline to crystalline faces ratio, F_{nc}, upon multiple-compression depending on fraction of small atoms, C_1, and radii ratio, R_2 / R_1.

The maximum reachable value, $y_0(F_{nc})$, of the parameter F_{nc} has a very similar form to the parameter F_{nc} itself, but the distribution range of the first one is broader and extends from (0.869, 1.088) to (0.853, 1.189) for the second one. The low regions become lower and the high ones become higher. The separation plane lies by the zero value of the parameter $a(F_{nc})$.

Parameter $a(F_{nc})$ indicates a tendency of the non-crystalline to crystalline faces ratio during compression. If $a(F_{nc})$ is positive, the system tends to a crystalline state; and *vice versa* in the case of negative parameter $a(F_{nc})$ the system increases its amount of non-crystalline faces during compression. The magnitude of these changes is proportional to the absolute value of the parameter $a(F_{nc})$.

Both surfaces have extrema in the area of 70 to 80 % of small atoms and radii ratio of 1.2 to 1.3 what makes this region attractive for reducing the trend of crystallization and accordingly enhancing of the glass-forming ability.

4.7.4 "Error tetrahedron" volume

The investigation of the relation between the unoccupied volume (error tetrahedron volume, ΔV_{err}) and number of compression runs was also performed by means of the exponential fitting with the function: $y = y_0 + a\exp(bx)$. The $adj.R^2$ of the fitting ranges between 0.78 and 0.99 and the average value amounts to 0.94 without any dependence on radii ratio, R_2/R_1, or concentration of atoms. Parameter b was found to be the same as for density and non-crystalline to crystalline faces ratio and amounts to -0.249.

Figure 4.11 presents parameters $y_0(\Delta V_{err})$ and $a(\Delta V_{err})$ of the exponential fitting for error tetrahedron volume, ΔV_{err}. In the whole range of concentration of small atoms, C_1, and radii ratios, R_2/R_1, limited to 2.0, parameter $a(\Delta V_{err})$ is positive and indicates a decreasing of the unoccupied volume during compression. This behavior conforms the idea that with the increasing of the density as well as with decreasing of disorder in the system the error tetrahedron volume, ΔV_{err}, shrinks and vanishes when system crystallizes.

The lowest achievable value of the error tetrahedron volume, $y_0(\Delta V_{err})$, without crystallization of the samples has a monotone increasing dependence on the radii ratio, R_2/R_1, and a maximum by 60 to 80 percent of small atoms, C_1. Its value is also

correlated to the parameter $a(\Delta V_{err})$, as well as for the density and for the parameter F_{nc}.

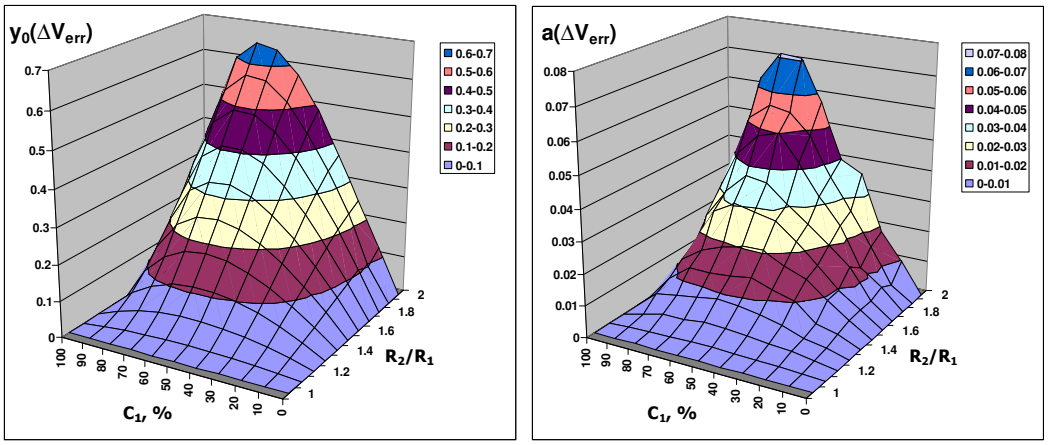

Figure 4.11: Parameters $y_0(\Delta V_{err})$ and $a(\Delta V_{err})$ of the exponential fitting $y = y_0 + a\exp(bx)$ for error tetrahedron volume, ΔV_{err}, upon multiple-compression depending on concentration of small atoms, C_1, and radii ratio, R_2 / R_1.

4.8 Real binary BMG's

In order to prove the validity of the parameter F_{nc}, density and fraction of dodecahedra as parameters responsible for glass-forming ability a number of binary bulk metallic (metal-metal) glasses were collected from literature. The data points in Figure 4.12 marked by capitals A–K denote these glasses listed in Table 4.2. All of these binary alloys have critical thickness of 1 mm and more and are the best binary metal-metal BMGs known up to date. The majority of listed BMGs have their mixing enthalpies up to -20 kJ/mole, except alloys $Zr_{66}Ni_{34}$ (A) and $Nb_{40}Ni_{60}$ (I) with values of about -30 kJ/mole.

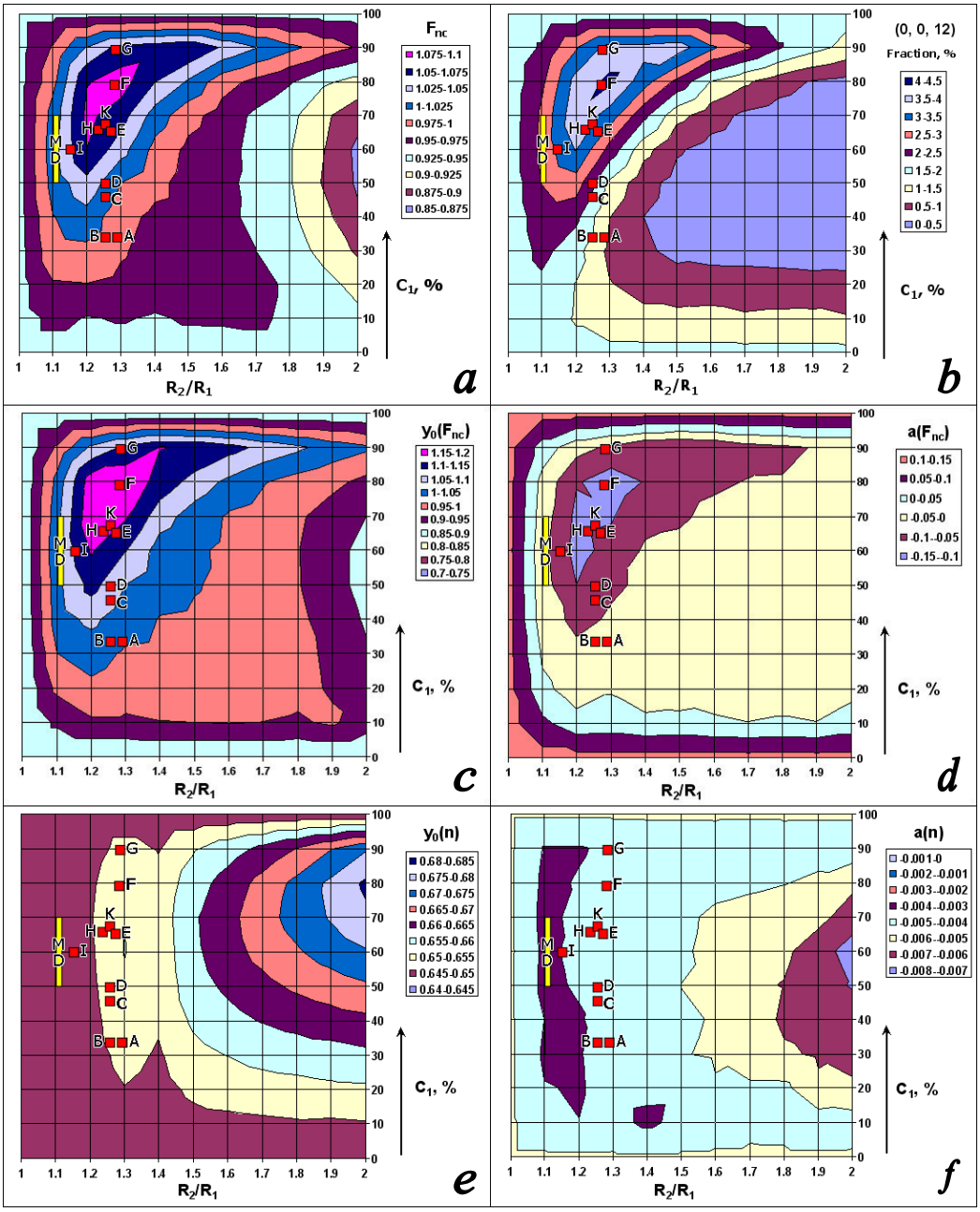

Figure 4.12: Distribution of binary metal-metal glasses relative to atomic size ratio, R_2 / R_1, and fraction of small atoms, C_1, in comparison to (a) parameter F_{nc}; (b) fraction of (0, 0, 12) polyhedron; (c-d) parameters $y_0(F_{nc})$ and $a(F_{nc})$ for the non-crystalline to crystalline faces ratio and (e-f) parameters $y_0(\eta)$, $a(\eta)$ of the density. Red squares represent the alloys listed in the Table 4.2; yellow rectangle displays data from molecular dynamics simulations [Wil08].

Table 4.2: Summary of binary bulk metal-metal glasses with corresponding mixing enthalpies, ΔH_{mix}, and sings in Figure 4.12.

BMG	ΔH_{mix}, kJ/mol	Point
$Zr_{66}Ni_{34}$ [Mat07]	-29.1	A
$Zr_{66}Cu_{34}$ [Mat07]	-11. 1	B
$Zr_{54}Cu_{46}$ [Yua08]	-12.8	C
$Zr_{50}Cu_{50}$ [Dua08]	-13.1	D
$Zr_{36}Cu_{64}$ [Dua08]	-12.7	E
$Zr_{21}Co_{79}$ [Hee00]	-17.0	F
$Zr_{10}Fe_{90}$ [Kau83]	-3.6	G
$Zr_{10}Co_{90}$ [Kau83]	-9.7	G
$Zr_{10}Ni_{90}$ [Kau83]	-14.6	G
$Sn_{35}Cu_{65}$ [Now99]	-4.3	H
$Nb_{40}Ni_{60}$ [Lu07]	-32.7	I
$Hf_{34}Cu_{66}$ [Dua05]	-16.0	K

Almost all real alloys in Figure 4.12 (a) are situated in the $F_{nc} > 1$ region (blue area). This is a region where non-crystalline faces are dominant. Two exceptions (points A and B) are placed very close but outside of this region. In the case of the multiple-compression all these point without exception are enveloped in the $y_0(F_{nc}) > 1$ region (Figure 4.12 (c)) and located at the minimum of the parameter $a(F_{nc})$ (Figure 4.12 (d)). (A comprehensive compilation of metallic glasses can be found in [Lon09].)

Quasi-velocity, $a(F_{nc})$, possesses two different regions separated by $a(F_{nc}) = 0$ curve. The inside region with $a(F_{nc}) < 0$ has tendency to increase fraction of non-crystalline faces and, accordingly, stabilize amorphous state. The outer region with $a(F_{nc}) > 0$ shows tendency towards crystallization and parameter F_{nc} decreases during densification. Position of the $a(F_{nc}) = 0$ boundary lies by radii ratio of about 1.08 - 1.12 and is in a good agreement with empirical 12% rule of Egami and Inoue.

Distribution of real binary metal-metal glasses shows good agreement with parameter F_{nc} and with results of multiple-compression ($y_0(F_{nc})$ and $a(F_{nc})$) as well confirming influence of these parameters on the glass-forming ability.

What is likewise important, all these BMG's are placed in the region of the maximum $y_0(\eta)$ (Figure 4.12 (e)) proving influence of the density on the glass-forming ability.

Parameter $a(\eta)$ has also a maximum but by the radii ratio of about 1.15. This maximum indicates a region where mixtures have the lowest tendency towards densification and is in a good correlation with empirical 12% rule for good glass-forming.

The results obtained in [Wil08] by means of molecular dynamics of binary hard-sphere systems with size ratio of $R_2/R_1 = 1.11$ in the composition range $C_1 = 0.05...1.00$ correspond to the present results though the packing fraction used in [Wil08] was 0.58 (0.643–0.645 in the present study). While the simulations for $C_1 \le 0.3$ and $C_1 \ge 0.825$ readily underwent a large degree of crystallization, for $0.5 \le C_1 \le 0.7$ the crystallization was almost totally suppressed on the time scale of the simulations [Wil08]. The data region corresponding to suppressed crystallization (marked by yellow rectangle) is situated in the $F_{nc} > 1$, $y_0(F_{nc}) > 1$ and $a(F_{nc}) < 0$ regions in Figures 4.12 (a), (c) and (d), respectively.

Using molecular dynamics simulations and Sutton–Chen many-body potentials Lee [Lee03] observed crystallization of binary $Cu_{50}Cu^*_{50}$ samples up to radii ratio of about $R(Cu)/R(Cu^*) \approx 1.053$ and amorphization from this point up to about 1.66. According to [Lee03] further increasing of the size difference causes phase separation in the samples. These results are in agreement with parameters F_{nc} and $y_0(F_{nc})$, since by radii ratios higher than about 1.7 both parameters decrease reflecting stabilization of crystalline state.

The aforesaid suggests that for binary dense random hard-sphere systems there exists a confined region in the size-ratio/concentration parameter range accentuated by an enhanced glass-forming ability. This specific region is determined by the condition

that the probability of finding 5-, 7-, … , -fold local symmetry is higher than that for the 3-, 4- and 6-fold one and by the local maximum of the density without crystallization. Both experimental and computer simulated data points for, respectively, binary metal–metal glasses and non-crystallizing hard-sphere systems as well as for maximum of the density are situated in the specified region. From this one can conclude that geometric aspects are important for the glass-forming ability of binary systems, especially of binary metallic alloys.

Figure 4.12 (b) shows distribution of binary metal-metal glasses in comparison to fraction of (0, 0, 12) polyhedron. It can be seen that real BMGs lie in area of the maximum and outside of the maximum as well and do not show any correlation. Results of simulations from Williams and Lee are also not connected to distribution of (0, 0, 12) polyhedron. Therefore, one can assume that icosahedral short-range order is not related to the glass-forming ability.

On other hand, from the comparison of parameters F_{nc} and $y_0(F_{nc})$ of Figures 4.12 (a, c) with distribution of dodecahedrons in Figure 4.12 (b) one can see some similarities like, for example, the same positions of maxima or similar bended form of maxima. From this comparison it seems clear, that icosahedral short-range order is a consequence of high non-crystallinity of the system and not *vice versa*. From the statistical point of view this relation is logical. Dodecahedron consists of only non-crystalline polygons and increasing of the total non-crystallinity in the systems raises probability to find fully non-crystalline polyhedra.

Thus, parameters F_{nc} and $y_0(F_{nc})$ are general description of the topology and are the ratio of non-crystallinity of the system. Concerning the glass-forming ability these two parameters do not limited to a certain type of short-range order, but envelope all possible atomic configuration on the sort-range order at the same time.

According to the empirical rules of Egami [Ega03] and Inoue [Ino00] negative enthalpy of mixing of the main elements and high atomic size ratio (above 12%) are necessary for good glass-forming ability. The first term refers to the chemical interaction of atoms and is fulfilled in all shown alloys. The second item of the empirical rules for good glass-forming ability of multi-component metallic alloys is related to the present results: the demand for the minimum size ratio of 12%

corresponds quantitatively to the lower bounds of the $F_{nc} > 1$, $y_0(F_{nc}) > 1$ and $a(F_{nc}) < 0$ regions in Figures 4.12 (a, c, d). These results substantiate the supposition that, irrespective of specific electronic properties, geometrical effects contribute essentially to the glass-forming ability of metallic alloys.

The results shown in Figures 4.12 also demonstrate that, from the geometrical point of view, there is also a maximum size ratio for good glass-forming ability of binary hard-sphere mixtures. This ratio depends distinctly from the concentration of small/big spheres as shown in Figures 4.11 (a-c). To our knowledge, the existence of a maximum size ratio for good glass-forming ability has not been discussed until now.

4.9 Probable good glass-formers

Taking into account maxima of parameters F_{nc}, $y_0(F_{nc})$ and $y_0(\eta)$ as well as negative mixing enthalpy, costs, toxicity and some other parameters a number of binary metal-metal systems was selected as hypothetical good glass formers. These systems are listed in the Table 4.3. All of them have the radii ratio of 1.25 to 1.3 and the mixing enthalpy up to -50 kJ/mol for $A_{50}B_{50}$ alloys, what coincide with both theoretical and experimental results.

Analysis of phase diagrams reduced systems listed in Table 4.3 to 6 eutectic or near eutectic alloys: $Al_{80}Y_{20}$, $Cr_{80}Sn_{20}$, $Cu_{70}In_{30}$, $Cu_{75}Nd_{25}$, $Ni_{65}Hf_{35}$ and $Zn_{60}Y_{40}$. All of these alloys are situated on maxima of F_{nc}, $y_0(F_{nc})$, $y_0(\eta)$ and on minima of $a(F_{nc})$, therefore in the region of enhanced glass-forming ability.

It would be also interesting to search for new glass formers by radii ratios of about 1.5 and 80% of small atoms, since both density and non-crystalline to crystalline faces ratio have high values in this area.

Table 4.3: Summary of metal-metal AB systems with radii ratios, R_B / R_A, in the range 1.25 to 1.3 and mixing enthalpies, ΔH_{mix}, for $A_{50}B_{50}$ alloys up to -50 kJ/mol. Radii are taken from [Sen01].

Element *A*	Element *B*	R_B / R_A	ΔH_{mix}, kJ/mol
Al	Y	1.26	-46.38
Co	Cd	1.25	-1.09
Co	Hf	1.26	-34.47
Co	Sn	1.29	-11.52
Cr	Hf	1.26	-9.22
Cr	Sn	1.3	-1.98
Cr	Zr	1.28	-11.98
Cu	In	1.3	-0.5
Cu	Nd	1.28	-20.99
Fe	Hf	1.27	-20.37
Mn	Pb	1.3	-4.77
Ni	Cd	1.26	-5.21
Ni	Hf	1.27	-41.86
Pt	Pb	1.26	-17.97
Zn	Y	1.29	-36.63

CHAPTER 5
TERNARY AND MULTI-COMPONENT AMORPHOUS ALLOYS

Present chapter summarizes results obtained for 3-, 4- and 5-component mixtures of hard-spheres simulated using the force-based algorithm of Jodrey and Tory. Since complexity of structures as well as amount of data strongly depend on number of elements the mixture consist of, only certain results are outlined in the current chapter.

A good convergence of results was received through the averaging of 30 identical mixtures consisting of 5000 spheres each. Thus, the total number of spheres in each system amounts to 150000; it accords to the particle of about 15-20 nm of a real alloy. The periodically boundary conditions were applied.

All spheres have an index 1, 2, 3…: 1 marks the smallest spheres. The radii ratios were limited to $R_{max} / R_1 = 2.0$, since almost all real alloys have their radii ratios in this region.

Each simulated structure was analyzed by means of Laguerre tessellation, RDF etc. and all results were averaged over 20 identical mixtures.

Results for monatomic and binary mixtures are taken from the previous Chapters 3.0 and 4.0, respectively.

5.1 Density and atomic size distribution plot

Most of the bulk metallic glasses can be classified by means of an atomic size distribution (ASD) plot which shows the concentration of the constituent metallic elements vs. the atomic size [Sen01]. Zr-based BMGs, for example, have an ASD plot with a concave shape. The base element has the maximum atomic radius and a

concentration of 40–80 at.%. The element with the smallest radius has typically the second-largest value of concentration. Hence, the corresponding ASD plot has a minimum at intermediate values of radii. In [Sen01] it was proposed that such a form of ASD plots defines an especially high density of BMGs, which, in turn, reduces the diffusivity and increases the glass-forming ability (GFA). (The reduction of diffusivity with increasing packing density can be understood in terms of the free volume approach for self-diffusion in metals [Shi00].)

Another specific characteristic of BMGs is the fact that the mass density is only 0.3–0.54% lower than the density of the corresponding crystallized alloy [Ino00]. This difference is significantly smaller for BMGs than for conventional glasses where it is of the order of 1–2% [Che80].

Both the existence of a characteristic shape of the ASD plot and the comparatively high density support the assumption that efficient packing plays an important role in the glass-forming process of BMGs. It should be noted that this is not the case for the conventional metal–metalloid glasses. In these, analysis of the density and its dependence on the metalloid content have shown that the local packing density of the metalloid atoms is smaller than the values expected from dense random hard sphere packing [Her83]. On the other hand, metal–metalloid glasses and BMGs may have similar local structure components. This was shown in [Gue01] where trigonal prismatic neighbor shells were observed in a $Ni_{25}Zr_{60}Al_{15}$ computer-simulated BMG. It is well known that the trigonal prismatic structure unit was proposed previously as a basic structure element for metal–metalloid glasses [Gas79, Gas83]. At that time, the trigonal prismatic coordination model was not successful because it did not reproduce the density. In the computer simulation [Gue01], non-additivity of atomic radii was identified as a precondition for the appearance of trigonal prisms in dense model systems.

For these reasons, it is obvious that the complexity of the structure of metallic glasses, especially of BMGs, cannot be understood on the basis of a sole simple principle. Nevertheless, dense packing is one of the important aspects of structure and GFA of multicomponent metallic melts and will therefore be analyzed in this contribution.

In the Section 2.1 it was explained how the maximum value of the packing fraction for a system of hard spheres with fixed size distribution is achieved. Considering discrete size distributions of radii, e.g. N different species, then a specific system is characterized by the concentrations, C_1, C_2, ... , C_N, of the N species, by the radii, R_1, R_2, . . . , R_N, and by the corresponding maximum packing fraction, $\eta = \eta(x)$, which can be achieved within the noncrystalline state where $\{x\}$ denotes the parameter set $\{C_1, C_2, \ldots C_N; R_1, R_2, \ldots R_N\}$. The problem considered here is to find parameter ranges $\{x\}$ where the function $\eta(x)$ takes exceedingly high values. This problem is not trivial in the case of multicomponent systems $(N = 3, 4, 5, \ldots)$ for two reasons: (i) the number of adjustable parameters is large and the search for maximum values of η takes place in the $2(N-1)$ dimensional parameter space; (ii) the calculation of one value of η for a given set of parameters takes of the order of 1–30 min computer time with a high-speed personal computer (for systems with about 10,000 spheres and periodic boundary conditions).

In the present study, the maximum density achievable for a non-crystalline system of hard spheres, η, is used as function F in the Nelder-Mead simplex algorithm (see Section 2.3). It is known from test simulations that the value of the maximum achievable density at a given parameter set {x} can vary for different sets of initial random coordinates within the limits of 0.01% for single component systems to up to 0.3% in multicomponent systems even if all the other parameters, such as the total number of spheres (of the order of 10^4-10^5) and the parameters controlling the details of the packing algorithm, are equal. To reduce the influence of this statistical factor, the density at each point was calculated 5-20 times, depending on the required accuracy of the calculation and the atomic size distribution. Thus, the statistical error of the calculated density remained within the limits of 0.05%.

The number of adjustable parameters, $2N$, can be reduced by the condition $\sum_{i=1}^{N} C_i = 1$, and by the normalization of the radii $R_1\{1, R_2/R_1, \ldots, R_N/R_1\}$, where the size of the simulation box is measured in atomic radii R_1. The new set of $2(N-1)$ adjustable

parameters is then $\{C_1, C_2, \ldots C_{N-1}; R_2/R_1, \ldots R_N/R_1\}$. Additionally, the quantity R_N/R_1 was not used as an adjustable parameter but as a parameter with a predefined value that is kept constant during each simulation. Considering the range of realistic atomic radii it was reasonable to restrict the simulations to values $R_N/R_1 = 1.1, 1.2, \ldots, 2.0$. It is known from empirical data that the parameter R_N/R_1 has a significant effect on the GFA of BMGs [Ino97b, Ino00, Ega03] which justified the separate treatment of this parameter in the simulations. In addition to parameter R_N/R_1, the number of species, N, was also kept constant during a specific simulation procedure. Systems with $N = 3-5$ were analyzed.

Results

For each simulation, $2(N-1)+1$ different initial configurations were generated to create the first Nelder–Mead simplex required to start the optimization procedure (see Section 2.3). Each of these configurations represents a dense-packed system of spheres with fixed values for the parameters $\{C_1, C_2, \ldots, C_N; R_1, R_2, \ldots, R_N\}$ generated by means of the force-biased algorithm. The result of each Nelder–Mead run is a system with the highest global packing fraction that can be obtained from the chosen initial set described by a refined data set for the size distribution $\{x\}$. Table 5.1 shows the results of our simulations regarding size distribution and maximum packing fraction achieved for N-component systems with fixed size ratio, R_N/R_1, of largest to smallest spheres, where the size ratio

$$\Delta = \frac{R_N - R_1}{R_1},\ R_1 < R_2 < \ldots < R_N \tag{5.1}$$

is used to characterize the width of the size distribution. The radii of sphere species are normalized, $R_1 = 1$, and the value of the largest one is determined by the size ratio and the value of R_1, $R_N = (1+\Delta)R_1$. The values of R_i, $i = 2, \ldots, N-1$, and C_j,

$i = 1, \ldots, N$, are determined by the simulation routine described in Section 2.1 under the condition that the global packing fraction, η, achieves a maximum.

The simulation results for $\Delta = 0.1$ show that very similar maximum packing fractions, η = 0.639 and 0.640, can be achieved by rather different radii distributions (Table 5.1). For $N = 3$, there is one system with $R_2 = 1.033$ ($R_1 = 1.000$, $R_2 = 1.100$) and $\eta = 0.639$. This system may be compared with the $N = 4$ simulation for the same ratio $\Delta = 0.1$ with the results $R_2 = 1.035$, $R_4 = 1.037$. The difference of 0.2% between the optimized radii R_2 and R_3 is very small compared to the difference of 10% between the largest radius and the smallest one so that both fractions of spheres can be combined to a single species. That way a $N^* = 3$ system was formed from an initial $N = 4$ structure. The change from initial $N = 4$ and $N = 5$ systems to $N^* = 3$ structures during optimization by convergence of radii of different species is a general trend for systems with $\Delta \leq 0.2$. All $N = 5$ systems studied in the range $0.1 \leq \Delta \leq 0.2$ changed from the initial $N = 5$ state to an $N^* = 4$ or even $N^* = 3$ distribution.

Figure 5.1 shows the ASD plots for the $N = 3$ ($\Delta = 0.1$) system and the $N^* = 3$ ($\Delta = 0.1$, $N = 4$) system mentioned above. While the maximum packing fraction takes the same value of 0.639 for both systems, the corresponding ASD plots differ, essentially showing convex and concave shapes, respectively. This illustrates the general finding that the maximum packing for a system with $\Delta \leq 0.2$ can be achieved by qualitatively different atomic size distributions.

The situation is different for systems with higher maximum size difference, $\Delta > 0.2$. Figure 5.2 shows the ASD plot for $\Delta = 0.25$ and for the collected $N = 3,\ 4,\ 5$ data taken from Table 5.1. There are concentration maxima at $r = R_1$ and at $r = R_N$ and a minimum at intermediate r values where the notation $\delta = (r - R_1)/R_1$ is used. This behavior is also observed for $\Delta = 0.5 - 1.0$ and modifies gradually from a parabola-like shape to a ‘‘nearly rectangular” shape (Figure 5.3).

Table 5.1: Results of the Nelder-Mead optimization of multi-component hard sphere systems. $\Delta = R_N / R_1 - 1$, relative size difference of largest and smallest spheres; N, number of components; R_i and C_i, sphere radius and concentration of species i, respectively; $R_1 = 1$, $R_N = (1+\Delta)R_1$; η, maximum packing fraction achieved for fixed values of Δ and N but variable radii and concentrations.

Δ	N	R_2	R_3	R_4	C_1	C_2	C_3	C_4	C_5	η
0.10	3	1.069	-	-	60.3	6.4	33.3	-	-	0.640
		1.033	-	-	62.1	17.4	20.5	-	-	0.639
	4	1.044	1.052	-	26.1	16.0	34.7	23.2	-	0.639
		1.035	1.037	-	41.0	38.4	10.2	10.4	-	0.639
0.15	3	1.071			63.8	5.9	30.3			0.641
		1.088			63.9	5.2	30.9			0.641
	4	1.054	1.078		59.2	5.2	6.2	29.4		0.641
		1.072	1.082		48.3	11.2	20.1	20.4		0.640
0.20	3	1.083			60.7	6.6	32.7			0.642
		1.081			62.4	5.4	32.2			0.642
	4	1.070	1.133		58.9	5.5	12.8	22.8		0.642
		1.085	1.100		65.4	6.7	6.2	21.7		0.641
0.25	3	1.109			64.6	4.4	31.0			0.643
		1.082			66.0	4.8	29.2			0.643
	4	1.049	1.184		59.2	8.8	5.3	26.7		0.643
		1.095	1.120		63.4	4.5	8.5	23.6		0.643
	5	1.035	1.066	1.094	36.8	22.6	9.9	11.3	19.4	0.642
		1.086	1.086	1.171	52 2	10.4	6.5	14.3	16.7	0.642
0.50	3	1.253			63.8	3.4	32.8			0.651
		1.209			72.3	3.5	24.2			0.651
	4	1.187	1.206		70.3	3.0	2.6	24.1		0.650
		1.229	1.252		69.3	2.6	3.0	25.1		0.650
	5	1.019	1.047	1.481	44.2	13.7	5.9	20.6	15.6	0.651
		1.049	1.236	1.385	53.0	14.4	2.9	9.8	19.9	0.649
0.75	3	1.289			73.5	3.0	23.5			0.661
		1.249			72.3	3.5	24.2			0.661
	4	1.165	1.309		65.9	13.9	2.0	18.2		0.658
		1.325	1.330		77.8	2.2	3.7	16.3		0.659
	5	1.075	1.133	1.659	66.4	3.8	6.7	5.4	17.7	0.660
		1.074	1.293	1.358	70.3	6.6	2.6	2.9	17.6	0.659
1.00	3	1.207			77.9	2.8	19.3			0.671
		1.336			72.9	2.2	24.9			0.670
	4	1.319	1.369		75.1	2.3	4.7	17.9		0.669
		1.434	1.436		76.7	3.7	2.2	17.4		0.669
	5	1.038	1.204	1.361	60.4	13.4	7.9	2.8	15.5	0.668
		1.387	1.415	1.448	70.3	12.0	3.2	2.6	11.9	0.664

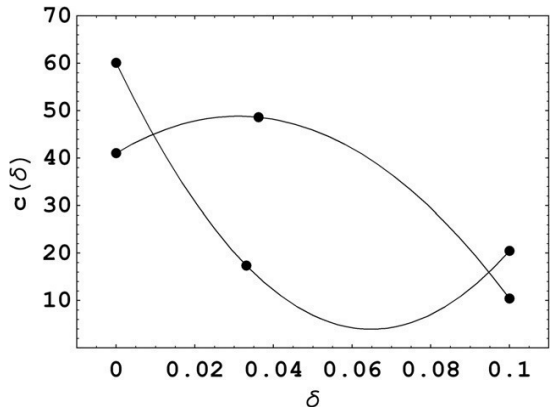

Figure 5.1: Atomic size distribution plots for $\Delta = 0.1$; $N = 3$ (convex) and $N^* = 3$ ($N = 4$, concave) both with maximum packing fraction of $\eta = 0.639$; concentration C vs. size ratio $\delta = (r - R_1)/R_1$ of species with radius r.

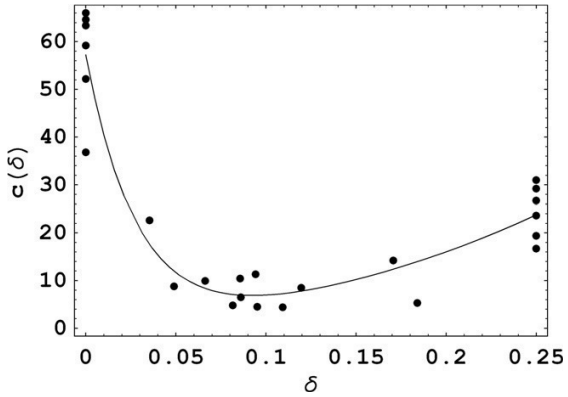

Figure 5.2: Atomic size distribution plot for $\Delta = 0.25$ (collected $N = 3,\ 4,\ 5$ data taken from Table 5.1); concentration C vs. size ratio $\delta = (r - R_1)/R_1$ of species with radius r.

The different character of systems with, respectively, low ($\Delta < 0.25$) and high ($\Delta > 0.25$) values of Δ is also reflected in the dependence of the ratio R_{N-1}/R_1 of second-largest to largest radii on the maximum relative size difference, Δ, where the (negative) ascent of the regression line changes its values at $\Delta = 0.25$ (Figure 5.4).

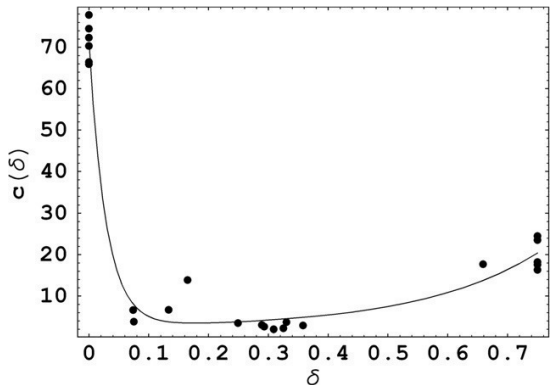

Figure 5.3: Atomic size distribution plot for $\Delta = 0.75$ (collected $N = 3,\ 4,\ 5$ data taken from Table 5.1); concentration C vs. size ratio $\delta = (r - R_1)/R_1$ of species with radius r.

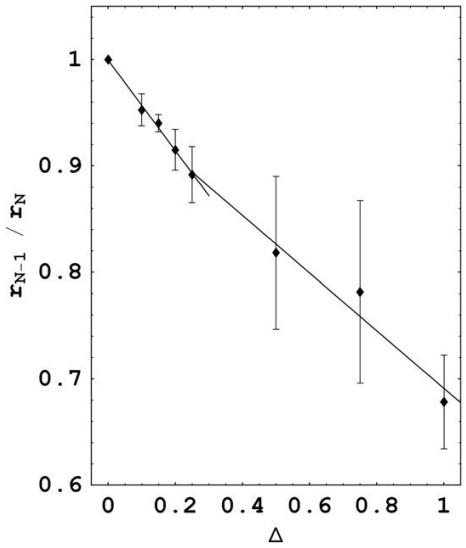

Figure 5.4: Dependence of the size ratio R_{N-1}/R_1 of second-largest to largest spheres vs. maximum size ratio Δ.

The simulation results for the characteristic shape of the size distribution for $\Delta \geq 0.25$ coincide substantially with experimental findings regarding the shape of the ASD of BMGs collected in [Sen01]. The only difference is that the ASD for BMGs has its absolute maximum at R_N [Sen01] while it is situated at R_1 for the systems considered in this work. It should be noted that the ASD can give a reasonable

impression of the situation only if the radii are distributed approximately uniformly in the interval $r \in (R_1, R_N)$ or $\delta \in (0, \Delta)$. If, for example, a system containing Cr ($R_{Cr} = 0.1249$ nm) and Co ($R_{Co} = 0.1251$ nm) atoms is considered, the question arises as to whether the Cr and Co concentrations should be marked separately or should be added and included in the experimental ASD plot at the position $r = 0.1250$ nm. However, the fact that in the present simulations the smallest spheres appear with the highest concentration does not fit the experimental situation for BMGs where, in most cases, the largest atoms play the role of the base element [Sen01].

Considering the results for the maximum global packing fraction, η, it is obvious that η does not depend essentially on the number, N, of species in the range $N = 3-5$ for constant Δ. In contrast, the dependence of η on the size ratio, Δ, proves to be significant. Figure 5.5 shows the plot of the values of the maximum packing fraction achieved for different values of the relative size difference, Δ. The error bars include not only the statistical error of η for fixed Δ and N, but also the distribution of data obtained for $N = 3-5$. A least-squares fit (solid line in Figure 5.5) yields

$$\eta = 0.636 + 0.0257\Delta + 0.0068\Delta^2 . \qquad (5.2)$$

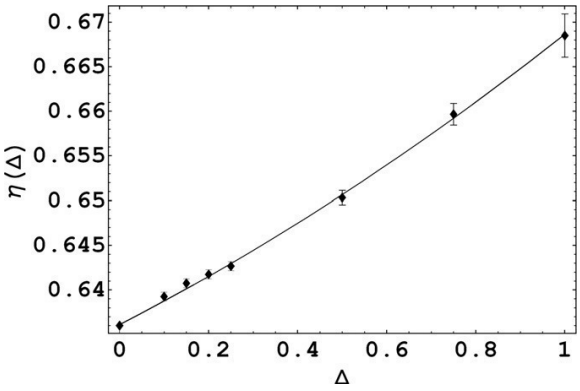

Figure 5.5: Maximum packing fraction, η, vs. relative size difference, $\Delta = R_N / R_1 - 1$, of largest and smallest spheres.

This means the maximum global packing fraction, η, of a randomly packed multicomponent system of spheres is mainly controlled by the relative size difference, Δ, of the largest and smallest spheres at least for the range of 3–5 components and Δ limited to 1.0 while the number $N = 3-5$ of different species plays only a tangential role.

Discussion

The atomic size effect in BMGs and its liquid precursors is related to empirical rules describing the conditions of good GFA. Inoue [Ino00] summarized the experimental data for a broad class of BMGs as follows: (i) multicomponent systems consisting of more than three elements are required; (ii) the difference in the atomic size between the three main constituent elements should be above 12%; (iii) negative heats of mixing among the three main constituent elements are necessary.

Egami [Ega03] extracted four conditions that would favor BMG formation from the melt: (i) increase the atomic size ratio of the constituent elements; (ii) increase the number of elements involved; (iii) increase the interaction between the small and large atoms; (iv) introduce repulsive interactions between small atoms.

Obviously, not all of these conditions are connected with the atomic size effect and with the hypothesis that the maximum packing fraction is a decisive requirement for good GFA of multicomponent metallic alloys. This concerns questions relating to the nature of chemical bonds such as interaction energy, spatially oriented covalent contributions and non-additivity of atomic radii. But the demand for a minimum value of the maximum size ratio and a minimum number of different elements as, for example, proposed for Zr- and Ln-based alloys, Mg–Ln–Cu, Fe–Zr–B, etc. [Ino00], can be discussed in terms of atomic size distribution and maximum packing fraction.

The present results show that there is a transition in the character of the size distribution required to achieve the maximum packing fraction with increasing size difference Δ. This transition occurs at $\Delta = 0.25$ (Figure 5.4). For smaller values of Δ, the maximum packing fraction can be achieved by different size distributions, while for $\Delta \geq 0.25$ always the same type of the shape of the ASD is achieved at maximum

packing fraction. The chance to realize the maximum packing fraction by means of different size distributions may have different consequences. (i) The enhanced number of possible realizations of the liquid or amorphous state increases the entropy of the system, especially if the compositional fluctuations appear on the nanometer scale. This would reduce the Gibb's free energy of the system and increase the stability of the liquid or amorphous state. (ii) Different amorphous phases may appear simultaneously if the correlation length of the compositional fluctuations exceeds significantly the 1 nm scale. (iii) Among the different size distributions resulting in the same maximum packing fraction for $\Delta < 0.25$ may be ones that favor crystalline phases. This would reduce the GFA.

The questions related to the options (i)–(iii) can be raised within the framework of the present model, but the answers will need to take into account more specific information about the interaction of the constituent elements within the dense random arrangements simulated here.

Additionally, the systems in the parameter range of $\Delta < 0.25$ tend to reduce the number of species from $N = 4$ and 5 to $N^* = 3$ during the Nelder–Mead optimization, which contradicts the demand for the high number of elements involved. Therefore, we believe that the value $\Delta = 0.25$ plays a specific role in the GFA of multicomponent Bernal's liquids. However, comparing this value with the minimum size difference of $\Delta = 0.12$ required for good GFA [Ino00], it is not yet clear whether both values differ only quantitatively or even qualitatively. The latter option would point to the presence of an additional effect beyond the idea of maximum packing density. Such an additional effect could be related to the presence of different types of local symmetry favoring either translational invariance of atomic arrangement.

The requirement to include more than three elements in order to obtain good GFA [Ino97b, Ino00, Ega03] can hardly be understood for systems with low relative atomic size difference in terms of the maximum packing fraction. Even for $\Delta > 0.20$, the influence of the number, N, of constituents on the maximum packing fraction, η, that can be achieved for fixed Δ is negligible compared to the effect of varying Δ (see Equation (5.2)).

Likewise, the experimental observation that in many cases the largest atoms are the base element with the highest concentration cannot be derived from the principle of maximum packing fraction. At least for $\Delta > 0.20$, this principle leads always to size distributions where the atoms with the smallest size are the main component while the largest atoms are only the component with the second-largest concentration.

In recent papers, the efficient cluster packing model was proposed as an approach to the structure of metallic glasses [Mir04b, Mir06]. There, in addition to solvent atoms (Ω), a species (α) of primary cluster-forming solute atoms is defined. Additionally, secondary (β) and ternary (γ) solutes are introduced, and are considered to occupy cluster-octahedral (β) and cluster-tetrahedral (γ) interstices, respectively. For a system where the α solutes have 12 next-nearest neighbors, the size ratio of α to Ω atoms is 0.902, corresponding to the close-packed icosahedral arrangement with an α atom in the center of the cluster and 12 Ω atoms surrounding it. It is interesting ask whether or not related clusters are spontaneously formed in the multicomponent systems considered in the present paper.

Remembering that the index of the largest spheres is N Equation (5.1), the ratio R_{N-1}/R_N plotted in Figure 5.4 vs. the maximum size ratio Δ corresponds to the size ratio of a solute atoms to Ω solvents according to [Mir04b, Mir06]. Values close to 0.902 appear for $\Delta = 0.15 - 0.20$ in Figure 5.4, e.g. in the system $\{R_1 = 1.0000,\ C_1 = 0.638;\ R_2 = 1.0708,\ C_2 = 0.059;\ R_3 = 1.1500,\ C_3 = 0.303\}$ with the packing fraction of $\eta = 0.641$ (see Table 5.1). In this system, a ratio $R_{N-1}/R_N = R_2/R_3 = 0.93$ appeared spontaneously, and the presence of icosahedral clusters could be expected. Therefore, this system was analyzed using the method of Laguerre tessellation. The result is: a small amount of 0.32% of the spheres of species 3 ($R_3 = 1.1500$, $C_3 = 0.303$), i.e. solvent atoms (Ω) in the notation used in Refs. [Mir04b, Mir06], are surrounded by (0, 0, 12) polyhedra, i.e. by polyhedra with icosahedral symmetry. The spheres of species 2 ($R_2 = 1.0708$, $C_2 = 0.059$) can be considered as primary clusterforming atoms of type α in the notation used in Refs. [Mir04b, Mir06] with the size ratio $R_{N-1}/R_N = R_2/R_3 = 0.93$ which is close to the value of 0.902 that occurs in

ideal icosahedral clusters. The Laguerre analysis showed that 4.00% of all spheres of species 2 are centers of (0, 0, 12) polyhedra, i.e. of icosahedral clusters. In other words, 4.00% of the spheres of species 2 in the system characterized by the parameter set $\{ R_1 = 1.0000,\ C_1 = 0.638;\ R_2 = 1.0708,\ C_2 = 0.059;\ R_3 = 1.1500,\ C_3 = 0.303 \}$ act as primary cluster-forming spheres of type α in the sense of the efficient cluster packing model proposed in Refs. [Mir04b, Mir06]. The same statement applies, however, also for species 1 ($R_1 = 1.0000,\ C_1 = 0.638$), where 4.66% of all spheres form centers of (0, 0, 12) icosahedral clusters. As the result of this discussion it can be stated that some aspects of the efficient cluster packing model proposed in Refs. [Mir04b, Mir06] can be identified in optimized multicomponent Bernal's liquids with a specific maximum size ratio of atoms. In general, we believe that the efficiency of packing of clusters seems to be heavily affected by collective effects exerted on a given cluster by its environment on the scale of medium-range order. There are specific size distributions of spheres that may favor the formation of clusters in the sense of the efficient cluster packing model [Mir04b, Mir06], but it seems to us that this model and the present approach of generalized Bernal's liquids are not completely compatible. Instead, more complex interactions seem to be more effective in forming clusters with specific short-range order. In [Her83] it was shown that competing central/non-central atomic interaction potentials [Her83] lead to the formation of model structures consisting of two types of randomly packed clusters. More recently, the effect of non-additivity of atomic radii was proven by means of molecular dynamics studies to be responsible for the formation of trigonal prismatic clusters [Gas79, Gas83] in ternary systems [Gue01].

Conclusion

Analyzing the aspect of maximum packing fraction, some of the properties of multicomponent liquids and glassy metallic systems can be understood. At least for systems consisting of 3-5 species, the maximum size ratio of the constituent elements plays an essential role in achieving maximum packing density. Assuming that high packing density favors good GFA, then the maximum size ratio is more important for

good GFA than the number of constituent elements, which plays a minor role. The relationship of the present approach to Miracle's efficient cluster packing model is neither straightforward nor conflicting. Spontaneous formation of atomic size distributions as proposed by Miracle's model was observed to some extent in a few of the simulated systems.

5.2 Coordination numbers

Since the $(R_2,\ C_1) = (1.3,\ 80\%)$ binary system corresponds to the maxima of parameters F_{nc}, $y_0(F_{nc})$ and $y_0(\eta)$, this system seems to be the most interesting binary one. Therefore, the binary system $(R_2,\ C_1) = (1.3,\ 80\%)$ was chosen as an initial system for investigations of ternary mixtures $\{R_1,\ R_2,\ R_3;\ C_1,\ C_2,\ C_3\}$ and two cuts (S1 and S2) with intersection at the point $(1.3,\ 80\%)$ were made:

$$\begin{aligned}
&\text{S1:} \quad R_1 = 1,\ R_2 = [1.1,\ 1.2,\ \ldots,\ 2.0],\ R_3 = [1.1,\ 1.2,\ \ldots,\ 2.0],\\
&\qquad\quad C_2 / C_1 = 80/20;\ C_3 = [10,\ 20,\ \ldots,\ 90]\ \%;\\
&\text{S2:} \quad R_1 = 1,\ R_2 = 1.3,\ R_3 = [1.1,\ 1.2,\ \ldots,\ 2.0],\\
&\qquad\quad C_2 / C_1 = [10/90,\ 20/80,\ \ldots,\ 90/10],\ C_3 = [10,\ 20,\ \ldots,\ 90]\ \%.
\end{aligned}$$

The surfaces in Figure 5.6 represent the total coordination numbers of three types of spheres for the cut S1 with $R_2 = 1.2$ and 1.9 depending on fraction, C_3, and radius, R_3, of the third atom type. The remaining coordination numbers for this cut are presented in Appendix A5.1.

All coordination numbers, CN_i, have a smooth dependence on all parameters (as well as for binary mixtures). The coordination number for small atoms, CN_1, of S1 vary between 13.49 for $(R_3,\ C_3) = (1.1,\ 10\%)$ and 10.18 for $(1.9,\ 90\%)$, respectively. According to Section 4.3, these values are slightly lower than 13.54 and 10.58 of the corresponding binary systems $(R_2,\ C_1) = (1.2,\ 72\%)$ and $(1.9,\ 8\%)$, respectively. This

deviation reflects the influence of the polydispersity on the manifoldness of possible atom arrangements.

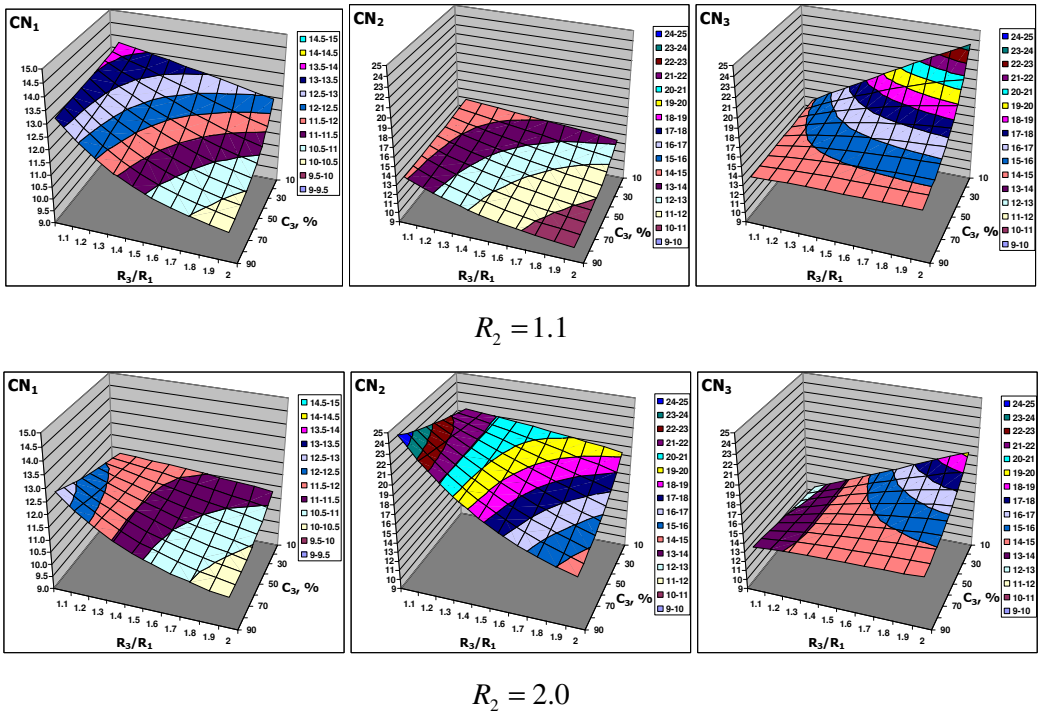

$R_2 = 1.1$

$R_2 = 2.0$

Figure 5.6: Total coordination numbers, CN_i, for three sphere types ($i = 1,\ 2,\ 3$) of ternary systems ($R_2 / R_1 = 1.1$ and 2.0, $C_2 / C_1 = 80/20$) vs. radii ratio R_3 / R_1 and concentration of third atoms, C_3.

With increasing R_2 up to 1.9 the coordination number of small atoms, CN_1, diminishes to 11.98 for $(R_3,\ C_3) = (1.1,\ 10\%)$ and does not change remarkably for systems with $C_3 = 90\%$. This shows that the coordination number of small atoms does not depend significantly on the sizes of other spheres, if the fraction of small spheres, C_1, is lower than about 10%. This effect is even stronger for greater radii differences.

The second type of spheres in the cut S1 can be smaller as well as bigger than the third one depending on the relation between R_2 and R_3. The coordination number for the second-type spheres, CN_2, ranges between 10.75 $(R_3,\ C_3) = (1.9,\ 90\%)$ and

15.65 $(R_3,\ C_3) = (1.1,\ 10\%)$ for systems with $R_2 = 1.2$. Increasing R_2 up to 1.9 causes a growth of the upper limit up to 23.62 ($R_3 = 1.1,\ C_3 = 90\%$), and the lower limit reaches 18.73 ($R_3 = 2.0,\ C_3 = 90\%$). The third type of spheres shows an inverse behavior of the total coordination number, CN_3. During the increasing of R_2 from 1.2 to 1.9 the interval of coordination numbers converges from 14.53 ($R_3 = 1.1,\ C_3 = 90\%$) and 23.08 ($R_3 = 2.0,\ C_3 = 10\%$) to 12.72 ($R_3 = 1.1,\ C_3 = 90\%$) and 19.80 ($R_3 = 2.0,\ C_3 = 10\%$), respectively.

All coordination numbers in the shown cut S1 of the ternary system have gradual dependences on radii R_2, R_3 as well as concentration of the third component, C_3 (see also Appendix A5.1).

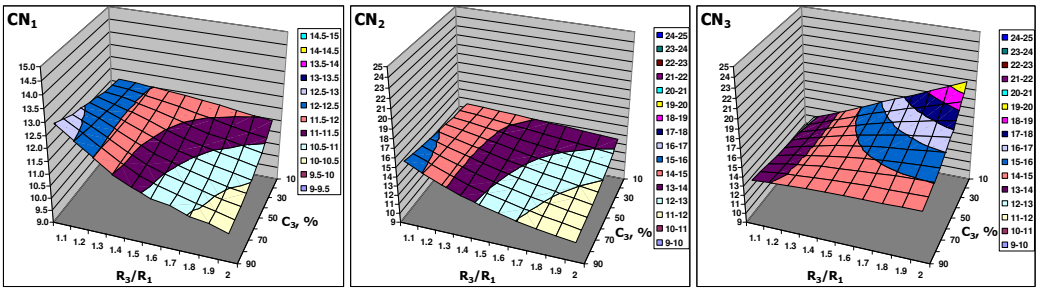

$C_1 / C_2 = 10/90$

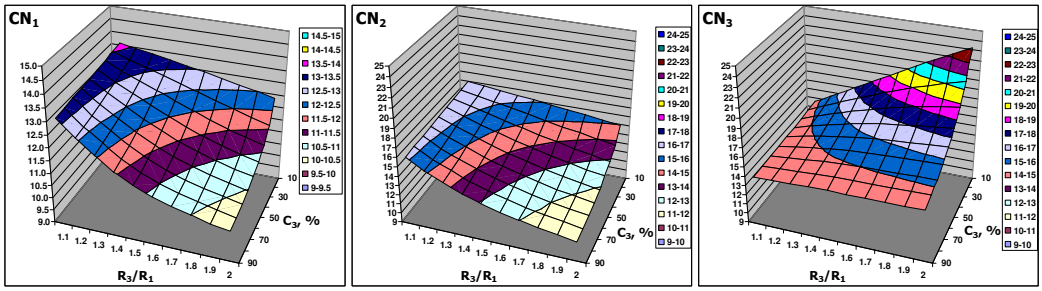

$C_1 / C_2 = 90/10$

Figure 5.7: Total coordination numbers, CN_i, for three sphere types ($i = 1,\ 2,\ 3$) of ternary system ($R_1 = 1,\ R_2 = 1.3,\ C_2 / C_1 = [10/90,\ 90/10]$) vs. $R_3 = [1.1,\ 1.2,\ \ldots,\ 2.0]$ and $C_3 = [10,\ 20,\ \ldots,\ 90]$ %.

The surfaces in Figure 5.7 show total coordination numbers, CN_i, for three sphere types in the cut S2 with $C_2/C_1 = 10/90$ and $90/10$ depending on fraction, C_3, and radius, R_3, of third sphere type. All coordination numbers in the cut S2 have a gradual dependence on the concentrations of all three components. Other results for coordination numbers of this cut are presented in Appendix A5.2.

For both cuts S1 and S2 as well as for binary systems the small atoms have a maximum number of neighboring atoms in the case of lowest radii ratios of other spheres. This value approaches the coordination number of a monatomic mixture in the limiting case of equal radii and does not exceed 14.04. The minimum value of the total coordination number for small spheres, $CN_1 \approx 10.12$, is reached for mixtures with the largest radii ratios and the smallest fractions of small atoms.

The second and third sphere types have an opposite behavior of the coordination numbers. The biggest values of CN_2 and CN_3 are reached for small amounts of largest spheres surrounded by big quantities of small spheres. The lowest values occur commonly in the opposite to the biggest value corner. The results shown in Appendix A5.2 have a similar behavior.

5.3 Polyhedra analysis

The most interesting polyhedron for amorphous structures is the dodecahedron (0, 0, 12), which corresponds to the icosahedral sort-range order. Figures 5.8 and 5.9 present the fraction of (0, 0, 12) polyhedra, $f^{(0,0,12)}$, for several compositions of cuts S1 and S2, respectively. Comparing to the dodecahedra fraction of binary systems (see Figure 4.5) even small additions of third element decrease $f^{(0,0,12)}$. So in the mixture with $R_2 = 1.3$ and 10 % of the third-type spheres the maximum fraction reaches about 3.7% by $(R_3, C_3) = (1.3, 10\%)$, which is lower than the maximal value of 4.1% for binary systems. Increasing of the radius of the second sphere type, R_2, causes a further monotone decrease of the dodecahedra fraction in the cut S1 (see also Appendix A5.3).

At $R_2 = 2.0$ the maximum fraction is about 2.5%. It is situated in the corner $(R_3,\ C_3) = (1.1,\ 90\%)$.

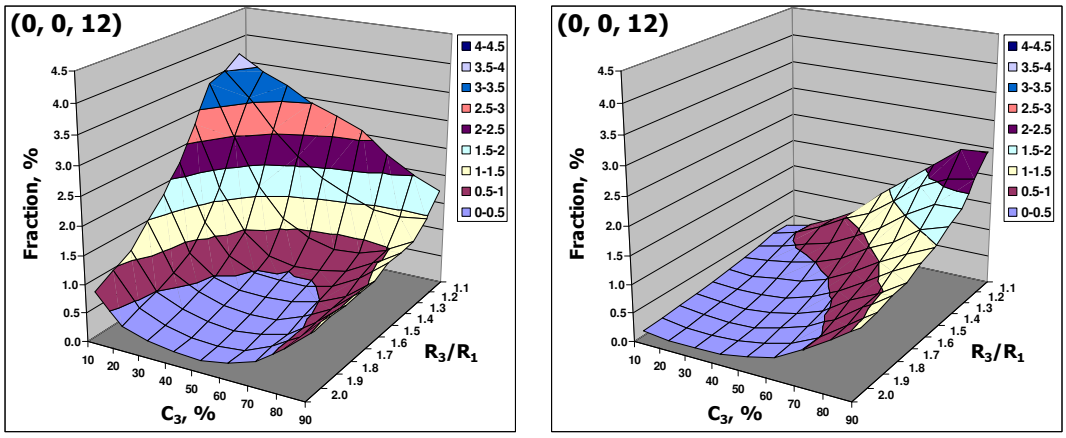

$R_2 = 1.3$ $R_2 = 2.0$

Figure 5.8: Fraction of (0, 0, 12) polyhedra of ternary systems: $R_1 = 1$, $R_2 = [1.3,\ 2.0]$, $R_3 = [1.1,\ 1.2,\ \ldots,\ 2.0]$, $C_2 / C_1 = 80/20$, $C_3 = [10,\ 20,\ \ldots,\ 90]$ % vs. R_3 and C_3.

The S2 cut with $C_2 / C_1 = 10/90$ shows two maxima of the dodecahedron fraction, pointing to two regions of enhanced icosahedral short-range order. The first maximum at $(R_3,\ C_3) = (1.1,\ 70\%)$ corresponds to the reduced maximum of the binary $(R_2,\ C_1) = (1.3,\ 80\%)$ mixture. The second maximum of ~3.0% is placed at $(R_3,\ C_3) = (1.6-1.7,\ 20\text{-}30\%)$. Since R_3 / R_2 for this maximum varies in the range of 1.23 to 1.31, this mixture can be also considered as nearly the same as the binary system $(R_2,\ C_1) = (1.23-1.31,\ 68-78\%)$ with 7-8% of additional spheres of the radius 0.77. Increasing C_1 / C_2 ratio leads to the vanishing of the second maximum (see also Appendixes A5.3 and A5.4) and shifting of the first one to the $(R_3,\ C_3) = (1.3,\ 10\%)$ by $C_1 / C_2 = 90/10$, which also corresponds to the binary system with the maximal fraction of dodecahedra.

This results show a similarity of the simulated binary and ternary mixtures. Thus, enhanced fractions of the icosahedral short-range order can be reached in multi-

component alloys if one pair of elements forms a binary system with the radii ratio of ~1.3 and ~80% of small atoms, or, in other words, if a multi-component systems is based on a binary mixture with a high fraction of (0, 0, 12) polyhedra.

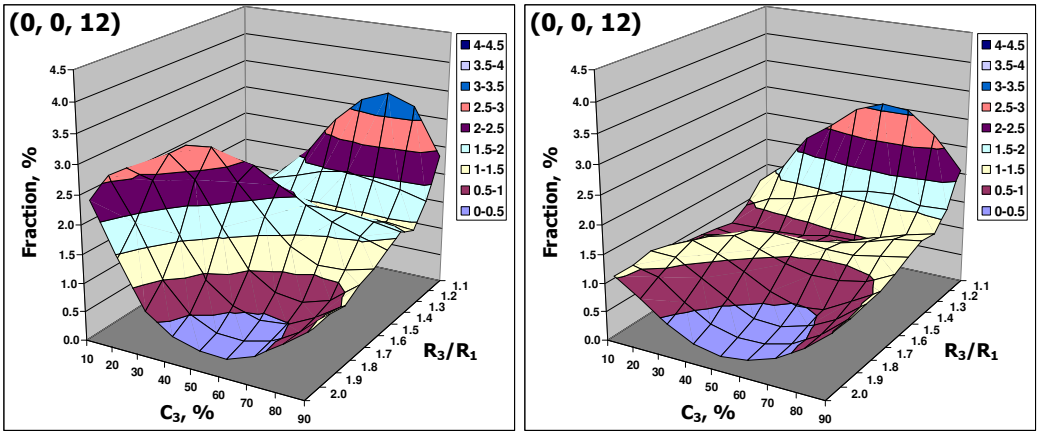

$C_1 / C_2 = 10/90$ $C_1 / C_2 = 40/60$

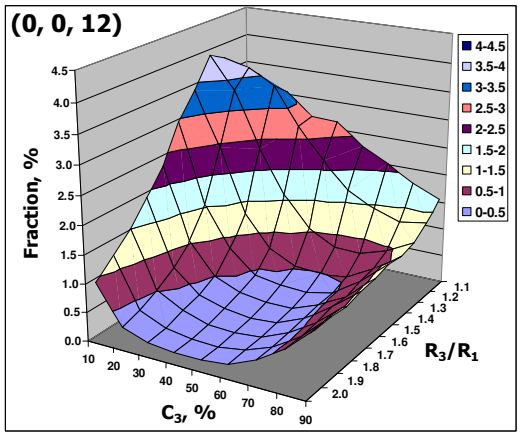

$C_1 / C_2 = 90/10$

Figure 5.9: Fraction of (0, 0, 12) polyhedra for ternary systems: $R_1 = 1$; $R_2 = 1.3$; $R_3 = [1.1,\ 1.2,\ \ldots,\ 2.0]$; $C_2 / C_1 = [10/90,\ 40/60,\ 80/20]$; $C_3 = [10,\ 20,\ \ldots,\ 90]$ %, vs. R_3 and C_3.

5.4 Non-crystalline to crystalline faces ratio

Figures 5.10 and 5.11 represent the non-crystalline to crystalline faces ratio, F_{nc}, depending on fraction, C_3, and radius, R_3, of the third atom type for several compositions of cuts S1 and S2, respectively. For the complete results for cuts S1 and S2 see also Appendixes A5.5 and A5.6. For all surfaces in Figure 5.10 the absolute maxima are placed on the boundaries. This means that maximum values of the parameter F_{nc} lie commonly in the binary alloys.

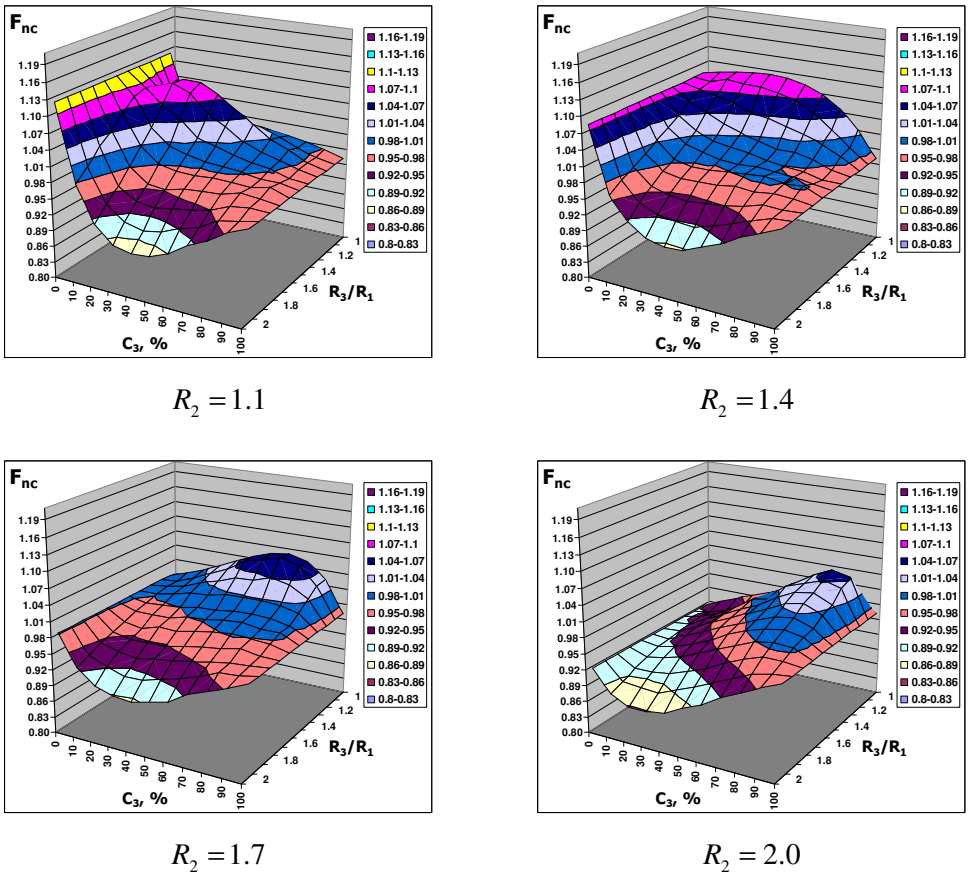

$R_2 = 1.1$ $R_2 = 1.4$

$R_2 = 1.7$ $R_2 = 2.0$

Figure 5.10: Non-crystalline to crystalline faces ratio, F_{nc}, of ternary systems: $R_1 = 1$, $R_2 = [1.1,\ 1.4,\ 1.7,\ 2.0]$, $R_3 = [1.1,\ 1.2,\ \ldots,\ 2.0]$, $C_1 / C_2 = 80/20$, $C_3 = [10,\ 20,\ \ldots,\ 90]$ %, vs. R_3 and C_3.

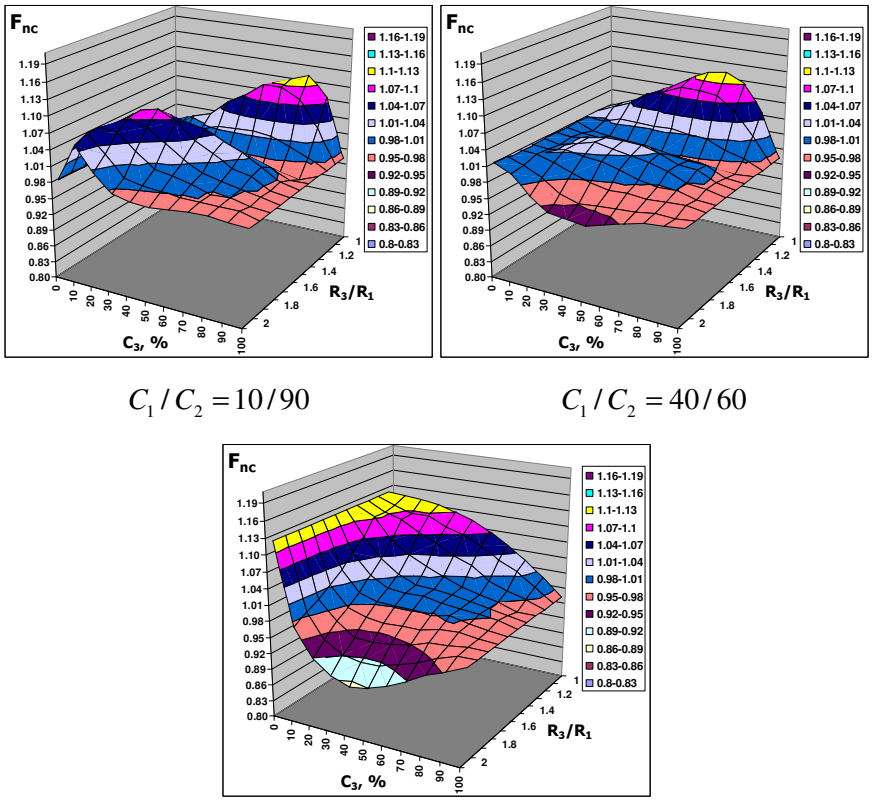

$C_1 / C_2 = 10/90$ $C_1 / C_2 = 40/60$

$C_1 / C_2 = 80/20$

Figure 5.11: Non-crystalline to crystalline faces ratio, F_{nc}, of ternary systems: $R_1 = 1$, $R_2 = 1.3$, $R_3 = [1.1,\ 1.2,\ \ldots,\ 2.0]$, $C_1 / C_2 = [10/90,\ 40/60,\ 80/20]$, $C_3 = [10,\ 20,\ \ldots,\ 90]$ %, vs. R_3 and C_3.

In addition to the global maximum at $C_3 = 0$, the cut S1 has a local maximum at $R_2 = 1.1$. This local maximum is situated at $(R_3,\ C_3) = (1.3,\ 20\text{-}30\%)$. With increasing R_2 it shifts to the lower radius of the third atoms, R_3, and to larger concentrations C_3.

After R_2 exceeds 1.3 the local maximum adheres to the $R_3 = 1.0$ border and becomes global. Further increasing of R_2 causes gradual decreasing of the non-crystalline to crystalline faces ratio, which indicates stabilization of crystalline state.

Figure 5.11 represents the non-crystalline to crystalline faces ratio, F_{nc}, depending on fraction, C_3, and radius, R_3, of the third atom type for several compositions of the cut S2.

Parameter F_{nc} has a similar behavior as $f^{(0,0,12)}$ (see Figures 5.8 and 5.9) for both S1 and S2 cuts. Like the distribution of dodecahedra, parameter F_{nc} has also a local maximum in the region $(R_3,\ C_3) = (1.6-1.7,\ 20\text{-}30\%)$, which can be considered as a binary mixture $(R_2,\ C_1) = (1.23-1.31,\ 68-78\%)$ alloyed with 7-8% spheres of the radius 0.77.

In the same way as for binary mixtures, the similarity of parameters F_{nc} and $f^{(0,0,12)}$ shows that prevalence of icosahedral short-range order is connected to a high fraction of non-crystalline faces and, accordingly, to high fractions of non-crystalline polyhedra. From the statistical point of view high non-crystallinity of the mixture is equivalent with high fractions of icosahedral structures characterized by non-crystalline faces.

Increasing radii ratio of the main (most widespread) elements in the system up to about 1.6 and higher causes a rapid decreasing of the non-crystalline to crystalline faces ratio in ternary as well as in binary systems. This observation leads to the conclusion that besides the empirical lower radii ratio of 12% there is an upper one of about 60%, which has a strong dependence on the composition.

5.5 Test of the Miedema methods

In order to test and compare all above mentioned methods experimental mixing enthalpies of more than 1200 different ternary (22 systems) and 216 quaternary alloys (2 systems) were collected from the literature. Table 5.2 presents absolute and relative average deviations between experimental mixing enthalpies and corresponding values calculated using Miedema's semi-empirical model and its 5 major modifications known from the literature. Red values correspond to the best coincidence with experimental results for a system, while the green color marks the second-best results.

For 15 from 24 systems the Ouyang's geometrical extrapolation yields better coincidence with experimental results in comparison to all other methods. The original Miedema's model with standard extrapolation to multi-component alloys made according to Equation (2.34) produces the best results for 9 and the second-best ones for 11 systems with average relative deviation of 33% which is 1 percent higher than Ouyang's geometrical extrapolation.

All other methods (R.F. Zhang, B. Zhang, L.C. Zhang and W.C. Wang) produce average deviations in the range 41 to 60 % and seem to be not appropriate for the calculation of the mixing enthalpy. Though, results of these methods have good coincidence with experimental results for some systems, for instance 19% difference for Fe-Ni-V system of B. Zhang's and L.C. Zhang's methods, in other cases these methods fail.

This comparison clearly shows that except the original idea of Miedema only Ouyang's geometrical extrapolation can be assumed as an adequate extension of the Miedema's model for multi-component alloys. All other extensions can be applied only to specific systems.

Table 5.3 shows absolute and relative deviations of the results calculated using the two "best" known methods and the new combination of Laguerre tessellation and Miedema's model described above. In order to reduce computation time a smaller amount of alloys were chosen for this comparison. For each system shown in Table 5.2 5 alloys were chosen in a random way under condition that each element has a concentration of higher than 5 at. %. Average deviations of Miedema's and Ouyang's models in Table 5.3 are very close to the values shown in Table 5.2. That confirms representativeness of sample.

For all three methods the average deviation is 30 %, while the average absolute difference makes 6.08, 5.94 and 5.42 kJ/mole for Miedema's model, Ouyang's geometrical extrapolation, and Laguerre plus Miedema combination, respectively. According to these values the combination of Laguerre tessellation and Miedema's model yields the best results of all models. In addition, this simple model does not use any superfluous parameters or approaches and allows the calculation of the contribution to the mixing enthalpy of separated atoms taking into account the specific local

structure of each atom. This feature allows a good estimation of the mixing and formation enthalpies for different alloys under different conditions without any additional formulae if the structure of an alloy is known.

Table 5.2: Absolute and relative average deviations from experimental values of the mixing enthalpy calculated using Miedema's model and its 5 modifications for 22 ternary systems (~1200 alloys) and 2 quaternary systems (216 alloys).

System	A.R. Miedema		Y. Ouyang		R.F. Zhang		B. Zhang		L.C. Zhang		W.C. Wang	
	Abs. Δ, kJ/mole	Rel. Δ	Abs. Δ, kJ/mole	Rel. Δ	Abs. Δ, kJ/mole	Rel. Δ	Abs. Δ, kJ/mole	Rel. Δ	Abs. Δ, kJ/mole	Rel. Δ	Abs. Δ, kJ/mole	Rel. Δ
Al-Cu-Ni-Zr [Wit99]	**3.78**	**0.13**	**4.09**	**0.14**	13.70	0.40	9.86	0.28	6.86	0.20	15.86	0.52
Cu-Ni-Si-Zr [Wit02]	**20.36**	**0.42**	20.80	0.43	39.12	0.80	33.50	0.68	26.41	0.53	**15.54**	**0.32**
Ag-Au-Bi [Zor05]	4.82	1.31	4.84	1.32	**4.19**	**1.12**	**4.55**	**1.24**	**4.54**	**1.24**	4.82	1.30
Ag-Au-Sn [Li08]	2.42	0.49	2.39	0.49	**1.53**	**0.22**	**1.77**	**0.35**	**1.80**	**0.35**	2.03	0.43
Al-Cu-Mg [Kim95]	**3.64**	**0.35**	**3.59**	**0.34**	7.58	0.77	4.84	0.48	5.02	0.49	3.64	0.37
Al-Cu-Ni [Sto93]	**11.72**	**0.51**	**11.61**	**0.50**	16.72	0.70	15.20	0.68	14.97	0.67	12.96	0.55
Al-Cu-Zr [Wit98]	**5.36**	**0.15**	**5.62**	**0.16**	22.53	0.59	13.09	0.34	12.45	0.32	9.02	0.24
Al-Li-Mg [Kry93]	**3.37**	**0.57**	**3.35**	**0.57**	5.04	0.87	3.84	0.65	3.88	0.66	**3.35**	**0.57**
Al-Ni-Zr [Wit99]	**5.75**	**0.16**	**5.77**	**0.16**	21.11	0.46	10.64	0.23	11.00	0.23	11.45	0.25
Al-Fe-Si [Kan03a]	**4.05**	**0.19**	**4.24**	**0.20**	13.07	0.62	9.34	0.43	9.59	0.44	13.67	0.62
Al-Ga-Sn [Bou95]	**0.04**	**0.02**	**0.04**	**0.02**	1.55	0.62	0.60	0.26	0.62	0.27	0.36	0.15
Al-Ga-Y [Kan06a]	**5.78**	**0.12**	**4.84**	**0.11**	20.02	0.47	12.63	0.29	12.10	0.28	7.59	0.26
Al-Ga-Zn [Bou99]	**1.48**	**0.72**	**1.48**	**0.72**	1.82	0.91	1.62	0.79	1.62	0.79	1.56	0.76
Cu-Mg-Y [Gan97]	**1.93**	**0.22**	**1.77**	**0.21**	8.33	0.71	3.01	0.33	3.40	0.36	2.83	0.32
Cu-Si-Zr [Wit02]	**9.05**	**0.37**	**8.94**	**0.36**	15.24	0.53	11.23	0.37	11.27	0.37	10.69	0.39
Fe-Ni-V [Zha02b]	2.98	0.51	3.02	0.52	1.51	0.28	**0.91**	**0.19**	**0.90**	**0.19**	1.79	0.32
Ga-Ge-Y [Kan05a]	**9.76**	**0.18**	**8.73**	**0.17**	24.82	0.51	18.39	0.34	18.16	0.34	8.75	0.28
Ge-Gd-Mn [Kan06b]	**8.21**	**0.19**	**8.09**	**0.18**	31.82	0.69	14.08	0.30	14.33	0.31	12.11	0.26
Ni-Si-Zr [Wit02]	**12.57**	**0.20**	**12.82**	**0.21**	36.56	0.66	19.54	0.33	20.06	0.34	20.63	0.35
Pb-Sn-Zn [Bou96]	**0.98**	**0.26**	**0.89**	**0.23**	2.54	0.72	1.67	0.45	1.72	0.46	1.41	0.38
Al-Cu-Ge [Kan03b]	1.59	0.29	1.46	0.28	2.01	0.35	**1.16**	**0.22**	**1.22**	**0.23**	5.99	1.05
Al-Cu-Si [Kan04a]	**0.99**	**0.08**	**0.97**	**0.08**	3.70	0.33	2.31	0.20	2.46	0.21	3.86	0.36
Al-Ga-Gd [Kan04b]	**6.66**	**0.16**	**6.08**	**0.15**	18.13	0.46	12.78	0.31	12.16	0.30	11.07	0.36
Ga-Gd-Si [Kan05b]	**11.79**	**0.23**	**10.57**	**0.21**	28.25	0.58	18.77	0.36	18.60	0.36	11.57	0.26
Average	**5.80**	**0.33**	**5.67**	**0.32**	14.20	0.60	9.39	0.42	8.97	0.41	8.02	0.44

Table 5.3: Absolute and relative deviations from experimental results over 110 ternary alloys and 10 quaternary alloys of 2 "best" methods comparing to the results of the combined Laguerre and Miedema model.

System	A.R. Miedema		Y. Ouyang		Laguerre + Miedema	
	Abs. Δ, kJ/mole	Rel. Δ	Abs. Δ kJ/mole	Rel. Δ	Abs. Δ kJ/mole	Rel. Δ
Al-Cu-Ni-Zr [Wit99]	3.82	0.10	3.98	0.11	4.86	0.13
Cu-Ni-Si-Zr [Wit02]	21.68	0.39	22.13	0.40	17.45	0.32
Ag-Au-Bi [Zor05]	5.86	1.33	5.88	1.33	5.84	1.32
Ag-Au-Sn [Li08]	1.28	0.17	1.23	0.16	2.05	0.26
Al-Cu-Mg [Kim95]	4.96	0.39	4.91	0.38	4.79	0.38
Al-Cu-Ni [Sto93]	13.52	0.50	13.37	0.50	12.06	0.45
Al-Cu-Zr [Wit98]	7.76	0.20	8.16	0.21	5.41	0.15
Al-Li-Mg [Kry93]	3.32	0.59	3.31	0.59	3.21	0.57
Al-Ni-Zr [Wit99]	7.51	0.16	7.66	0.17	6.81	0.16
Al-Fe-Si [Kan03a]	4.07	0.19	4.25	0.20	3.49	0.16
Al-Ga-Sn [Bou95]	0.04	0.02	0.05	0.02	0.18	0.08
Al-Ga-Y [Kan06a]	8.51	0.15	7.07	0.12	5.89	0.11
Al-Ga-Zn [Bou99]	1.45	0.71	1.45	0.71	1.41	0.69
Cu-Mg-Y [Gan97]	2.23	0.21	2.09	0.20	1.72	0.17
Cu-Si-Zr [Wit02]	10.37	0.34	10.10	0.33	10.45	0.38
Fe-Ni-V [Zha02b]	2.24	0.35	2.29	0.35	3.00	0.45
Ga-Ge-Y [Kan05a]	8.58	0.14	7.44	0.12	6.25	0.12
Ge-Gd-Mn [Kan06b]	10.49	0.16	10.35	0.16	8.91	0.15
Ni-Si-Zr [Wit02]	10.29	0.16	10.45	0.16	10.10	0.16
Pb-Sn-Zn [Bou96]	0.96	0.25	0.84	0.22	0.74	0.19
Al-Cu-Ge [Kan03b]	1.83	0.30	1.61	0.27	2.32	0.37
Al-Cu-Si [Kan04a]	1.37	0.10	1.36	0.10	1.40	0.12
Al-Ga-Gd [Kan04b]	7.92	0.18	7.37	0.18	8.08	0.21
Ga-Gd-Si [Kan05b]	5.93	0.16	5.14	0.14	3.73	0.11
Average	**6.08**	**0.30**	**5.94**	**0.30**	**5.42**	**0.30**

CHAPTER 6
CONCLUSIONS

Bulk metallic glasses are complex materials. The complexity can be illustrated by the following example: In Ref. [Lon09] there is a summary of a series of reported bulk metallic glasses based on 15 different metallic elements. It is known from basic mathematics that the number of different combinations of n constituents taken from a list of 15 elements is given by the binomial $\binom{15}{n}$. For $n = 2,\ 3,\ 4,\ 5,\ \ldots$ one obtains 105, 455, 1365, 3003, … possible combinations of elements. Each of these combinations corresponds to a formally admissible alloy each characterized by $(n-1)$ independent additional free parameters describing the concentration of the elements. Obviously, it is a challenging task to find out which structural characteristics are common to all known and unknown bulk metallic glasses and how these characteristics could be determined.

It is a matter of fact that computer simulations are valuable to achieve progress in this problem. In view of the complexity of the problem models are required which are as simple as possible. Here, the generalized Bernal's model was applied to generate structure models for metallic glasses consisting of atoms with approximately spherical shape. The models are analyzed using the Voronoi/Laguerre method. The most important results are:

- The determination of the geometrical contribution to the glass-forming ability of bulk metallic glasses.
- The optimization of N-component systems with respect to maximal packing fraction.
- The prediction of mixing enthalpies for N-component metallic glasses by a new method which combines the generalized Bernal's model, the Voronoi/Laguerre

method and the Miedema's model for the prediction of the mixing enthalpies of binary alloys.

Monatomic mixtures

The results for the simulated monatomic structures confirm the validity of Bernal's model as a good approximation for monatomic metallic liquids and simple metallic glasses. So, for instance, density, coordination number and radii distribution function determined for simulated structures are very similar to experimental values. Therefore, simulated models fulfill Bernal's necessary conditions for amorphous materials: homogeneity, coherence and irregularity.

One of the most important characteristics of Bernal's model is the packing density. Scott [Sco69] determined the random close-packed density of ball-bearing to be 0.6366 ± 0.0005. Other researchers obtained different values in the range 0.61-0.665 [Ber83] and it is not clear, if there is a limiting value of the packing density of the random close packed structure, and at which density an amorphous structure transforms into the crystalline state.

Results of the multiple-compression simulations show two different types of behavior of the density during compression. The transition from one type to the other one occurs at the density of about 0.647, which is in a good agreement with previous results [Ber83]. Thorough analysis of the densification yielded that the density of 0.64635 is the limiting value for random packing and further densification occurs only with a certain degree of crystallization.

This limiting value is maintained on several observations:

- Exponential fitting of the "amorphous" region of the density yields the maximum achievable density of 0.64635 for amorphous state without crystallization.
- Up to the density of 0.64635 only separated crystalline polyhedra (crystalline cells) with a fraction of < 0.4 % are observed. From the statistical point of view it is possible to find separated crystalline cells in each real metallic glass.

- Increasing of the density above ~ 0.64635 results in interaction of crystalline cells, which are starting to agglomerate to nano-crystalline regions.
- Above the density of ~0.647 the total fraction of crystalline regions exceeds 1% and can be determined using experimental methods like XRD, and "crystalline" peaks arise in the radial pair distribution function.

The new proposed parameter F_{nc} (non-crystalline to crystalline faces ratio) shows a clear tendency towards crystallization of monatomic mixtures, what is also in a good agreement with experimental results, since pure metals are very unstable in the amorphous state and tend to crystallize.

The distribution of the local density (ratio between atomic and polyhedron volumes) shows an interesting behavior. On the atomic scale the density varies in the broad range from 55 to 75 % pointing to inhomogeneity of the samples on the atomic scale. By contrast, the fluctuation of the density of the whole samples (5000 atoms) is small. Thus, these mixtures are homogeneous on the linear scale of about 15 atomic diameters (about 5 nm of real structures).

Binary mixtures

Binary mixtures of hard spheres have much more complicated structure than monatomic ones. So, for example, even at the radii ratio, R_2 / R_1, of 1.1 the number of different types of polyhedra amounts to about 1400, what is about 400 more than of monatomic systems. This amount increases rapidly with increasing degree of polydispersity. Coordination numbers in the range from ~11 to ~14 for small spheres and from ~14 to ~24 for big ones also represent a great variety of possible atomic configurations.

Radial distribution functions as well as polyhedra analyses confirm amorphism of the simulated structures. The multiple-compression tests yield very similar curves for density and parameter F_{nc} in comparison to monatomic mixtures. Thus, exponential fitting of the results of multiple-compression tests is also valid for binary systems.

While the packing density, η, of binary mixtures has a monotone dependence on the radii ratio, parameter $y_0(\eta)$ of the exponential fitting has a strong maximum at radii ratio of 1.3.

The positions of real binary metal-metal glasses (best known up to date) in the concentration/size ratio plot are in a very good agreement with positions of:

- maximum of the parameter $y_0(\eta)$ describing the maximum achievable density without crystallization;
- maxima of parameters F_{nc}, $y_0(F_{nc})$ giving the non-crystalline to crystalline faces ratio after the first compression cycle and the maximum achievable value without crystallization, respectively;
- minimum of parameter $a(F_{nc})$ representing a quasi-velocity of crystallization or amorphization (negative values - amorphization) during densification.

The well known empirical rules of Inoue and Egami demand radii ratios of more than 12 % of the base elements on order to get good glass-forming alloy. This rule coincides very well with the lower boundary of the $a(F_{nc}) = 0$ curve, which separates regions with tendencies towards crystallization and towards amorphization.

These observations confirm the supposition that density and non-crystalline to crystalline faces ratio are connected to the glass-forming ability.

High densities reduce the diffusivity and increase the viscosity, which in its turn reduces crystal nucleation and growth and, thereby, stabilizes the amorphous state.

Parameter F_{nc} describes the extent of atomic rearrangements which are necessary for crystallization. High values of F_{nc} mean high amount of rearrangements, which in its turn demand time and energy. Thus, F_{nc} is connected to the critical cooling rate and, accordingly, to the glass-forming ability.

The polyhedron (0, 0, 12) was shown to be only a consequence of the high non-crystallinity of the mixtures, and not *vice versa*. The statistic of non-crystalline polygons is much more important than the fraction of (0, 0, 12) polyhedra. Thus, parameter F_{nc} is a more general description than the fraction of (0, 0, 12) polyhedra.

According to shown results several alloys were proposed as probable good glass formers: $Al_{80}Y_{20}$, $Cr_{80}Sn_{20}$, $Cu_{70}In_{30}$, $Cu_{75}Nd_{25}$, $Ni_{65}Hf_{35}$ and $Zn_{60}Y_{40}$.

Ternary and multi-component mixtures

The parameters of N-component mixtures are determined which correspond to the highest possible density under the constraints of given radii ratios of the biggest and smallest spheres, $\Delta = (R_{\max} - R_{\min})/R_{\min}$, and fixed number of elements, N. These results were achieved by means of the Nelder-Mead optimization method.

The analysis of the atomic size distributions (ASD) of the mixtures with the maximal packing fraction presents that there is a transition in the character of the size distribution required to achieve the maximum packing fraction with increasing size difference Δ. This transition occurs at $\Delta = 0.25$. For $\Delta < 0.25$ the maximum packing fraction can be achieved with different size distributions, while for $\Delta \geq 0.25$ always the same type of the shape of the ASD is achieved at maximum packing fraction.

The ASD of simulated systems with parameter $\Delta \geq 0.25$ are similar to the ASD obtained from real multi-component bulk metallic glasses collected in [Sen01]. The only difference is that the ASD for bulk metallic glasses has its absolute maximum at R_{max} [Sen01] while it is situated at R_{min} for the systems considered in the present study.

The systems in the parameter range of $\Delta < 0.25$ tend to reduce the number of species from $N = 4$ and 5 to 3 during the Nelder–Mead optimization, which contradicts the demand for the high number of elements involved.

The maximum global packing fraction, η, of a randomly packed multi-component system of spheres is mainly controlled by the relative size difference, Δ, of the largest and smallest spheres at least for the range of 3–5 components and Δ limited to 1.0 while the number $N = 3-5$ of different species plays only a marginal role.

The polyhedra analysis shows that global maxima of the fraction of the (0, 0, 12) polyhedra, $f^{(0,0,12)}$, are always placed at the boundaries, i.e. in the limits of binary mixtures. Mixtures corresponding to the local maxima of the $f^{(0,0,12)}$ fraction are very similar to the binary $(R_2/R_1,\ C_1) = (1.3,\ 80\%)$ mixture, which has the maximal value of

about 4.1 %. Thus, high fractions of dodecahedra can be obtained in the multi-component systems based on the binary $(R_2 / R_1,\ C_1) = (1.3,\ 80\%)$ one.

Parameter F_{nc} has a very similar behavior. It was found to have global maxima on the boundaries (binary mixtures) of the distributions and the local ones at the mixtures corresponding to the binary $(R_2 / R_1,\ C_1) = (1.3,\ 80\%)$ system.

The similar behavior of $f^{(0,0,12)}$ and F_{nc} for ternary mixtures confirms the results obtained for binary ones. High fractions of dodecahedra (icosahedral short-range order) are generally caused by high non-crystallinity of the system and not vice versa.

A new and improved extension of Miedema's model

Comparison of the new proposed approach with 5 known extensions of Miedema's model as well as with the original Miedema's model over more than 1400 ternary and quaternary alloys shows that the lowest average deviation from experimental results is achieved by the new approach. The proposed method is based on the combination of the original Miedema's model and Laguerre tessellation. This combination allows the calculation of the mixing and formation enthalpies for different kinds of multi-component metallic alloys without additional approximation or extrapolations. This method takes into account the local structure of each atom.

APPENDIXES

A4 Appendixes to Chapter 4

A4.1: Radial distribution functions of binary systems depending on concentration of small atoms, C_1, and radii ratio, R_2 / R_1.

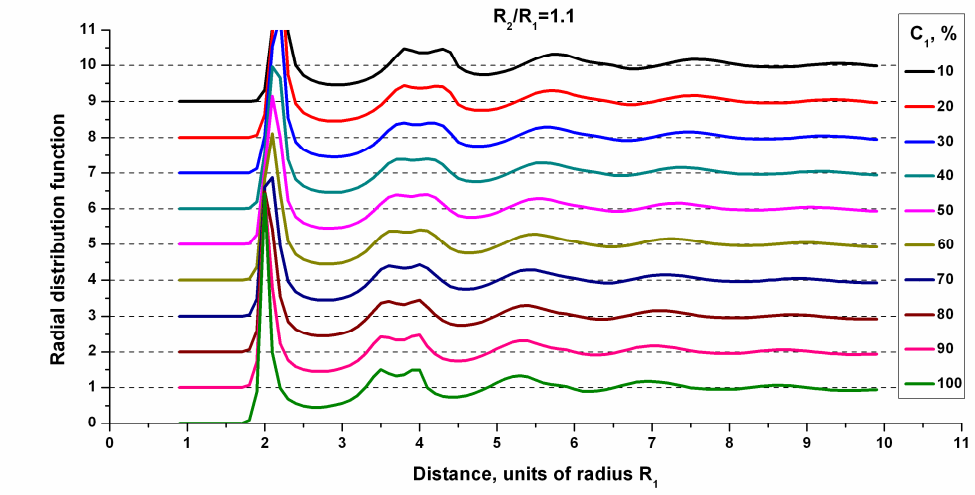

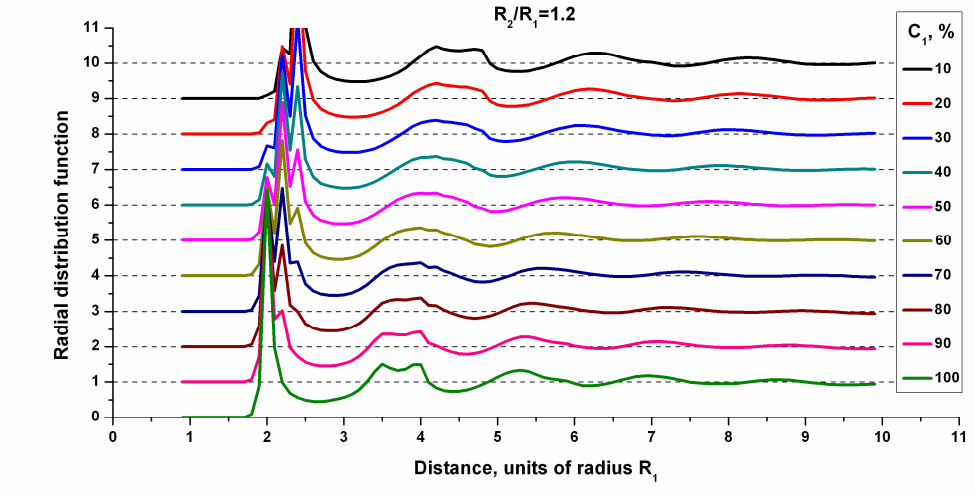

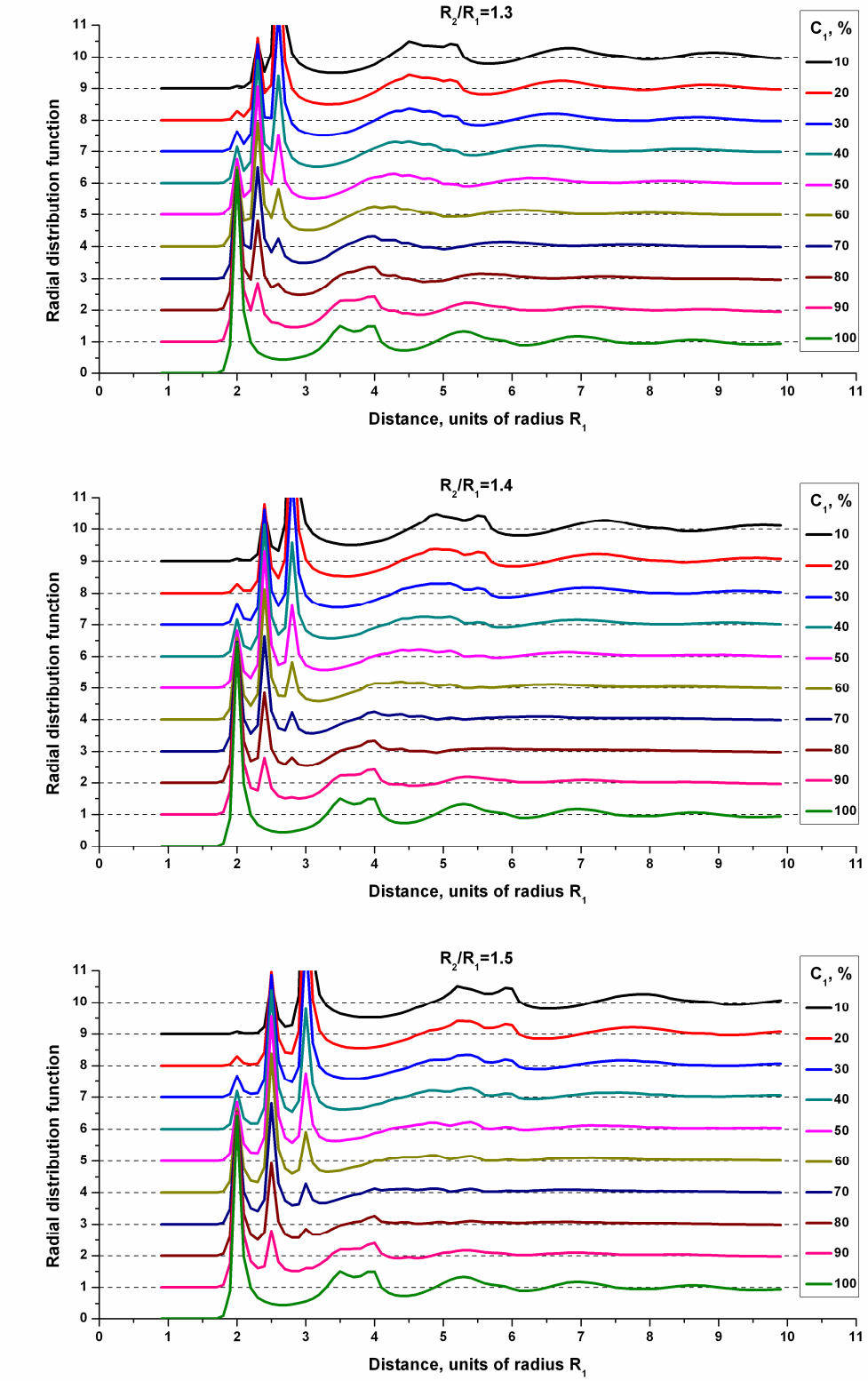
R2/R1=1.3
R2/R1=1.4
R2/R1=1.5
Radial distribution function
Distance, units of radius R1
C1, %
10
20
30
40
50
60
70
80
90
100

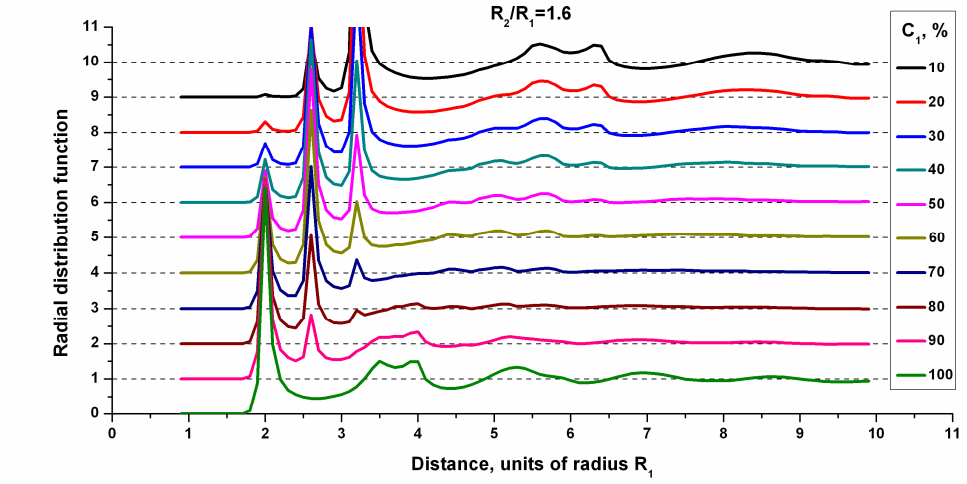
R2/R1=1.6
Radial distribution function
Distance, units of radius R1
C1, %
10
20
30
40
50
60
70
80
90
100

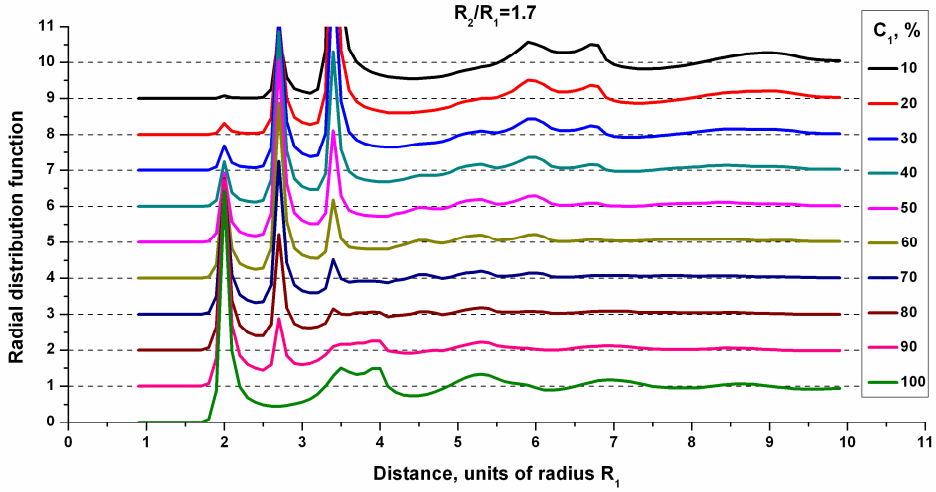
R2/R1=1.7
Radial distribution function
Distance, units of radius R1
C1, %
10
20
30
40
50
60
70
80
90
100

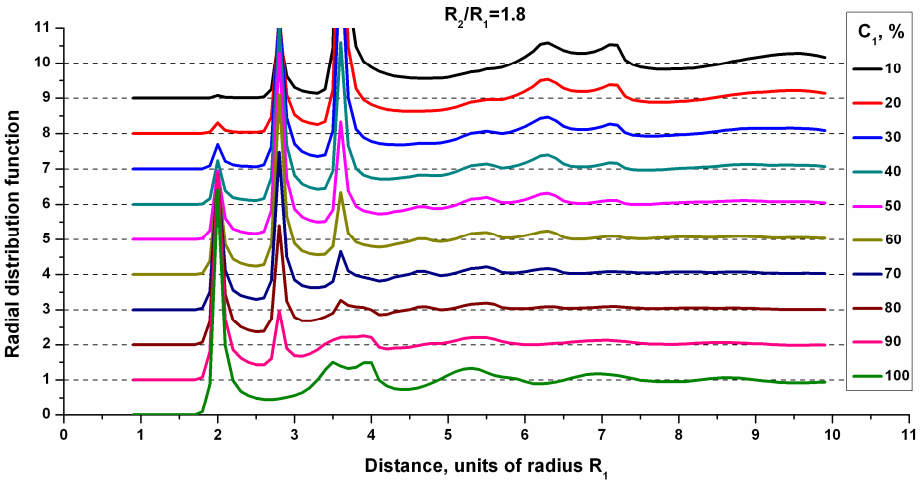
R2/R1=1.8
Radial distribution function
Distance, units of radius R1
C1, %
10
20
30
40
50
60
70
80
90
100

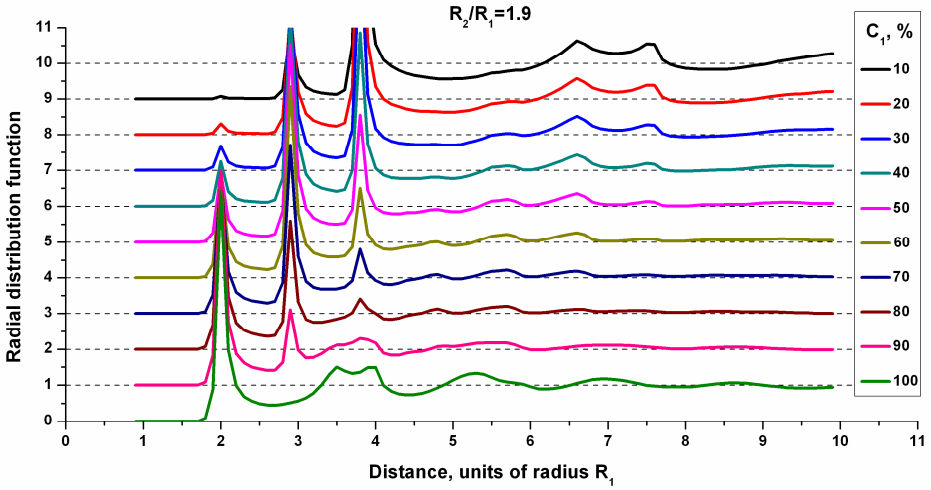
R2/R1=1.9
C1, %
10
20
30
40
50
60
70
80
90
100
Radial distribution function
Distance, units of radius R1

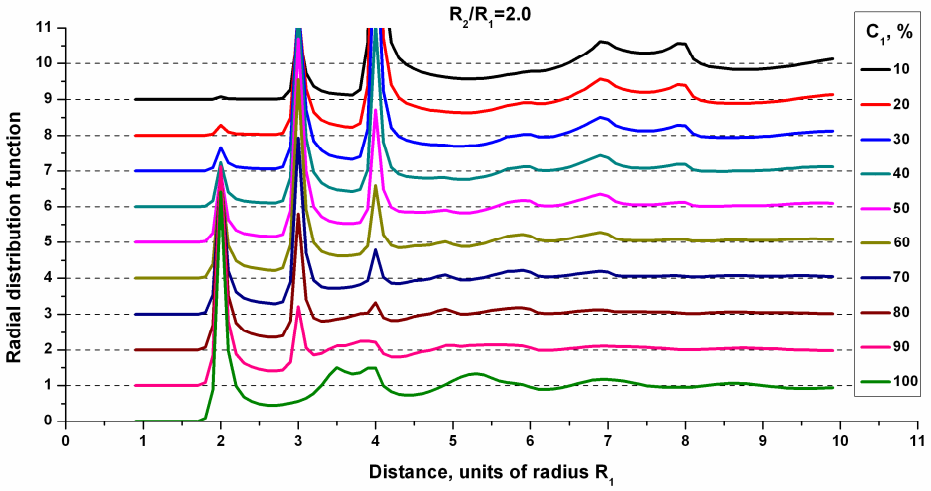
R2/R1=2.0
C1, %
10
20
30
40
50
60
70
80
90
100
Radial distribution function
Distance, units of radius R1

A4.2: Partial coordination numbers, CN_{i-j}, of binary mixtures of hard spheres depending on concentration of small atoms, C_1, and radii ratio, R_2 / R_1.

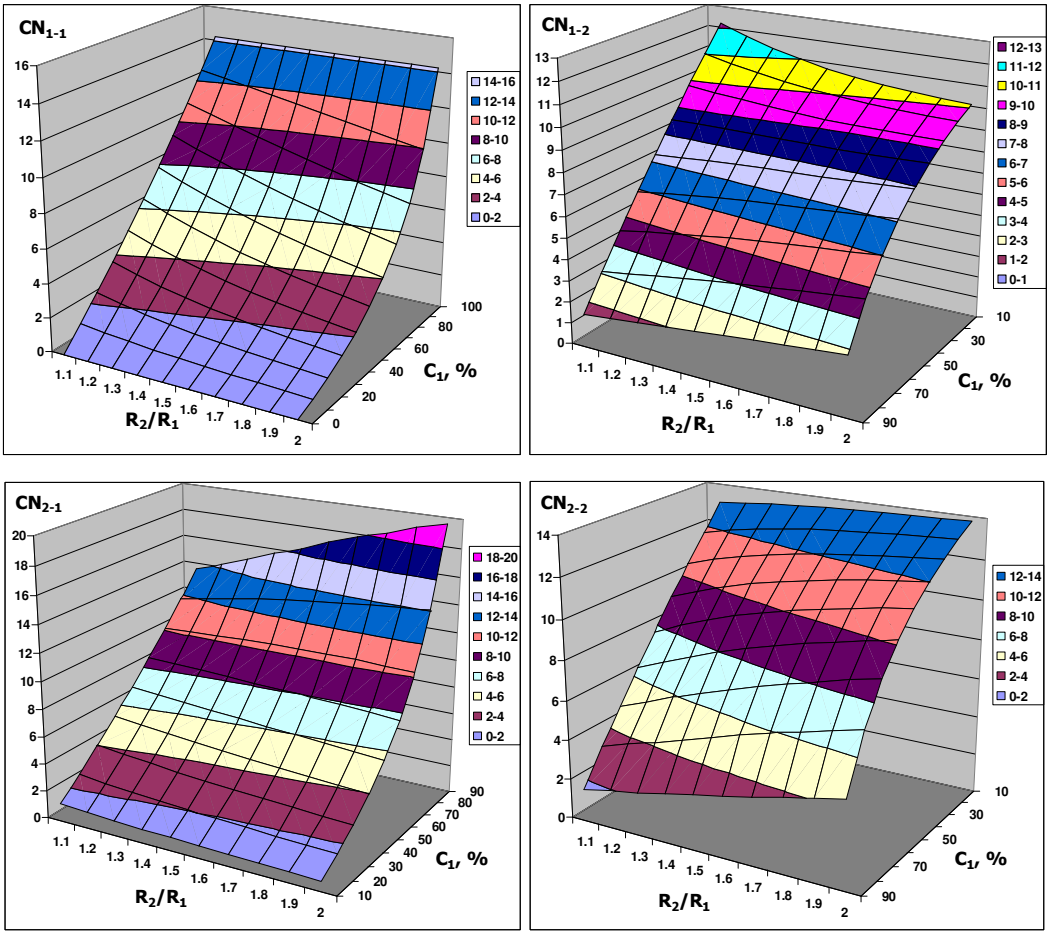

A4.3: Fractions of the major polyhedra groups (except (0, 2, 8, x) and (0, 3, 6, x)) in binary systems depending on radii ratio, R_2 / R_1, and concentration of small atoms, C_1.

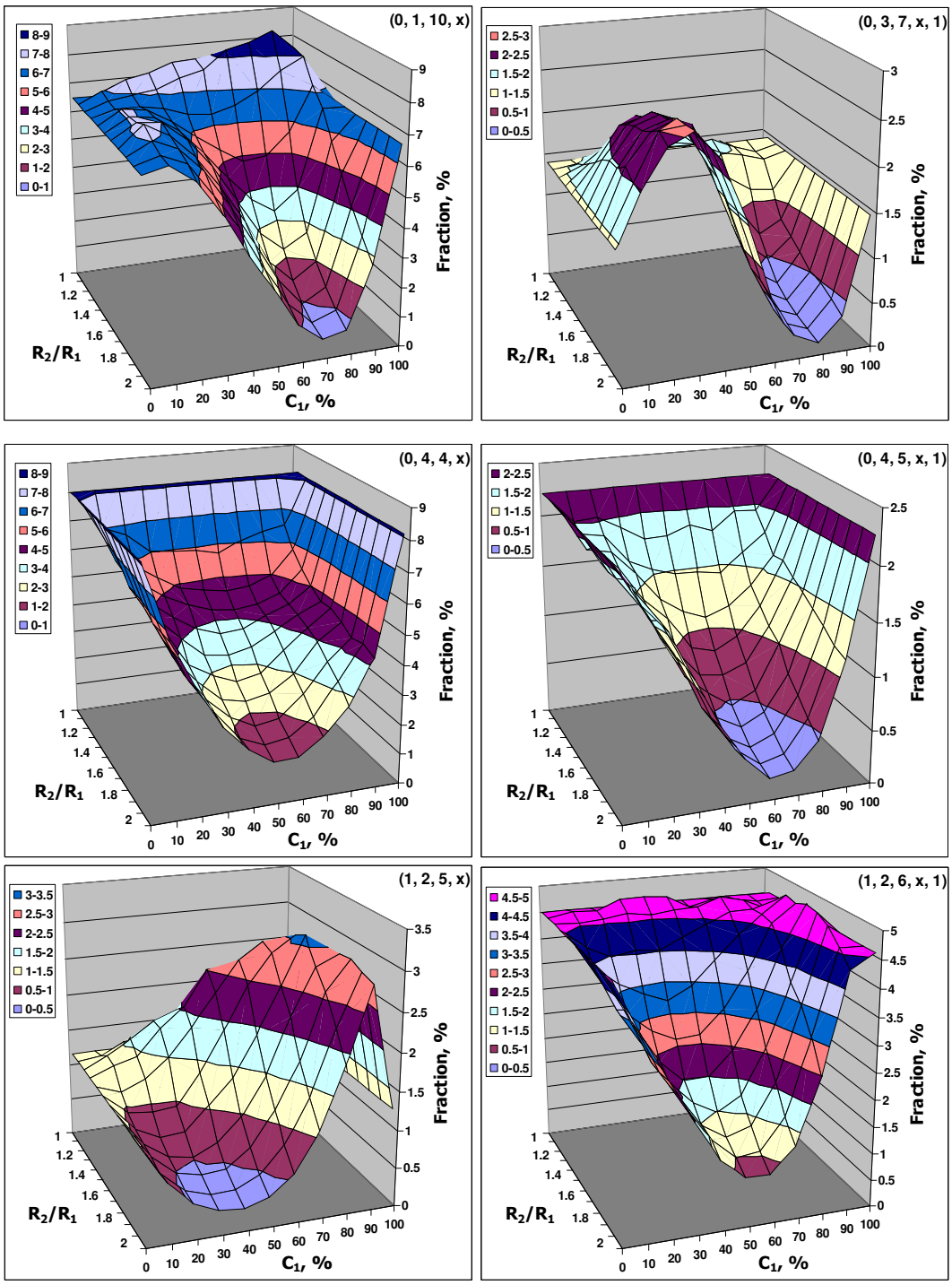

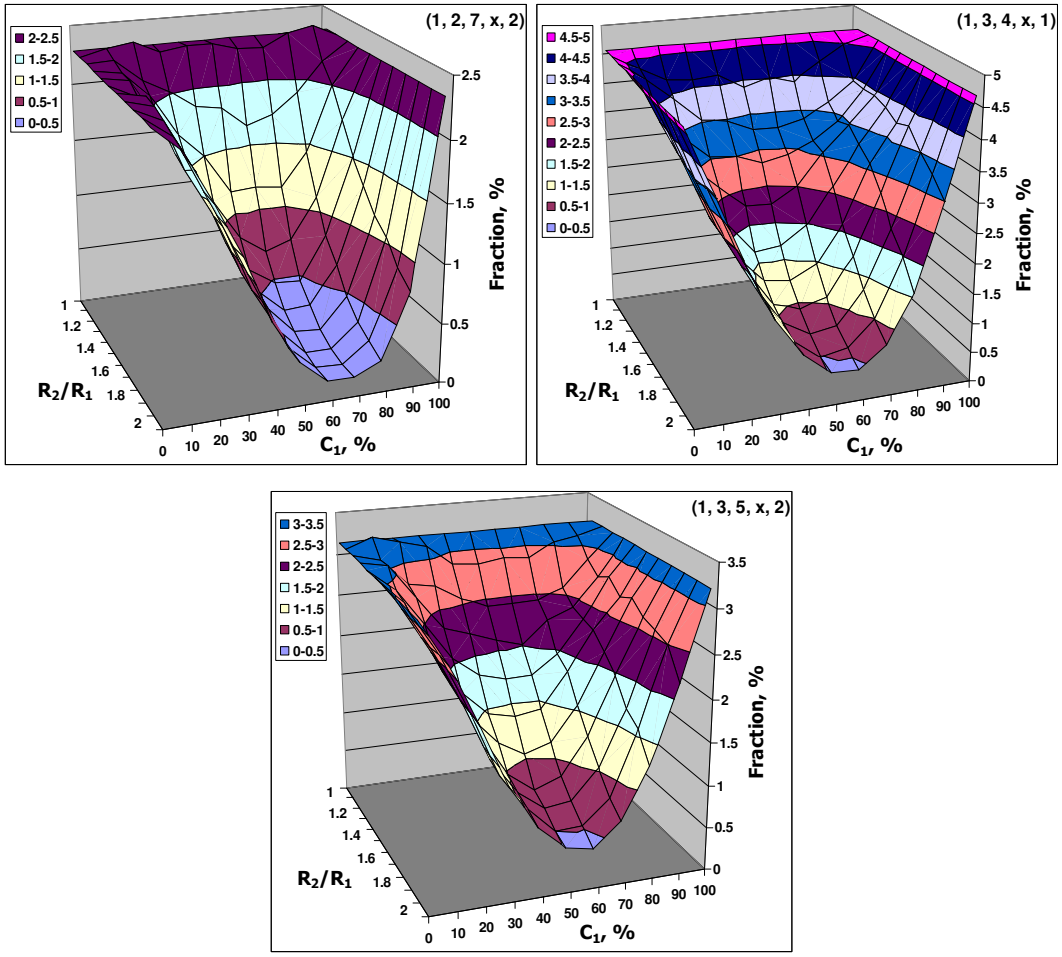
(1, 2, 7, x, 2)
2-2.5
1.5-2
1-1.5
0.5-1
0-0.5
Fraction, %
R_2/R_1
C_1, %
(1, 3, 4, x, 1)
4.5-5
4-4.5
3.5-4
3-3.5
2.5-3
2-2.5
1.5-2
1-1.5
0.5-1
0-0.5
Fraction, %
R_2/R_1
C_1, %
(1, 3, 5, x, 2)
3-3.5
2.5-3
2-2.5
1.5-2
1-1.5
0.5-1
0-0.5
Fraction, %
R_2/R_1
C_1, %

A4.4: Distribution of polygons in binary mixtures depending on radii ratio, R_2 / R_1, and concentration of small atoms, C_1.

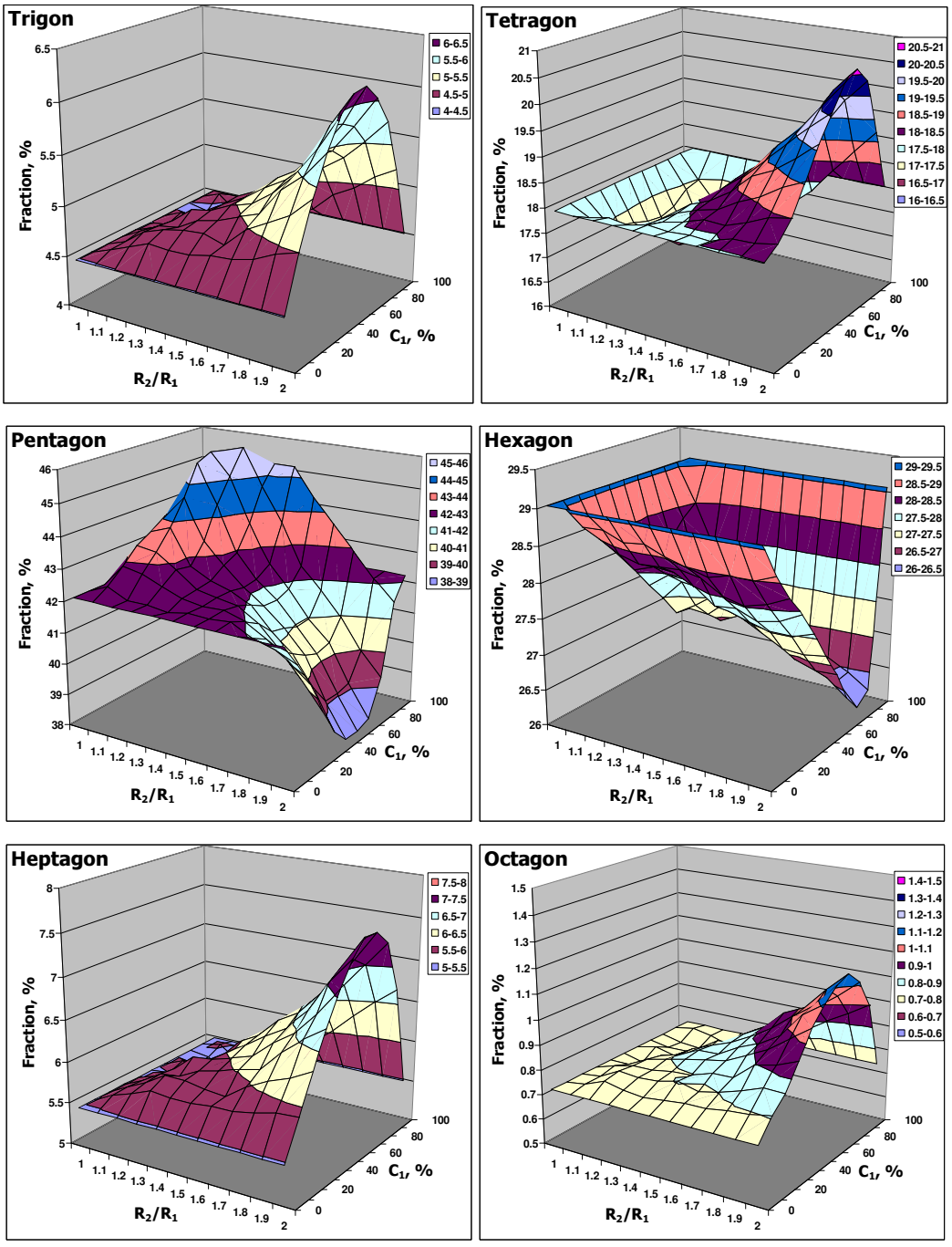

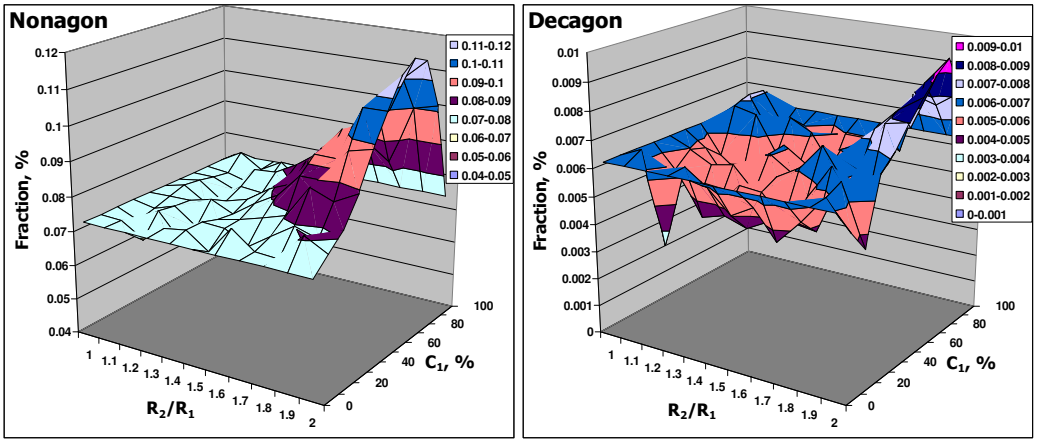
Nonagon
Fraction, %
0.12
0.11
0.1
0.09
0.08
0.07
0.06
0.05
0.04
0.11-0.12
0.1-0.11
0.09-0.1
0.08-0.09
0.07-0.08
0.06-0.07
0.05-0.06
0.04-0.05
1
1.1
1.2
1.3
1.4
1.5
1.6
1.7
1.8
1.9
2
R2/R1
0
20
40
60
80
100
C1, %
Decagon
Fraction, %
0.01
0.009
0.008
0.007
0.006
0.005
0.004
0.003
0.002
0.001
0
0.009-0.01
0.008-0.009
0.007-0.008
0.006-0.007
0.005-0.006
0.004-0.005
0.003-0.004
0.002-0.003
0.001-0.002
0-0.001
1
1.1
1.2
1.3
1.4
1.5
1.6
1.7
1.8
1.9
2
R2/R1
0
20
40
60
80
100
C1, %

A5 Appendixes to Chapter 5

A5.1: Total coordination numbers, CN_i, for three sphere types of ternary systems: R_2/R_1, $R_3/R_1 = [1.1,\ 1.2,\ \ldots,\ 2.0]$; $C_1/C_2 = 80/20$; $C_3 = [10,\ 20,\ \ldots,\ 90]$ %, vs. R_3/R_1 and C_3.

$R_2/R_1 = 1.1$

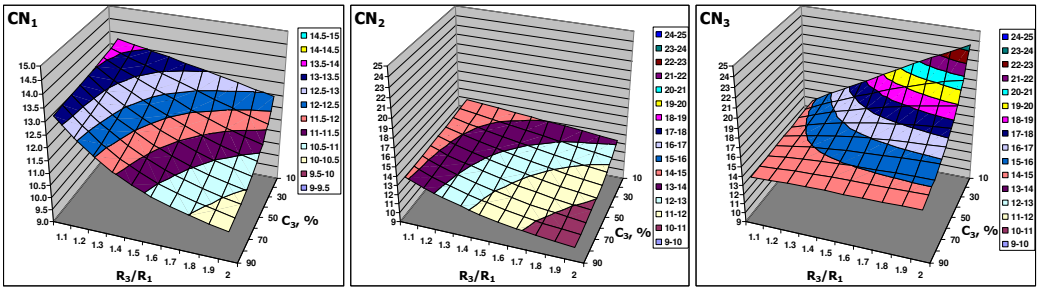

$R_2/R_1 = 1.2$

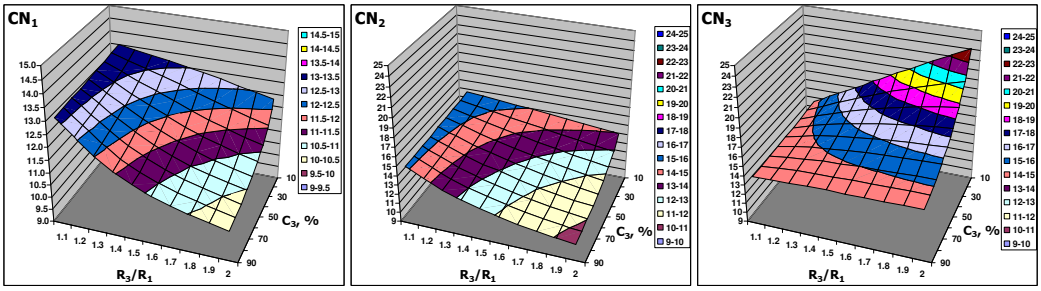

$R_2/R_1 = 1.3$

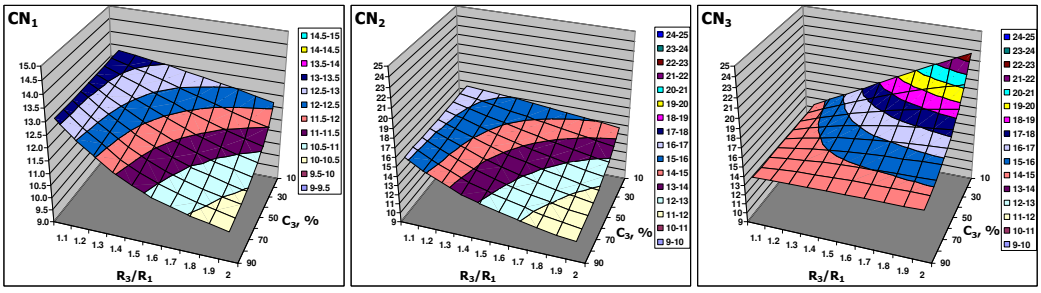

$R_2 / R_1 = 1.4$

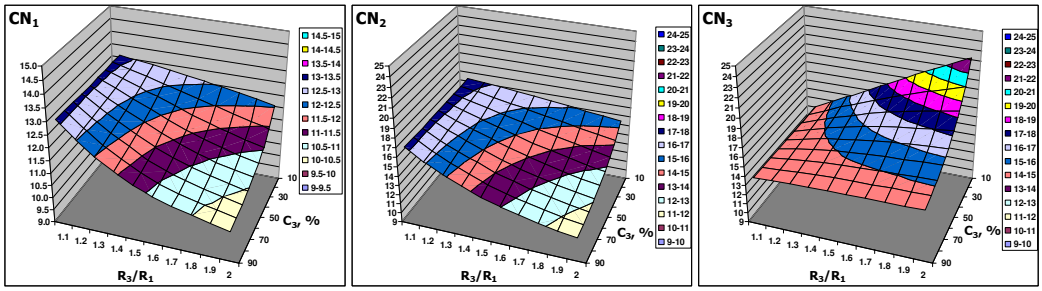

$R_2 / R_1 = 1.5$

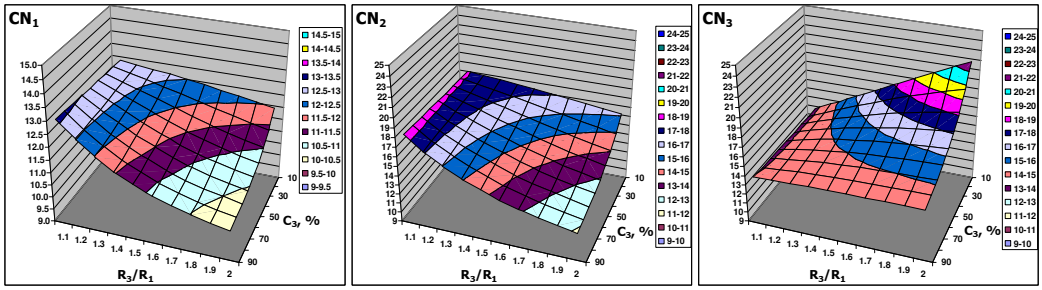

$R_2 / R_1 = 1.6$

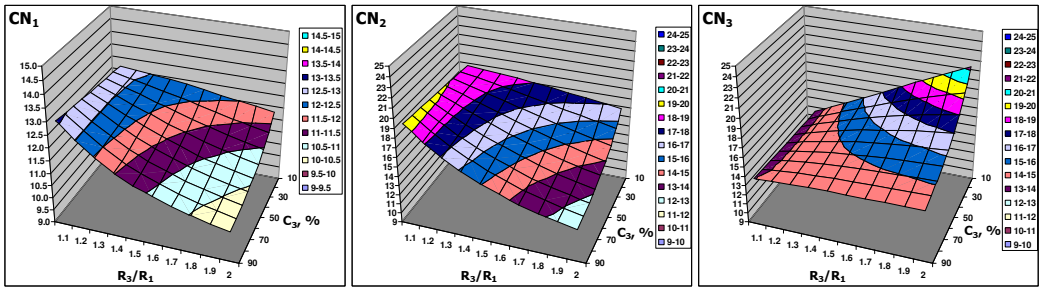

$R_2 / R_1 = 1.7$

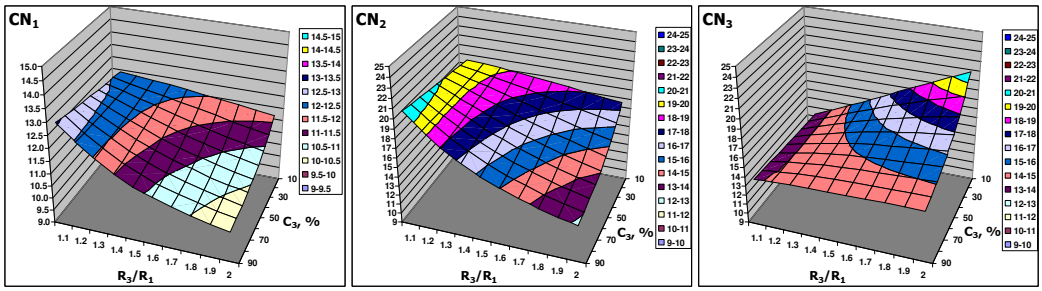

$R_2 / R_1 = 1.8$

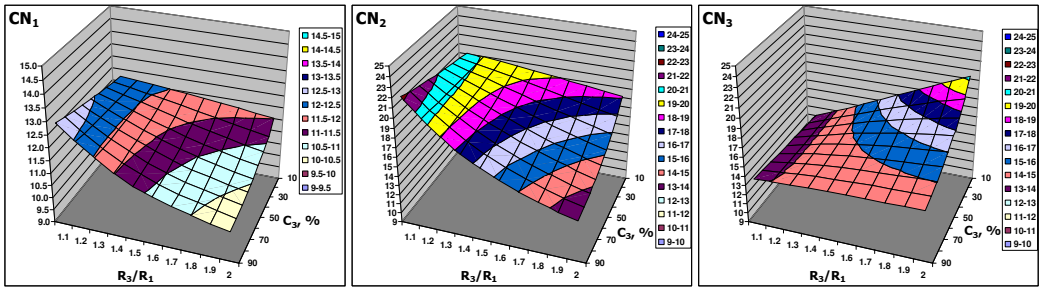

$R_2 / R_1 = 1.9$

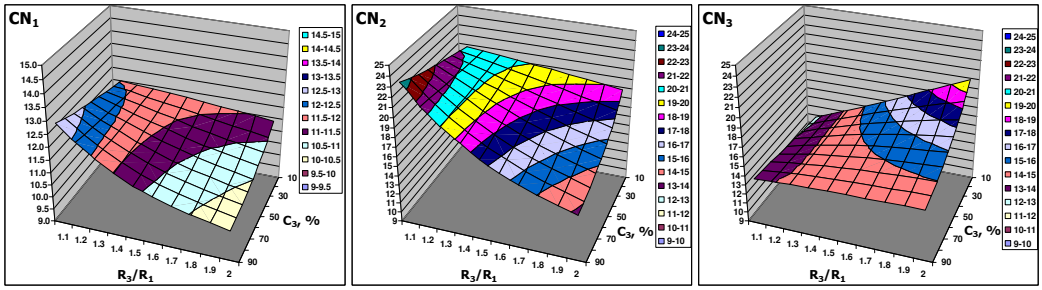

$R_2 / R_1 = 2.0$

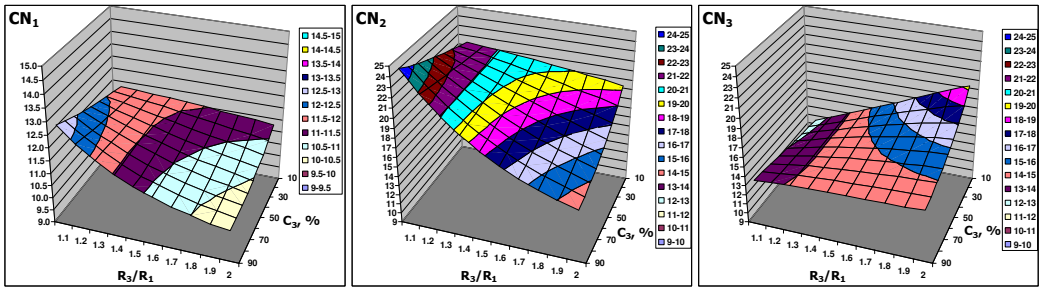

A5.2: Total coordination numbers, CN_i, for three sphere types of ternary systems: $R_2/R_1 = 1.3$; $R_3/R_1 = [1.1,\ 1.2,\ \ldots,\ 2.0]$; $C_1/C_2 = [10/90,\ 20/80,\ \ldots,\ 90/10]$; $C_3 = [10,\ 20,\ \ldots,\ 90]$ %, vs. R_3/R_1 and C_3.

$C_1/C_2 = 10/90$

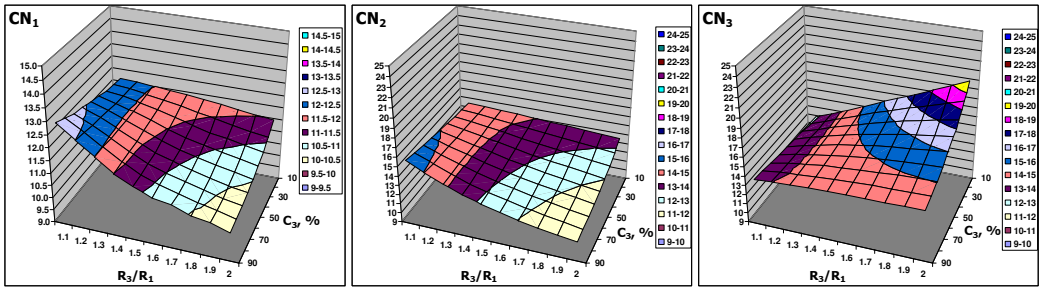

$C_1/C_2 = 20/80$

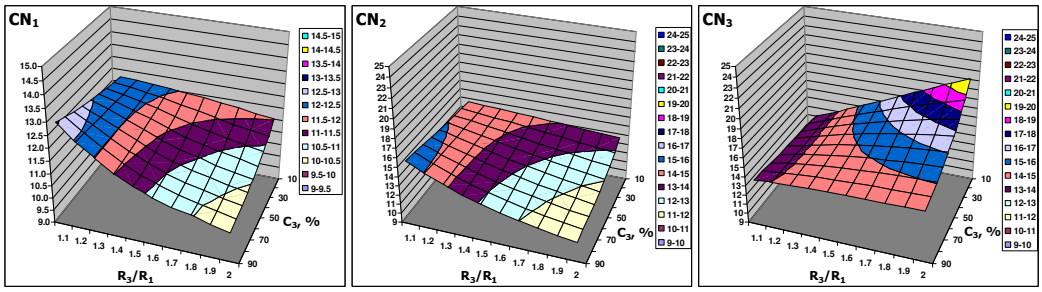

$C_1/C_2 = 30/70$

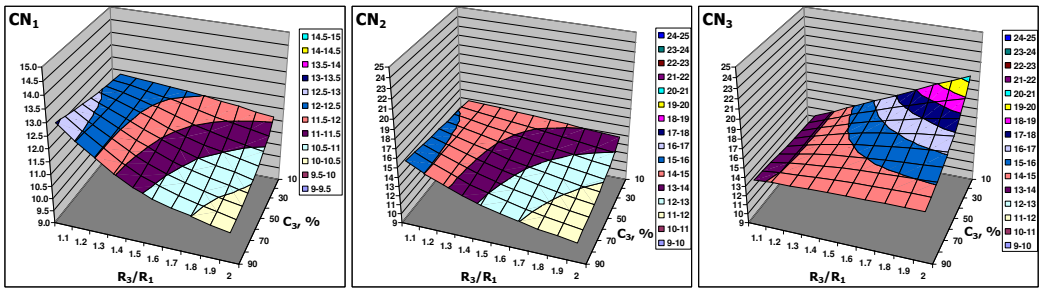

$C_1 / C_2 = 40 / 60$

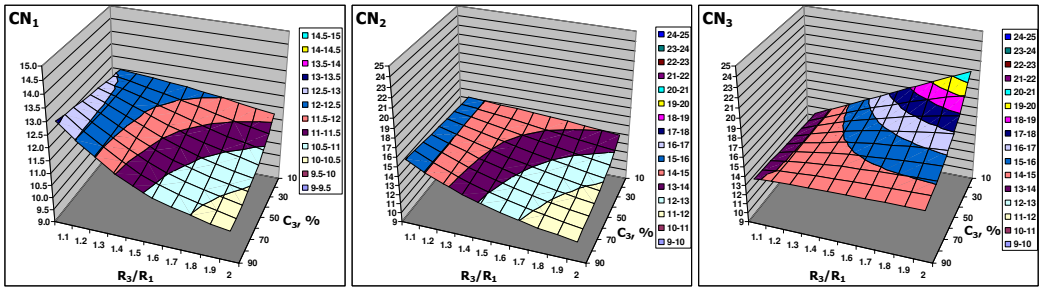

$C_1 / C_2 = 50 / 50$

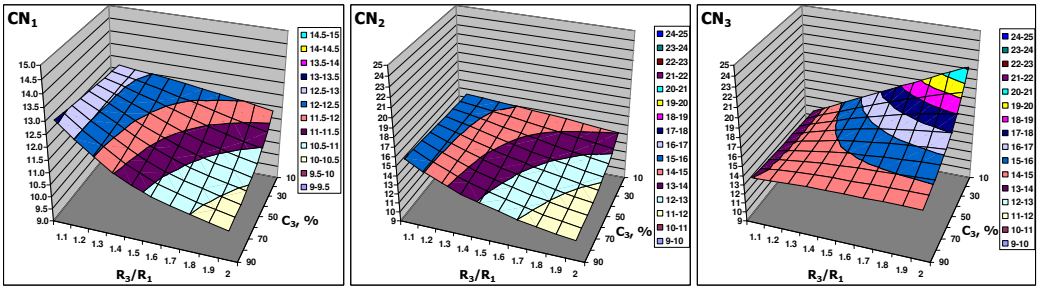

$C_1 / C_2 = 60 / 40$

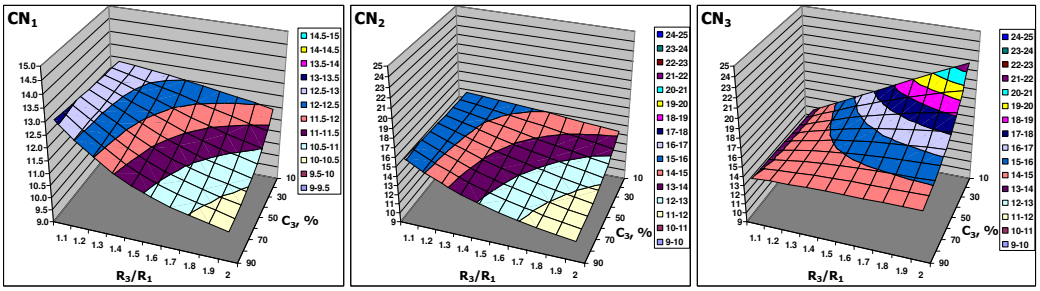

$C_1 / C_2 = 70 / 30$

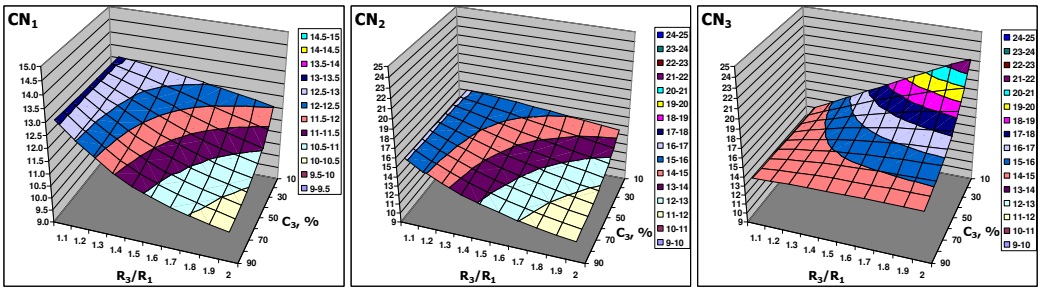

$$C_1 / C_2 = 80/20$$

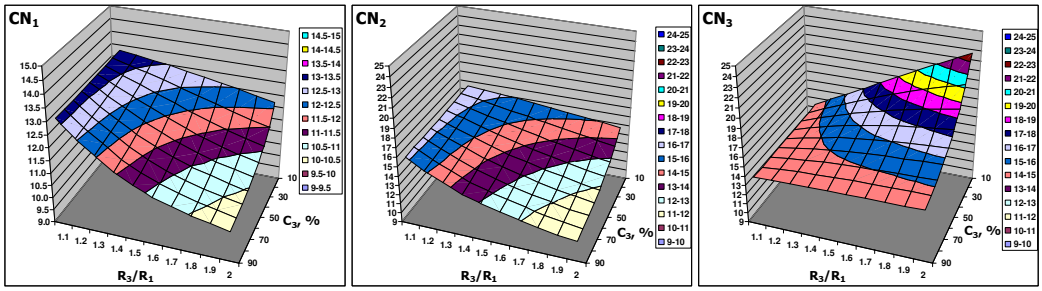

$$C_1 / C_2 = 90/10$$

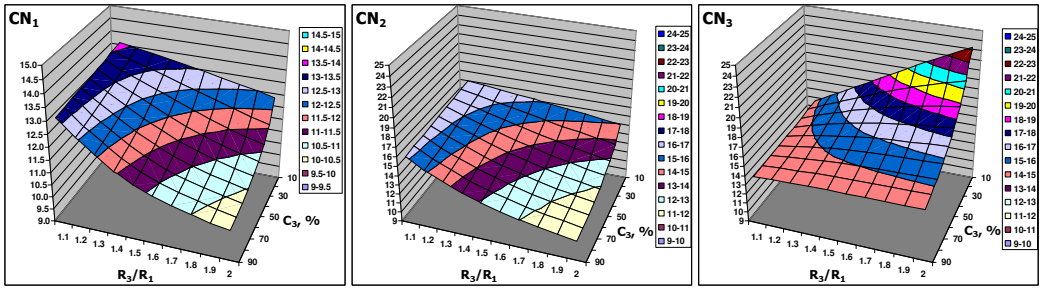

A5.3: Fraction of (0, 0, 12) polyhedron, $f^{(0,0,12)}$, of ternary systems: R_2/R_1, $R_3/R_1 = [1.1,\ 1.2,\ \ldots,\ 2.0]$; $C_1/C_2 = 80/20$; $C_3 = [10,\ 20,\ \ldots,\ 90]$ %, vs. R_3/R_1 and C_3.

$R_2/R_1 = 1.1$

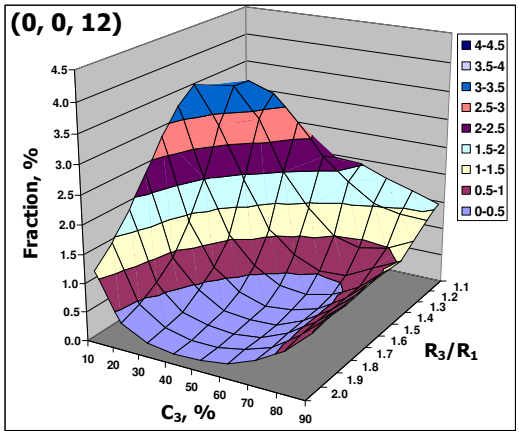

$R_2/R_1 = 1.2$

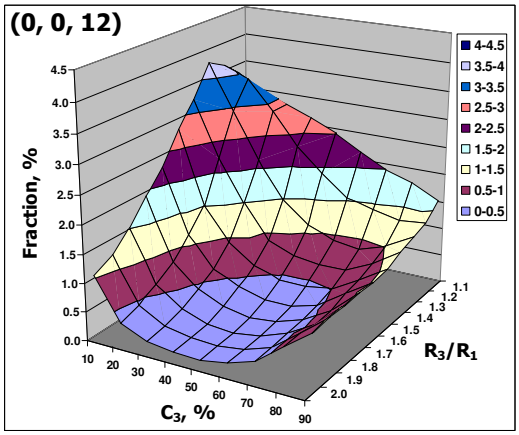

$R_2/R_1 = 1.3$

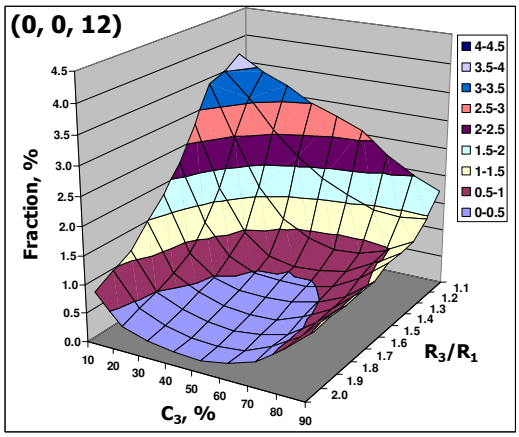

$R_2/R_1 = 1.4$

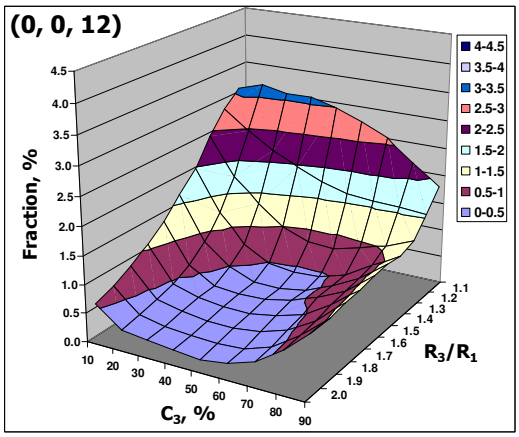

$R_2 / R_1 = 1.5$

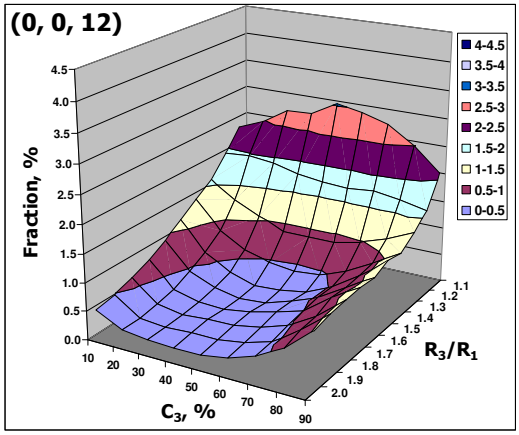

$R_2 / R_1 = 1.6$

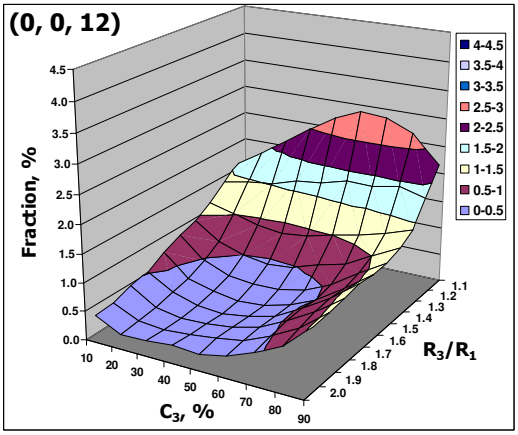

$R_2 / R_1 = 1.7$

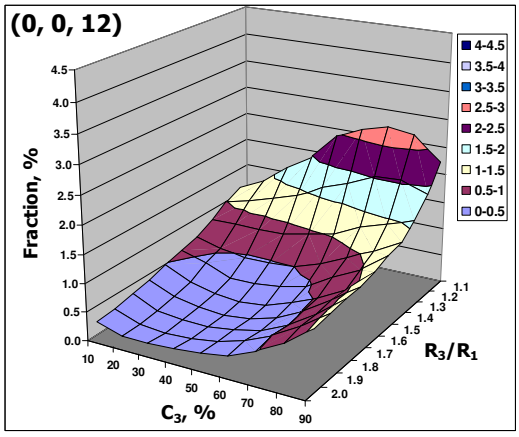

$R_2 / R_1 = 1.8$

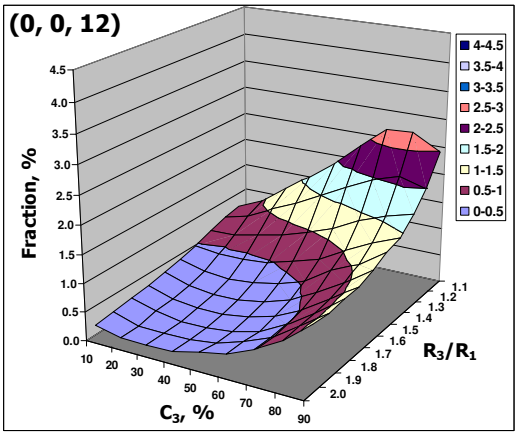

$R_2 / R_1 = 1.9$

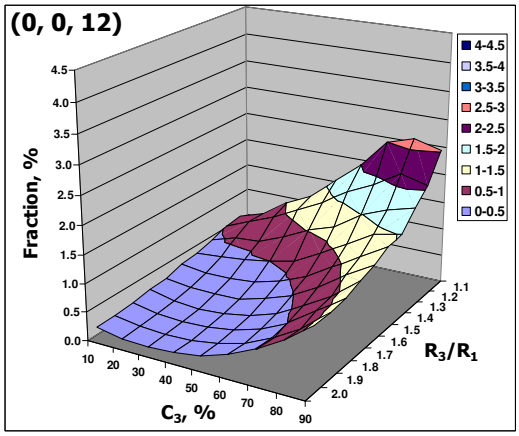

$R_2 / R_1 = 2.0$

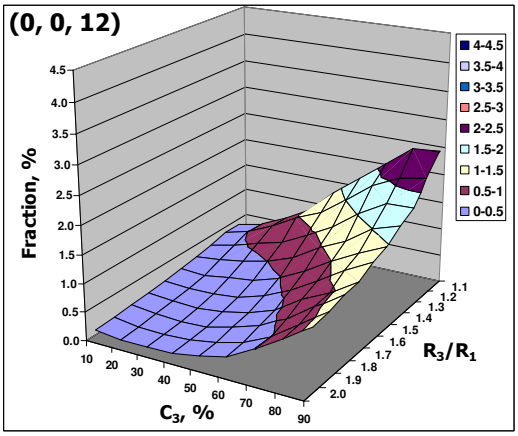

A5.4: Fraction of (0, 0, 12) polyhedron, $f^{(0,0,12)}$, of ternary systems: $R_2/R_1 = 1.3$; $R_3/R_1 = [1.1,\ 1.2,\ \ldots,\ 2.0]$; $C_1/C_2 = [10/90,\ 20/80,\ \ldots,\ 90/10]$; $C_3 = [10,\ 20,\ \ldots,\ 90]$ %, vs. R_3/R_1 and C_3.

$C_1/C_2 = 10/90$

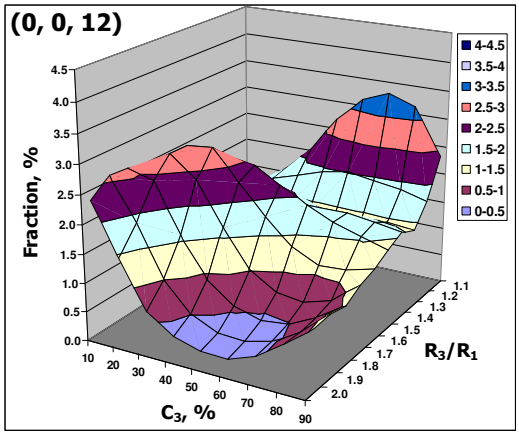

$C_1/C_2 = 20/80$

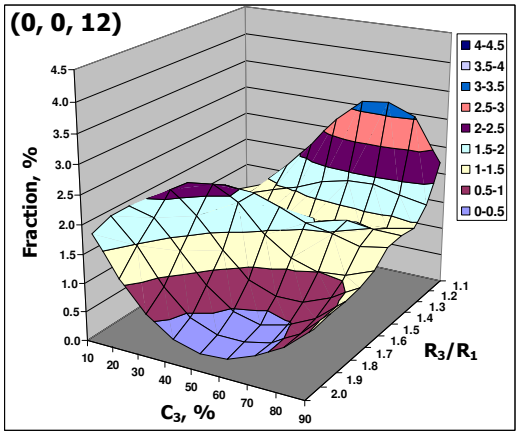

$C_1/C_2 = 30/70$

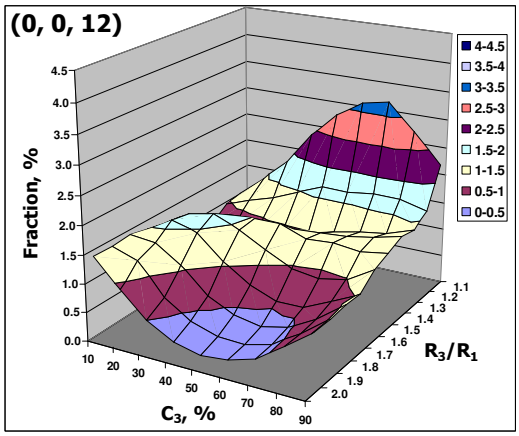

$C_1/C_2 = 40/60$

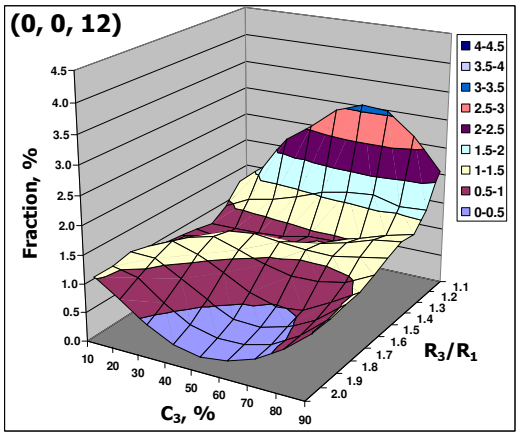

$C_1 / C_2 = 50/50$

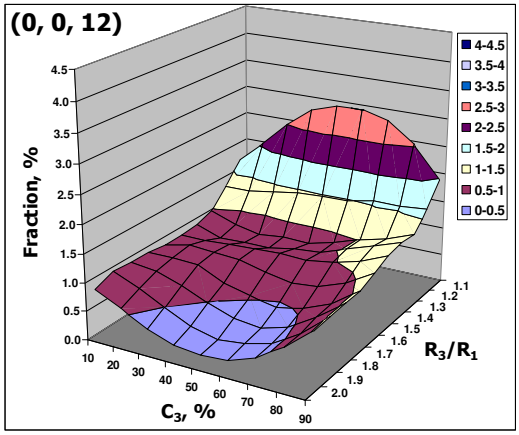

$C_1 / C_2 = 60/40$

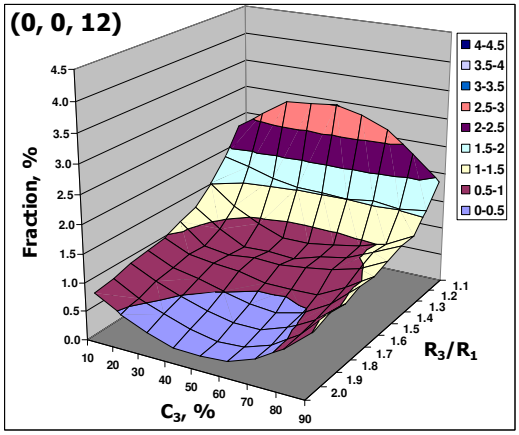

$C_1 / C_2 = 70/30$

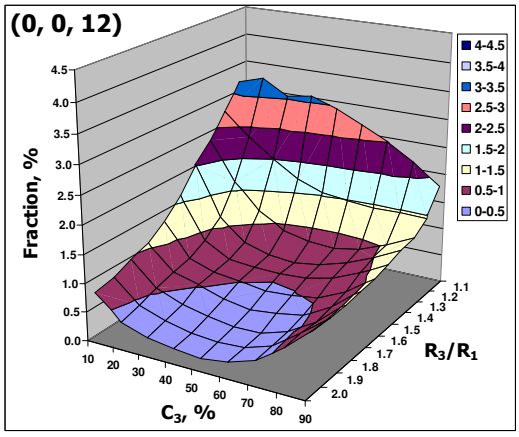

$C_1 / C_2 = 80/20$

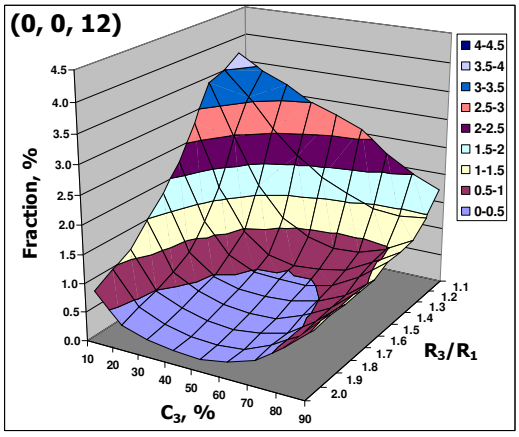

$C_1 / C_2 = 90/10$

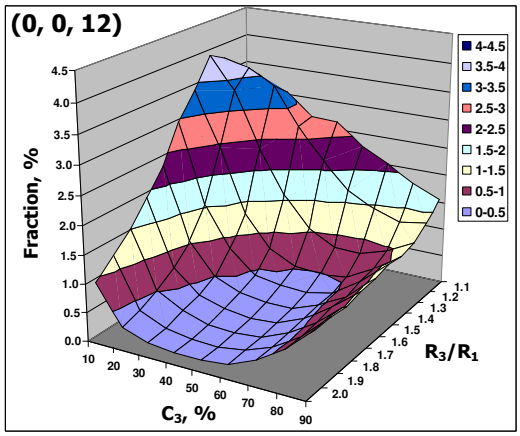

A5.5: Non-crystalline to crystalline faces ratio, F_{nc}, of ternary systems: R_2/R_1, $R_3/R_1 = [1.1,\ 1.2,\ \ldots,\ 2.0]$; $C_1/C_2 = 80/20$; $C_3 = [10,\ 20,\ \ldots,\ 90]$ %, vs. R_3/R_1 and C_3.

$R_2/R_1 = 1.1$

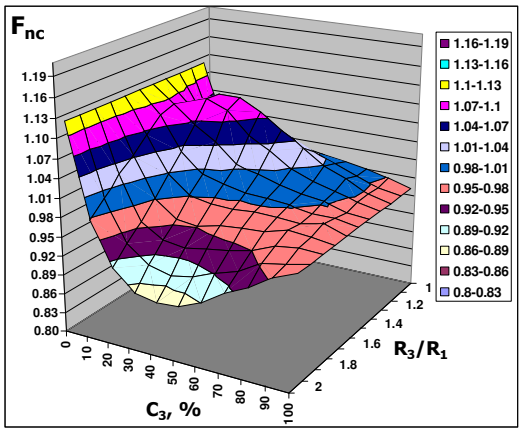

$R_2/R_1 = 1.2$

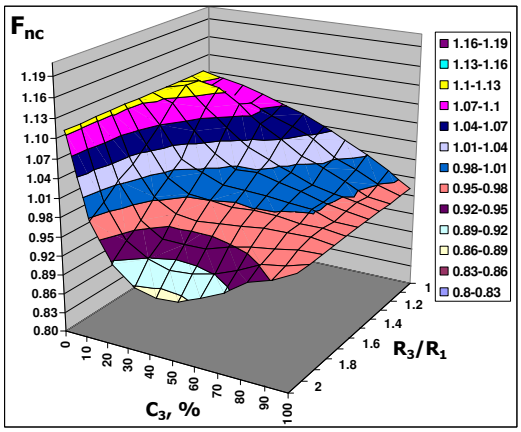

$R_2/R_1 = 1.3$

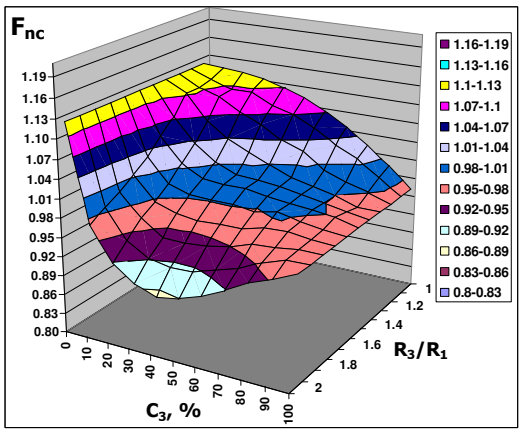

$R_2/R_1 = 1.4$

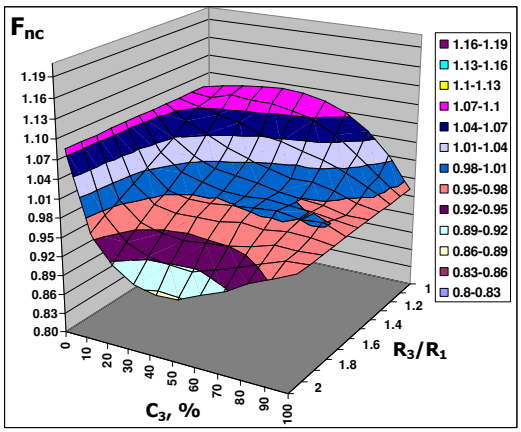

$R_2 / R_1 = 1.5$

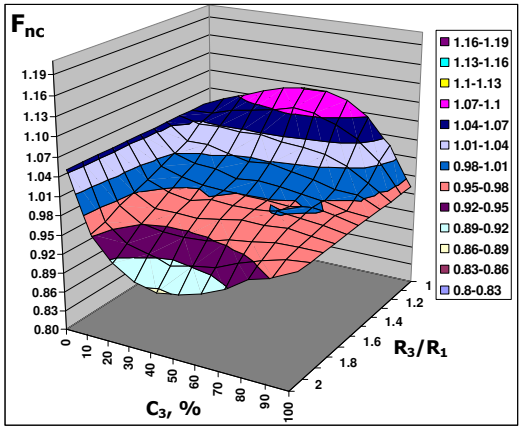

$R_2 / R_1 = 1.6$

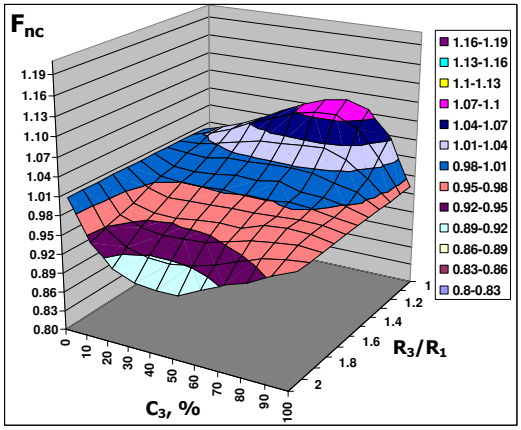

$R_2 / R_1 = 1.7$

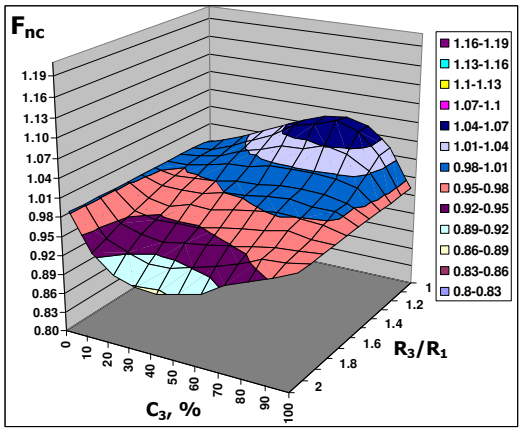

$R_2 / R_1 = 1.8$

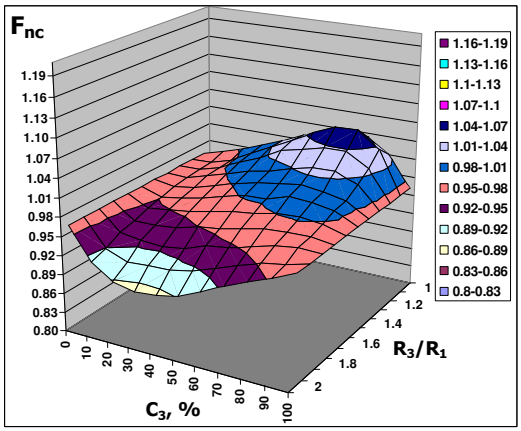

$R_2 / R_1 = 1.9$

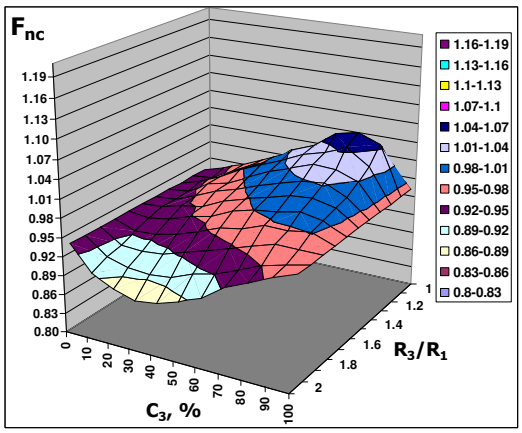

$R_2 / R_1 = 2.0$

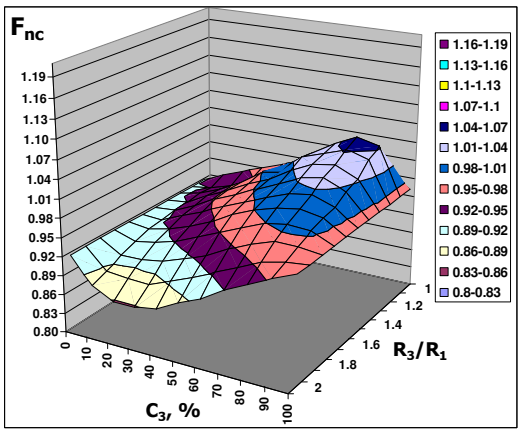

A5.6: Non-crystalline to crystalline faces ratio, F_{nc}, of ternary systems: $R_2/R_1 = 1.3$; $R_3/R_1 = [1.1,\ 1.2,\ \ldots,\ 2.0]$; $C_2/C_1 = [10/90,\ 20/80,\ \ldots,\ 90/10]$; $C_3 = [10,\ 20,\ \ldots,\ 90]$ %, vs. R_3/R_1 and C_3.

$C_1/C_2 = 10/90$

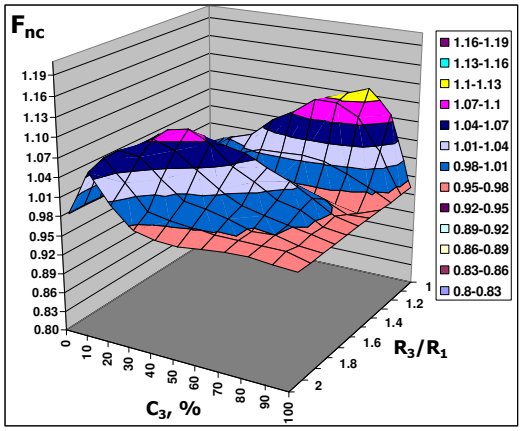

$C_1/C_2 = 20/80$

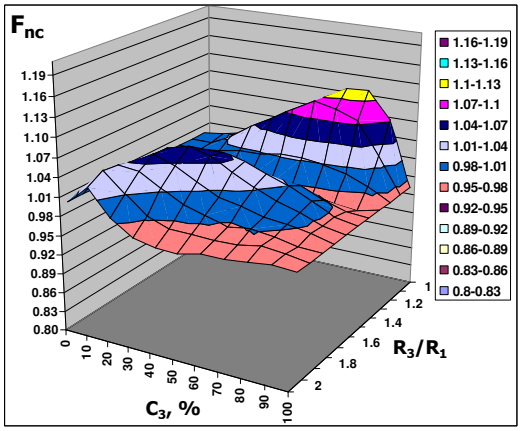

$C_1/C_2 = 30/70$

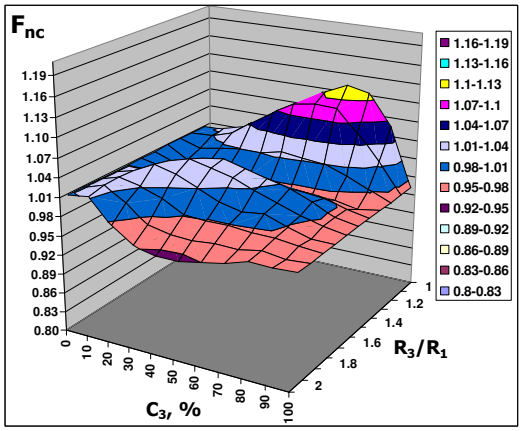

$C_1/C_2 = 40/60$

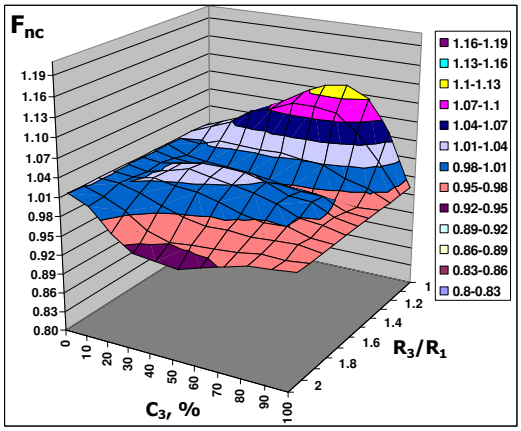

$C_1 / C_2 = 50/50$

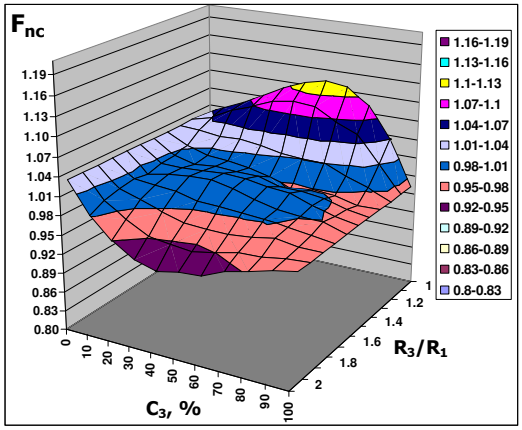

$C_1 / C_2 = 60/40$

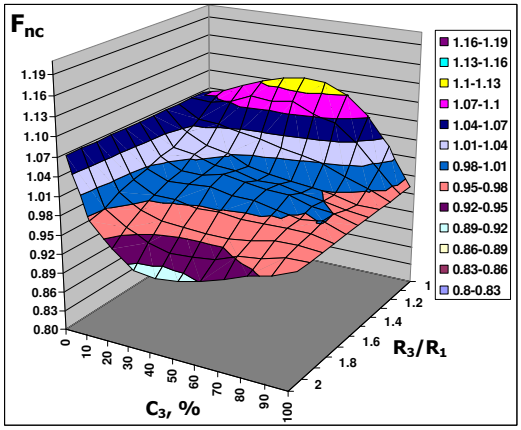

$C_1 / C_2 = 70/30$

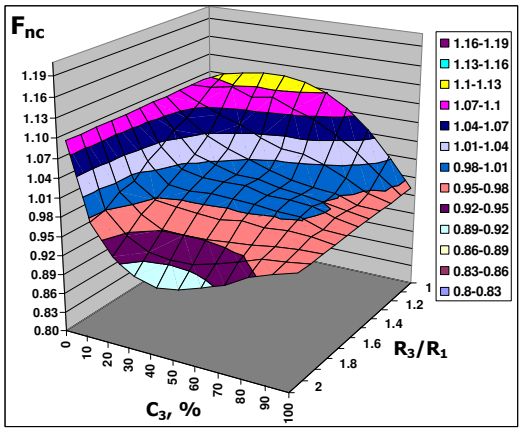

$C_1 / C_2 = 80/20$

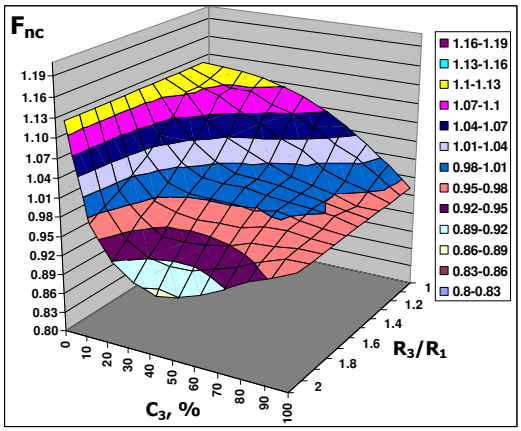

$C_1 / C_2 = 90/10$

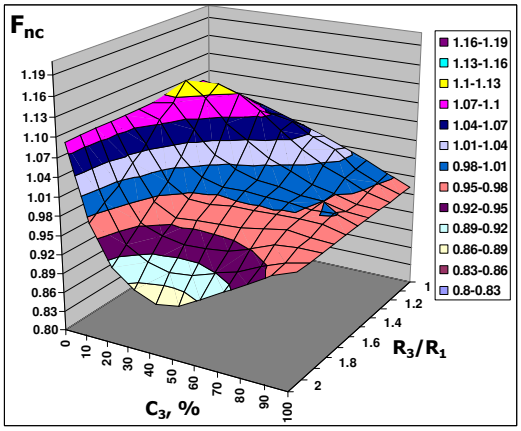

REFERENCES

[Ada72] D.J. Adams, A.J. Matheson: "Computation of dense random packings of hard spheres", *J. Chem. Phys.* **56**, (1972) 1989.

[Alc08] A.N. Alcaraz, R.S. Duhau, J.R. Fernández, P. Harrowell, D.B. Miracle: "Dense amorphous packing of binary hard sphere mixtures with chemical order: The stability of a solute ordered approximant", *J. Non-Cryst. Solids* **354**, (2008) 3171.

[Ald57] B.J. Alder, T.E. Wainright: "Phase transition for a hard sphere system", *J. Chem. Phys.* **27**, (1957) 1208.

[Alf05] D. Alfe: "Melting curve of MgO from first-principles simulations", *Phys. Rev. Lett.* **94**, (2005) 235701.

[And88] P.N. Andrade, M.A. Fortes: "Distribution of cell volumes in a Voronoi partition", *Phil. Mag. B* **58**, (1988) 671.

[Bak95] H. Bakker, G.F. Zhou, H. Yang: "Mechanically driven disorder and phase transformation in alloys", *Prog. Mater. Sci.* **39**, (1995) 159.

[Bak98] H. Bakker: *Enthalpies in alloys – Miedema's semi-empirical model*, Trans Tech Publications Ltd, Switzerland, (1998).

[Bar91] M. Bargieł, J. Mościński: "C-language program for the irregular close packing of hard spheres", *Computer Phys. Commun.* **64**, (1991) 183.

[Bas92] M.I. Baskes: "Modified embedded-atom potentials for cubic materials and impurities", *Phys. Rev. B* **46**, (1992) 2727.

[Bau07] J. Baumgart, R.P.A. Dullens, M. Dijkstra, R. Roth, C. Bechinger: "Experimental observation of structural crossover in binary mixtures of colloidal hard spheres", *Phys. Rev. Lett.* **98**, (2007) 198303.

[Ben72] C.H. Bennett: „Serially deposited amorphous aggregates of hard spheres", *J. Appl. Phys.* **43**, (1972) 2727.

[Ben86] U. Bengtzelius: "Dynamics of a Lennard-Jones system close to the glass-transition", *Phys.Rev. A* **34**, (1986) 5059.

[Ber37] J.D. Bernal: „An attempt at a molecular theory of liquid structure", *Trans. Farad. Soc.* **33**, (1937) 27.

[Ber59] J.D. Bernal: „A geometrical approach to the structure of liquids", *Nature* **183**, (1959) 141.

[Ber60] J.D. Bernal: „Geometry of the structure of monatomic liquids", *Nature* **185**, (1960) 68.

[Ber64] J.D. Bernal: „The Bakerian lecture, 1962. The structure of liquids", *Proc. Roy. Soc.* **A 280**, (1964) 299.

[Ber67] J.D. Bernal, J.L. Finney: "Random close-packed hard-sphere model. II. Geometry of random packing of hard spheres", *Discuss. Faraday Soc.* **43**, (1967) 62.

[Ber83] J.G. Berryman: "Random close packing of hard spheres and disks", *Phys. Rev. A* **27**, (1983) 1053.

[Bez02] A. Bezrukov, M. Barguel, D. Stoyan: "Statistical analysis of simulated random packings of spheres", *Part. Part. Syst. Charact.* **19**, (2002) 111.

[Boe89] F.R. De Boer, R. Boom, W.C.M. Mattens, A.R. Miedema, A.K. Niessen: *Cohesion in Metalls*, North-Holland, Amsterdam, The Netherlands, (1989).

[Bou77] D.S. Boudreaux, J.M. Gregor: „Structure simulation of transition-metal-metalloid glasses", *J. Appl. Phys.* **48**, (1977) 152.

[Bou95] A. Bourkba, M. Azzanaoui, N. David, J. Hertz: "Experimental mixing enthalpy of the liquid (Al, Ga, Sn) solution: Darken and Redlich-Kister modeling", *Z. Metallkd.* **86**, (1995) 326.

[Bou96] A. Bourkba, J.M. Fiorani, C. Naguet, J. Hertz: "The mixing enthalpy of the ternary (Pb, Sn, Zn) liquid phase – calorimetric measurements and modeling outside and inside the miscibility gap", *Z. Metallkd.* **87**, (1996) 773.

[Bou99] A. Bourkba, J.M. Fiorani, N. David, J. Hertz: "Experimental enthalpy of mixing of liquid Al-Ga-Zn alloys and Redlich-Kister modeling", *Z. Metallkd.* **90**, (1999) 407.

[Bro82] J.Q. Broughton, G.H. Gilmer, and K.A. Jackson: "Crystallization rates of a Lennard-Jones liquid", *Phys. Rev. Lett.* **49**, (1982) 1496.

[Buc54] W. Buckel: „Elektronenbeugungs-Aufnahmen von dünnen Metallschichten bei tiefen Temperaturen", *Z. Physik* **138**, (1954) 136.

[Che01] Z. Cheng, P.M. Chaikin, W.B. Russel, W.V. Meyer, J. Zhu, R.B. Rogers, R.H. Ottewill: "Phase diagram of hard spheres", *Materials and Design* **22**, (2001) 529.

[Che05] X.Q. Chen, R. Podloucky, P. Rogl: "Comment on 'Proposed model for calculating the standard formation enthalpy of binary transition-metal systems' [Appl. Phys. Lett. 81, 1219 (2002)]", *Appl. Phys. Lett.* **86**, (2005) 216103.

[Che69] H.S. Chen, D. Turnbull: „Formation, stability and structure of palladium-silicon based alloy glasses", *Acta Metall.* **17**, (1969) 1021.

[Che74] H.S. Chen: „Thermodynamic consideration on the formation and stability of metallic glasses", *Acta Metall.* **22**, (1974) 1505.

[Che76] H.S. Chen: „Glass temperature, formation and stability of Fe, Co, Ni, Pd and Pt based glasses", *Mater. Sci. Eng.* **23**, (1976) 151.

[Che80] H.S. Chen: "Glassy metals", *Rep. Prog. Phys.* **43**, (1980) 353.

[Cho87] K.-C. Chou: "A new solution model for predicting ternary thermodynamic properties", *CALPHAD* **11**, (1987) 293.

[Cho95] K.-C. Chou: "A general solution model for predicting ternary thermodynamic properties", *Calphad* **19**, (1995) 315.

[Cla87] A.S. Clarke, J.D. Wiley: "Numerical simulation of the dense random packing of a binary mixture of hard spheres: amorphous metals", *Phys. Rev. B* **35**, (1987) 7350.

[Dir50] G. L. Dirichlet: „Über die Reduction der positiven quadratischen Formen mit drei unbestimmten ganzen Zahlen.", *J. Reine Angew. Math.* **40**, (1850) 209.

[Dre82] A.J. Drehman, A.L. Greer, D. Turnbull: „Bulk formation of a glass: $Pd_{40}Ni_{40}P_{20}$", *Appl. Phys. Lett.* **41**, (1982) 716.

[Dua05] G. Duan, D. Xu, W. L. Johnson: "High copper content bulk glass formation in bimetallic Cu-Hf system", *Metallurg. Mater. Trans. A* **36**, (2005) 455.

[Dua08] G. Duan, K.D. Blauwe, M.L. Lind, J.P. Schramm, W.L. Johnson: "Compositional dependence of thermal, elastic, and mechanical properties in Cu–Zr–Ag bulk metallic glasses", *Scripta Mater.* **58**, (2008) 159.

[Duw60] P. Duwez, R.H. Willens, W. Klement (jun.): „Continuous series of metastable solid solutions in silver-copper alloys", *J. App. Phys.* **31**, (1960) 1136.

[Eck02] T. Eckert, E. Bartsch: „Re-entrant glass transition in a colloid-polymer mixture with depletion attractions", *Phys. Rev. Lett.* **89**, (2002) 125701.

[Ega03] T. Egami: "Atomistic mechanism of bulk metallic glass formation", *J. Non-Cryst. Solids* **317**, (2003) 30.

[Ega84] T. Egami T, Y. Waseda: "Atomic size effect on the formability of metallic glasses", *J. Non-Cryst. Solids.* **64**, (1984) 113.

[Erc94] F. Ercolessi, J.B. Adams: "Interatomic potentials from first-principles calculations: The force-matching method", *Europhys. Lett.* **26**, (1994) 583.

[Esh56] D.J. Eshelby: *Solid state physics*, Academic Press, New York, USA, 1956.

[Fin67] J.L. Finney, J.D. Bernal: "Random close packing and the heat of fusion of simple liquids", *Nature* **213**, (1967) 1079.

[Fin70a] J.L. Finney: "Random packing and the structure of liquids. II. The molecular geometry of simple liquids", *Proc. Roy. Soc.* **A 319**, (1970) 495.

[Fin70b] J.L. Finney: "Random packing and the structure of liquids. I. The geometry of random close packing", *Proc. Roy. Soc.* **A 319**, (1970) 479.

[Fin77] J.L. Finney: "Modeling the structures of amorphous metals and alloys", *Nature* **266**, (1977) 309.

[Fra58] F.C. Franc, J.S. Kasper: "Complex alloy structures regarded as sphere packings. I. Definition and basic principles", *Acta Cryst.* **11**, (1958) 184.

[Fre02] D. Frenkel, B. Smit: *Understanding Molecular Simulation*, Academic press, London, Great Britain, (2002).

[Gan97] V. Ganesan, F. Schuller, H. Feufel, F. Sommer, H. Ipser: „Thermodynamic properties or ternary liquid Cu-Mg-Y alloys", *Z. Metallkd.* **88**, (1997) 701.

[Gas79] P.H. Gaskell: "A new structural model for amorphous transition metal silicides, borides, phosphides and carbides", *J. Non-Cryst. Solids* **32**, (1979) 207.

[Gas83] P.H. Gaskell: "Models for the structure of amorphous metals", *Top Appl. Phys.* **53**, (1983) 5.

[Ger95] M. Gerstein, J. Tsai, M. Levitt: „The volume of atoms on the protein surface: calculated from simulation, using Voronoi polyhedra", *J. Mol. Biol.* **249**, (1995) 955.

[Goe97] A. Goede, R. Preissner, C. Frömmel: „Voronoi cell: New method for allocation of space among atoms: Elimination of avoidable errors in calculation of atomic volume and density", *J. Comput. Chem.* **18**, (1997) 1113.

[Got78] K. Gotoh, W.S. Jodrey, E.M. Tory: "A random packing structure of equal spheres – statistical analysis of tetrahedral configurations", *Powder Technol.* **20**, (1978) 233.

[Gou01] Q. Guo, O.J. Kleppa: "The standard enthalpies of formation of the compounds of early transition metals with late transition metals and with noble metals as determined by Kleppa and co-workers at the University of Chicago — A review", *J. Alloys Comp.* **321**, (2001) 169.

[Gue01] M. Guerdane, H. Teichler: "Structure of the amorphous, massive-metallic-glass forming $Ni_{25}Zr_{60}Al_{15}$ alloy from molecular dynamics simulations", *Phys. Rev. B* **65**, (2001) 014203.

[Hee00] A. Heesemann, V. Zöllmer, K. Rätzke, F. Faupel: „Evidence of highly collective Co diffusion in the whole stability range of Co-Zr glasses", *Phys. Rev. Lett.* **84**, (2000) 1467.

[Hen57] D.G. Henshaw: "Atomic distribution in liquid argon by neutron diffraction and the cross section of A^{36} and A^{40}", *Phys. Rev.* **105**, (1957) 976.

[Hen58] D.G. Henshaw: "Atomic distribution in liquid and solid neon and solid argon by neutron diffraction", *Phys. Rev.* **111**, (1958) 1470.

[Hen60] D.G. Henshaw: "Effect of the λ transition on the atomic distribution in liquid helium by neutron diffraction", Phys. Rev. 119, (1960) 9.

[Her05] H. Hermann, A. Elsner, T. Gemming: "Influence of the packing effect on stability and transformation of nanoparticles embedded in random matrices", *Mater. Sci.-Poland* **23**, (2005) 541.

[Her07a] H. Hermann, A. Elsner, K. Lochmann, D. Stoyan: "Optimization of multi-component hard sphere liquids with respect to the dense packing", *Mater. Sci. Eng. A* **449-451**, (2007) 666.

[Her07b] H. Hermann, A. Elsner, D. Stoyan: "Behavior of icosahedral clusters in computer simulated hard sphere systems", *J. Non-Cryst. Solids* **353**, (2007) 3693.

[Her83] H. Hermann: "Influence of directed chemical bonding on the structure of metallic glasses", *Phys. Stat. Sol. (B)* **117**, (1983) 185.

[Hey97] B. Heyd, I. Bardot, Ph. Bourriot: "Comparison of optimization algorithms in formulation on a sensory basis", *Food Quality and Preference* **8**, (1997) 73.

[Hil80] M.Hillert: "Empirical methods of predicting and representing thermodynamic properties of ternary solution phases", *CALPHAD* **4**, (1980) 1.

[Ino00] A. Inoue: "Stabilization of metallic supercooled liquid and bulk amorphous alloys", *Acta Mater.* **48**, (2000) 279.

[Ino89a] A. Inoue, T. Zhang, T. Masumoto: „Al-La-Ni amorphous alloys with a wide supercooled liquid region", *Mater. Trans. JIM* **30**, (1989) 965.

[Ino89b] A. Inoue, M. Kohinata, A.P. Tsai, T. Masumoto: "Mg-Ni-La amorphous alloys with a wide supercooled liquid region", *Mater. Trans. JIM* **30**, (1989), 378.

[Ino90a] A. Inoue, T. Zhang, T. Masumoto: „ Al-La-Cu amorphous alloys with a wide supercooled liquid region", *Mater. Trans. JIM* **31**, (1990) 104.

[Ino90b] A. Inoue, T. Zhang, T. Masumoto: „Production of amorphous cylinder and sheet of $La_{55}Al_{25}Ni_{20}$ alloy by a metallic mold casting method", *Mater. Trans. JIM* **31**, (1990) 425.

[Ino91] A. Inoue, A. Kato, T. Zhang, S.G. Kim, T. Masumoto: „Mg-Cu-Y amorphous alloys with high mechanical strengths produced by a metallic mold casting method", *Mater. Trans. JIM* **32**, (1991) 609.

[Ino93a] A. Inoue, T. Nakamura, T. Sugita, T. Zhang, T. Masumoto: „Bulky La-Al-TM (TM = Transition Metal) amorphous alloys with high tensile strength produced by a high-Pressure die casting method", *Mater. Trans. JIM* **34**, (1993) 351.

[Ino93b] A. Inoue, T. Zhang, N. Nishiyama, K. Ohba, T. Masumoto: „Preparation of 16 mm diameter rod of amorphous $Zr_{65}Al_{7.5}Ni_{10}Cu_{17.5}$ alloy", *Mater. Trans. JIM* **34**, (1993) 1234.

[Ino97a] A. Inoue, N. Nishiyama, H. Kimura: „Preparation and thermal stability of bulk amorphous $Pd_{40}Cu_{30}Ni_{10}P_{20}$", *Mater. Trans. JIM* **38**, (1997) 179.

[Ino97b] A. Inoue: "Bulk amorphous alloys with soft and hard magnetic properties", *Mater. Sci. Eng. A* **226-228**, (1997) 357.

[Jac87] K.W. Jacobsen, J.K. Norskov, M.J. Puska: "Interatomic interactions in the effective medium theory", *Phys. Rev. B* **35**, (1987) 7423.

[Jod79] W.S. Jodrey, E.M. Tory: "Simulation of random packing of spheres", *Simulation* **32**, (1979) 1.

[Jod81] W.S. Jodrey, E.M. Tory: "Computer simulation of isotropic, homogeneous, dense random packing of equal spheres", *Powder Technol.* **30**, (1981) 111.

[Jod85] W.S. Jodrey, E.M. Tory: "Computer simulation of close random packing of equal spheres", *Phys. Rev. A* **32**, (1985) 2347.
W.S. Jodrey, E.M. Tory: "Erratum: Computer simulation of close random packing of equal spheres [Phys. Rev. A 32, 2347 (1985)]", *Phys. Rev. A* **34**, (1986) 675.

[Kan03a] D. S. Kanibolotsky, O.A. Bieloborodova, N.V. Kotova, V.V. Lisnyak: "Enthalpy of mixing in liquid Al–Fe–Si alloys at 1750 K", *Thermochimica Acta* **408** (2003) 1.

[Kan03b] D.S. Kanibolotsky, N.V. Kotova, O.A. Bieloborodova, V.V. Lisnyak: "Thermodynamics of liquid aluminium–copper–germanium alloys", *J. Chem. Termodynamics* **35**, (2003) 1763.

[Kan04a] D. S. Kanibolotsky, O.A. Bieloborodova, V.A. Stukalo, N.V. Kotova, V. V. Lisnyak: "Thermodynamics of liquid aluminium–copper–silicon alloys", *Thermochimica Acta* **412**, (2004) 39.

[Kan04b] D.S. Kanibolotsky, N.V. Golovataya, O.A. Bieloborodova, V.V. Lisnyak: "Calorimetric investigation of liquid Al–Ga–Gd alloys", *Thermochimica Acta* **421**, (2004) 111.

[Kan05a] D.S. Kanibolotsky, O.A. Bieloborodova, V.V. Lisnyak: "Calorimetric study of enthalpies of mixing in liquid gallium–germanium–yttrium alloys", *Thermochimica Acta* **438**, (2005) 51.

[Kan05b] D.S. Kanibolotsky, N.V. Golovataya, O.A. Bieloborodova, V.V. Lisnyak: "Enthalpy of mixing of liquid (gallium–gadolinium–silicon) alloys measured by high-temperature isoperibolic calorimetry", *J. Chem. Thermodynamics* **37**, (2005) 449.

[Kan06a] D. S. Kanibolotsky, O.A. Bieloborodova, V.V. Lisnyak: "Calorimetric study of enthalpies of mixing in liquid (aluminium–gallium–yttrium) alloys", *J. Chem. Thermodynamics* **38**, (2006) 1150.

[Kan06b] D.S. Kanibolotsky, N.V. Kotova, O.A. Bieloborodova, V.V. Lisnyak: "High temperature calorimetric examination of enthalpies of mixing in liquid (gadolinium–germanium–manganese) alloys", *J. Chem. Termodynamics* **38**, (2006) 849.

[Kau83] S.N. Kaul: "Weak itinerant ferromagnetism in amorphous $M_{90}Zr_{10}$ (M=Fe,Co,Ni) alloys", *Phys. Rev. B* **27**, (1983) 6923.

[Kim95] Y.B. Kim, F. Sommer, B. Predel: „Determination of the enthalpy of mixing of liquid Aluminum-Copper-Magnesium alloys", *Z. Metallkd.* **86** (1995) 597.

[Kle60] W. Klement (jun.), R.H. Willens, Pol Duwez: „Non-crystalline structure in solidified gold-silicon alloys", *Nature* **187**, (1960) 869.

[Koh60] F. Kohler: "Zur Berechnung der thermodynamischen Daten eines ternären Systems aus den zugehörigen binären Systemen", *Mh. Chem.* **91**, (1960) 738.

[Kok08] V. Kokotin, H. Hermann: "Computational analysis of the atomic size effect in bulk metallic glasses and their liquid precursors", *Acta Mater.* **56**, (2008) 5058.

[Kry93] A.S. Krylov, A.M. Katsnelson: "The application of the model of Quasi-ideal associated solutions to the calculation of the thermodynamics of ternary melts", *Z. Metallkd.* **84**, (1993) 641.

[Kui84] W.H. Kui, A.L. Greer, D. Turnbull: „Formation of bulk metallic glass by fluxing", *Appl. Phys. Lett.* **45**, (1984) 615.

[Lag98] J.C. Lagarias, J.A. Reeds, M.H. Wright, P.E. Wright: "Convergence properties of the Nelder-Mead simplex method in low dimensions", *SIAM J. Optim.* **9**, (1998) 112.

[Lai89] B.B. Laird, A.D.J. Haymet: "The crystal liquid interface of a body-centered-cubic-forming substance – Computer-simulations of the R-6 potential", *J. Chem. Phys.* **91**, (1989) 3638.

[Lee03] H.J. Lee, T. Cagin, W.L. Johnson, W.A. Goddard III: "Criteria for formation of metallic glasses: The role of atomic size ratio", *J. Chem. Phys.* **119**, (2003) 9858.

[Lee82] M.C. Lee, J.M. Kendall, W.L. Johnson: „Spheres of the metallic glass $Au_{55}Pb_{22.5}Sb_{22.5}$ and their surface characteristics", *Appl. Phys. Lett.* **40**, (1982) 382.

[Lek07] Ch.E. Lekka, A. Ibenskas, A.R. Yavari, G.A. Evangelakisa: "Tensile deformation accommodation in microscopic metallic glasses via subnanocluster reconstructions", *Appl. Phys. Lett.* **91**, (2007) 214103.

[Li08] Z. Li, M. Dallegri, S. Knott: "Calorimetric measurements of the ternary Ag–Au–Sn system", *J. Alloys Comp.* **453**, (2008) 442.

[Loc06] K. Lochmann, A. Anikeenko, A. Elsner, N. Medvedev, D. Stoyan: „Statistical verification of crystallization in hard sphere packings under densification", *The Europ. Phys. J. B* **53**, (2006) 67.

[Loe03] J.F. Löffler: „Bulk metallic glasses", *Intermetallics* **11**, (2003) 529.

[Lon09] Z. Long, H. Wei, Y. Ding, P. Zhang, G. Xie, A. Inoue: "A new criterion for predicting the glass-forming ability of bulk metallic glasses", *J. Alloys Compd.* **475**, (2009) 207.

[Lu02] Z.P. Lu, C.T. Liu: "A new glass-forming ability criterion for bulk metallic glasses", *Acta Mater.* **50**, (2002) 3501.

[Lu07] Z.P. Lu, H. Bei, C.T. Liu: "Recent progress in quantifying glass-forming ability of bulk metallic glasses", *Intermetallics* **15**, (2007) 618.

[Lüc86] R. Lück, U. Gerling, B. Predel: "Über die Interpolation thermodynamischer Mischungsfunktionen höherkomponentiger Systeme aus binären Randsystemen", *Z. Metalkd.* **77**, (1986) 442.

[Mat07] N. Mattern: "Structure formation in liquid and amorphous metallic alloys", *J. Non-Cryst. Solids* **353**, (2007) 1723.

[Mat09] N. Mattern, P. Jóvári, I. Kaban, S. Gruner, A. Elsner, V. Kokotin, H. Franz, B. Beuneu, J. Eckert: "Short-range order of Cu–Zr metallic glasses", *J. Alloys Compd.* **485**, (2009) 163.

[Mat74] A.J. Matheson: „Computation of a random packing of hard spheres“, *J. Phys. C* **7**, (1974) 2569.

[Met53] N. Metropolis, A.W. Rosenbluth, M.N. Rosenbluth, A.N. Teller, E. Teller: “Equation of state calculations by fast computing machines”, *Chem. Phys.* **21**, (1953) 1087.

[Mih04] M. Mihalkovic, M. Widom: “Ab initio calculations of cohesive energies of Fe-based glass-forming alloys”, *Phys. Rev. B* **70**, (2004) 144107.

[Mil02] M.K. Miller, T.D. Shen, R.B. Schwarz: “Atom probe tomography study of the decomposition of a bulk metallic glass”, *Intermetallics* **10**, (2002) 1047.

[Mil08] M. Miller, P. Liaw: *Bulk metallic glasses – an overview*, Springer, New York, USA, (2008).

[Mir04a] D.B. Miracle: “Efficient local packing in metallic glasses”, *J. Non-Cryst. Solids* **342**, (2004) 89.

[Mir04b] D.B. Miracle: “A structural model for metallic glasses”, *Nat. Mater*. **3**, (2004) 697.

[Mir06] D.B. Miracle: “The efficient cluster packing model – An atomic structural model for metallic glasses”, *Acta Mater.* **54**, (2006) 4317.

[Moh93] T. Mohri, S. Takizawa, K. Terakura: “First-principles calculation of heats of formation for Au-Cu, Au-Pd and Au-Ag alloys with thermal vibration effects”, *J. Phys.: Condens. Matter.* **5**, (1993) 147.

[Moo93] R.E.M. Moore, I.O. Angell: “Voronoi polygons and polyhedra”, *J. Comput. Phys.* **105**, (1993) 301.

[Mra74] P. Mrafko, P. Duhaj: “X-Ray study of an amorphous $Pd_{80}Si_{20}$ alloy”, *Phys. Stat. Sol.* **22**, (1974) 151.

[Mug75] Y.M. Muggianu, M. Gambino, J.P. Bros: “Choices of an analytical representation of integral and partial excess quantities of mixing”, *J. Chem. Phys.* **72**, (1975) 83.

[Nel65] J.A. Nelder, R. Mead: “A simplex method for function minimization”, *Comput. J.* **7**, (1965) 308.

[Nel89] D.R. Nelson, F. Spaepen: „Polytetrahedral order in condensed matter“, *Solid State Phys.* **42**, (1989) 1.

[Now99] H. Nowak and P. Häussler: “Concept of resonances in disordered metallic matter”, *J. Non-Cryst. Solids* **250-252**, (1999) 389.

[Obe09] H.J. Oberle: “Optimierung. 4. Simplexmethode nach Nelder, Mead”, Universität Hamburg, So*Se* **2009**.

[Ouy06a] Y. Ouyang, X. Zhong, Y. Du, Z. Jin, Y. He, Z. Yuan: “Formation enthalpies of Fe-Al-RE ternary alloys calculated with a geometric model and Miedema’s theory”, *J. Alloys Comp.* **416**, (2006) 148.

[Ouy06b] Y. Ouyang, X. Zhong, Y. Du, Y. Feng, Y. He: "Enthalpies of formation for the Al-Cu-Ni-Zr quaternary alloys calculated via a combined approach of geometric model and Miedema theory", *J. Alloys Comp.* **420**, (2006) 175.

[Par05] G. Parisi, F. Zamponi: "The ideal glass transition of hard spheres", *J. Chem. Phys.* **123**, (2005) 144501.

[Par07a] J. Park, Y. Shibutani: "Weighted Voronoi tessellation technique for internal structure of metallic glasses", *Intermetallics* **15**, (2007) 187.

[Par07b] K.W. Park, J.J. Jang, M. Wakeda, Y. Shibutani, J.C. Lee: "Atomic packing density and its influence on the properties of Cu–Zr amorphous alloys", *Scripta Mater.* **57**, (2007) 805.

[Pas88] W. Paszkowicz: "Contribution of a hard-spheres packing model to the determination of binary alloy phase diagrams", *J. Phys. F: Met. Phys.* **18**, (1988) 1761.

[Pau52] L. Pauling: *The nature of the chemical bond 2nd Edition*, Cornell University Press, Ithaca, USA, 1952.

[Pek93] A. Peker, W.L. Johnson: „A high processable metallic glass: $Zr_{41.2}Ti_{13.8}Cu_{12.5}Ni_{10}Be_{22.5}$", *Appl. Phys. Lett.* **63**, (1993) 2342.

[Pri36] J.A. Prins, H. Petersen: „Theoretical diffraction patterns corresponding to some simple types of molecular arrangement in liquids", *Physica* **3**, (1936) 147.

[Qi99] Y. Qi, T. Çağin, Y. Kimura, W.A. Goddard III: "Molecular-dynamics simulations of glass formation and crystallization in binary liquid metals: Cu-Ag and Cu-Ni", *Phys. Rev. B* **59**, (1999) 3527.

[Ric74] F.M. Richards: "The interpretation of protein structures: Total volume, group volume distributions and packing density", *J. Mol. Biol.* **82**, (1974) 1.

[Ros89] V. Rosato, M. Guillope, B. Legrand: "Thermodynamical and structural-properties of fcc transition metals using a simple tight-binding model", *Phil. Mag. A* **59**, (1989) 321.

[Rub95] G. Rubin, A. Finel: "Application of first-principles methods to binary and ternary alloy phase diagram predictions", *J. Phys.: Condens. Matter.* **7**, (1995) 3139.

[Sad03] J.F. Sadoc, R. Jullien, N. Rivier: "The Laguerre polyhedral decomposition: application to protein folds", *Eur. Phys. J. B* **33**, (2003) 355.

[Sch67] G.E.R. Schulze: *Metallphysik*, Akademie-Verlag, Berlin, Germany, (1967).

[Sch98] T.B. Schrøder, J.C. Dyre: "Hopping in a supercooled binary Lennard-Jones liquid", *J. Non-Cryst. Solids* **235–237**, (1998) 331.

[Sco60] G.D. Scott: "Packing of spheres", *Nature* **188**, (1960) 908.

[Sco62] G.D. Scott: "Radial distribution of the random close packing of equal spheres", *Nature* **194**, (1962) 956.

[Sco69] G.D. Scott, D.M. Kilgour: "The density of random close packing of spheres", *Brit. J. Appl. Phys. (J. Phys. D)* **2**, (1969) 863.

[Sen01] O.N. Senkov, D.B. Miracle: "Effect of the atomic size distribution on glass forming ability of amorphous metallic alloys", *Mater. Res. Bull.* **36**, (2001) 2183.

[Sen03] O.N. Senkov, D.B. Miracle: "A topological model for metallic glass formation", *J. Non-Cryst. Solids* **317**, (2003) 34.

[She06] H.W. Sheng, W.K. Luo, F.M. Alamgir, J.M. Bai, E. Ma: „Atomic packing and short-to-medium-range order in metallic glasses", *Nature* **439**, (2006) 419.

[Shi00] F.G. Shi, T.G. Nieh, Y.T. Chou: " A free volume approach for self-diffusion in metals", *Scripta Mater.* **43**, (2000) 265.

[Sib02] R. Sibug-Aga, B.B. Laird: "Simulations of binary hard-sphere crystal–melt interfaces: Interface between a one-component fcc crystal and a binary fluid mixture", *J. Chem. Phys.* **116**, (2002) 3410.

[Spe62] W. Spendley, G.R. Hext, F.R. Himsworth: "Sequential application of simplex designs in optimization and evolutionary operation", *Technometrics* **4**, (1962) 441.

[Ste30] G.W. Stewart: „X-Ray Diffraction in liquids", *Rev. Mod. Phys.* **2**, (1930) 116.

[Sto93] U.K. Stolz, I. Arpshofen, F. Sommer: "Determination of the enthalpy of mixing of liquid Aliminium-Copper-Nickel ternary alloys", *Z. Metallkd.* **84**, (1993) 552.

[Sut90] A.P. Sutton, J. Chen: "Long-range Finnis Sinclair potentials", *Phil. Mag. Lett.* **61**, (1990) 139.

[Tel04] M. Telford: „The case for bulk metallic glass", *Materials Today* **7**, Issue 3, (2004) 36.

[Too65] G.W. Toop: "Predicting ternary activities using binary data", *Trans. Met. Soc. AIME* **233**, (1965) 850.

[Tor00] S. Torquato, T.M. Truskett, P.G. Debenedetti: "Is random close packing of spheres well defined?", *Phys. Rev. Lett.* **84**, (2000) 2064.

[Tor68] E.M. Tory, N.A. Cochrane, S.R. Waddell: "Anisotropy in simulated random packing of equal spheres", *Nature* **220**, (1968) 1023.

[Vis72] W.M. Visscher, M. Bolsterli: "Random packing of equal and unequal spheres in two and three dimensions", *Nature* **239**, (1972) 504.

[Vla03] A.Yu. Vlasov, A.J. Masters: "Binary mixtures of hard spheres: how far can one go with the virial equation of state?", *Fluid Phase Equilibria* **212**, (2003) 183.

[Vor08] G. Voronoi: "Nouvelles applications des paramètres continus à la théorie des formes quadratiques.", *J. Reine Angew. Math.* **134**, (1908) 198.

[Wah91] G. Wahnström: "Molecular-dynamics study of a supercooled 2-component Lennard-Jones system", *Phys. Rev. A* **44**, (1991) 3752.

[Wan03] X.L. Wang, J. Almer, C.T. Liu, Y.D. Wang, J.K. Zhao, A.D. Stoica, D.R. Haeffner, W.H. Wang: "In situ synchrotron study of phase transformation behaviors in bulk metallic glass by simultaneous diffraction and small angle scattering", *Phys. Rev. Lett.* **91**, (2003) 265501.

[Wan04] S. Wang, C.Z. Wang, F.C. Chuang, J.R. Morris, K.M. Ho: "Ab initio molecular dynamics simulation of liquid Al_xGe_{1-x} alloys", *Phys. Rev. B* **70**, (2004) 224205.

[Wan07a] W.H. Wang: "Roles of minor additions in formation and properties of bulk metallic glasses", *Prog. Mater. Sci.* **52**, (2007) 540.

[Wan07b] W.C. Wang, J.H. Li, H.F. Yan, B.X. Liu: "A thermodynamic model proposed for calculating the standard formation enthalpies of ternary alloy systems", *Scripta Mat.* **56**, (2007) 975.

[Wan08] L. Wang, K.-C. Chou, S. Seetharaman: "A comparison of traditional geometrical models and mass triangle model in calculating the surface tensions of ternary sulphide melts", *CALPHAD* **32**, (2008) 49.

[Wee87] A.W. Weeber: ""Application of the Miedema model to formation enthalpies and crystallization temperatures of amorphous alloys", *J. Phys. F: Met. Phys.* **17**, (1987) 809.

[Wig33] E. Wigner, F. Seitz: "On the constitution of metallic sodium", *Phys. Rev.* **43**, (1933) 804.

[Wil08] S.R. Williams, C.P. Royall, G. Bryant: "Crystallization of dense binary hard-sphere mixtures with marginal size ratio", *Phys. Rev. Lett.* **100**, (2008) 225502.

[Wit02] V.T. Witusiewicz, I. Arpshofen, H.J. Seifert, F. Sommer, F. Aldinger: "Enthalpy of mixing of liquid and undercooled liquid ternary and quaternary Cu–Ni–Si–Zr alloys", *J. Alloys Comp.* **337**, (2002) 155.

[Wit98] V.T. Witusiewicz, U.K. Stolz, I. Arpshofen, F. Sommer: "Thermodynamics of liquid Al-Cu-Zr alloys", *Z. Metallkd.* **89**, (1998) 704.

[Wit99] V.T. Witusiewicz, F. Sommer: "Thermodynamics of liquid Al–Ni–Zr and Al–Cu–Ni–Zr alloys", *J. Alloys Comp.* **289**, (1999) 152.

[Woo60] W.W. Wood, L.D. Jacobson: "Preliminary results from a recalculation of the Monte Carlo equation of state of hard spheres", *J. Chem. Phys.* **33**, (1960) 1207.

[Yua08] Z.Z. Yuan, S.L. Bao, Y.Lu, D.P. Zhang, L. Yao: "A new criterion for evaluating the glass-forming ability of bulk glass forming alloys", *J. Alloys Compd.* **459**, (2008) 251.

[Zha02a] R.F. Zhang, B. X. Liu: „Proposed model for calculating the standard formation enthalpy of binary transition-metal systems", *Appl. Phys. Lett.* **81**, (2002) 1219.

[Zha02b] B. Zhang, W.A. Jesser: "Formation energy of ternary alloy systems calculated by an extended Miedema model", *Phys. B* **315**, (2002) 123.

[Zha05] R.F. Zhang, B.X. Liu: "Response to "Comment on 'Proposed model for calculating the standard formation enthalpy of binary transition-metal systems' " [Appl. Phys. Lett. 86, 216103 (2005)] ", *Appl. Phys. Lett.* **86**, (2005) 216104.

[Zha07a] L.C. Zhang, K.B. Kim, P. Yu, W.Y. Zhang, U. Kunz, J. Eckert: "Amorphization in mechanically alloyed (Ti, Zr, Nb)–(Cu, Ni)–Al equiatomic alloys", *J. Alloys Comp.* **428**, (2007) 157.

[Zha07b] R.F. Zhang, S.H. Sheng, B.X. Liu: "Predicting the formation enthalpies of binary intermetallic compounds", *Chem. Phys. Lett.* **442**, (2007) 511.

[Zha91] T. Zhang, A. Inoue, T. Masumoto: „Amorphous Zr-Al-TM (TM = Co, Ni, Cu) alloys with significant supercooled liquid region of over 100 K", *Mater. Trans. JIM* **32**, (1991) 1005.

[Zho06] S.H. Zhou, R.E. Napolitano: "Phase equilibria and thermodynamic limits for partitionless crystallization in the Al–La binary system", *Acta Mater.* **54**, (2006) 831.

[Zor05] E. Zoro, D. Boa, C. Servant, B. Legendre: "Enthalpies of mixing of the liquid phase in the ternary system Ag–Au–Bi", *J. Alloys Comp.* **398**, (2006) 106.

ACKNOWLEDGMENTS

I would like to take this opportunity to thank the following persons for their special contributions, without many of which it would have been impossible to have this work done.

First of all I want to thank Prof. Helmut Eschrig for the scientific supervision of this work and interesting lectures.

It also gives me a pleasure to take this occasion to thank Prof. Dr. Jürgen Eckert for the opportunity to work in ICM.

I must also express my gratitude towards my advisor, Dr. Helmut Hermann, for giving me the opportunity to work at IFW-Dresden. His faith, pleasant working relationship and patience have helped me very much to accomplish this work.

The supportive atmosphere inherent to the whole group of IFW Dresden contributed essentially to the final outcome of my studies. In this context I would like to thank particularly to Dr. Mihai Stoica, Dr. Norbert Mattern, Dr. Helmut Ehrenberg, Dr. Antje Elsner and Dr. Laichang Zhang for their advices and helpful scientific discussions. It has been a pleasure working with them.

I am grateful to Mr. Michael Frey, Mr. Heiko Schulze and Mr. Sven Donath for helping me with experimental environment and casting.

At the end, but not less, I also thank to my colleagues and especially departments 32 and 34, which had supported me with a cheerful mood during this work. Many peoples should be listed here.

And now I would like to express all my gratitude to my family and my friends. Thank you for your trust, kindness, help and patience!

Declaration

I hereby declare that the thesis, submitted for partial fulfillment of the requirements for the degree of Doctor rerum naturalium (Dr. rer. nat.) and entitled *"Polyhedra-based analysis of computer simulated amorphous structures"* represents my own work and has not been previously submitted to this or any other institution for any degree, diploma or other qualification.

The research was done at Leibniz-Institut für Festkörper- und Werkstoffforschung Dresden, under the scientific supervision of Prof. Dr. Helmut Eschrig.

I declare that I know the graduation regularity of Faculty of Mathematics and Natural Sciences of Technical University Dresden, from 20.03.2000.

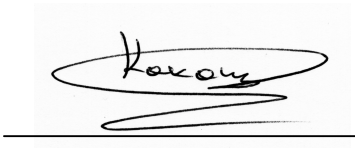

Valentin Kokotin

Dresden, 12 January 2010